Studies on Crystal Structures and Functions of Amide Group-Containing Coordination Polymers

Kazuhiro Uemura

2004

Preface

The study presented in this thesis has been curried out under the direction of Professor Susumu Kitagawa during April 1999 – March 2004 at the Department of Synthetic Chemistry and Biological Chemistry, Graduate School of Engineering, Kyoto University.   In this thesis the author described the relationship between structures and functions of coordination polymers.

The author would like to express his supreme gratitude to Professor Susumu Kitagawa for his kindest guidance, valuable suggestions and warm encouragement in the laboratory.

The author would like to express his sincere gratitude to Associate Professor Mitsuru Kondo (Shizuoka University) for his helpful advises and discussions during the course of this work.   The author would like to express his deep gratitude to Professor Tadashi Mizutani (Doshisya University), Dr. Ho-Chol Chang and Dr. Takashi Uemura for his kind advises and valuable discussions.

The author is thankful to Dr. Yusuke Yamada (National Institute of Advanced Industrial Science and Technology) for his kind technical supports of XRPD.   The author is thankful to Dr. Kazuya Saito (Osaka University) for their valuable suggestions and discussion.   The author is thankful to Dr. Kôichi Fukui (Regional Joint Research Project of Yamagata Prefecture) for his kind technical supports of EPR.

The author is thankful to Dr. Tapas Kumar Maji, Dr. Shin-ichiro Noro (RIKEN), Mr. Shigeyuki Masaoka, Mr. Katsunori Mochizuki, Mr. Ryotaro Matsuda, Mr. Shuhei Furukawa, Mr. Yasunori Nakanishi and Ms. Yuki Kumamoto for their valuable suggestions and kind technical supports. The author is thankful to Mrs. Hiroko Hirohata for her secretarial works and warm encouragement. Acknowledgement is made to all other members of the group of Professor Kitagawa for their encouragement and friendship.

Finally the author expresses his deep appreciation to his parents, Mr. Zenji Uemura and Mrs. Akiko Uemura for constant financial supports and affectionate encouragement.

Kazuhiro Uemura

Department of Synthetic Chemistry and Biological Chemistry
Graduate School of Engineering
Kyoto University

March, 2004

Contents

General Introduction

1. Background of Coordination Polymers.

Recently, a remarkable progress has been made in molecularly inorganic-organic hybrid compounds. The synthesis and characterization of infinite one-, two-, and three-dimensional (1-, 2-, and 3-D) networks has been an area of rapid growth in recent years.[1] In the last decade coordination compounds with infinite structures have been intensively studied, in particular, compounds with backbones constructed by metal ions as "nodes" and ligands as "linkers" form a family of polymers, which are called "coordination polymers". Since the early 1990s, research into materials with polymeric structures based on metal ions and organic bridging ligands has increased greatly. In principle, through the wide choice of metal, and infinite choice and design of ligands, a broad range of structural, magnetic, electrical, optical, and catalytic properties might be rationally incorporated into such materials. Early papers by Robson,[2] Moore,[3] Yaghi,[4] and Zaworotko[5] pointed out the rich possibilities for new material structures and properties offered by these coordination polymers.

The recent developments in coordination polymer research have accelerated the search in the direction of constructing desired framework. That the architecture of coordination polymers can be reasonably well predicted rests upon the simple premise that the coordination geometry of metals can be propagated with rigid bridging ligands ("spacer"). It is therefore unsurprising that a wide range of 1-D, 2-D, and 3-D infinite frameworks have already been generated with simple, linear spacers such as 4,4'-bpy (4,4'-bipyridine) (Scheme 1).
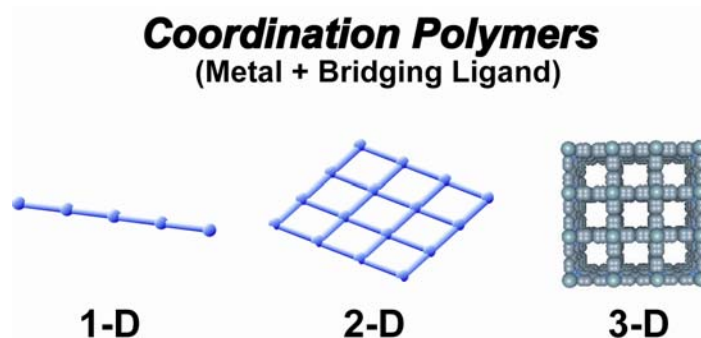
Scheme 1.

Porous compounds have attracted the attention of chemists, due to the interest in the creation of nanometer-sized spaces and finding of novel phenomena as well as commercial interest in their application in separations, storage, and heterogeneous catalysis. In 1994, the study on a catalytic properties was done by Fujita *et al.* using porous $[Cd(NO_3)_2(4,4'-bpy)_2]_n$ coordination polymer.[6]

1

That result stimulated the host-guest chemistry in coordination polymers, subsequently in 1995, a guest adsorption was studied by Yaghi's[4] and Moore's[7] groups, then gas adsorption at ambient temperature was carried out in 1997 by Kitagawa's group.[8]   Porous coordination polymers recently have appeared, which are beyond the scope of the zeolites and activated carbons, because of their complete regularity, high porosity, and highly designable frameworks.   One can take advantages in the synthesis that the reactions occur at mild conditions and choice of a certain combination of discrete molecular units leads to a desired extended network.

## 2. Crystal Engineering for Stable Porous Coordination Polymers.

Coordination polymers have exemplified how crystal engineering has become a paradigm for the design of new supramolecular architectures.[9]   Recent activity in crystal engineering has afforded several examples of coordination polymers which have rigid open framework network structures and therefore have the potential to be functionally related to zeolites.   The $[Cu(SiF_6)(4,4'\text{-bpy})_2]_n$ was reported as a prototype in the context of coordination polymers since it can be regarded as having been generated from square-grid coordination polymers that are cross-linked by $\mu\text{-SiF}_6$ anions.[10]   Also, the $[Zn_4O(BDC)_3]_n$ (BDC = benzenedicarboxylic acid) was synthesized on the basis of the ideas from metal carboxylate cluster chemistry, where an organic dicarboxylate linker is used in a reaction that gives supertetrahedron clusters when capped with monocarboxylates.[11]   This porous coordination polymer was realized by utilizing geometrical shapes of the cluster referred to a secondary building units (SBUs).[12]   Both coordination polymers afford the rigid and divergent character of the added linker allows the articulation into a 3-D framework resulting in structure with higher apparent surface area and pore volume.


$[Cu(SiF_6)(4,4'\text{-bpy})_2]_n$ $[Zn_4O(BDC)_3]_n$
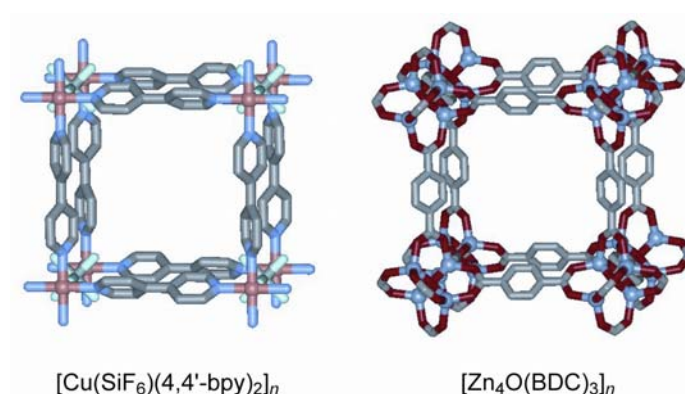
Scheme 2.

2

3. Soft Materials Assembled with Discrete Molecules.

Host-guest chemistry with organic hydrogen bonded networks in the solid state has largely studied since 1970s,[13] which have revealed that discrete organic molecules crystallize enclathlating guest molecules (= solvent) with elastic hydrogen bonds.   The reliability of these researches is a direct consequence of conformation flexibility exhibited by these hosts that, unlike rigid systems, enables them to achieve optimal packing with guest molecules (Scheme 3).   The state of the host component without guest molecules is referred to as the "apohost".   The structural rearrangement of molecules proceeds from the "apohost phase" to the clathrate phase responding to guest molecules like eq. (1).[14]
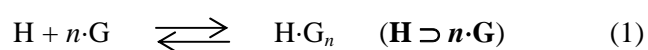
$$H + n \cdot G \quad \rightleftharpoons \quad H \cdot G_n \quad (\mathbf{H \supset n \cdot G}) \quad\quad (1)$$

where H is apohost, G is guest molecule, and n is stoichiometry of accommodated guest vs. apohost.[15] The Werner complexes, $M(NCS)_2(4\text{-Me-py})_4$, has also been studied intensively.[16]   This compound includes small guest molecules such as methane and xylene accompanying with the structural rearrangement.
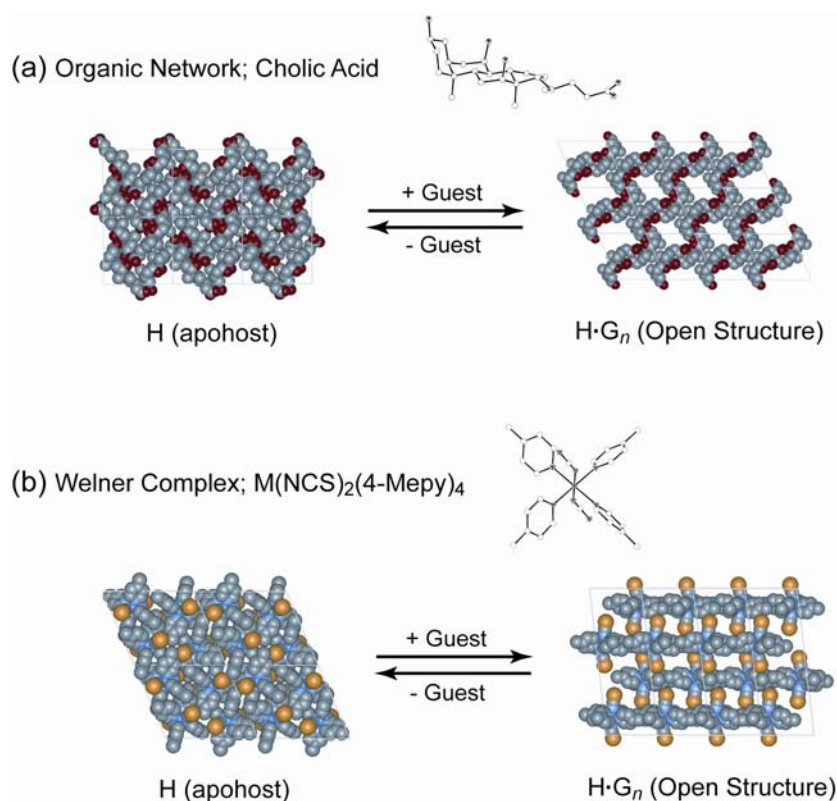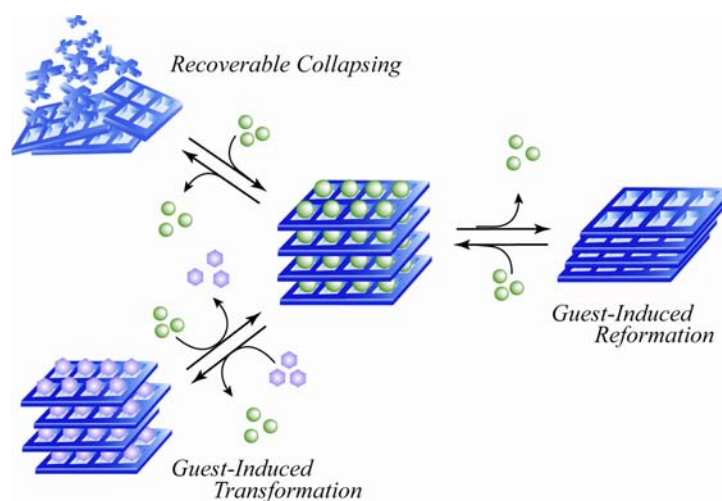

Scheme 3.

3

4. Dynamic Porous Coordination Polymers.

Compared with flexible discrete ensembles, the flexibility of coordination polymers have been overlooked for a long time. This is because flexibility in coordination polymers is incompatible with robustness such that porous frameworks are maintained without guest molecules.[10,11] Nevertheless, any indications of the softness were recognized as new generation coordination polymers.[17] Although the some efforts for construction of stable porous coordination polymers thorough understanding of the porosity in view of the substantial energy difference between the coordination bonds sustaining these frameworks and the very strong Si/Al-O bonds in zeolites, in general, the weak links like as Cu(II)-N coordination bond (= about 90 kJ/mol) afford the softness in the frameworks.

Until present-day, several flexible coordination polymers have been reported.[18-55] Such dynamic structural transformation based on flexible porous frameworks is one of the most interesting phenomena in coordination polymers, which are categorized as the three types are listed in Scheme 3:[31]

Scheme 4.

(1) Type I framework of "recoverable collapsing" has a property that by removal of guest molecules a network collapses due to the close packing force, however it regenerates under the initial condition.[26,31-33,44,52]

(2) Type II framework of "guest-induced transformation" has a property that structural shifts in the network are induced by the simultaneously exchanging of guest molecules.[18-22]

(3) Type III framework of "guest-induced reformation" has a property that removal of guest molecules makes a structure change in network to another one, however it reverts to the original one under the initial condition.[24,25,27-31,34-43,45-51,53-56]

Type I is regarded as "crystal-to-amorphous transformation", therefore, the approach to create such a transformation could be applicable to brittle materials systems.[57] Whereas, type II and III compounds show "crystal-to-crystal transformation", in a sense, this property results from advantage of molecularly inorganic-organic hybrid system.

5. Definition of "Porous" by Thermodynamic Analysis.

There are numerous reports about "porous coordination polymers", which could be classified into two types, "rigid pores" and "dynamic pores". In many cases, such solids are interchangeably referred to as "porous" and "open-framework", without definitive proof of porosity. Yaghi pointed out that "porous" implies having pores, and pores are, a "minute opening through which fluids or gases can pass", thus, demonstration of porosity through gas sorption isotherms is necessary to prove permanent porosity.[12] Undoubtedly, many structures titled with "porous …" were analyzed by only X-ray crystallography.

As well, in the organic host-guest compounds, host molecules may be broadly classified into two main types:[58] (A) those that form lattice inclusion compounds by packing in such a manner as to leave cavities, channels, or layers in the crystal structure so as to accommodate various guest molecules, and (B) those that form molecular complexes by fitting convex guests into the concave cavity of the host. Needless to say, compounds of type (A) are corresponding to porous compounds pointed by Yaghi.

In flexible compounds (type (B)) on the basis of mononuclear complex assembles and organic networks, thermal analysis have been done to clear their mechanism. Scheme 5 shows the schematic representation of the k_{obs} vs guest pressure in the reaction of eq. (1), where k_{obs} is observed reaction rate constant. In the case of flexible compounds like type (B), the phenomenon arises from the threshold pressure, P_{th}, required to start the enclathration reaction. These threshold pressures increase with increasing temperatures, which is generally consistent with the inclusion compound having a greater propensity to decompose at higher temperatures. The graph of $\ln P_{th}$ vs $1/T$ has a slope of $\Delta H_{ad}/R$, yielding adsorption enthalpy change value (ΔH_{ad}) using the Clausius-Clapeyron equation as eq.2.

$$\text{d} \ln P_{th}/\text{d}(1/T)) = \Delta H_{ad}/R \qquad (2)$$

Also, the graph of $\ln k_{obs}$ vs $1/T$ has a slope of $-E_{ad}/R$, yielding activation energy of adsorption (E_{ad}) using the Arrhenius equation as eq.3.

$$k_{obs} = A \exp(-E_{ad}/RT) \qquad (3)$$

5

Sometimes, an interesting feature of the kinetics is observed that for a given pressure of guest vapor, the rate of the reaction decreases with increasing temperature. Such an anti-Arrhenius behavior has been observed for enclathration of guest molecules.[59]

In the case of rigid porous materials like type (A), it is clear that the graph of the k_{obs} vs guest pressure pass through the zero point. Therefore, we can recognize porous material from the thermodynamic analysis; line (a) indicates "rigid pores", and line (b) indicates "dynamic pores". Recently there has been a keen interest in dynamic porous coordination polymers that transform under some sort of external stimuli to take on different functions, these sometimes being referred to as smart, responsive, or new generation materials.
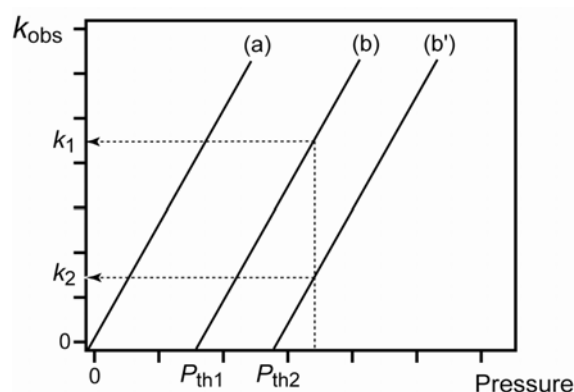
Scheme 5.

6. Expected Functionalities Induced by Dynamic Pores.

Dynamic pores could come from a sort of "soft" framework with bistability, whose two states go back from and forth to one of counter parts; a system could exist in one or two states for the same values of external field parameters. Such flexible porous coordination polymers offer an application to unique class of materials, which cannot be obtained in rigid porous material. For example, $\{[Fe(NCS)_2(azpy)_2]\cdot Guest\}_n$ (azpy = *trans*-4,4'-azopyridine) displays Fe(II) spin crossover induced by reversible uptake and release of guest molecules, due to a considerable flexibility of framework causing substantial changes in the local geometry of the Fe(II) centers.[53] Other several examples of properties that framework functionalities change by inclusion and removal of guest molecules, which induce the change of environment of metal centers, have been also known.[33,40,60-62] The generation of a host lattice that interacts with exchangeable guest species in a switchable fashion has implications for the generation of previously undeveloped advanced materials with applications in areas such as molecular sensing.

6

As well, the size, shape, and physicochemical character of the inclusion cavities can be adjusted by interchanging framework components while maintaining infinite framework motif, enabling highly selective guest inclusions. Dynamic porous coordination polymers, $[Ni(NO_3)_2(L)_2]_n$ (L = 4,4'-bis(4-pyridyl)biphenyl), selectively includes *o*-xylene but not *m*-xylene.[30] Such kinds of compound may have distinct advantages for the separations of fine chemicals, making use of the diffusion of the guest molecules in to pre-existing pores.

The difference from the case of discrete molecules is that coordination polymers form infinite network, therefore the extensive cooperativity would be expected between the molecules throughout the crystal, such that rearrangement can occur in a well-concerted fashion, in order to maintain its macroscopic integrity.

7. Contrivance for Construction of Dynamic Porous Frameworks.

Reported dynamic porous frameworks indicate that cooperative interactions in systems based on supposedly weaker interactions can yield softer yet functional networks with behavior unlike that observed in more rigid inorganic frameworks. Consequently, the mutual relationship among each motif (1-D, 2-D and 3-D) is significant to attain flexible frameworks. The achieved frameworks are grouped roughly by architectural type/dimensionality: 1-D, 2-D, and 3-D (Scheme 6).

I. 1-D Chain.[18-24] Most 1D coordination polymers have the simplest topology of a single-strand chain, particularly when a two-coordinate Ag(I) atoms interacts with a bidentate ligand. Although much of attention have been focused on their unique topologies like helix, the packing manner of each 1-D chain in the whole crystal is overlooked. Since a charged framework would also have to accommodate counterions as guest molecules, anions may play key roles in determining the polymer structure. Therefore, the heterogeneous anion exchange accompanying with framework structural changes have been done.

II. 2-D Stacked Layer.[25-34] 2-D sheets such as square grids and rectangular grids stack on the neighboring those with weak interactions. Square grids and rectangular grids have the potential to provide dynamic pores as they can adopt changes caused by external stimuli, either within the layers or between the layers. The crystal-to-crystal sliding of 2-D nets between two packing modes, staggered and edge-to-edge manner, is triggered by guest exchanges, and results in considerable increase in the dimensions of channels.

III. 2-D Interdigitated Layer.[35,36] 2-D sheets based on coordination polymers weakly interact with the neighboring 2-D sheets. The interlocked layer, where some interlayer interaction act together within the layer to impart a 3-D character to a structure, produces the channel for guest

molecules.   The robustness nature of the framework is reflected in the retention upon desorption of guest molecules, however a void volume is decrease with multiple interaction between layers.
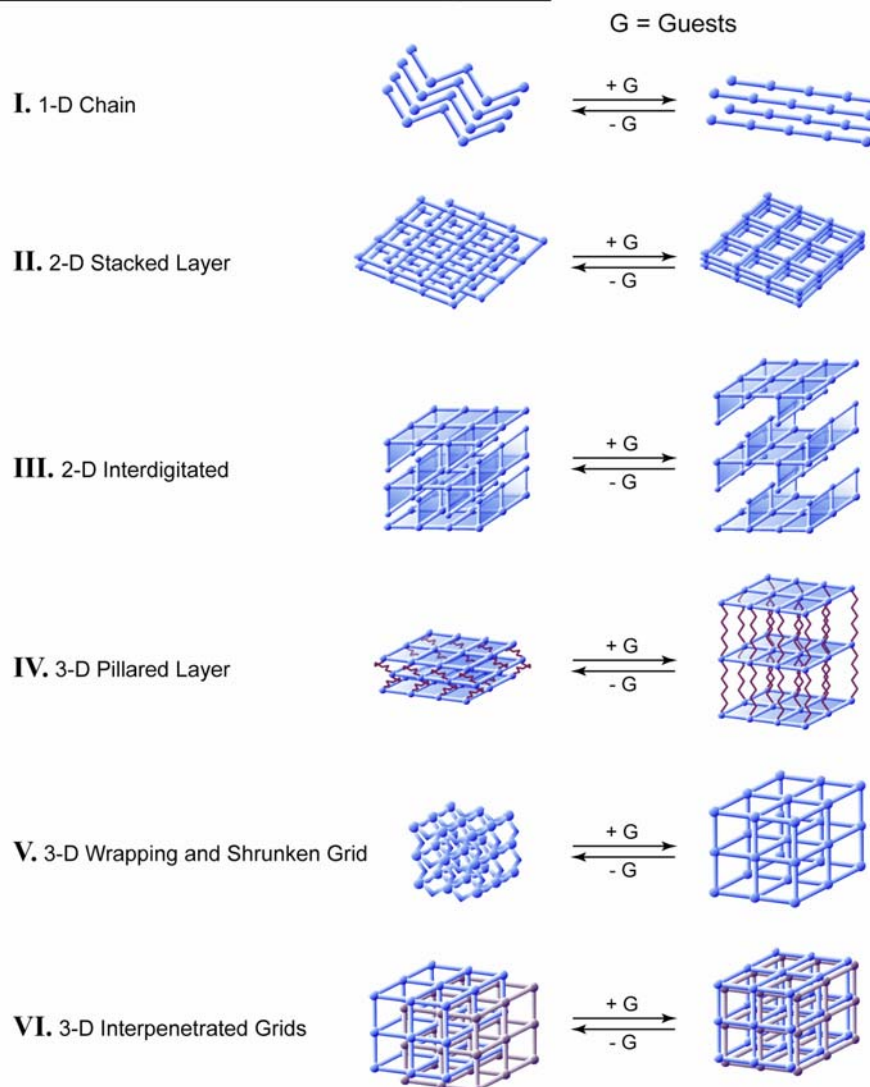
IV. 3-D Pillared Layer.[37-39]   The organic bridging ligands serve as pillars to build the lattice in third dimension and introduce tunable chemical functionality to the resulting lattice.   The simplest architecture is a "pillared layer", in which two adjacent sheets are connected by organic pillars that span galleries between sheets.   The connecting of these layers generates the complete 3-D crystal structure.   This generally affords inclusion cavities that are occupied by guest molecules during assembly of the lattice.   We note that these cavities are "virtual" as they do not exist in the absence of the guests.   The volumes, heights, shapes, and chemical environments of the inclusion cavities, created in the gallery regions between adjacent sheets, can be manipulated by adsorption/desorption of guest molecules.

V. 3-D Wrapping and Shrunken Grid.[40-49]   The introduction of hydrogen bond sites in pores induces to that these frameworks are somewhat flexible, enabling them to "shrink-wrap" about slightly undersized guests to achieve dense packing and optimized host-guest interaction.   Guest molecules inclusion indicates that the shrink-wrapping principally involves conformational changes of the host rather than shortening of the hydrogen bond length.

VI. 3-D Interpenetrated Grid.[50-55]   The 3-D linked grids are intimately inter-locked with other(s) in the same sort of topological relationship.   Although the interpenetration has been considered that this type of structure is not consistent with the creation of porous structure, the presence of voids for small-molecules inclusion could be still expected.   When the affinity between frameworks and guest molecules are stronger, guest molecules could penetrated into the pre-existing pore with slightly framework sliding.

Although such structural categorization for dynamic porous coordination polymers is obtained, consideration of the family of structures is necessary, due to the general difficulty of the prediction of structures.   The outcome of crystallization depends a great deal on experimental variables such as temperature, solvent, rates of heating and cooling, impurities and shock.   Therefore, the knowledge of the generality of new systems and their characterization provides a route to a priori determination of key metric parameters, that can guide the design and synthesis of these materials.

Dynamic Porous Coodination Polymers

G = Guests

I. 1-D Chain

II. 2-D Stacked Layer

III. 2-D Interdigitated

IV. 3-D Pillared Layer

V. 3-D Wrapping and Shrunken Grid

VI. 3-D Interpenetrated Grids

Scheme 6.

8. Survey of this thesis.

The main purpose of this thesis is to establish rational synthesis (= crystal engineering) by finding a general principle for controlling frameworks and to elucidate the relationship between crystal structures and functional properties or dynamic phenomena of frameworks of coordination polymers. Particularly, this thesis mainly describes coordination polymers containing amide groups as a function origin have been synthesized and categorized as "Metal-Organic Polymer with

9

Amide Groups" (**MOPA**).   The idea of combining coordination polymers and ligand-based hydrogen bonds has been recently introduced.   There are some advantages to this approach because it allows a combination of strength, imparted by a coordination network, and flexibility, allowed by the softer hydrogen-bond interactions.   Hence, assemblies of coordination complexes that have ligand-based hydrogen-bond functionalities, in which subunits can be formed independently and then later connected to themselves or other (complementary) subunits, are a useful addition to the field of crystal engineering.   Bridging ligands used in this study are given in Scheme 7 along with their abbreviations.

The Bridging Ligands

bpe

4-pia

dpds

3-pia

3-pna

4-pcia

3-pcia

4-pcna

4-peia
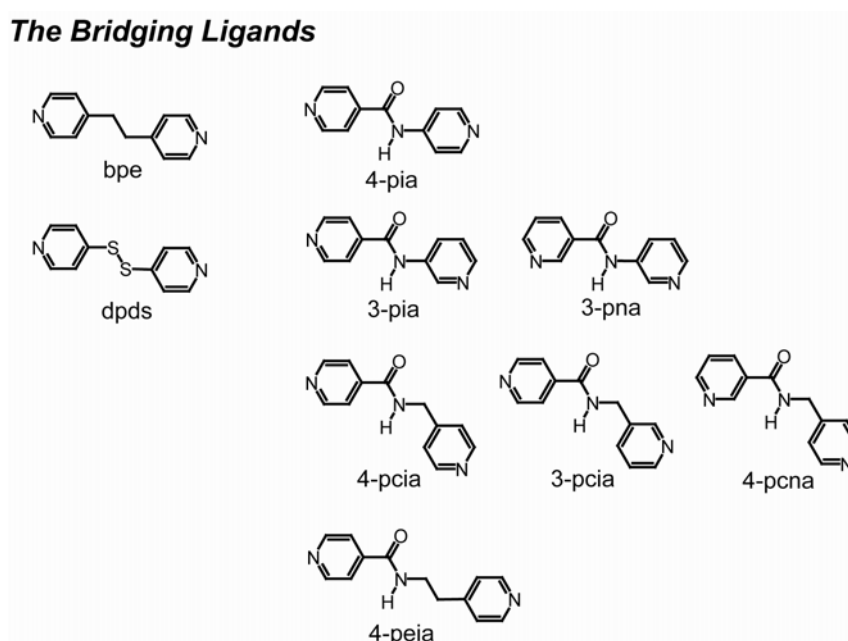
Scheme 7.

Chpater 1 describes 1-D chains the general formula $\{[AgL]\cdot X\}_n$ constructed by self-assembly of py-amide-py ligands (L) with various AgX (X = NO_3^-, BF_4^-, ClO_4^-, PF_6^-).   All these species contain cationic 1-D chains showing interesting features: with L = 4-pia, 4-pcia and 3-pcia, the cationic $[AgL]_n$ (**A1**, **A2** and **A3**, respectively) network exhibits the parallel alignment of 1-D chains with amide hydrogen bond among motif chains, so called "β-sheet" (Scheme 8).   When L = 4-pcna, four holded "helical" chains are obtained that show chiral single crystals (**A4** and **A5**).   **A1** ~ **5** accommodate anions as guest molecules with elastic hydrogen bond.   The anion exchange of **A1** ~ **3** with NO_3^-, BF_4^-, ClO_4^- and PF_6^- has been accomplished in aqueous media.

1-D Chains

A1
"β-Sheet Structure"
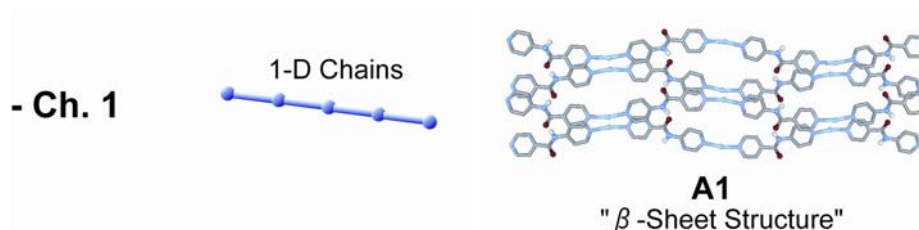
Scheme 8.

Chapter 2 deal with two repeated rhomboid typed new coordination polymers, [Mn(bpe)$_2$(NCS)$_2$]$_n$ (**R1**) and {[Cd(dpds)$_2$(H$_2$O)$_2$]·2NO$_3$·2EtOH·2H$_2$O}$_n$ (**R2 ⊃ 2EtOH·2H$_2$O**), were synthesized and structurally characterized. For both compounds, the basal plane is filled with the four pyridine donors and each metal ion in these compounds is linked by the two bridging ligands to make up a one-dimensional structure with large cavities. The network of **R2** demonstrates unique redox property in solid state. A cyclic voltammogram of this compound reveals redox activity, which is ascribed to the reduction of the disulfide bond to thiolate and reoxidation of the thiolate to disulfide.

Chapter 3 deal with three new coordination polymers of formulae [CoCl$_2$(4-pcna)$_2$]$_n$ (**R3**), {[Co(NCS)$_2$(4-pcna)$_2$]·2Me$_2$CO}$_n$ (**R4 ⊃ 2Me$_2$CO**) and {[Co(4-pcna)$_2$(H$_2$O)$_2$]·2NO$_3$·2CH$_3$OH}$_n$ (**R5 ⊃ 2H$_2$O·2MeOH**), have been synthesized and characterized by single crystal X-ray analysis. In three compounds, cobalt(II) atoms are bridged by 4-pcna ligand to form double stranded 1-dimensional chains, "repeated rhomboid-typed chains", with rectangular shaped cavities in the chains (Scheme 9). In **R3**, each chain slips and obstructs neighboring cavities to afford no guest-incorporated pores. **R4 ⊃ 2Me$_2$CO** and **R5 ⊃ 2H$_2$O·2MeOH** eschew such staggered fashions to attain pores fulfilled with guest molecules. **R5 ⊃ 2H$_2$O·2MeOH** trapped guest molecules with multiple hydrogen bonds, and shows *crystal* (**R5 ⊃ 2H$_2$O·2MeOH**) *-to-crystal* (**R5**) structural rearrangement in adsorption/desorption process. Thermodynamic analysis (DSC and TG) becomes apparent that two crystalline states are stabilized with multiple hydrogen bonds.


1-D Repeated rhomboids

R5 ⊃ 2H$_2$O·2MeOH
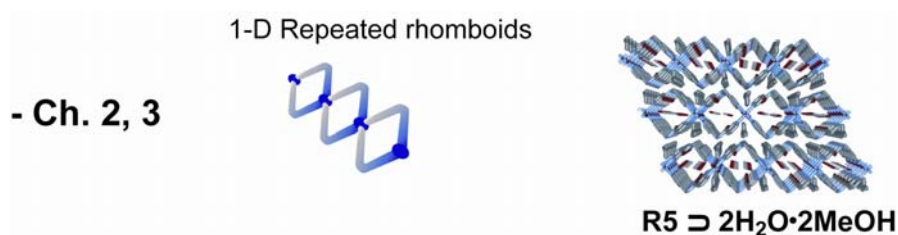
Scheme 9.

Chapter 4 deal with four porous crystalline coordination polymers with 2-D frameworks of a double edged axe-shaped motif, {[Co(NCS)$_2$(3-pia)$_2$]·2EtOH·11H$_2$O}$_n$ (**MOPA-1 ⊃ 2EtOH·11H$_2$O**), {[Co(NCS)$_2$(3-pia)$_2$]·4Me$_2$CO}$_n$ (**MOPA-1 ⊃ 4Me$_2$CO**), {[Co(NCS)$_2$(3-pia)$_2$]·4THF}$_n$ (**MOPA-1 ⊃ 4THF**) and [Co(NCS)$_2$(3-pna)$_2$]$_n$ (**MOPA-2**), have been synthesized from reactions of cobalt(II) thiocyanate 3-pia or 3-pna. X-ray crystallographic characterization reveals that the adjacent layers are stacked such that channels are created except for **MOPA-2**. The channels form a hydrogen bonding interior for guest molecules, in practice, **MOPA-1 ⊃ 2EtOH·11H$_2$O** contains ethanol and water molecules as guests in the channels with hydrogen bonds, whereas **MOPA-1 ⊃ 4THF** (**MOPA-1 ⊃ 4Me$_2$CO**) includes tetrahydrofuran (acetone) molecules. Spectroscopic measurements (Visible, EPR, and IR) indicate a clue to the crystal-to-crystal transformation; on removal of the guests the amide groups are used to form the β-sheet type hydrogen bonding between the sheets, and thus the framework withstands significant stress on removal of guest molecules (Scheme 10). This mechanism is attributed to the arrangement of the adjacent sheets so suited in regularity that the β-sheet type structure forms efficiently. The apohost **MOPA-1** shows a guest-selectivity that in addition to the size, the hydrogen bonding capability is required for the guest molecules.

Chpater 5 describes bispyridyl ligands with a spacer of amide group afford 2-D motifs with a deformed square grid, resulting in 3-D frameworks of [Co(NO$_3$)$_2$(3-pna)$_2$]$_n$ (**MOPA-3**), [Co(Br)$_2$(3-pna)$_2$]$_n$ (**MOPA-4**) and {[Co(NCS)$_2$(4-peia)$_2$]·4Me$_2$CO}$_n$ (**MOPA-5 ⊃ 4Me$_2$CO**), where the 2-D motifs are bound by complementary hydrogen bond between the amide groups. In the case of the **MOPA-5 ⊃ 4Me$_2$CO**, the amide groups form a contrivance for a dynamic porous framework because of their relevant position and orientation in the mutual nearest neighboring motifs. Consequently, **MOPA-5 ⊃ 4Me$_2$CO** shows *amorphous* (non-porous)-to-*crystal* (porous) structural rearrangement in Me$_2$CO adsorption/desorption process, where 2-D motifs are maintained. This cooperative phenomena associated with guest inclusion is examined by thermodynamic analysis.
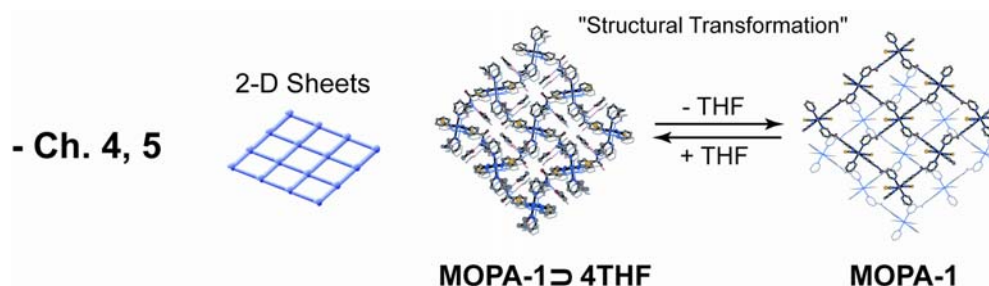
Scheme 10.

Chapter 6 demonstrates equilibrium adsorption isotherms of *n*-pentane and isoprene were measured on two kinds of 3-D porous coordination polymer, $[Cu_2(p\text{-OOC-Ph-COO})_2TED]_n$ (**1**) and $[Cu_2(1,4\text{-OOC-Nap-COO})_2TED]_n$ (**2**) (Scheme 11). All adsorption isotherm exhibit Type-I curve confirming the presence of micropores. For each of these isotherms, Langmuir, Freundlich and Dubinin-Radushkevich (DR) adsorption parameters were calculated.
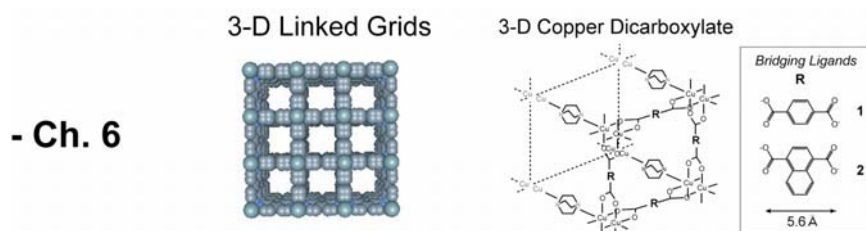
Scheme 11.

References and Notes

(1) Moulton, B.; Zaworotko, M. J. *Chem. Rev.* **2001**, *101*, 1629-1658.

(2) Hoskins, B. F.; Robson, R. *J. Am. Chem. Soc.* **1990**, *112*, 1546-1554.

(3) Gardner, G. B.; Venkataraman, D.; Moore, J. S.; Lee, S. *Nature* **1995**, *374*, 792-795.

(4) Yaghi, O. M.; Li, G.; Li, H. *Nature* **1995**, *378*, 703-706.

(5) Zaworotko, M. J. *Chem. Soc. Rev.* **1994**, 283-288.

(6) Fujita, M.; Kwon, J. Y.; Washizu, S.; Ogura, K. *J. Am. Chem. Soc.* **1994**, *116*, 1151-1152.

(7) Venkataraman, D.; Gardner, G. B.; Lee, S.; Moore, J. S. *J. Am. Chem. Soc.* **1995**, *117*, 11600-11601.

(8) Kondo, M.; Yoshitomi, T.; Seki, K.; Matsuzaka, H.; Kitagawa, S. *Angew. Chem. Int. Ed.* **1997**, *36*, 1725-1727.

(9) Zaworotko, M. J. *Chem. Comm.* **2001**, 1-9.

(10) Noro, S.-I.; Kitagawa, S.; Kondo, M.; Seki, K. *Angew. Chem. Int. Ed.* **2000**, *39*, 2082-2084.

(11) Li, H.; Eddaoudi, M.; O'Keeffe, M.; Yaghi, O. M. *Nature* **1999**, *402*, 276-279.

(12) Yaghi, O. M.; O'Keeffe, M.; Ockwig, N. W.; Chae, H. K.; Eddaoudi, M.; Kim, J. *Nature* **2003**, *423*, 705-714.

(13) MacNicol, D. D.; McKendrick, J. J.; Wilson, D. R. *Chem. Soc. Rev.* **1978**, *7*, 65-87.

(14) Miyata, M.; Shibakami, M.; Chirachanchai, S.; Takemoto, K.; Kasai, N.; Miki, K. *Nature* **1990**, *343*, 446-447.

(15) Hereafter, the number *n* is defined for the ratio of [the amount of adsorbed guest molecules]/[asymmetric unit of the crystal].

(16) Atwood, J. L.; Davies, J. E. D.; MacNicol, D. D. *Inclusion Compounds* **1984**, vol 1, Academic Press: London.

(17) Kitagawa, S.; Kondo, M. *Bull. Chem. Soc. Jpn.* **1998**, *71*, 1739-1753.

(18) Yaghi, O. M.; Li, H. *J. Am. Chem. Soc.* **1996**, *118*, 295-296.

(19) Jung, O.-S.; Kim, Y. J.; Lee, Y.-A.; Park, J. K.; Chae, H. K. *J. Am. Chem. Soc.* **2000**, *122*, 9921-9925.

(20) Jung, O.-S.; Kim, Y. J.; Lee, Y.-A.; Chae, H. K.; Jang, H. G.; Hong, J. *Inorg. Chem.* **2001**, *40*, 2105-2110.

(21) Pan, L.; Woodlock, E. B.; Wang, X.; Lamb, K.-C.; Rheingoldb, A. L. *Chem. Comm.* **2001**, 1762-1763.

(22) Muthu, S.; Yip, J. H. K.; Vittal, J. J. *J. Chem. Soc. Dalton Trans* **2002**, 4561-4568.

(23) Khlobystov, A. N.; Champness, N. R.; Roberts, C. J.; Tendler, S. J. B.; Thompson, C.; Schroder, M. *CrystEngComm* **2002**, *4*, 426-431.

(24) Takamizawa, S.; Nakata, E.-i.; Yokoyama, H.; Mochizuki, K.; Mori, W. *Angew. Chem. Int. Ed.* **2003**, *42*, 4331-4334.

(25) Kiang, Y.-H.; Gardner, G. B.; Lee, S.; Xu, Z.; Lobkovsky, E. B. *J. Am. Chem. Soc.* **1999**, *121*, 8204-8215.

(26) Choi, H. J.; Lee, T. S.; Suh, M. P. *Angew. Chem. Int. Ed.* **1999**, *38*, 1405-1408.

(27) Edgar, M.; Mitchell, R.; A. M. Z. Slawin; Lightfoot, P.; Wright, P. A. *Chem. Eur. J.* **2001**, *7*, 5168-5175.

(28) Min, K. S.; Suh, M. P. *Chem. Eur. J.* **2001**, *7*, 303-313.

(29) Li, D.; Kaneko, K. *Chem. Phys. Lett.* **2001**, *335*, 50-56.

(30) Biradha, K.; Hongo, Y.; Fujita, M. *Angew. Chem. Int. Ed.* **2002**, *41*, 3395-3398.

(31) Uemura, K.; Kitagawa, S.; Kondo, M.; Fukui, K.; Kitaura, R.; Chang, H.-C.; Mizutani, T. *Chem. Eur. J.* **2002**, *8*, 3586-3600.

(32) Uemura, K.; Kitagawa, S.; Fukui, K.; Saito, K. *J. Am. Chem. Soc.* **2003**, submitted.

(33) Maspoch, D.; Ruiz-molina, D.; Wurst, K.; Domingo, N.; Cavallini, M.; Biscarini, F.; Tejada, J.; Rovira, C.; Veciana, A. J. *Nature Mater.* **2003**, *2*, 190-195.

(34) Cai, J.; Zhou, J.-S.; Lin, M.-L. *J. Mater. Chem.* **2003**, *13*, 1806-1811.

(35) Suh, M. P.; Ko, J. W.; Choi, H. J. *J. Am. Chem. Soc.* **2002**, *124*, 10976-10977.

(36) Kitaura, R.; Seki, K.; Akiyama, G.; Kitagawa, S. *Angew. Chem. Int. Ed.* **2003**, *42*, 428-431.

(37) Alberti, G.; Murcia-Mascaros, S.; Vivani, R. *J. Am. Chem. Soc.* **1998**, *120*, 9291-9295.

(38) Alberti, G.; Brunet, E.; C. Dionigi; Juanes, O.; Mata, M. J. d. l.; RodrIguez-Ubis, J. C.; Vivani, R. *Angew. Chem. Int. Ed.* **1999**, *38*, 3351-3353.

(39) Kitaura, R.; Fujimoto, K.; Noro, S.-i.; Kondo, M.; Kitagawa, S. *Angew. Chem. Int. Ed.* **2002**, *41*, 133-135.

(40) Larionova, J.; Chavan, S. A.; Yakhmi, J. V.; Froystein, A. G.; Sletten, J.; Sourisseau, C.; Kahn, O. *Inorg. Chem.* **1997**, *36*, 6374-6381.

(41) Li, H.; Davis, C. E.; Groy, T. L.; Kelley, D. G.; Yaghi, O. M. *J. Am. Chem. Soc.* **1998**, *120*, 2186-2187.

(42) Beauvais, L. G.; Shores, M. P.; Long, J. R. *J. Am. Chem. Soc.* **2000**, *122*, 2763-2772.

(43) Chen, B.; Eddaoudi, M.; Reineke, T. M.; Kampf, J. W.; O'Keeffe, M.; Yaghi, O. M. *J. Am. Chem. Soc.* **2000**, *122*, 11559-11560.

(44) Tabares, L. C.; Navarro, J. A. R.; Salas, J. M. *J. Am. Chem. Soc.* **2001**, *123*, 383-387.

(45) Makinen, S. K.; Melcer, N. J.; Parvez, M.; Shimizu, G. K. H. *Chem. Eur. J.* **2001**, *7*, 5176-5182.

(46) Barthelet, K.; Marrot, J.; Riou, D.; Ferey, G. *Angew. Chem. Int. Ed.* **2002**, *41*, 281-284.

(47) Millange, F.; Serre, C.; Ferey, G. *Chem. Comm.* **2002**, 822-823.

(48) Serre, C.; Millange, F.; Thouvenot, C.; Nogues, M.; Marsolier, G.; Louer, D.; Ferey, G. *J. Am. Chem. Soc.* **2002**, *124*, 13519-13526.

(49) Lu, J. Y.; Babb, A. M. *Chem. Comm.* **2002**, 1340-1341.

(50) Carlucci, L.; Ciani, G.; Gudenberg, D. W. v.; Proserpio, D. M. *New J. Chem.* **1999**, *23*, 397-401.

(51) Kepert, C. J.; Prior, T. J.; Rosseinsky, M. J. *J. Am. Chem. Soc.* **2000**, *122*, 5158-5168.

(52) Carlucci, L.; Ciani, G.; Moret, M.; Proserpio, D. M.; Rizzato, S. *Angew. Chem. Int. Ed.* **2000**, *39*, 1506-1510.

(53) Halder, G. J.; Kepert, C. J.; Moubaraki, B.; Murray, K. S.; Cashion, J. D. *Science* **2002**, *298*, 1762-1765.

(54) Biradha, K.; Fujita, M. *Angew. Chem. Int. Ed.* **2002**, *41*, 3392-3395.

(55) Seki, K. *Phys. Chem. Chem. Phys.* **2002**, *4*, 1968-1971.

(56) Cussen, E. J.; Claridge, J. B.; Rosseinsky, M. J.; Kepert, C. J. *J. Am. Chem. Soc.* **2002**, *124*, 9574-9581.

(57) White, S. R.; Sottos, N. R.; Geubelle, P. H.; Moore, J. S.; Kessler, M. R.; Sriram, S. R.; Brown, E. N.; Viswanathan, S. *Nature* **2001**, *409*, 794-797.

(58) Nassimbeni, L. R. *Acc. Chem. Res.* **2003**, *36*, 631-637.

(59) Barbour, L. J.; Caira, M. R.; Nassimbeni, L. R. *J. Chem. Soc. Perkin Trans. II* **1993**, 2321-2322.

(60) Codjovi, E.; Sommier, L.; Kahn, O. *New J. Chem.* **1996**, *20*, 503-505.

(61) Garcia, Y.; Koningsbruggen, P. J. v.; Codjovi, E.; Lapouyade, R.; Kahn, O.; Rabardel, L. *J. Mater. Chem.* **1997**, *7*, 857-858.

(62) Usuki, N.; Ohba, M.; Okawa, H. *Bull. Chem. Soc. Jpn.* **2002**, *75*, 1693-1698.

Cationic Ag(I)-Amide One-dimensional Coordination Polymers with β-Sheet and Helical Structures.   New Second Structure Motif Constructed by Metallo-Amino Acids

Abstract

Coordination polymers containing amide groups as a function origin have been synthesized and categorized as "Metal-Organic Polymer with Amide Groups" (**MOPA**).   The self-assembly of py-amide-py ligands (L) with various AgX (X = NO_3^-, BF_4^-, ClO_4^-, PF_6^-) afforded new polymeric coordination networks with the general formula $\{[AgL]\cdot X\}_n$.   All these species contain cationic 1-dimensional (1-D) chains showing interesting features: with L = *N*-(4-pyridyl)isonicotinamide (4-pia), *N*-(4-pycolyl)isonicotinamide (4-pcia) and *N*-(3-pycolyl)isonicotinamide (3-pcia), the cationic $[AgL]_n$ (**A1**, **A2** and **A3**, respectively) network exhibits the parallel alignment of 1-D chains with hydrogen bond in amide moieties among motif chains, so called "β-sheet".   When L = *N*-(4-pycolyl)nicotinamide (4-pcna), four-hold "helical" chains are obtained that show chiral single crystals (**A4** and **A5**).   **A1** ~ **5** accommodate anions as guest molecules with elastic hydrogen bond. The anion exchange of **A1** ~ **3** with NO_3^-, BF_4^-, ClO_4^- and PF_6^- has been accomplished in aqueous media.

Introduction

Supramolecular chemistry[1] is currently in the middle of an avalanche-like process of experimental data accumulation and the extensive studies within the last decade have produced hundreds of new supramolecule compounds, especially in the area of coordination supramolecules[2-8] The next level of the development of this modern branch of chemistry will be based upon the classification of the experimental material, and this mode of construction of nanoscale structures and nanosystems represents the so-called 'bottom-up' or 'engineering-up' approach to fabrication. Hydrogen bond is also widely used in self-assembly of organic networks by considering its strength, specificity and directionality.[9-13] We utilize hydrogen bond in coordination polymers with fundamental knowledge of biological structures self-assemble in search of viable paradigms for the construction of large assemblies.

In the field of coordination polymers, 4,4'-bipyridine (4,4'-bpy) and the py-X-py type derivatives have been used in rational construction and provided various network materials, in which X are alkane, arene, alkyne, aromatic, azo, disulfide, and so on. However the synthetic studies of coordination network with py-X-py ligands containing interactive sites are sparse due to the difficulty of structure perspective. Particulaly, introduction of unique functional groups as X has afforded network materials showing new redox properties or network motifs. For example, azo or disulfide groups, i.e. py-N=N-py and py-S-S-py, have yieled redox active networks,[14,15] while py-$(CH_2)_3$-py has formed a double helical network.[16] Although hydrogen bonding interaction is quite important for the construction of new network motifs,[10,17] the synthetic studies of coordination network with py-X-py ligands containing hydrogen bonding sites such as hydroxy or amide are quite rare.

Recently we have shown that py-CONH-py ligand is useful for the construction of new coordination networks containing directed hydrogen bonded linkages between the amide groups of the ligands.[18,19] It is well known that the hydrogen bonds between amide moieties in the poly-peptide chains are quite important for the construction of well-ordered protein foldings, which contain α-helical or β-sheet structures.[20] Since the basic repetition is formulated as CONH-CHR, self-assembled syntheses and structural characterizations of one-dimensional coordination networks with CONH-CHR moieties are of great current interest toward the understanding translation process of one-dimensional peptide into the high-dimensional structures. Therefore, "Metal-Organic Polymers with Amide Groups" (**MOPA**) could be utilized as like metallo-amino acids for their synthetic studies and their structures. We chose *N*-(4-pyridyl)isonicotinamide (4-pia) and three py-CONH-CH_2-py type ligands (Scheme 1) for the synthetic studies, and have succeeded in the similar synthesis of one-dimensional silver(I) coordination network, **A1 ~ 5**. These ligands have, in the X part, two functional groups; one is amide sites for hydrogen bonding, and another is methylene site for free-rotation. As a result, two kinds of

coordinating pyridine site are set, due to their unsynmetrical structures. In this paper we report the unique self-assembled network topologies with inter chains amide-amide hydrogen bonding interactions.
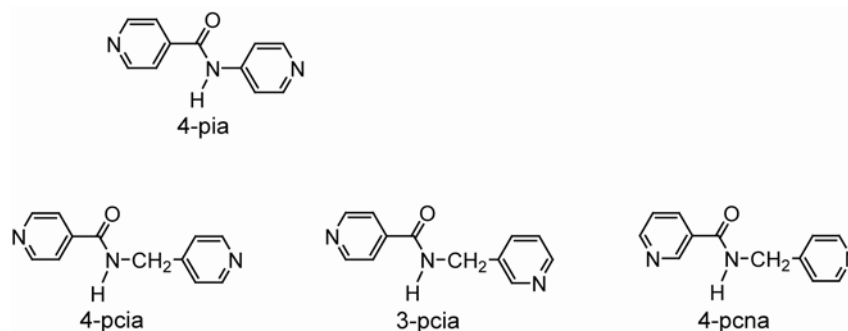
Scheme 1.

Table 1. Crystal Data and Structure Refinement.

Compound	A1 ⊃ NO₃⁻	A1 ⊃ BF₃⁻	A1 ⊃ ClO₄⁻
Chemical formula	$C_{11}H_9AgN_4O_4$	$C_{11}H_9BAgF_4N_3O$	$C_{11}H_9AgClN_3O_5$
Formula weight	369.08	393.88	406.53
Crystal system	monoclinic	monoclinic	monoclinic
Space group	*C2/c*	*C2/c*	*C2/c*
Temperature [K]	293	293	293
Color	Colorless	Colorless	Colorless
a [Å]	19.67(1)	19.670(8)	19.760(10)
b [Å]	6.728(4)	7.908(3)	8.112(3)
c [Å]	18.67(1)	16.980(7)	16.797(8)
α [°]	90	90	90
β [°]	91.663(9)	92.943(6)	93.519(7)
γ [°]	90	90	90
V [Å³]	2470(2)	2637(1)	2687(2)
Z	8	8	8
Goodness-of-fit on F^2	1.524	1.658	2.896
no. of unique data	2740	2974	2999
no. of variables	181	190	159
R [a]	0.044	0.050	0.1037
R_w [b]	0.124	0.140	0.3362

A1 ⊃ PF$_6^-$	A2 ⊃ NO$_3^-$·H$_2$O	A2 ⊃ ClO$_4^-$·H$_2$O	A2 ⊃ PF$_6^-$
C$_{11}$H$_9$AgF$_6$N$_3$OP	C$_{12}$H$_{11}$AgN$_4$O$_5$	C$_{12}$H$_{11}$AgClN$_3$O$_6$	C$_{12}$H$_{11}$AgF$_6$N$_3$OP
452.04	399.11	436.56	466.07
monoclinic	orthorhombic	orthorhombic	monoclinic
C2/c	*Pbca*	*Pbca*	*P2$_1$/n*
293	293	293	293
Colorless	Colorless	Colorless	Colorless
20.222(8)	12.903(5)	13.4092(9)	9.704(4)
8.652(3)	9.022(4)	9.3825(7)	25.40(1)
16.482(6)	24.54(1)	25.048(1)	12.458(5)
90	90	90	90
92.282(6)	90	90	94.893(6)
90	90	90	90
2881(1)	2856(2)	3151.3(3)	3058(2)
8	8	8	8
1.787	1.255	0.932	1.734
3179	3199	3312	6334
208	194	203	428
0.070	0.048	0.069	0.071
0.209	0.129	0.240	0.188

A3 ⊃ NO$_3^-$·H$_2$O	A3 ⊃ BF$_4^-$	A3 ⊃ ClO$_4^-$	A3 ⊃ PF$_6^-$
C$_{12}$H$_{11}$AgN$_4$O$_5$	C$_{12}$H$_{11}$BAgF$_4$N$_3$O	C$_{12}$H$_{11}$AgClN$_3$O$_5$	C$_{12}$H$_{11}$AgF$_6$N$_3$OP
399.11	407.91	420.56	466.07
monoclinic	monoclinic	monoclinic	monoclinic
P2$_1$/a	*P2$_1$/c*	*P2$_1$/c*	*P2$_1$/c*
293	293	293	293
Colorless	Colorless	Colorless	Colorless
8.951(5)	8.514(4)	8.4895(4)	8.501(1)
13.049(7)	18.763(9)	18.888(7)	19.951(3)
12.215(7)	9.071(4)	9.227(2)	9.6221(2)
90	90	90	90
94.210(9)	104.630(6)	105.094(2)	108.4339(4)
90	90	90	90
1422(1)	1402(1)	1428.5(6)	1548.2(2)
4	4	4	4
1.007	1.452	1.365	2.102
3145	3057	2927	3358
194	199	199	217
0.034	0.044	0.039	0.053
0.088	0.119	0.132	0.155

A4 ⊃ PF$_6^-$·MeOH	A5 ⊃ PF$_6^-$·MeOH
C$_{13}$H$_{11}$AgF$_6$N$_3$O$_2$P	C$_{13}$H$_{11}$AgF$_6$N$_3$O$_2$P
494.08	494.08
tetragonal	tetragonal
$P4_1$ [c]	$P4_3$ [c]
223	223
Colorless	Colorless
7.9389(7)	7.9357(7)
7.9389(7)	7.9357(7)
28.250(3)	28.283(3)
90	90
90	90
90	90
1780.5(3)	1781.1(3)
4	4
1.743	1.682
1801	2048
216	216
0.080	0.073
0.161	0.165

[a] $R = \Sigma||Fo| - |Fc||/\Sigma|Fo|$.   [b] $R_w = [(\Sigma w (|Fo| - |Fc|)^2/\Sigma wFo^2)]^{1/2}$.   [c] Space group is determined based on Flack Parameters.

Table 2.   Selected Bond Lengths and Angles around Silver(I) Atoms in **A1 ~ 5**.

MOPAs	Ag-N^C	Ag-N^N	N-Ag-N
A1 ⊃ NO$_3^-$	2.167(3)	2.155(3)	168.4(1)
A1 ⊃ BF$_3^-$	2.144(4)	2.140(4)	169.2(1)
A1 ⊃ ClO$_4^-$	2.139(8)	2.147(8)	168.1(3)
A1 ⊃ PF$_6^-$	2.122(5)	2.110(5)	172.1(2)
A2 ⊃ NO$_3^-$·H$_2$O	2.164(3)	2.159(3)	173.3(1)
A2 ⊃ ClO$_4^-$·H$_2$O	2.165(5)	2.163(5)	174.6(2))
A2 ⊃ PF$_6^-$	2.160(5), 2.152(5)	2.152(5), 2.134(6)	161.0(2), 162.0(2)
A3 ⊃ NO$_3^-$·H$_2$O	2.161(2)	2.159(2)	172.25(8)
A3 ⊃ BF$_4^-$	2.136(3)	2.144(3)	173.5(1)
A3 ⊃ ClO$_4^-$	2.162(3)	2.156(3)	172.9(1)
A3 ⊃ PF$_6^-$	2.149(3)	2.143(3)	174.9(1)
A4 ⊃ PF$_6^-$·MeOH	2.17(2)	2.13(2)	178.5(3)
A5 ⊃ PF$_6^-$·MeOH	2.16(2)	2.14(1)	178(1)

Table 3. Guest Occupied Area, Network Motif and N_A---O_A Lengths in **A1 ~ 5**.

MOPAs	Guest occupied area [%][a]	Network motif	N_A---O_A [Å]
A1 ⊃ NO₃⁻	5.3	β-Sheet	3.135(5)
A1 ⊃ BF₃⁻	16.0	β-Sheet	3.361(6)
A1 ⊃ ClO₄⁻	20.7	β-Sheet	3.35(1)
A1 ⊃ PF₆⁻	29.3	β-Sheet	3.203(8)
A2 ⊃ NO₃⁻·H₂O	9.5[b]	water-linked HB	-
A2 ⊃ ClO₄⁻·H₂O	17.1[b]	water-linked HB	-
A2 ⊃ PF₆⁻	23.5	[c]	-
A3 ⊃ NO₃⁻·H₂O	10.3[b]	water-linked HB	-
A3 ⊃ BF₄⁻	18.2	β-Sheet	2.823(4)
A3 ⊃ ClO₄⁻	19.6	β-Sheet	2.829(4)
A3 ⊃ PF₆⁻	23.6	β-Sheet	2.831(4)
A4 ⊃ PF₆⁻·MeOH	35.9[b]	Helical	-
A5 ⊃ PF₆⁻·MeOH	36.1[b]	Helical	-

[a] calculated by using PLATON.   [b] Solvent molecules are included as guest molecules.   [c] Oxygen atoms in amide moieties are contact to Ag(I) atoms.

Table 4. Ag(I)---Ag(I) Distances and Ag(I)---Anion Distances in **A1 ~ 5**.

MOPAs	Ag(I)---Ag(I) [Å]	Ag(I)---Anion [Å]
A1 ⊃ NO₃⁻	3.2824(9)	2.866(6)
A1 ⊃ BF₃⁻	3.2692(7)	2.986(5)
A1 ⊃ ClO₄⁻	3.293(2)	3.08(2)
A1 ⊃ PF₆⁻	3.622(1)	2.764(7)
A2 ⊃ NO₃⁻·H₂O	-	2.785(5)
A2 ⊃ ClO₄⁻·H₂O	-	2.769(7)
A2 ⊃ PF₆⁻	-	3.00(1)
A3 ⊃ NO₃⁻·H₂O	-	2.673(3)
A3 ⊃ BF₄⁻	3.342(1)	2.753(5)
A3 ⊃ ClO₄⁻	3.3214(7)	2.777(5)
A3 ⊃ PF₆⁻	3.5764(9)	2.915(4)
A4 ⊃ PF₆⁻·MeOH	-	3.13(4)
A5 ⊃ PF₆⁻·MeOH	-	3.11(4)

Results and Discussion

Crystal Structures.

Crystal data and details of the structure determinations are summarized in Table 1.   Selected bond distances and angles are listed in Table 2-4.   Due to unsymmetrical amide moiety (-CO$_A$N$_A$H-) two kinds of coordinating pyridine sites (N^C = carbonyl pyridine and N^N = amino pyridine (or N^M = methylene pyridine)) are available, by which coordination orientation can be controlled by the position

of nitrogen in the pyridine ring. The amide moiety of their ligands could create hydrogen bonding interaction sites in the network and cross-linking to coordination-based motifs. We tried self-assembly synthesis and add a new structural dimension to coordination networks with β-sheet motif having a linking capability to a network structure.

{[Ag(4-pia)]·X}$_n$ (A1 ⊃ X) (X = NO$_3^-$, BF$_4^-$, ClO$_4^-$ and PF$_6^-$). {[Ag(4-pia)]·NO$_3$}$_n$ (**A1 ⊃ NO$_3^-$**) is comprised of crystallographically independent one Ag(I) atom and one 4-pia ligand. The 4-pia molecules are linked by Ag(I) atoms to provide one-dimensional network. Each Ag(I) atom is coordinated by two pyridine nitrogen atoms of 4-pia molecules, N^C and N^N, leading to the electronically unsymmetric Ag(I) center (Figure 1a). The two Ag(I)-N distances are similar; Ag(I)-N^C = 2.167(3) Å, Ag(I)-N^N = 2.155(3) Å, N^C-Ag(I)-N^N = 168.4(1)°. All chains run along the *c* axis, and the pyridine rings are perpendicular to the *ac* plane. Adjacent chains run with the opposite direction as shown in Figure 1a. The one-dimensional chains are not linear but waving; the Ag(I) atom is in the top and bottom of the wave. The closest Ag(I)---Ag(I) distance (3.2824(9) Å; bottom-to top) in the two chains run parallel is separated to about 7.1 Å in the adjacent top-to-bottom point. The NO$_3^-$ anion, which is trapped in the space between chains, is weakly associate with Ag(I) atom (Ag(I)---O (NO$_3^-$) = 2.866(6) Å) as shown in Figure 1b. Furthermore, amide groups in the adjacent chains are hydrogen bonded in a way, via NH---O=C (N$_A$---O$_A$ = 3.135(5) Å), to yield a β–sheet type structure. Although the anions exhibit substantial differences both in shape and size (PF$_6^-$ = 54 Å^3, ClO$_4^-$ = 47 Å^3, BF$_4^-$ = 38 Å^3),[21] Ag(I)-(4-pia) chains take β-sheet network modifying with elastic amide-amide hydrogen bonding.
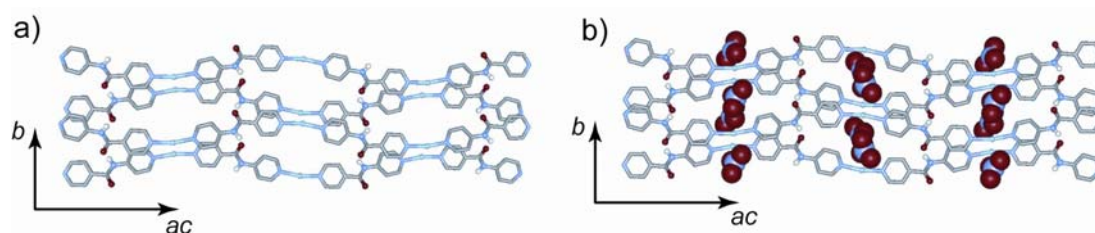
Figure 1. Crystal structure of {[Ag(4-pia)]·NO$_3$}$_n$ (**A1 ⊃ NO$_3^-$**). (a) Crystal view of **A1 ⊃ NO$_3^-$** along the *ac* plane. Four chains are bound with hydrogen bond of amide moieties between the chains. (b) Crystal view of **A1 ⊃ NO$_3^-$** along the *ac* plane. **NO$_3^-$** anions are accommodated among chains.

{[Ag(4-pcia)]·X}$_n$ (A2 ⊃ X) (X = NO$_3^-$·H$_2$O, ClO$_4^-$·H$_2$O and PF$_6^-$). Figure 2a shows the overall structure of **A2 ⊃ NO$_3^-$·H$_2$O**. Coordinations of two types of pyridine donor in 4-pcia ligands afford a slightly bent geometry (N^C-Ag-N^M = 173.3(1)°). Although these pyridine donors are unequivalent because of the unsymmetric structure of this ligand, the two Ag-N bond distances are similar;

Ag(I)-N^C = 2.164(3) Å and Ag(I)-N^M = 2.159(3) Å.   Each silver atom is linked by the 4-pcia ligands to provide an one-dimensional chain of $\{[Ag(pcia)]\cdot NO_3\cdot H_2O\}_n$ which forms a zigzag shape turning at methylene moiety.   These chains are aligned along a axis to form overall structure like wave sheet. Each chain direction (-CH_2-NH-CO- or –CO-NH-CH_2-) is opposing to neighboring chains.   Oxygen atoms of amide moieties stick out to be hydrogen bonded to water molecules.   These water molecules are hydrogen bonded to oxygen atoms of amide moieties, oxygen atoms of nitrate anions and nitrogen atoms in amide moieties.   Nitrate anions interact with silver atom (Ag---O(NO_3^-) = 2.785(5) Å), and are placed among these zigzag chains.

$A2 \supset ClO_4^-\cdot H_2O$ form iso-structure of $A2 \supset NO_3^-\cdot H_2O$, whereas $A2 \supset PF_6^-$ has different packing fashion (Figure 2a).   The most remarkable difference is that $A2 \supset PF_6^-$ does not include water molecules, and each chain slip against neighboring chains, where oxygen atoms in amide moieties interact with Ag(I) atoms (Ag(I)---O_A = 2.611(5), 2.685(5) Å).
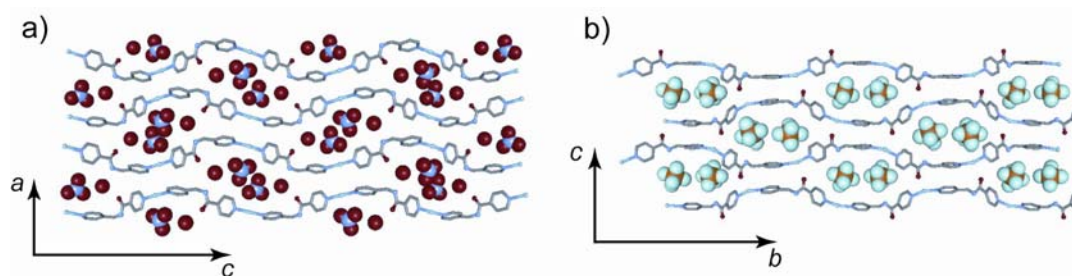
Figure 2.   Crystal structure of $\{[Ag(4\text{-pcia})]\cdot NO_3\cdot H2O\}_n$ ($A2 \supset NO_3^-\cdot H_2O$) and $\{[Ag(4\text{-pcia})]\cdot PF_6\}_n$ ($A2 \supset PF_6^-$).   (a) Crystal view of $A2 \supset NO_3^-\cdot H_2O$ along the b axis.   Four chains are bound with water linked hydrogen bond.   (b) Crystal view of $A2 \supset PF_6^-$ along the b axis.   Four chains are bound with Ag(I)---O_A contacts.

$\{[Ag(3\text{-pcia})]\cdot X\}_n$ ($A3 \supset X$) ($X = NO_3^-\cdot H_2O$, BF_4^-, ClO_4^- and PF_6^-).   In $A3 \supset PF_6^-$, each silver atoms are bridged by 3-pcia ligand with distorted linear geometry (N^C-Ag-N^M = 174.9(1)°, Ag-N^C = 2.149(3) Å, Ag-N^M = 2.143(3) Å), to afford an infinite zigzag chain in the bc plane as well as **A1** and **-10**.   It is worth noting that hydrogen-bonding links of the NH---O=C (N_A---O_A = 2.831(4) Å) groups between the adjacent chains create complementary-amide binding network (Figure 3b).   The β–sheet of $A3 \supset PF_6^-$ is a wavelike sheet with about 10 Å thickness.   The closest distance of Ag(I)---Ag(I) among the chains is 3.5764(9) Å.   In the protein structure, β-sheet structure is classified in two types; one is parallel type, and the other is the antiparallel type.[20]   In the former sheet, all chains are oriented at the same direction.   On the other hand, in the latter sheet, the chains are oriented at the opposite direction alternatively, and often observed in the single chain folding.   As shown in Figure 3b, the arrangement of the hydrogen bonding linkages found in $A3 \supset PF_6^-$ has the latter antiparallel form, i.e.

24

the direction of Ag-(py-CH$_2$-NH-CO-py)-Ag is changed to Ag-(py-CO-NH-CH$_2$-py)-Ag in the adjacent chain. These wavelike sheets interdigitate along the a axis, in which pyridine(N^M) rings stack with the about 4 Å distance. There is no hydrogen bonding between the adjacent sheets.

A3 ⊃ BF$_4$$^-$ and **A3 ⊃ ClO$_4$$^-$** form iso-structure of **A3 ⊃ PF$_6$$^-$**, to afford β-sheet structures. On the other hand, **A2 ⊃ NO$_3$$^-$·H$_2$O** include water molecules, These water molecules are hydrogen bonded to oxygen atoms of amide moieties, oxygen atoms of nitrate anions and nitrogen atoms in amide moieties (Figure 3a).
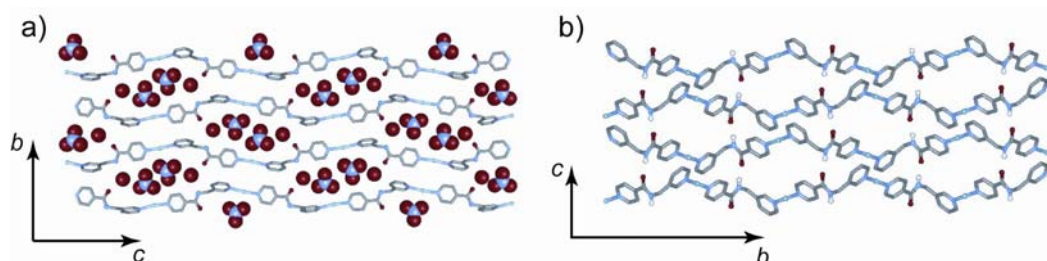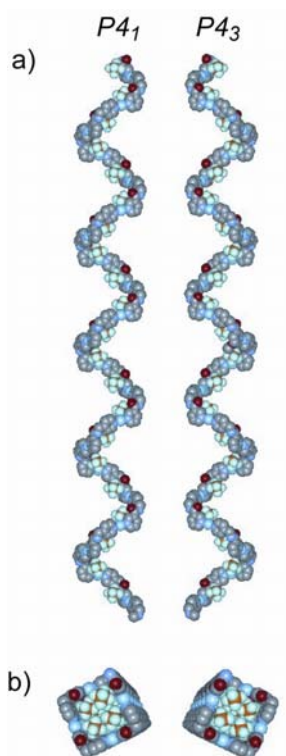

Figure 3. Crystal structure of {[Ag(3-pcia)]·NO$_3$·H2O}$_n$ (**A3 ⊃ NO$_3$$^-$·H$_2$O**) and {[Ag(3-pcia)]·PF$_6$}$_n$ (**A3 ⊃ PF$_6$$^-$**). (a) Crystal view of **A3 ⊃ NO$_3$$^-$·H$_2$O** along the a axis. Four chains are bound with water linked hydrogen bond. (b) Crystal view of **A3 ⊃ PF$_6$$^-$** along the a axis. PF$_6$$^-$ molecules are omitted for clarity. Four chains are bound with with hydrogen bond of amide moieties between the chains.

{[Ag(4-pcna)]·PF$_6$·MeOH}$_n$ (A4 ⊃ PF$_6$$^-$·MeOH). In **A4 ⊃ PF$_6$$^-$·MeOH**, each silver atom is linearly coordinated to 4-pcna ligands (N^C-Ag-N^M = 178.5(3)°) to provide an one-dimensional chain. In spite of the unequivalent pyridine donors, no significant difference is observed for the two Ag-N bond distances; Ag-N^C = 2.17(2) Å, Ag-N^M = 2.13(2) Å. The interesting feature in this chain is the formation of a helical framework with a repetition of 28 Å along the c axis (Figure 4a). **A4 ⊃ PF$_6$$^-$·MeOH** crystallizes in space group *P4$_1$*, resulting in unique structure of single right-handed helicity. **A4 ⊃ PF$_6$$^-$·MeOH** has the four hold axis along the c axis. Hexafluorophosphate anions and methanol molecules are located within the helical columns with closely contact distances; Ag(I)---O(MeOH) = 2.76(2) Å, Ag(I)---F(PF$_6$$^-$) = 3.13(4) Å. One helical column is interdigitated with adjacent columns, in which the oxygen atom at the amide moiety weakly associate with silver atom in the adjacent chain (Ag(I)---O$_A$ = 2.79(5) Å).[22-24] It is well-known that the helical structure of protein is mostly driven and stabilized by intramolecular hydrogen-bond interactions between carbonyl groups (H-bond donor) originated from the flexible polypeptide backbone.[20] In **A4 ⊃ PF$_6$$^-$·MeOH**, however, carbonyl oxygen atoms do not hydrogen bond to N-H, but weakly interact to Ag atoms in neighboring chain. Whereas, **A5 ⊃ PF$_6$$^-$·MeOH** crystallizes in space group *P4$_3$*, resulting in unique structure of single left-handed helicity.

Figure 5. Ramachandran Plot of **A2** (open triangle), **A3** (open circle), **A4** ⊃ **PF$_6$$^-$·MeOH** (open square) and **A5** ⊃ **PF$_6$$^-$·MeOH** (filled square) with reported pairs (dot) found in protein structures.

Figure 4. Crystal structure of {[Ag(4-pcna)]·PF$_6$·MeOH}$_n$ (**A4** ⊃ **PF$_6$$^-$·MeOH**) and {[Ag(4-pcna)]·PF$_6$·MeOH}$_n$ (**A5** ⊃ **PF$_6$$^-$·MeOH**) shown at left and right sides, respectively. Both helix chains have 28 Å pitch.

Comparison with Ramachandran Plot.

In protein structures, amide plane is planar. This structural rigidity is also found in **MOPA** ($\omega \approx$ 0) as shown in Table 5. By contrast, a rotation can occur about the C$^\alpha$-C bond, whose angle on rotation is called φ, and about the N-C$^\alpha$ bond whose angle on rotation is called ϕ (Scheme2). The conformation of the main-chain in a protein is determined by a certain pair of φ and ϕ values for each amino acid; because of steric repulsion within each amino acid, most pairs of φ and ϕ angles do not be permitted. In this so-called Ramachandran plot, each dot represents an observed pair of angles in a protein.[20] Figure 5 shows pairs of φ and ϕ angles found in **A1 ∼ 5** with Ramachandran plot. The β-sheet formed **A3** and right-handed helical **A4** ⊃ **PF$_6$$^-$·MeOH** is nicely met with the corresponding areas.

In the field of coordination polymers, helix structures with various metals and oligopyridines have been studied and reported to date,[25-27] and are controlled in their lengths or fashion taking advantage of metal geometries and ligand shapes. [28-31] Nevertheless, to the best of our knowledge, the report of the β-sheet type hydrogen bonded network motif in coordination polymers is only one.[11] Therefore it is

an unique finding that the single helix and β-sheet type structures found in **A1** and **-3** are obtained from two isomeric py-X-py type ligands, reminiscent of the self-assembled structures of the protein folding.
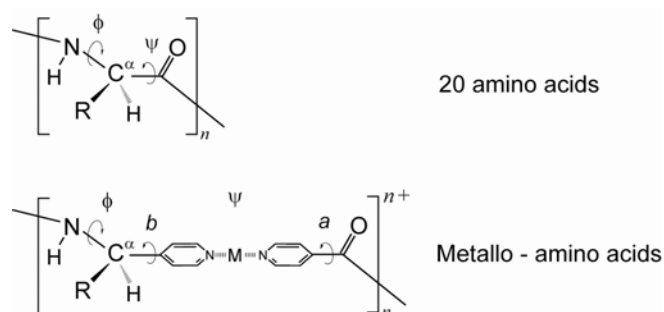
Scheme 2.

Table 5. Selected Torsion Angles in **A1 ~ 5**.

MOPAs	amide Plane, ω [°]	φ [°]	ϕ [°]	a [°]
A1 ⊃ NO$_3^-$	-6.0(7)	-	-	14.3
A1 ⊃ BF$_3^-$	3.6(8)	-	-	14.8
A1 ⊃ ClO$_4^-$	6.2(18)	-	-	16.2
A1 ⊃ PF$_6^-$	-3.2(10)	-	-	17.8
A2 ⊃ NO$_3^-$·H$_2$O	-0.1(5)	-65.6	76.8	70.9
A2 ⊃ ClO$_4^-$·H$_2$O	3.1(9)	-66.9	80.7	101.5
A2 ⊃ PF$_6^-$	-4.3(9)	-104.5	116.0	55.7, 65.7
A3 ⊃ NO$_3^-$·H$_2$O	0.0(4)	64.1	-87.9	111.5
A3 ⊃ BF$_4^-$	0.8(6)	112.9	-80.4	6.1
A3 ⊃ ClO$_4^-$	-0.4(6)	119.5	-77.6	6.4
A3 ⊃ PF$_6^-$	2.5(6)	109.7	-73.5	6.9
A4 ⊃ PF$_6^-$·MeOH	-3.8(14)	5.8	-88.0	9.1
A5 ⊃ PF$_6^-$·MeOH	7.4(13)	-2.7	83.9	8.5

IR Spectra.

As mentioned previously, all 1-D chains in **A1 ~ 3** are aligned in parallel with some weak interaction such as the Ag(I)---O contact and hydrogen bond in the amide moiety. Table 6 summarizes the length of hydrogen bond and IR bands in the amide moiety of **A1 ~ 3**. The N-H stretching and amide-I/-II bands appear in the regions of 3500 - 3100 cm^{-1} and 1700 - 1500 cm^{-1}, respectively.[10,32] **A1** and **A3 ⊃ BF$_4^-$** (**ClO$_4^-$**, **PF$_6^-$**), so-called β-sheet form, afford structured bands; the sharp bands of N-H stretching vibrations and amide-I/II. Pseudo-β-sheet form, **A2 ⊃ NO$_3^-$·H$_2$O**, **A2 ⊃ ClO$_4^-$·H$_2$O** and **A3 ⊃ NO$_3^-$·H$_2$O**, where each chain is linked by water molecules with hydrogen

bond, also afford the characteristic bands for hydrogen bonds. Similar to the results of single X-ray crystallography, IR spectra shows the elastic hydrogen bond in amide moieties, exhibiting that all 1-D chains are flexible packed with modulated length and angles of hydrogen bonds.

Table 6. Distances of Hydrogen Bonds and IR Bands of Amide Moieties in **A1 ~ 3**.

MOPAs	d(D---A) [Å]	NH	amide-I	amide-II
A1 ⊃ NO₃⁻	3.135(5)	3273 (br)	1695	1524
A1 ⊃ BF₃⁻	3.361(6)	3350	1690	1516
A1 ⊃ ClO₄⁻	3.35(1)	3328	1689	1515
A1 ⊃ PF₆⁻	3.203(8)	3393	1694	1518
A2 ⊃ NO₃⁻·H₂O	2.828(4) [a]	3290	1645	1547
A2 ⊃ ClO₄⁻·H₂O	2.841(8) [a]	3290	1644	1547
A2 ⊃ PF₆⁻	-	3431, 3413	1661	1543
A3 ⊃ NO₃⁻·H₂O	2.867(3) [a]	3264	1659	1553
A3 ⊃ BF₄⁻	2.823(4)	3365	1661	1548
A3 ⊃ ClO₄⁻	2.829(4)	3285	1657	1552
A3 ⊃ PF₆⁻	2.831(4)	3295	1660	1553

[a] Amide moieties are hydrogen bonded to water molecules.

The arrangement of chains in the solid state (Heterogenious Anion Exchange).

The cationic **A1 ~ 5** accommodate counteranions as guests.[33]   The anions of NO_3^- (36.0 cm^3/g), BF_4^- (51.0 cm^3/g), ClO_4^- (52.1 cm^3/g) and PF_6^- (56.2 cm^3/g) exhibit substantial different in size.[34] For the cationic chains, the counteranion exchange should be able to tune the mode of hydrogen bond.

Initial evaluation revealed that the counteranion exchange of **A2** with NO_3^-, ClO_4^- and PF_6^- smoothly occurs.   The reverse exchange was easily achieved under the same condition.   To investigate the exchange procedure, counteranion exchange of **A2 ⊃ PF₆⁻** with NO_3^- monitored of characteristic IR band of counteranion.[34,35]   The counteranion exchange in water at room temperature was checked after 3, 6, 9 and 12 days.   The IR spectra shows the gradually disappearance of intense PF_6^- bands (834 cm^{-1}) and the appearance and growth of new NO_3^- bands (1400-1320 cm^{-1}) (Figure 6). The PF_6^- bands disappear completely after 12 days.   The counteranion are easily exchanged, but the exchange rate is some or less dependent upon the counteranions, reaction temperature, the mole ration and the concentration.

In **A1**, the counteranion exchange does not proceed.   In the system of **A3**, the counteranion exchange of **A3 ⊃ NO₃⁻·H₂O** and **A3 ⊃ BF₄⁻** with other counteranions smoothly occurs, whereas **A3 ⊃ ClO₄⁻** and **A3 ⊃ PF₆⁻** do not release their anion.   All the exchanged species were characterized by

X-ray powder diffraction (XRPD). They show similar relative peak intensity and positions, indicating clearly retention of the skeletal structure after counteranion exchange. Although the report[36] suggested that the transformation of one coordination polymer to another is driven by the differences in the solubility of the two phases, the thermodynamic reversibility of cationic 1-D chains provide the selective anion accommodation.
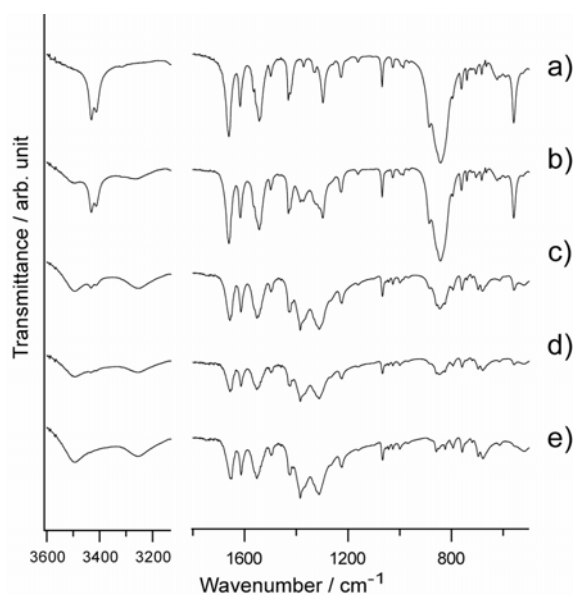
Figure 6. IR spectra in the region of N-H stretching (left) and 1800-500 cm^{-1} at room temperature of (a) as-synthesized **A2** ⊃ **PF$_6$**$^-$, **A2** ⊃ **PF$_6$**$^-$ immersed in 0.25 M NaNO$_3$ aqua for (b) 3 days, (c) 6 days, (d) 9 days, and (e) 12 days.

Conclusion

In this manuscript, we synthesized novel coordination polymers, **A1 ∼ 5**, with coordination bond and hydrogen bond. Among the factors that induce the self-assembly processes, the design of the ligand plays a crucial role in deciding between discrete and extended structures of the metal complexes. Although structural controls in this new topological system with the py-CO-NH-CH$_2$-py organic ligands are rather difficult because of the free rotation of NH-CH$_2$ bond, **A1 ∼ 3** form 1-D chains aligned in parallel in the crystal. **MOPA** form cationic 1-D chain to accommodate anions as guest molecules with elastic hydrogen bonds. The tunable chain will be intended to the contribution to the development of molecular-based recognition materials such as sensor, molecular switch, chemical separator, drug and chemical delivery and DNA control. Moreover, complementary-amide bindings are useful for the construction as linkages of the network.

Experimental Section

Materials. Isonicotinoyl chloride hydrochloride, nicotinoyl chloride hydrochloride, 4-aminopyridine, 3-aminopyridine, 4-picolylamine, 3-picolylamine and $NaPF_6$ were obtained from Tokyo Kasei Industrial Co. $AgNO_3$, $NaNO_3$ and $NaBF_4$ were obtained from Wako Co. $AgPF_6$ was obtained from Aldrich Chemical Co. $AgBF_4$ and $AgClO_4$ were obtained from Nacalai Tesque Co. $NaClO_4$ was obtained from Kishida Chemical Co.

Synthesis of *N*-(4-pyridyl)isonicotinamide (4-pia)

The ligand was prepared by the reaction of isonicotinic chloride hydrochloride (34 g, 0.19 mol) with 4-aminopyridine (18 g, 0.19 mol) in dry tetrahydrofuran (500 mL) in the presence of triethylamine (28 mL, 0.2 mol) under N_2.   The product was recrystallized from acetone/hexane in 60 % yield (23.2 g): ^{1}H NMR (DMSO) δ 7.76 (d, J = 7.0 Hz, 2H), δ 7.85 (d, J = 6.0 Hz, 2H), δ 8.50 (d, J = 7.0 Hz, 2H), δ 8.80 (d, J = 6.0 Hz, 2H), δ 10.83 (s, 1H).   Elemental analysis calcd for $C_{11}H_9N_3O$: C, 66.32; H, 4.55; N, 21.09; found: C, 65.65; H, 4.70; N, 20.77.

Synthesis of *N*-(4-pycolyl)isonicotinamide (4-pcia)

The ligand was prepared by the reaction of isonicotinic chloride hydrochloride (13.0 g, 73.0 mmol) with 4-pycolylamine (7.4 mL, 73.0 mmol) in dry tetrahydrofuran (250 mL) in the presence of triethylamine (21 mL, 150 mmol) under N_2.   The product was recrystallized from acetone/hexane in 36 % yield (5.7 g): ^{1}H NMR (DMSO) δ 4.51 (d, J = 6.0 Hz, 2H), δ 7.31 (d, J = 5.5 Hz, 2H), δ 7.80 (d, J = 6.0 Hz, 2H), δ 8.50 (d, J = 5.5 Hz, 2H), δ 8.74 (d, J = 6.0 Hz, 2H), δ 9.41 (t, J = 6.0 Hz, 1H). Elemental analysis calcd for $C_{12}H_{11}N_3O$: C, 67.59; H, 5.20; N, 19.71; found: C, 67.39; H, 5.25; N, 19.58.

Synthesis of *N*-(3-pycolyl)isonicotinamide (3-pcia)

The ligand was prepared by the reaction of isonicotinic chloride hydrochloride (6.5 g, 36.5 mmol) with 3-pycolylamine (3.7 mL, 36.5 mmol) in dry tetrahydrofuran (125 mL) in the presence of triethylamine (10.5 mL, 75 mmol) under N_2.   The product was recrystallized from acetone/hexane in 45 % yield (3.5 g):   ^{1}H NMR (DMSO) δ 4.51 (d, J = 6.0 Hz, 2H), δ 7.36 (dd, J = 8.0 Hz; 5.0 Hz, 1H), δ 7.72 (d, J = 8.0 Hz, 1H), δ 7.78 (d, J = 6.0 Hz, 2H), δ 8.46 (d, J = 5.0 Hz, 1H), δ 8.56 (s, 1H), δ 8.73 (d, J = 6.0 Hz, 2H), δ 9.37 (t, J = 6.0 Hz, 1H).   Elemental analysis calcd for $C_{12}H_{11}N_3O$: C, 67.59; H, 5.20; N, 19.71; found: C, 67.02; H, 5.04; N, 19.62.

{[Ag(4-pia)]·NO₃}ₙ (A1 ⊃ NO₃⁻)

An ethanol solution (1.5 mL) of 4-pia (14.9 mg, 0.075 mmol) was carefully layered on a water solution (1.5 mL) of AgNO₃ (6.37 mg, 0.038 mmol), where a mixed solvent of ethanol/water (v/v 1:1) was placed between two layers (yield: 42 %). Elemental analysis calcd for $C_{11}H_9AgN_4O_4$: C, 35.80; H, 2.46; N, 15.18; found: C, 35.91; H, 2.60; N, 15.33. FT-IR (KBr Pellet, cm⁻¹): ν (N-H stretching band); 3273 (m, br), ν (Amide-I); 1695 (s), δ (Amide-II); 1524 (s), ν (NO₃); 1385 (s).

{[Ag(4-pia)]·BF₄}ₙ (A1 ⊃ BF₃⁻)

An ethanol solution (1.5 mL) of 4-pia (14.9 mg, 0.075 mmol) was carefully layered on a water solution (1.5 mL) of AgBF₄ (7.30 mg, 0.038 mmol), where a mixed solvent of ethanol/water (v/v 1:1) was placed between two layers (yield: 5.5 %). Elemental analysis calcd for $C_{11}H_9AgBF_4N_3O$: C, 33.54; H, 2.30; N, 10.67; found: C, 33.71; H, 2.41; N, 10.79. FT-IR (KBr Pellet, cm⁻¹): ν (N-H stretching band); 3350 (m), ν (Amide-I); 1690 (s), δ (Amide-II); 1516 (s), ν (BF₄); 1075 (s, multibands).

{[Ag(4-pia)]·ClO₄}ₙ (A1 ⊃ ClO₄⁻)

An ethanol solution (1.5 mL) of 4-pia (14.9 mg, 0.075 mmol) was carefully layered on a water solution (1.5 mL) of AgClO₄·nH₂O (7.77 mg, 0.038 mmol), where a mixed solvent of ethanol/water (v/v 1:1) was placed between two layers (yield: 19 %). Elemental analysis calcd for $C_{11}H_9AgClN_3O_5$: C, 32.50; H, 2.23; N, 10.34; found: C, 32.30; H, 2.30; N, 10.33. FT-IR (KBr Pellet, cm⁻¹): ν (N-H stretching band); 3328 (m), ν (Amide-I); 1689 (s), δ (Amide-II); 1515 (s), ν (ClO₄); 1089 (s, multibands).

{[Ag(4-pia)]·PF₆}ₙ (A1 ⊃ PF₆⁻)

An ethanol solution (1.5 mL) of 4-pia (2.99 mg, 0.015 mmol) was carefully layered on a water solution (1.5 mL) of AgPF₆ (1.90 mg, 0.008 mmol), where a mixed solvent of ethanol/water (v/v 1:1) was placed between two layers (yield: 99 %). Elemental analysis calcd for $C_{11}H_9AgF_6N_3OP$: C, 29.23; H, 2.01; N, 9.30; found: C, 29.37; H, 2.16; N, 9.31. FT-IR (KBr Pellet, cm⁻¹): ν (N-H stretching band); 3393 (m), ν (Amide-I); 1694 (s), δ (Amide-II); 1518 (s), ν (PF₆); 842 (s, br).

{[Ag(4-pcia)]·NO₃·H₂O}ₙ (A2 ⊃ NO₃⁻·H₂O)

An ethanol solution (1.5 mL) of 4-pcia (16 mg, 0.075 mmol) was gently layered on an aqua solution (1.5 mL) of AgNO₃ (6.4 mg, 0.037 mmol), where a mixed solvent of ethanol/water (v/v 1:1, 1.5 mL) was placed between the two layers. After five months, colorless single crystals formed at

room temperature (yield: 55%). For elemental analysis these crystals were collected, and dried *in vacuo* for 2 hours. Elemental analysis calcd for $C_{12}H_{11}AgN_4O_4$: C, 35.93; H, 3.27; N, 13.97; found: C, 36.34; H, 3.02; N, 14.28. FT-IR (KBr Pellet, cm^{-1}): ν(H$_2$O); 3484 (m, br), ν(N-H stretching band); 3290 (m), ν(Amide-I); 1645 (s), δ(Amide-II); 1547 (s), ν(NO$_3$); 1384 (s).

{[Ag(4-pcia)]·ClO$_4$·H$_2$O}$_n$ (A2 ⊃ ClO$_4^-$·H$_2$O)

An ethanol solution (1.5 mL) of 4-pcia (16 mg, 0.075 mmol) was gently layered on an aqua solution (1.5 mL) of AgClO$_4$ (7.8 mg, 0.037 mmol), where a mixed solvent of ethanol/water (v/v 1:1, 1.5 mL) was placed between the two layers. After five months, colorless single crystals formed at room temperature (yield: 72%). For elemental analysis these crystals were collected, and dried *in vacuo* for 2 hours. Elemental analysis calcd for $C_{12}H_{11}AgN_3O_5Cl$: C, 32.86; H, 2.99; N, 9.58; found: C, 32.76; H, 2.81; N, 9.65. FT-IR (KBr Pellet, cm^{-1}): ν(H$_2$O); 3450 (m, br), ν(N-H stretching band); 3290 (m), ν(Amide-I); 1644 (s), δ(Amide-II); 1547 (s), ν(ClO$_4$); 1089 (s, multibands).

{[Ag(4-pcia)]·PF$_6$}$_n$ (A2 ⊃ PF$_6^-$)

An ethanol solution (1.5 mL) of 4-pcia (32 mg, 0.15 mmol) was carefully layered on an aqua solution (1.5 mL) of AgPF$_6$ (19 mg, 0.075 mmol), where a mixed solvent of ethanol/water mixed (v/v 1:1) was placed between two layers (yield: 74%). Elemental analysis calcd for $C_{12}H_{11}AgN_3OPF_6$: C, 30.92; H, 2.38; N, 9.02; found: C, 31.62; H, 2.44; N, 9.53. FT-IR (KBr Pellet, cm^{-1}): ν(N-H stretching band); 3431 (m), 3413 (m), ν(Amide-I); 1661 (s), δ(Amide-II); 1543 (s), ν(PF$_6$); 842 (s, br).

{[Ag(3-pcia)]·NO$_3$·H$_2$O}$_n$ (A3 ⊃ NO$_3^-$·H$_2$O)

An ethanol solution (1.5 mL) of 3-pcia (32 mg, 0.15 mmol) was gently layered on an aqua solution (1.5 mL) of AgNO$_3$ (13 mg, 0.075 mmol), where a mixed solvent of ethanol/water (v/v 1:1, 1.5 mL) was placed between the two layers. After five months, colorless single crystals formed at room temperature (yield: 80%). For elemental analysis these crystals were collected, and dried *in vacuo* for 2 hours. Elemental analysis calcd for $C_{12}H_{11}AgN_4O_4$: C, 35.93; H, 3.27; N, 13.97; found: C, 35.66; H, 3.20; N, 14.08. FT-IR (KBr Pellet, cm^{-1}): ν(H$_2$O); 3480 (m, br), ν(N-H stretching band); 3264 (m), ν(Amide-I); 1659 (s), δ(Amide-II); 1553 (s), ν(NO$_3$); 1384 (s).

{[Ag(3-pcia)]·BF$_4$}$_n$ (A3 ⊃ BF$_4^-$)

An ethanol solution (1.5 mL) of 3-pcia (32.0 mg, 0.150 mmol) was carefully layered on a methanol/chloroform mixed (v/v 9:1) solvent (1.5 mL) of AgBF$_4$ (14.6 mg, 0.075 mmol), where a

mixed solvent of ethanol/chloroform (v/v 19:1) was placed between two layers (yield: 27 %). Elemental analysis calcd for $C_{12}H_{11}AgBF_4N_3O$: C, 35.33; H, 2.72; N, 10.30; found: C, 35.50; H, 2.75; N 10.09. FT-IR (KBr Pellet, cm^{-1}): ν (N-H stretching band); 3365 (m), ν (Amide-I); 1661 (s), δ (Amide-II); 1548 (s), ν (BF$_4$); 1074 (s, multibands).

{[Ag(3-pcia)]·ClO₄}ₙ (A3 ⊃ ClO₄⁻)

An ethanol solution (1.5 mL) of 3-pcia (16.0 mg, 0.075 mmol) was carefully layered on a water solution (1.5 mL) of AgClO$_4$·nH$_2$O (7.77 mg, 0.038 mmol), where a mixed solvent of ethanol/water (v/v 1:1) was placed between two layers (yield: 72 %). Elemental analysis calcd for $C_{12}H_{11}AgN_3O_5Cl$: C, 32.86; H, 2.99; N, 9.58; found: C, 34.11; H, 2.56; N 10.08. FT-IR (KBr Pellet, cm^{-1}): ν (N-H stretching band); 3285 (m), ν (Amide-I); 1657 (s), δ (Amide-II); 1552 (s), ν (ClO$_4$); 1089 (s, multibands).

{[Ag(3-pcia)]·PF₆}ₙ (A3 ⊃ PF₆⁻)

An ethanol solution (1.5 mL) of 3-pcia (32.0 mg, 0.150 mmol) was carefully layered on a methanol/chloroform mixed (v/v 9:1) solvent (1.5 mL) of AgPF$_6$ (19.0 mg, 0.075 mmol), where a mixed solvent of ethanol/chloroform (v/v 19:1) was placed between two layers (yield: 80 %). Elemental analysis calcd for $C_{12}H_{11}AgN_3OPF_6$: C, 30.92; H, 2.38; N, 9.02; found: C, 31.29; H, 2.39; N 9.09. FT-IR (KBr Pellet, cm^{-1}): ν (N-H stretching band); 3295 (m), ν (Amide-I); 1660 (s), δ (Amide-II); 1553 (s), ν (PF$_6$); 836 (s, br).

{[Ag(4-pcna)]·PF₆·MeOH}ₙ (A4 ⊃ PF₆⁻·MeOH and A5 ⊃ PF₆⁻·MeOH)

An ethanol solution (1.5 mL) of 4-pcna (16 mg, 0.075 mmol) was carefully layered on a methanol/chloroform mixed (v/v 9:1) solvent (1.5 mL) of AgPF$_6$ (9.5 mg, 0.038 mmol), where a mixed solvent of ethanol/chloroform (v/v 19:1) was placed between two layers (yield: 60%). Elemental analysis calcd for $C_{13}H_{15}AgN_3O_2PF_6$: C, 31.35; H, 3.04; N, 8.44; found: C, 31.87; H, 3.01; N, 8.63. FT-IR (KBr Pellet, cm^{-1}): ν (MeOH); 3618 (m), ν (N-H stretching band); 3448 (m), ν (Amide-I); 1664 (s), δ (Amide-II); 1533 (s), ν (PF$_6$); 841 (s, br).

X-ray crystal analysis. All single crystals were mounted on a glass fiber and coated with epoxy resin. For each compound X-ray data collections were carried out by a Rigaku Mercury diffractometer with graphite monochromated Mo-Kα radiation (λ = 0.71069 Å) and CCD two-dimensional detector. Two different χ settings were used and ω were changed by 0.5º per frame. Intensity data were collected with a ω scan width of 0.5º. Empirical absorption correction using

REQABA[37] was performed for all data. Crystal data and details of the structure determinations are summarized in Table 1. For **A1 ⊃ NO₃⁻, A2 ⊃ PF₆⁻, A3 ⊃ NO₃⁻·H₂O, A3 ⊃ BF₄⁻** and **A3 ⊃ ClO₄⁻**, the structure was solved by a direct method using the SIR97 program[38] and expanded using Fourier techniques.[39] For **A2 ⊃ ClO₄⁻·H₂O**, the structure was solved by a direct method using the SIR92 program[40] and expanded using Fourier techniques.[39] For **A1 ⊃ BF₃⁻, A1 ⊃ ClO₄⁻, A1 ⊃ PF₆⁻, A2 ⊃ NO₃⁻·H₂O, A4 ⊃ PF₆⁻·MeOH** and **A5 ⊃ PF₆⁻·MeOH**, the structure was solved by a direct method using the DIRDIF (Patty) program[41] and expanded using Fourier techniques.[39] For **A3 ⊃ PF₆⁻**, the structure was solved by a direct method using the SAPI91 program[42] and expanded using Fourier techniques.[39] The final cycles of the full-matrix least-squares refinements were based on the observed reflections. All calculations were performed using the teXsan crystallographic software package of Molecular Structure Corporation.[43,44] For all compounds the non-hydrogen atoms were refined anisotropically and all the hydrogen atoms were placed in the ideal positions. In compound **A1 ⊃ ClO₄⁻**, the disorder of the perchlorate anion containing Cl(1) and O(2)-C(4) was found at final stage, and thus its atom positions were isotropically refined under a rigid condition. In compound **A2 ⊃ NO₃⁻·H₂O**, water molecule of O(5) atom was refined isotropically. In compound **A2 ⊃ ClO₄⁻·H₂O**, water molecule of O(6) atom was refined isotropically. In compound **A2 ⊃ PF₆⁻**, F(8) atom was refined isotropically. In compound **A3 ⊃ NO₃⁻·H₂O**, water molecule of O(5) atom was refined isotropically. In compound **A4 ⊃ PF₆⁻·MeOH**, F(3)-F(4) atoms and O(2) atom were refined isotropically. In compound **A4 ⊃ PF₆⁻·MeOH**, F(2)-F(3) atoms and O(2) atom were refined isotropically.

Physical Measurements. IR spectra were recorded on a Perkin-Elmer 2000 FT-IR spectrophotometer with samples prepared as KBr pellets. X-ray powder diffraction (XRPD) data were collected on a Rigaku RINT-2200HF (Ultima) diffractometer by using Cu-Kα radiation.

Ion Exchange in the Solid State. A freshly bulk-synthesized powder of **A1 ⊃ PF₆⁻** (0.20 g, 0.50 mmol) was immersed in the aqueous solution of NaNO₃ (5 M, 5 mL) for 3 days. The resulting anion-exchanged solid was filtered off, washed several times with water, and then dried in air. The product was characterized by FT-IR spectra and XRPD pattern. Similar experiments were performed with the bulk-synthesized **A1 ⊃ X, A2 ⊃ X** and **A3 ⊃ X** (X = anions and water) by immersing it in 5 M aqueous solutions of NaNO₃, NaBF₄, NaClO₄, and NaPF₆. The ion-exchange experiments were also carried out with in 0.25 - 5 M NaNO₃ (2 mL), where the crystals of **A2 ⊃ PF₆⁻** (20 mg, 0.043 mmol) were immersed for a few days, and the products were filtered off, washed several times with water, dried, and then identified by FT-IR spectra and elemental analysis.

References

(1)   Lehn, J.-M. *Supramolecular Chemisitry; Concepts and perspectives*, VCH, Weinhein **1995**.

(2)   Hoskins, B. F.; Robson, R. *J. Am. Chem. Soc.* **1990**, *112*, 1546-1554.

(3)   Fujita, M.; Oguro, D.; Miyazawa, M.; Oka, H.; Yamaguchi, K. *Nature* **1995**, *378*, 469-471.

(4)   Batten, S. R.; Robson, R. *Angew. Chem. Int. Ed.* **1998**, *37*, 1460-1494.

(5)   Hagrman, P. J.; Hagrman, D.; Zubieta, J. *Angew. Chem. Int. Ed.* **1999**, *38*, 2638-2684.

(6)   Moulton, B.; Zaworotko, M. J. *Chem. Rev.* **2001**, *101*, 1629-1658.

(7)   Eddaoudi, M.; Kim, J.; Rosi, N.; Vodak, D.; Wachter, J.; O'Keeffe, M.; Yaghi, O. M. *Science* **2002**, *295*, 469-472.

(8)   Kitagawa, S.; Kondo, M. *Bull. Chem. Soc. Jpn.* **1998**, *71*, 1739-1753.

(9)   Desiraju, G. R. *Angew. Chem. Int. Ed.* **1995**, *34*, 2311-2327.

(10)   Ghadiri, M. R.; Granja, J. R.; Milligan, R. A.; McRee, D. E.; Khazanovich, N. *Nature* **1993**, *366*, 324-327.

(11)   Karle, I. L.; Ranganathan, D.; Kurur, S. *J. Am. Chem. Soc.* **1999**, *121*, 7156-7157.

(12)   Gauthier, D.; Baillargeon, P.; Drouin, M.; Dory, Y. L. *Angew. Chem. Int. Ed.* **2001**, *40*, 4635-4638.

(13)   Steiner, T. *Angew. Chem. Int. Ed.* **2002**, *41*, 48-76.

(14)   Noro, S.-I.; Kondo, M.; Ishii, T.; Kitagawa, S.; Matsuzaka, H. *J. Chem. Soc., Dalton Trans.* **1999**, 1569-1574.

(15)   Kondo, M.; Shimamura, M.; Noro, S.-i.; Kimura, Y.; Uemura, K.; Kitagawa, S. *J. Solid State Chem.* **2000**, *152*, 113-119.

(16)   Carlucci, L.; Ciani, G.; Gudenberg, D. W. v.; Proserpio, D. M. *Inorg. Chem.* **1997**, *36*, 3812-3813.

(17)   Endo, K.; Koike, T.; Sawaki, T.; Hayashida, O.; Masuda, H.; Aoyama, Y. *J. Am. Chem. Soc.* **1997**, *119*, 4117-4122.

(18)   Kondo, M.; Asami, A.; Chang, H.-c.; Kitagawa, S. *Cryst. Eng.* **1999**, *2*, 115-122.

(19)   Uemura, K.; Kitagawa, S.; Kondo, M.; Fukui, K.; Kitaura, R.; Chang, H.-C.; Mizutani, T. *Chem. Eur. J.* **2002**, *8*, 3586-3600.

(20)   Branden, C.; Tooze, J. *Introduction to Protein Structure*, 2nd ed. Garland, New York, **1999**.

(21)   Mingos, D. M. P.; Rohl, A. L. *Inorg. Chem.* **1991**, *30*, 3769-3771.

(22)   Robinson, F.; Zaworotko, M. J. *J. Chem. Soc., Chem. Commun.* **1995**, 2413-2414.

(23)   Yaghi, O. M.; Li, H. *J. Am. Chem. Soc.* **1996**, *118*, 295-296.

(24)   Withersby, M. A.; Blake, A. J.; Champness, N. R.; Hubberstey, P.; Li, W.-S.; Schroder, M. *Angew. Chem. Int. Ed.* **1997**, *36*, 2327-2328.

(25)   Lehn, J.-M.; Rigault, A.; Siegel, J.; Harrowfield, J.; Chevrier, B.; Moras, D. *Proc. Natl. Acad. Sci. USA* **1987**, *84*, 2565-2569.

(26)   Constable, E. C. *Tetrahedron* **1992**, *48*, 10013-10059.

(27)   Piguet, C.; Bernardinelli, G.; Hopfgartner, G. *Chem. Rev.* **1997**, *97*, 2005-2062.

(28)   Piguet, C.; Bernardinelli, G.; Bocquet, B.; Quattropani, A.; Williams, A. F. *J. Am. Chem. Soc.* **1992**, *114*, 7440-7451.

(29)   Carina, R. F.; Bernardinelli, G.; Williams, A. F. *Angew. Chem. Int. Ed.* **1993**, *32*, 1463-1465.

(30)   Goodgame, D. M. L.; Hill, S. P. W.; Williams, D. J. *J. Chem. Soc., Chem. Commun.* **1993**, 1019-1021.

(31)   Ohata, N.; Masuda, H.; Yamauchi, O. *Angew. Chem. Int. Ed.* **1996**, *35*, 531-532.

(32)   Nakamoto, K. *Infrared and Raman Spectra of Inorganic and Coordination Compounds*, 5th Edition, Wiley, New York, **1997**.

(33)   Vilar, R. *Angew. Chem. Int. Ed.* **2003**, *42*, 1460-1477.

(34)   Jung, O.-S.; Kim, Y. J.; Lee, Y.-A.; Park, J. K.; Chae, H. K. *J. Am. Chem. Soc.* **2000**, *122*, 9921-9925.

(35)   Jung, O.-S.; Kim, Y. J.; Lee, Y.-A.; Chae, H. K.; Jang, H. G.; Hong, J. *Inorg. Chem.* **2001**, *40*, 2105-2110.

(36)   Khlobystov, A. N.; Champness, N. R.; Roberts, C. J.; Tendler, S. J. B.; Thompson, C.; Schroder, M. *CrystEngComm* **2002**, *4*, 426-431.

(37)   Jacobson, R. A. REQABA Empirical Absorption Correction Version 1.1-0301998, Molecular Structure Corp. The Woodlands, TX, (USA) **1996**-**1998**.

(38)   Altomare, A.; Burla, M. C.; Camalli, M.; Cascarano, G. L.; Giacovazzo, C.; Guagliardi, A.; Moliterni, A. G. G.; Polidori, G.; Spagna, R. *J. Appl. Cryst.* **1999**, *32*, 115-119.

(39)   Beurskens, P. T.; Admiraal, G.; Beurskens, G.; Bosman, W. P.; deGelder, R.; Israel, R.; Smits, J. M. M., The DIRDIF-94 program system, Technical Report of the Crystallography Laboratory, University of Nijmegen, (The Netherlands), **1994**.

(40)   Altomare, A.; Burla, M. C.; Camalli, M.; Cascarano, M.; Giacovazzo, C.; Guagliardi, A.; Polidori, G. *J. Appl. Cryst.* **1994**, *27*, 435.

(41)   Beurskens, P. T.; Admiraal, G.; Beurskens, G.; Bosman, W. P.; Garcia-Granda, S.; Gould, R. O.; Smits, J. M. M.; Smykalla, C., The DIRDIF program system, Technical Report of the Crystallography Laboratory, University of Nijmegen, (The Netherlands), **1992**.

(42)   Hai-Fu, F.,Structure Analysis Programs with Intelligent Control, Rigaku Corporation, Tokyo, Japan, **1991**.

(43)   teXsan Crystal Structure Analysis Package, Molecular structure Corporation **1985, 1992**.

(44)   teXsan Crystal Structure Analysis Package, Molecular structure Corporation **1985, 1999**.

Chapter 2

Synthesis and Structures of Coordination Polymers with 4,4'-Dipyridylsulfide

Abstract

Two new coordination compounds, $[Mn(bpe)_2(NCS)_2]_n$ (bpe = 4,4'-bipyridylethane) (**R1**) and $\{[Cd(dpds)_2(H_2O)_2]\cdot 2NO_3\cdot 2EtOH\cdot 2H_2O\}_n$ (dpds = 4,4'-dipyridyldisulfide) (**R2 ⊃ 2EtOH·2H₂O**), were synthesized and structurally characterized. **R1** crystallizes in the monoclinic space group $C2/c$ (#15) with a = 19.928(3) Å, b = 10.060(3) Å, c = 14.680(3) Å, β = 110.30(1) °, V = 2760.1(9) Å^3, and Z = 4. **R2 ⊃ 2EtOH·2H₂O** crystallizes in the monoclinic space group $P21/n$ (#14) with a = 8.9735(9) Å, b = 19.835(1) Å, c = 10.778(2) Å, β = 112.29(1) °, V = 1775.1(1) Å^3, and Z = 2. **R1** has an elongated octahedral manganese center with the two NCS$^-$ anions in the axial sites, while **R2 ⊃ 2EtOH·2H₂O** provides a distorted octahedral center with water molecules in the axial sites. For both compounds, the basal plane is filled with the four pyridine donors. Each metal ion in these compounds is linked by the two bridging ligands to make up a one-dimensional structure with large cavities. Assembled structures of these compounds contain 3 × 2 Å and 5 × 4 Å of microchannels for **R1** and **R2 ⊃ 2EtOH·2H₂O**, respectively. Although the channels of **R2 ⊃ 2EtOH·2H₂O** have enough dimension for small molecules, the dried compound shows no methane adsorption property because this pore structure is not retained after removal of the guest molecules. On the other hand, the network of **R2** demonstrates unique redox property in solid state. A cyclic voltammogram of this compound reveals redox activity, which is ascribed to the reduction of the disulfide bond to thiolate and reoxidation of the thiolate to disulfide. The redox activity of the coordination polymer shows a new class of network material.

Introduction

Design and construction of coordination networks with unique functions are a great challenge in the field of network materials.[1-10]   Much effort has been devoted to modifying the building units and to controlling the assembled motifs and the unique functions such as molecular magnets[9,11] electric conductors,[12] or the zeolite-like porous materials.[3,7,13-15]   We have obtained various coordination networks from bis(pyridine)-type ligands, for example, pyrazine, 4,4'-bipyridine,[16,17] pyrazine-2,3-dicarboxylate,[18] 1,4-bis(4-pyridoxy)benzene (bpob),[19] 4,4'-azopyridine (azpy),[20,21] and *N*-(4-pyridyl)isonicotinamide (pia).[18,22]   It has been demonstrated that their structures and functions are directed by the type of bridging ligands.

Recently we have studied redox properties of the bridging ligand azpy in the coordination networks of $\{[Fe(azpy)(NCS)_2(MeOH)_2] \cdot azpy\}_n$ and $[Fe(azpy)_2(NCS)_2]_n$.[21]   The azpy ligand held by hydrogen bonding shows a redox reaction similar to that of the free azpy molecule, while the azpy ligand directly binds to the iron atom and shows no redox properties. This fact indicates the restriction of the coordination network on the redox activities of bridging ligands.

In addition to the ligand, we selected 4,4'-dipyridyldisulfide (dpds) (Scheme 1) in this work for the creation of a new functional coordination network that could yield a redox active framework and have succeeded in the synthesis and characterization of a new coordination polymer, $\{[Cd(dpds)_2(H_2O)_2] \cdot 2NO_3 \cdot 2EtOH \cdot 2H_2O\}_n$.   Although a skeleton of dpds is similar to that of 4,4'-bipyridylethane (bpe), the network structures obtained by the combination with cadmium nitrate are quite different; it has been reported that the cadmium nitrate with bpe yields a one-dimensional compound, $[Cd_2(bpe)_3(NO_3)_4]_n$, with a T-shaped metal center.[23]   In order to study the effect of disulfide moiety on network topology, the new coordination polymer, $[Mn(bpe)_2(NCS)_2]_n$, was also synthesized and crystallographically characterized.   In this paper, structures and functions of a coordination network with dpds ligand are described.
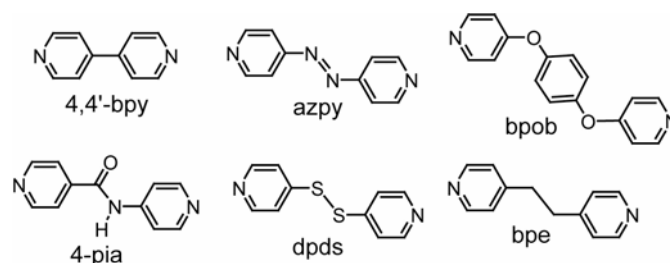
Scheme 1.

Table 1. Crystal data and structure refinement $[Mn(bpe)_2(NCS)_2]_n$ (**R1**) and $\{[Cd(dpds)_2(H_2O)_2]\cdot 2NO_3\cdot 2EtOH\cdot 2H_2O\}_n$ (**R2 ⊃ 2EtOH·2H₂O**).

Compound	R1	R2 ⊃ 2EtOH·2H₂O
Chemical formula	$C_{26}H_{24}MnN_6S_2$	$C_{24}H_{36}CdN_6O_{12}S_4$
Formula weight	539.57	841.23
Crystal system	monoclinic	monoclinic
Space group	*C2/c*	*P2₁/n*
Temperature [K]	296	296
Unit cell dimensions		
a [Å]	19.928(3)	8.9735(9)
b [Å]	10.060(3)	19.835(1)
c [Å]	14.680(3)	10.778(2)
α [°]	90	90
β [°]	110.30(1)	112.29(1)
γ [°]	90	90
V [Å³]	2760.1(9)	1775.1(4)
Z	4	2
D_c [g cm⁻¹]	1.298	1.574
μ (MoKα) [mm⁻¹]	0.654	0.915
2θ range [°]	6.0 - 55.0	6.0 - 55.0
R[a]	0.045	0.049
R_w[b]	0.047	0.053

[a] $R = \Sigma||Fo| - |Fc||/\Sigma|Fo|$, [b] $R_w = \{\Sigma w[(|Fo| - |Fc|)^2/\Sigma wFo^2]\}^{1/2}$.

Results and Discussion

Crystal Structures.

$[Mn(bpe)_2(NCS)_2]_n$ (R1).   Figure 1a shows the ORTEP drawing of manganese center of **R1** with a numbering scheme, where the metal sites are in the crystallographic twofold axis.   The manganese has a distorted elongated octahedral environment with two thiocyanate nitrogen donors in the axial sites and four pyridine nitrogen donors in the basal plane.   The pyridine rings are arranged in a propeller fashion around the equatorial plane.   The *trans* N-Mn-N bond angles for NCS and pyridine ligands are 176.4(3)° and 174.1(2)°, respectively.   The *cis* N-Mn-N bond angles range from 85° to 94°, indicative of a distorted octahedral environment.   The NCS ligands are coordinated to the manganese atom in a bent fashion with the angle C(13)-N(3)-Mn(1) of 150.7(4)°.   The NCS ligand itself is almost linear; the N(3)-C(13)-S(1) is 179.5(5)°.

Each manganese atom is linked by two bpe ligands to afford a one-dimensional framework along the *b* axis (Figure 1b).   The chain framework contains large cavities (about 4 × 4 Å) formed by two

manganese atoms and two bpe ligands, in which the nonbonded distance between the two manganese atoms is about 10.1 Å. The torsion angle of the (CH$_2$-CH$_2$) moiety, i.e., C(3)-C(11)-C(12)-C(8), is 68.4(6)°, which is close to the value (60°) expected for the gauche-staggered conformation of the methylene bond.

Although there are no direct bondings between the chains, these are regularly assembled to yield small size channels (about 3×2 Å), which contain no guest molecules, along the *a* axis as shown in Figure 1c, whose porosity of this compound is comparable to some zeolite materials, i.e., analcime (about 2×2 Å), natrolite, or thomsonite (about 3×4 Å). This size of channel could adsorb water molecules, but is too small to adsorb usual guest molecules. Actually, this compound shows no effective methane adsorption property at a pressure range 1 to 36 atm at room temperature.
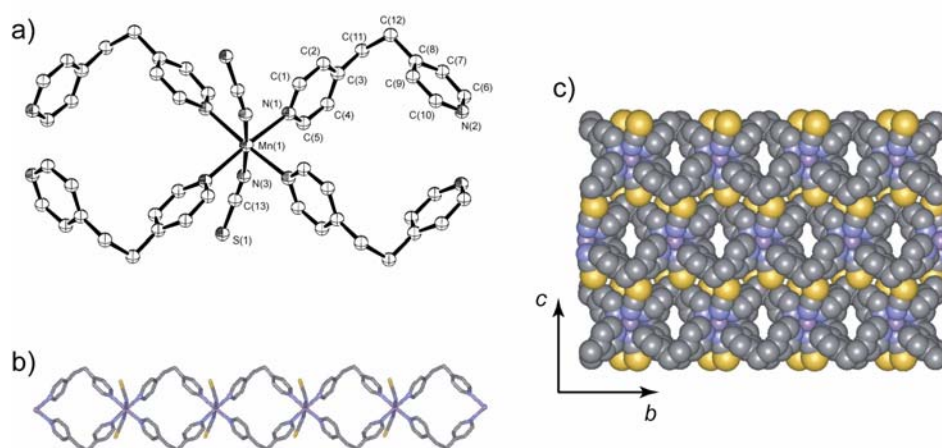
Figure 1. (a) ORTEP drawing of the manganese center of **R1** with the nonhydrogen atoms at the 30% probability level. (b) View of the one-dimensional structure. (c) A space-filling model of **R1** with the nonhydrogen atoms along the *a* axis, indicating the aspects of the 3×2 Å channel structure.

{[Cd(dpds)$_2$(H$_2$O)$_2$]·2NO$_3$·2EtOH·2H$_2$O}$_n$ (R2 ⊃ 2EtOH·2H$_2$O). Figure 2a shows the ORTEP drawing of the cadmium center of **R2 ⊃ 2EtOH·2H$_2$O** with a numbering scheme, where the metal sites are in the crystallographic inversion center. The cadmium has a distorted elongated octahedral environment with two water oxygens in the axial sites and four pyridine nitrogen donors in the basal plane. The *trans* N-Cd-N and O-Cd-O bond angles are crystallographically 180°. On the other hand, *cis* N-Cd-O and N-Cd-N bond angles range from 88° to 92° indicative of distorted octahedral environment.

Each cadmium center is bridged by two dpds ligands to form a one-dimensional framework along the $(a + c)$ vector. The nonbonded distance between the cadmium centers is about 11.1 Å. Although

42

this network motif is similar to that of **R1**, the framework structure is slightly different.   The torsion angle formed by the disulfide moiety, i.e., C(4)-S(1)-S(2)-C(8), is about 90°, whose value is close to that of the usual disulfide normal for the sulfide compounds.   The cavity framework defined by two dpds ligands and two cadmium atoms has a crystallographic inversion center.

The assembled structure of this compound shows a clear difference from that of **R1** in the channels (about 5×4 Å), which run along the *a* axis and are filled with guest ethanol molecules.   Oxygen atoms of the ethanol molecules and nitrate counter anions are hydrogen bonded to the coordinating water molecules (O(1)-O(5*) = 2.710(6) Å).   Nitrate anions are not included in the channel-like cavities but are positioned above or below the one-dimensional chains without blocking the channels.   To the best of our knowledge, this is the first example of the well-characterized coordination network of dpds ligands.

The single-crystal X-ray diffraction study clearly demonstrates that the reaction of dpds with cadmium nitrate yields crystals of a product that was formulated as $\{[Cd(dpds)_2(H_2O)_2] \cdot 2NO_3 \cdot 2EtOH \cdot 2H_2O\}_n$.   The uncoordinated ethanol and water molecules could be removed under reduced pressure; the dried compound is formulated as $\{[Cd(dpds)_2(H_2O)_2] \cdot 2NO_3\}_n$ by elemental analysis.
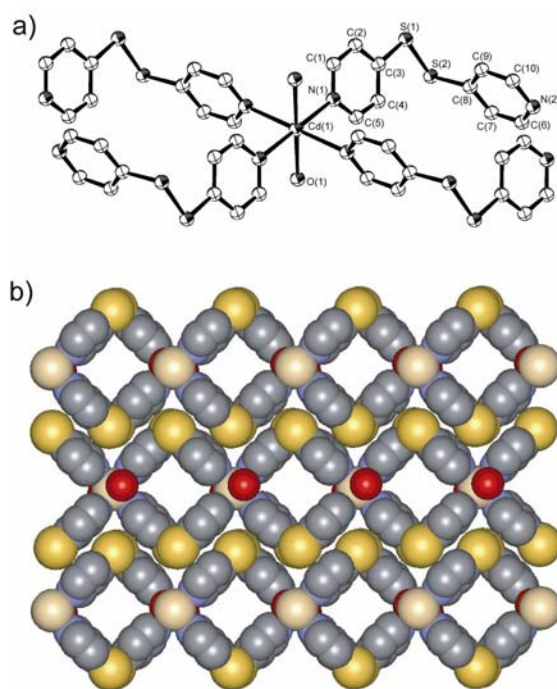
Figure 2.   (a) ORTEP drawing of the cadmium center of **R2 ⊃ 2EtOH·2H₂O** with the non-hydrogen atoms at the 30% probability level.   (b) The channel structure.   A space-filling model of **R2 ⊃ 2EtOH·2H₂O** with the nonhydrogen atoms along the *a* axis, indicating the formation of large size (5×4 Å) of channels.   Guest ethanol and water molecules are omitted for clarity.

Function of dpds network.

Although the single-crystal X-ray diffraction study clearly demonstrates that the crystals of the product **R2 ⊃ 2EtOH·2H$_2$O** form channels with a dimension of 5 × 4 Å, we have demonstrated that such channels reversibly adsorb large amounts of gas molecules under high pressure at room temperature when the network is tightly held.[16,18]   However, the dried compound **R2** does not show an appreciable gas adsorption property because of the phase transition, coupled with the deformation of the porous structure, upon removal of the included guest molecules.   These findings were confirmed by the measurements of X-ray powder diffraction (XRPD) pattern of the dried compound.   In the case of **R1**, the observed XRPD pattern shows a good agreement with the simulated pattern, while the peak positions and the pattern observed for **R2** are apparently different from those of the simulated pattern.

Although detailed structure is unknown, intense and sharp XRPD diffraction of **R2** implies the formation of a new assembled phase of its one-dimensional chains.   The redox activity of the dpds moiety incorporated in the network was estimated by using a CV measurement in the solid state. Figure 3 shows the CV charts of **R2** and free dpds, which were measured for comparison.   Free dpds shows redox waves at -1.1 and 0.3 V (vs SCE), which are ascribed to reduction of the disulfide bond to thiolate anions and reoxidation to disulfide, respectively eq. 1.

$$\text{py-S-S-py} + 2e^- \quad \rightleftarrows \quad 2 \text{ py-S}^- \qquad\qquad (1)$$
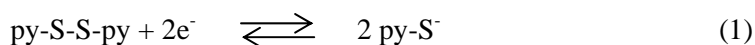
R2 shows the corresponding redox waves at -1.2 and 1.0 V.   The potentials slightly shift compared with those of the free dpds.   Moreover, the reduction wave is sharper than that of the free dpds, and the wave corresponding to the reoxidation to disulfide is quite small.   These aspects are likely due to the effect of the restriction of the network on the redox property.

We have prepared the coordination networks with azpy ligands, {[Fe(azpy)(NCS)$_2$(MeOH)$_2$]·azpy}$_n$ and [Fe(azpy)$_2$(NCS)$_2$]$_n$.[21]   The azo group is also a redox active moiety, whose mechanism is represented by eq. 2.

$$\text{py-N=N-py} + 2e^- + 2H^+ \quad \rightleftarrows \quad \text{py-NH-NH-py} \qquad (2)$$
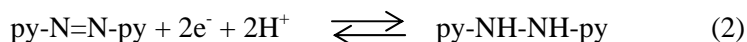
The two types of azpy ligands are found in these network materials, i.e., one is directly bonded to the iron center and the other is associated by hydrogen bonds.   The hydrogenbonded azpy ligands are redox active in the solid state, while the azpy ligands that directly bind to the iron centers are not redox active in the range 1.2 to -1.2 V (vs SCE).   In contrast with the case of the azpy ligand, dpds ligand undergoes reduction at the potential close to that of free dpds even when the ligand is tightly

incorporated in the network by coordination bonds.   According to eq. 1, the reduced product possibly contains a py-S$^-$ moiety, which is coordinated to the cadmium atom.   The lower irreversibility, i.e., weak intensity of the reoxidation wave, of **R2** is ascribed to the separation of the terminal S$^-$ sites so far apart, in which the pyridine donor site is anchored at the cadmium atom, that the S$^-$ sites hardly recombine for the production of original dpds.
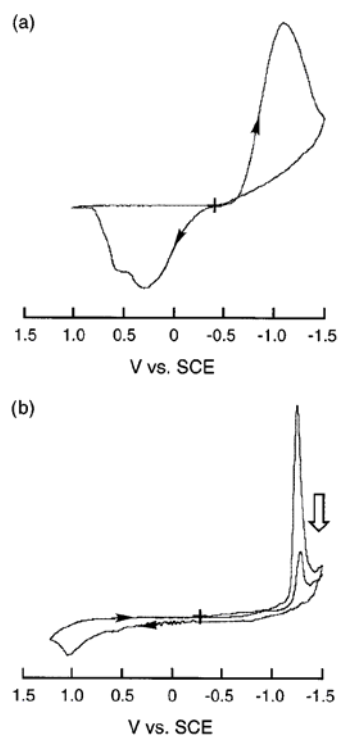
Figure 3.   CV of free dpds (a) and **R2** (b) in the solid state.

Conclusion

We demonstrate the synthesis, crystal structures, and redox properties of two coordination network compounds, **R1** and **R2 ⊃ 2EtOH·2H$_2$O**, from bpe and dpds ligands, respectively.   Although their network motifs are similar to each other, **R2 ⊃ 2EtOH·2H$_2$O** affords large microchannels, this network is not so robust that the porous network is deformed when the guest molecules are removed.   The phase transition was confirmed by XRPD measurements.   This coordination network shows a unique redox property based on the disulfide. These results indicate the designed construction for a functional coordination network.

Experimental Section

[Mn(bpe)$_2$(NCS)$_2$]$_n$ (R1)

An ethanol solution (20 mL) of bpe (0.76 g, 4.1 mmol) was slowly di!used into an aqueous solution (20 mL) of MnCl$_2$·6H$_2$O (0.43 g, 1.8 mmol) and NH$_4$SCN (0.32 g, 4.2 mmol). White brick crystals were obtained in 1 week. One of them was used for X-ray analysis. The residual crystals were collected by filtration and dried *in vacuo* (yield: 72 %). Elemental analysis calcd for C$_{26}$H$_{24}$MnN$_6$S$_2$: C, 57.87; H, 4.48; N, 15.57; found: C, 57.95; H, 4.51; N 15.28.

{[Cd(dpds)$_2$(H$_2$O)$_2$]·2NO$_3$·2EtOH·2H$_2$O}$_n$ (R2 ⊃ 2EtOH·2H$_2$O)

An aqueous solution (15 mL) of Cd(NO$_3$)$_2$·4H$_2$O (0.24 g, 0.78 mmol) in H$_2$O was slowly diffused into an ethanol solution (15 mL) of dpds (0.488 g, 2.2 mmol). White plate crystals of **R2 ⊃ 2EtOH·2H$_2$O** were formed in 1 week. One of them was used for X-ray analysis, and the residual crystals were collected by filtration, washed with H$_2$O and EtOH, and dried *in vacuo*. Although the single-crystal structure involves guest ethanol and water molecules, solvent molecules were lost during the drying process. Elemental analysis calcd for C$_{2o}$H$_{20}$CdN$_6$O$_8$S$_4$: C, 33.69; H, 2.83; N, 11.79; found: C, 32.69; H, 2.52; N 10.74.

Physical measurements. X-ray powder diffraction data were collected on a MAC Science MXP18 automated diffractometer by using Cu$K\alpha$ radiation. A cyclic voltammogram (CV) was taken on a BAS CV-50W polarographic analyzer according to the described in the literature method.[21] A SCE electrode was used as a reference. Each bulk sample of free dpds or **R2** was added to carbon paste (graphite and mineral oil) and mixed well. By using this mixture a working electrode was prepared: platinum wire. Another platinum wire was used as a counter electrode. Threeelectrode system was employed in 0.1 mol dm^{-3} NaClO$_4$ aqueous solution, using a scan rate of 10 mVs^{-1} in the range -1.2 to 1.2 V.

X-ray structure determination. For each compound, a suitable crystal was sealed in a glass capillary. For **R1** data collections were carried out on a Rigaku AFC7R diffractometer with a monochromatic Mo$K\alpha$ radiation source (λ = 0.71069 Å). Unit-cell constants were obtained from a least-squares refinement using the setting angles of 25 well-centered reflections in the ranges $25.22 < 2\theta < 29.89°$. Crystallographic data are given in Table 1. An empirical absorption correction based on azimuthal scans of several reflections was applied. The data were corrected for Lorentz and polarization effects. For **R2 ⊃ 2EtOH·2H$_2$O**, X-ray data collection was carried out by an oscillation method using a Rigaku

R-AXIS IV imaging-plate system on a rotating-anode X-ray generator operated at 50 kV, 100 mA. Crystallographic data are given in Table 1. Laue group and unit-cell parameters were determined by data-processing software (PROCESS) attached to the R-AXIS system. Lorentz and polarization corrections were applied.

The structures were solved by a direct method and expanded using Fourier techniques. The nonhydrogen atoms were refined anisotropically. Hydrogen atoms were placed in idealized positions and were included but not refined. The refinements were carried out using full-matrix least-squares techniques. All calculations were performed using the *teXsan* crystallographic software package of Molecular Structure Corporation.

References

(1)   Lehn, J.-M. *Supramolecular Chemisitry; Concepts and perspectives, VCH, Weinhein* **1995**.

(2)   MacDonald, J. C.; Whitesides, G. M. **1994**, *94*, 2383.

(3)   Yaghi, O. M.; Li, H.; Davis, C.; Richardson, D.; Groy, T. L. *Acc. Chem. Res.* **1998**, *31*, 474-484.

(4)   Zaworotko, M. J. *Chem. Soc. Rev.* **1994**, 283-288.

(5)   Zaworotko, M. J. *Angew. Chem. Int. Ed.* **1998**, 1211-1213.

(6)   Munakata, M.; Wu, L. P.; Kuroda-Sowa, T. *Bull. Chem. Soc. Jpn.* **1997**, *70*, 1727-1743.

(7)   Kitagawa, S.; Kondo, M. *Bull. Chem. Soc. Jpn.* **1998**, *71*, 1739-1753.

(8)   Janiak, C. *Angew. Chem. Int. Ed.* **1997**, *36*, 1431-1434.

(9)   Kahn, O. *Molecular Magnetism*, VCH: New York, 1993.

(10)   Hagrman, D.; Hammond, R. P.; Haushalter, R.; Zubieta, J. *Chem. Mater.* **1998**, *10*, 2091-2100.

(11)   Muller, J. S.; Epstein, A. J.; Reiff, W. M. *Chem. Rev.* **1988**, *88*, 201.

(12)   Law, K.-Y. *Chem. Rev.* **1993**, *93*, 449.

(13)   Fujita, M.; Kwon, J. Y.; Washizu, S.; Ogura, K. *J. Am. Chem. Soc.* **1994**, *116*, 1151-1152.

(14)   Venkataraman, D.; Gardner, G. B.; Lee, S.; Moore, J. S. *J. Am. Chem. Soc.* **1995**, *117*, 11600-11601.

(15)   Choi, H. J.; Suh, M. P. *J. Am. Chem. Soc.* **1998**, *120*, 10622-10628.

(16)   Kondo, M.; Yoshitomi, T.; Seki, K.; Matsuzaka, H.; Kitagawa, S. *Angew. Chem. Int. Ed.* **1997**, *36*, 1725-1727.

(17)   Noro, S.; Kondo, M.; Kitagawa, S.; Ishii, T.; Matsuzaka, H. *Chem. Lett.* **1999**, 727.

(18)   Kondo, M.; Okubo, T.; Asami, A.; Noro, S.-I.; Yoshitomi, T.; Kitagawa, S.; Ishii, T.; Matsuzaka, H.; Seki, K. *Angew. Chem. Int. Ed.* **1999**, *38*, 140-143.

(19)   Kondo, M.; Asami, A.; Fujimoto, K.; Noro, S.; Kitagawa, S.; Ishii, T.; Matsuzaka, H. *J. Inorg. Mater.* **1999**, *1*, 73.

(20)   Kondo, M.; Shimamura, M.; Noro, S.-i.; Yoshitomi, T.; Minakoshi, S.; Kitagawa, S. *Chem. Lett.* **1999**, 285-286.

(21)   Noro, S.-I.; Kondo, M.; Ishii, T.; Kitagawa, S.; Matsuzaka, H. *J. Chem. Soc., Dalton Trans.* **1999**, 1569-1574.

(22)   Kondo, M.; Asami, A.; Chang, H.-c.; Kitagawa, S. *Cryst. Eng.* **1999**, *2*, 115-122.

(23)   Fujita, M.; Kwon, Y. J.; Miyazawa, M.; Ogura, K. *J. Chem. Soc., Chem. Commun.* **1994**, 1977-1978.

Chapter 3

Construction of Repeated Rhomboid-Typed Coordinatin Polymers Having
Guest-Incorporated Cavities.   Analysis of Flexible Structural Transformation with
Thermodynamic Analysis

Abstract

Flexible porous coordination polymers containing amide groups as a function origin have been synthesized and categorized as "Metal-Organic Polymer with Amide Groups" (**MOPA**).   Three new coordination polymers of formulae $[CoCl_2(4\text{-pcna})_2]_n$ (**R3**), $\{[Co(NCS)_2(4\text{-pcna})_2]\cdot2Me_2CO\}_n$ (**R4** ⊃ **2Me₂CO**) and $\{[Co(4\text{-pcna})_2(H_2O)_2]\cdot2NO_3\cdot2CH_3OH\}_n$ (**R5** ⊃ **2H₂O·2MeOH**), (4-pcna = *N*-4-pycolylnicotinamide) have been synthesized and characterized by single crystal X-ray analysis. In three compounds, cobalt(II) atoms are bridged by 4-pcna ligand to form double stranded 1-dimensional chains, "repeated rhomboid-typed chains", with rectangular shaped cavities in the chains.   In **R3**, each chain slips and obstructs neighboring cavities to afford no guest-incorporated pores.   **R4** ⊃ **2Me₂CO** and **R5** ⊃ **2H₂O·2MeOH** eschew such staggered fashions to attain pores fulfilled with guest molecules.   **R5** ⊃ **2H₂O·2MeOH** trapped guest molecules with multiple hydrogen bonds, and shows *crystal* (**R5** ⊃ **2H₂O·2MeOH**) *-to-crystal* (**R5**) structural rearrangement in adsorption/desorption process.   Thermodynamic analysis (DSC and TG) becomes apparent that two crystalline states are stabilized with multiple hydrogen bonds.

Introduction

The rational design of new coordination polymers is of current interest in the field of supramolecular chemistry and crystal engineering.[1]   During the last few decades, large number of structures has been successfully designed and synthesized through the rational combination of organic ligands (spacers) and metals (nodes).   Since the main goal is to obtain stable pores in frameworks, rigid 3-dimensional (3-D) coordination polymers have been tried to construct and achieved.[2-4]   In the case of 2-dimensional (2-D) and 1-dimensional (1-D) motifs, which include some weak interaction among each motifs, it must be took into account for their integrity in the whole crystals to attain pores.[5]

There are two types of popular array for strategy of construction of coordination polymers: one is the introduction functional groups, and another is the introduction of flexible moiety.   To control the stacking of infinite networks (low dimensional motifs), some interaction rationally must be included. "Metal-Organic Polymer with Amide Groups" (**MOPA**) is one of candidates in relevant to those having unique topologies with hydrogen bond, where **MOPA** including L-Amide-L type ligand (L = ligand containing coordination donor atom) form hydrogen bonding between infinite motifs.[5,6]   In this manuscript, we chose the py-CONH-CH$_2$-py type ligands, N-4-pycolylnicotinamide (4-pcna), for the synthetic studies (Scheme 1).   This ligand has, in the X part, two functional groups; one is amide sites for hydrogen bonding, and another is methylene site for free-rotation.   As a result, two kinds of coordinating pyridine site (N^C = carbonyl pyridine and N^M = metylene pyridine) is set, due to its unsynmetrical structure.

If an arrangement of hydrogen bond could be changed by a variation of counter anions, whole crystal structures would be changed.[7-9]   However, we have succeeded in the similar network motif of three kinds of 1-D double stranded cobalt(II) coordination polymer in different stacking manners; [CoCl$_2$(4-pcna)$_2$]$_n$ (**R3**), {[Co(NCS)$_2$(4-pcna)$_2$]·2Me$_2$CO}$_n$ (**R4** ⊃ **2Me$_2$CO**) and {[Co(4-pcna)$_2$(H$_2$O)$_2$]·2NO$_3$·2CH$_3$OH}$_n$ (**R5** ⊃ **2H$_2$O·2MeOH**).   We report here the preparation and structural characterization of three new amide-containing Co(II) compounds which are obtained by reacting 4-pcna and CoX$_2$ (X = Cl$^-$ (**R3**), SCN$^-$ (**R4** ⊃ **2Me$_2$CO**), NO$_3^-$ (**R5** ⊃ **2H$_2$O·2MeOH**)) and their guest enclathlate properties with thermodynamic analysis.
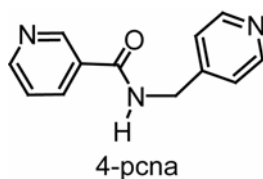
4-pcna

Scheme 1.

Table 1. Crystal data and structure refinement $[CoCl_2(4\text{-pcna})_2]_n$ (**R3**), $\{[Co(NCS)_2(4\text{-pcna})_2]\cdot 2Me_2CO\}_n$ (**R4 ⊃ 2Me₂CO**) and $\{[Co(4\text{-pcna})_2(H_2O)_2]\cdot 2NO_3\cdot 2CH_3OH\}_n$ (**R5 ⊃ 2H₂O·2MeOH**).

Compound	R3	R4 ⊃ 2Me₂CO	R5 ⊃ 2H₂O·2MeOH
Chemical formula	$C_{24}H_{22}Cl_2CoN_6O_2$	$C_{32}H_{22}CoN_8O_4S_2$	$C_{26}H_{28}CoN_8O_{12}$
Formula weight	556.32	705.63	703.49
Crystal system	triclinic	monoclinic	triclinic
Space group	$P\bar{1}$	$P2_1/n$	$P\bar{1}$
Temperature [K]	293	293	213
Unit cell dimensions			
a [Å]	7.899(7)	11.371(2)	8.0720(7)
b [Å]	8.782(7)	10.063(1)	9.760(1)
c [Å]	8.980(8)	15.5356(4)	11.260(1)
α [°]	84.70(2)	90	107.235(5)
β [°]	81.32(2)	104.6391(7)	104.600(6)
γ [°]	82.50(2)	90	101.293(3)
V [Å³]	608.8(9)	1720.0(4)	784.0(1)
Z	1	2	1
D_c [g cm⁻¹]	1.517	1.362	1.490
μ (MoKα) [mm⁻¹]	0.959	0.668	0.622
$F(000)$	285	722	363
2θ range [°]	5.5 - 55.0	5.5 - 55.0	5.5 - 53.4
Goodness-of-fit on F^2	1.691	1.998	1.901
R_1,[a] wR_2[b] [$I > 2\delta(I)$]	0.041, 0.181	0.064, 0.208	0.050, 0.172
R_1,[a] wR_2[b] (all data)	0.041, 0.183	0.065, 0.225	0.051, 0.193

[a] $R = \Sigma||Fo| - |Fc||/\Sigma|Fo|$, [b] $R_w = \{\Sigma w[(Fo^2 - Fc^2)^2]/[(\Sigma wFo^2)^2]\}^{1/2}$.

Result and Discussion

Design Principle.

The 4-pcna ligand consists of two structural parts: (1) pyridyl groups that can coordinate to a metal, (2) a amide group, which can have hydrogen bonding interactions through the amide nitrogen atom as well as via the carbonyl oxygen atom (Scheme 1). In our design, (1) the metal centers assemble the ligands into the required geometrical orientations to promote unique intermolecular connections, and (2) included solvent and coordinated counterion assist in the formation of infinite ensembles of hydrogen bonding interactions. Crystal data and details of the structure determinations for **R3**, **R4 ⊃ 2Me₂CO** and **R5 ⊃ 2H₂O·2MeOH** are summarized in Table 1. Selected bond lengths and angles are given in Tables 2. In all three compounds, the Co(II) metal centers adopt octahedral geometry and coordinate with 4-pcna ligand in a 1:2 ratio to form a repeated rhomboid coordination polymers containing 22 membered rings with a Co---Co intra chain

distance of 11.5 Å. Such networks afford rhomboid shaped cavities with the dimension of about 8.0 × 6.5 Å.
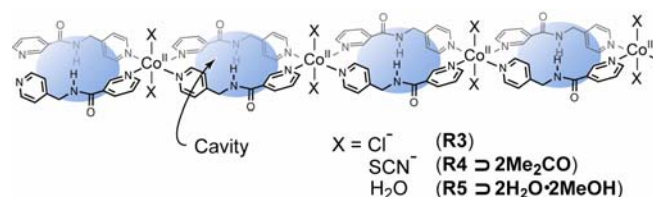
Scheme 2.

Table 2. Selected bond lengths [Å] and angles [°] for **R3**, **R4 ⊃ 2Me₂CO** and **R5 ⊃ 2H₂O·2MeOH**.

R3			
Co(1)-Cl(1)	2.447(1)	Co(1)-N(1b)	2.208(2)
Co(1)-N(2)	2.237(2)		
Cl(1)-Co(1)-Cl(1a)	180	Cl(1)-Co(1)-N(1b)	90.20(7)
N(1b)-Co(1)-N(1c)	180	Cl(1a)-Co(1)-N(2)	89.44(8)
N(2)-Co(1)-N(2a)	180	N(1b)-Co(1)-N(2)	89.50(10)
R4 ⊃ 2Me₂CO			
Co(1)-N(1)	2.218(3)	Co(1)-N(2b)	2.203(3)
Co(1)-N(4)	2.090(3)	S(1)-C(13)	1.633(3)
N(4)-C(13)	1.143(4)		
N(1)-Co(1)-N(1a)	180	N(1)-Co(1)-N(2b)	87.33(10)
N(2b)-Co(1)-N(2c)	180	N(1)-Co(1)-N(4)	89.24(10)
N(4)-Co(1)-N(4a)	180	N(2b)-Co(1)-N(4)	90.2(1)
Co(1)-N(4)-C(13)	165.0(2)	S(1)-C(13)-N(4)	179.0(3)
R5 ⊃ 2H₂O·2MeOH			
Co(1)-O(2)	2.082(2)	Co(1)-N(1b)	2.187(2)
Co(1)-N(2)	2.203(2)		
O(2)-Co(1)-O(2a)	180	O(2)-Co(1)-N(1b)	89.27(8)
N(1b)-Co(1)-N(1c)	180	O(2)-Co(1)-N(2)	90.50(9)
N(2)-Co(1)-N(2a)	180	N(1b)-Co(1)-N(2)	87.99(9)

Symmetry codes for: **R3** (a) –x+1, -y, -z+1; (b) x, y+1, z-1; (c) –x+1, -y-1, -z+2. **R4 ⊃ 2Me₂CO** (a) –x+2, -y, -z+2; (b) x+1, y, z; (c) -x+1, -y, -z+2. **R5 ⊃ 2H₂O·2MeOH** (a) –x+2, -y, -z+2; (b) x-1, y-1, z; (c) -x+3, -y+1, -z+2.

[CoCl₂(4-pcna)₂]ₙ (R3). Figure 1(a) shows a coordination environment of the cobalt ion in **R3**. The cobalt(II) center is octahedrally coordinated to the four nitrogen atoms of 4-pcna ligands in equatorial plane, in which two types of the nitrogen donors (N^C and N^M) are coordinated to the cobalt ion in a trans fashion. All the Co-N bond distances are close to each other; Co-N(1) =

52

2.208(2) Å, Co-N(2) = 2.237(2) Å.   In addition, two chlorate anions are coordinated axially with the distance of Co-Cl(1) = 2.447(1) Å.   The cobalt ions are linked by 4-pcna ligands to form a 1-D chain with repeated rhomboid motif, in which 4-pcna ligand forms L-shaped fashion (Figure 1(b)). The amide planes are perpendicular to the planes of rhomboid shaped cavities, and each repeated rhomboid typed chains are connected along the $(b + c)$ axis by hydrogen bonding between amide moiety and chlorate anion (N---Cl = 3.274(3) Å) (Figure 1(c)).   The nearest Co-Co distance in a chain is about 12.0 Å, and 7.9 Å in the adjacent chain.
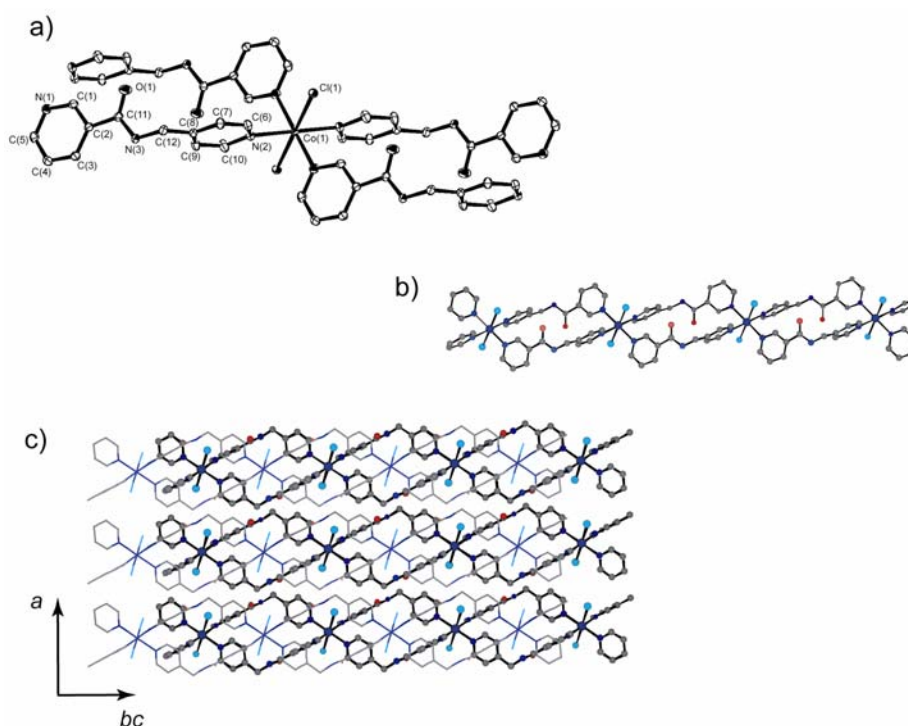
Figure 1.   Crystal structure of $[CoCl_2(4\text{-}pcna)_2]_n$ (**R3**).   (a) ORTEP drawing of **R3** at the 30% probability level.   Hydrogen atoms are omitted for clarity.   (b) A repeated rhomboid typed chain of **R3**.   (c) Crystal view of **R3**.   Repeated rhomboid typed chains connected by Cl---HN hydrogen bond to afford 2-D sheet.   Two sheets stack with staggered manner, and the thin and thick lines show the upper and lower sheet, respectively.

$\{[Co(NCS)_2(4\text{-}pcna)_2]\cdot 2Me_2CO\}_n$ (**R4** ⊃ **2Me₂CO**).   Figure 2(a) shows a coordination environment of the cobalt ion in **R4** ⊃ **2Me₂CO**.   The cobalt(II) center is octahedrally coordinated to the six nitrogen atoms of 4-pcna ligands and two NCS groups.   In equatorial plane, N^C and N^M atoms in 4-pcna ligands are coordinated to the cobalt ion in a *trans* fashion.   All the Co-N bond distances are close to each other; Co-N(1) = 2.218(3) Å, Co-N(2) = 2.203(3) Å.   In addition, the NCS groups are coordinated axially in a linear fashion with the angles of 179.0(3)° (N-C-S).   The *trans* N-Co-N bond angles for NCS and pyridine ligands are 180°.   The *cis* N-Co-N bond angles

53

range from 87° to 93°, indicative of a distorted octahedral environment. The cobalt ions are linked by L-shaped 4-pcna ligands to form a 1-D chain with repeated rhomboid motif as well as compound **R3** (Figure 2(b)). Each repeated rhomboid chain is connected with the hydrogen bond between amide moiety and sulfur atom in NCS group (N---S = 3.361(2) Å) (Figure 2(c)). Among each chain, acetone molecules are accommodated without significant interaction to any atoms. The volume fraction occupied by solvent molecules is estimated to be 30 % out of the total space.[10] The nearest Co-Co distance in a chain is about 11.4 Å, and 9.8 Å in the adjacent chain.
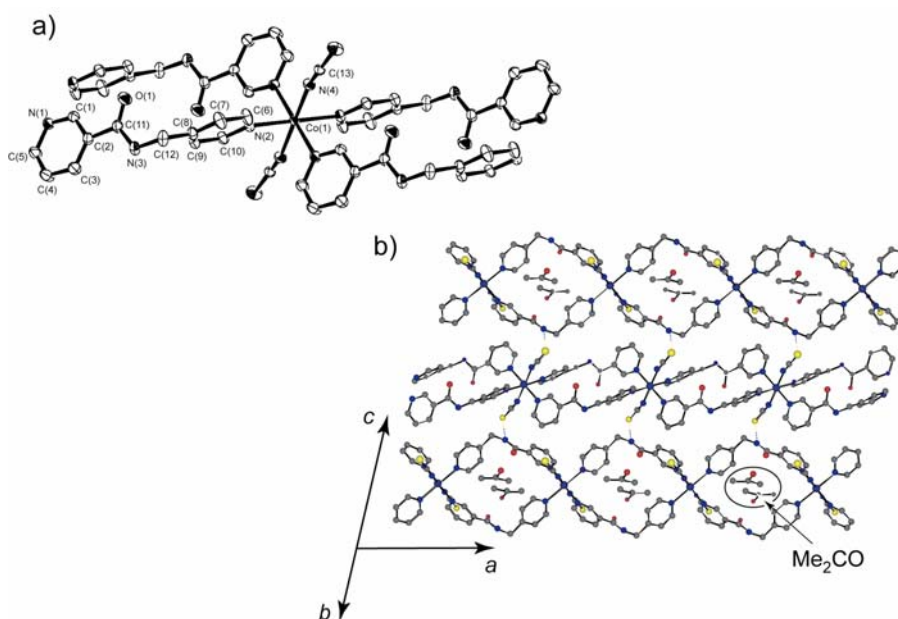
Figure 2. Crystal structure of $\{[Co(NCS)_2(4\text{-pcna})_2]\cdot 2Me_2CO\}_n$ (**R4 $\supset$ 2Me$_2$CO**). (a) ORTEP drawing of **R4 $\supset$ 2Me$_2$CO** at the 30% probability level. Hydrogen atoms and acetone molecules are omitted for clarity. (b) Three repeated rhomboid typed chains which are connected by S---HN hydrogen bond, including acetone molecules.

$\{[Co(4\text{-pcna})_2(H_2O)_2]\cdot 2NO_3\cdot 2CH_3OH\}_n$ (R5 $\supset$ 2H$_2$O·2MeOH). Figure 3(a) shows a coordination environment of the cobalt ion in **R5 $\supset$ 2H$_2$O·2MeOH**. The cobalt(II) center is octahedrally coordinated to the four nitrogen atoms of 4-pcna ligands in equatorial plane, in which N^C and N^N, are coordinated to the cobalt ion in a trans fashion. All the Co-N bond distances are close to each other; Co-N(1) = 2.187(2) Å, Co-N(2) = 2.203(2) Å. In addition, the water molecules are coordinated axially with the distance of 2.082(2) Å. The cobalt ions are linked by 4-pcna ligands to form a 1-D chain with repeated rhomboid motif, as well as compound **R3** and **R4 $\supset$ 2Me$_2$CO**. Each chain is connected by hydrogen bond via nitrate anions as shown in Figure 3(c). In the repeated rhomboid chain, 3.6 Å $\times$ 3.0 Å cavities are surrounded by two L-shaped 4-pcna

ligands, which are fulfilled with methanol molecules. Methanol molecules are hydrogen bonded to oxygen atoms of amide moieties (O(MeOH)---O(1) = 2.724(3) Å), and to water molecules which are coordinated to the cobalt(II) atom (O(MeOH)---O(2) = 2.694(3) Å). The volume fraction occupied by solvent molecules is estimated to be 16 % out of the total space.[10] The nearest Co-Co distance in a chain is about 11.4 Å, and 8.1 Å in the adjacent chain.
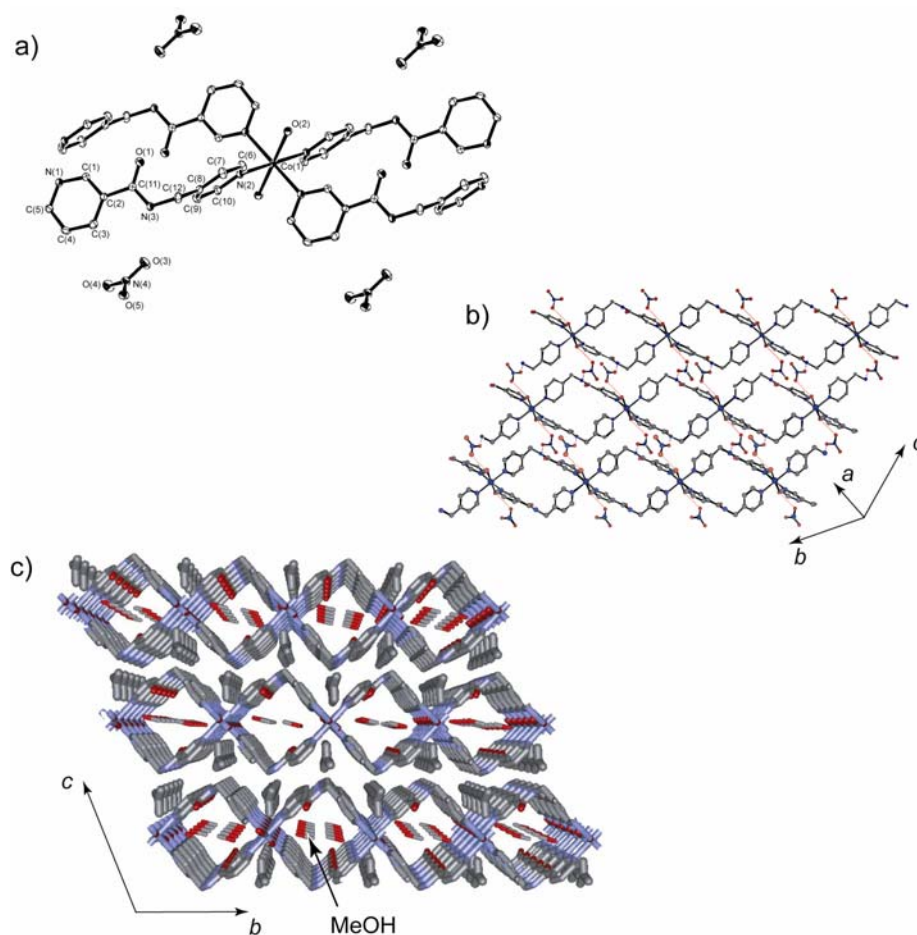
Figure 3. Crystal structure of {[Co(4-pcna)$_2$(H$_2$O)$_2$]·2NO$_3$·2CH$_3$OH}$_n$ (**R5 ⊃ 2H$_2$O·2MeOH**). (a) ORTEP drawing of **R5 ⊃ 2H$_2$O·2MeOH** at the 30% probability level. Hydrogen atoms, nitrate anions and methanol molecules are omitted for clarity. (b) A repeated rhomboid typed chain of **R5 ⊃ 2H$_2$O·2MeOH** including methanol molecules with hydrogen bond. (c) Three repeated rhomboid typed chains which are connected by O(water)-NO$_3^-$-N(amide) hydrogen bond.

R3 ~ 5 have same network topologies, repeated rhomboid-typed chains, which is attributed that torsion angles between carbonyl pyridine, methylene pyridine and amide plane in **R3 ~ 5** are similar (Table 3). Although these unique topologies were already synthesized and reported,[11-14] the study about relationships among infinite chains in whole crystals is sparse. We hypothesized that because 4-pcna, as a consequence of conjugation, has planar functional groups, its reactions with

various metal ions capable of forming complexes with different coordination numbers and geometries would generate molecular scaffolds with unique directional hydrogen bonding that might direct via self-assembly well-defined structural motifs.   In this case, the rational introduction of hydrogen bond with guest molecules affords open spaces in the frameworks like **R5** ⊃ **2H₂O·2MeOH** (Scheme 3).

Table 3.   Torsion angles and hydrogen bonds in **R3**, **R4** ⊃ **2Me₂CO** and **R5** ⊃ **2H₂O·2MeOH**.

	R3	**R4** ⊃ **2Me₂CO**	**R5** ⊃ **2H₂O·2MeOH**
Amide Plane ^{a} [°]	1.9(5)	5.2(5)	3.0(5)
∠(*py*---C=O) ^{b} [°]	7.8(4)	12.3(5)	5.3(4)
∠(*py*---N-H) ^{c} [°]	176.1(3)	-10.2(5)	-20.3(4)
D-H---A	N-H---Cl	N-H---S(NCS⁻)	N-H---O(Nitrate)
d(D---A) [Å]	3.274(3)	3.361(2)	2.919(4)
∠(DHA) [°]	143.694	147.056	145.132

^{a}O(1)-C(11)-N(3)-C(12), ^{b}C(3)-C(2)-C(11)-N(3), ^{c}C(7)-C(8)-C(12)-N(3)
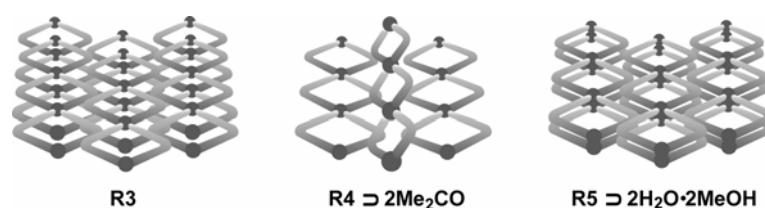
Scheme 3.

Thermogravimetry (TG) and Differential Scanning Calorimetry (DSC).

Figure 4 shows the TG thermograms for **R3**, **R4** ⊃ **2Me₂CO** and **R5** ⊃ **2H₂O·2MeOH** over the temperature range from 30 to 500 °C at a heating rate of β = 5 °C/min.   **R3** remains stable up to 250 °C, but the temperature exceeds 250 °C, it slowly decomposes with the loss of the 4-pcna ligands.   The weight loss continued to 400 °C and final residue was amorphous one.   For **R4** ⊃ **2Me₂CO**, TG showed a weight loss corresponding to two acetone molecules (observed 15.6 %, calculated 16.2 %) in the temperature range 25-250 °C, immediately followed by another weight loss corresponding to one 4-pcna ligand (observed 29.6 %, calculated 29.7 %) from 250-285 °C.   Since

the X-ray powder diffraction (XRPD) pattern of **R4** was broaden, **R4 ⊃ 2Me₂CO** cannot stand from closed packing force to be amorphous when guest molecules are removal from **R4 ⊃ 2Me₂CO**.

The TG for **R5 ⊃ 2H₂O·2MeOH** showed weight loss corresponding to two methanol molecules and two coordinated water (observed 15.0 %, calculated 14.1 %) in the temperature range of 50-90 °C. The resulting adduct, **R5**, is stable up to 170 °C, and then gradually decomposes with the loss of 4-pcna ligand. DSC curve of **R5 ⊃ 2H₂O·2MeOH** indicates that the guest is lost in a single endothermic step (peak A), with the enthalpy change for the guest-release reaction measured as ΔH_{de} = -198 kJ/mol (Figure 5). This is followed by peak B, an endotherm with ΔH = -40 kJ/mol. We ascribe second endotherm to a possible phase change in the host compound, as observed similar behavior in the decomposition of organic compounds.[15]
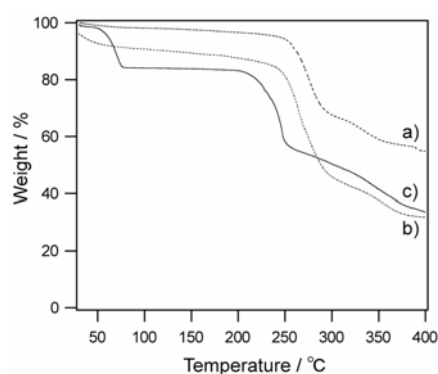
Figure 4. TG analysis of (a) **R3**, (b) **R4 ⊃ 2Me₂CO** and (c) **R5 ⊃ 2H₂O·2MeOH**, over the temperature range from 25 to 400 °C at a heating rate of β = 5 °C/min under the N₂ atmosphere.
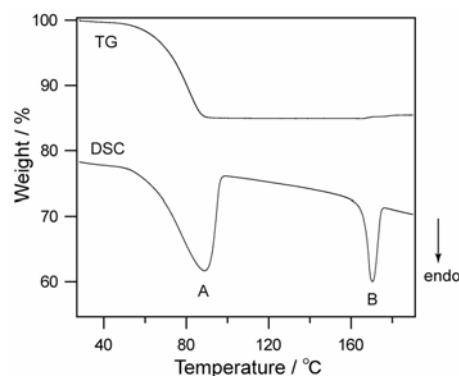
Figure 5. TG and DSC thermograms of **R5 ⊃ 2H₂O·2MeOH** over the temperature range from 30 to 190 °C at a heating rate of β = 5 °C/min under the N₂ atmosphere.

Reversible Structural Change Induced by Guest Molecule.

Removal of guest molecules causes a significant change on the framework of **R5 ⊃ 2H₂O·2MeOH**. **R5** was obtained by treating **R5 ⊃ 2H₂O·2MeOH** under reduced pressure at 100 °C, which was readily detected by XRPD and IR. The sharp XRPD pattern of **R5** exhibits new crystalline phase which is different from those of **R5 ⊃ 2H₂O·2MeOH** (Figure 6b, right). On the other hand, the original crystal structure comes back completely upon exposing to methanol vapor in the atmosphere because the peak positions and relative intensities coincide with original ones. The XRPD pattern in Figure 6c is in good agreement with those calculated from single crystal data of **R5 ⊃ 2H₂O·2MeOH**.
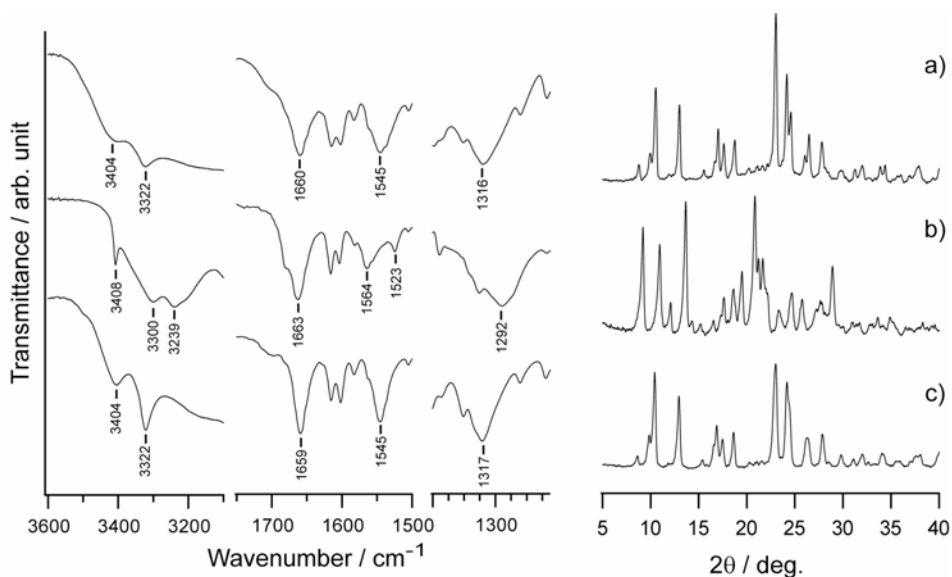
Figure 6. IR spectra (left) and XRPD patterns (right) of (a) as-synthesized **R5 ⊃ 2H₂O·2MeOH**, (b) **R5** obtained by drying *in vacuo* for 20 hours at 373 K, and (c) **R5 ⊃ 2H₂O·2MeOH** obtained by exposing **R5** to methanol vapor under atmosphere for 4 days.

Infrared spectra measurements afford the information of **R5** crystal structure. The O-H stretching band of solvents, the N-H stretching band of amide moiety, amide-I/-II bands appear in the region of 3650 - 3200, 3500 - 3100, 1700 - 1500 cm^{-1}, respectively.[16-20] The amide moieties in **R5 ⊃ 2H₂O·2MeOH** provide structured bands as shown at Figure 6a; O-H stretching, N-H stretching and amide-I/-II bands are observed at 3404 cm^{-1}, 3322 cm^{-1}, 1660 cm^{-1} and 1545 cm^{-1}, respectively. Whereas, in **R5**, the bands are observed as follows; N-H stretching vibrations at 3408, 3300 and 3239 cm^{-1}, the amide-I bands at 1663 cm^{-1}, and the amide-II band at 1564 and 1523 cm^{-1}. Such IR data afford amide moieties in 4-pcna ligands have various environments, as indicating strong hydrogen bond (3408, 3300 and 1564 cm^{-1}) and free hydrogen bond (3239 and 1523 cm^{-1}). However, IR data also shows the regeneration of structure because all main bands in regenerated one are similar to those in original **R5 ⊃ 2H₂O·2MeOH**.

In this case, IR data also afford the information of environment around cobalt(II) in **R5**. The NO stretching band appears around 1300 cm^{-1}. In adsorption/desorption process of this compound, the NO stretching band change with 1316 cm^{-1} (**R5 ⊃ 2H₂O·2MeOH**), 1292 cm^{-1} (**R5**) and 1317 cm^{-1} (regenerated **R5 ⊃ 2H₂O·2MeOH**). It is worth noting that the NO stretching band in **R5** show 1292 cm^{-1}, which red shift suggest that NO$_3^-$ anions are coordinated to cobalt(II) considering removal of coordinated waters. We concluded that there are two different states about this compound in relation to the guest molecule, namely {[Co(4-pcna)₂(H₂O)₂]·2NO₃·2CH₃OH}$_n$ (**R5 ⊃ 2H₂O·2MeOH**) and [Co(4-pcna)₂(NO₃)₂]$_n$ (**R5**), which are summarized as reaction equation of eq. 1.

58

$$R5 + 2H_2O + 2MeOH \rightleftharpoons R5 \supset 2H_2O \cdot 2MeOH \qquad (1)$$
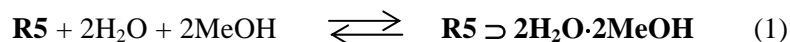
Desorption and Energetics.

From TG and DSC curve profile, **R5 $\supset$ 2H$_2$O·2MeOH** is desolvated to be crystalline **R5** in a single step with the enthalpy change for the guest-release (ΔH_{de} = 198 kJ/mol). The thermal decomposition of the inclusion compound could be investigated using three kinds of method; (1) Ozawa-Flynn-Wall Method, (2) Kissinger Method, and (3) Kinetics of desorption. By TG and differential thermal analysis (DTA) these analyses yield an approximate value of the activation energy (E_{de}) of the desolvation process.

E_{de} Estimated by Ozawa-Flynn-Wall Method. In desorption process, the activation energy of desorption (E_{de}) is estimated by recording TG curves at various heating rates (β) and by plotting $\log\beta$ vs $1/T$ at a given extent of desorption, using eq. 2.[21-23]

$$\ln\beta = -1.0516 E_{de}/RT + \text{const.} \qquad (2)$$

The decomposition curves recorded at various heating rates β, ranging from 2 to 20 °C/min are shown in Figure7a. It is apparent that these curves can be superposed by lateral shifts. For the process of "**R5 $\supset$ 2H$_2$O·2MeOH $\rightarrow$ R5**" at 50% desorption, T = 67.4 (340.4), 71.7 (344.7), 75.8 (348.8), 81.8 (354.8), 85.2 (358.2) and 94.9 °C (367.9 K) at β = 2, 3, 5, 7, 10 and 20 °C/min. In the Figure7b, the logarithms of the heating rates are plotted against the reciprocal absolute temperature. Straight lines are obtained and the method of the least squares affords the activation energies determined; E_{de1} = 82 kJ/mol. The corresponds to several degrees of decomposition, varying between 10 % and 90 % of guest loss. The slopes of the lines corresponding to a range of activation energies which vary from 88 to 78 kJ/mol. This result of changed values is not entirely unexpected in view of the fact that recent results show that the activation energy of desorption of hydrocarbons from zeolites was depend on coverage, that is the degree to which the host lattice was covered by the guest molecules.

E_{de} Estimated by Kissinger Method. In this method,[23,24] from the correlation between peak temperature T_p and heating rate (β) for DTA curves, the apparent activation energy can be determined according to the equation
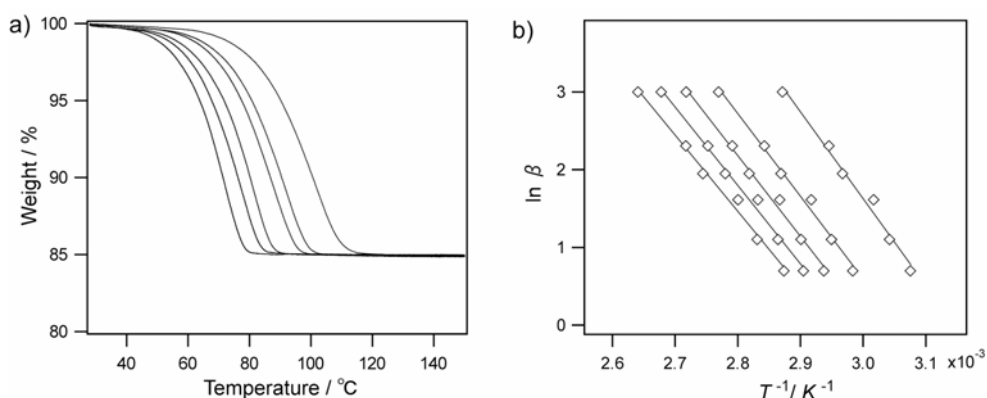
Figure 7. (a) The thermogravimetric curves of **R5 ⊃ 2H₂O·2MeOH** plotted against the reciprocal absolute temperature. Heating rate; 2, 3, 5, 7, 10 and 20 °C/min. (b) The plots of logarithms of heating rate (β) versus the conversions of reciprocal absolute temperature of 10, 30, 50, 70 and 90 % desorption for **R5 ⊃ 2H₂O·2MeOH**.
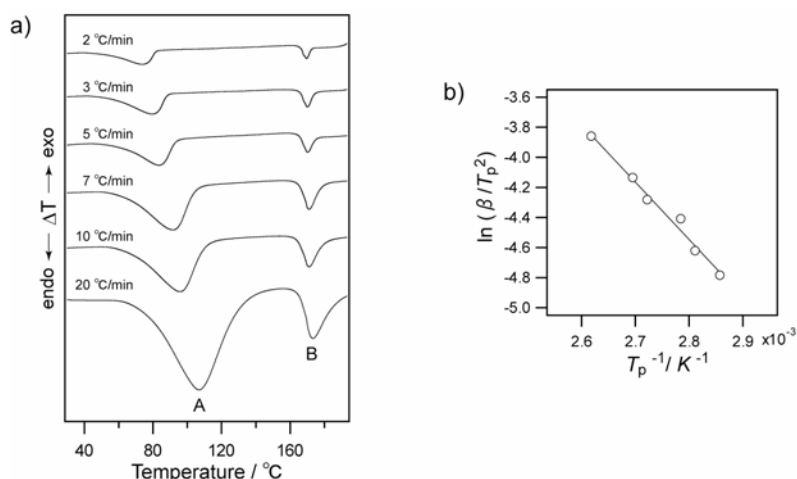
Figure 8. (a) DTA curves of **R5 ⊃ 2H₂O·2MeOH** over the temperature range from 30 to 190 °C under the N₂ atmosphere at a heating rate of $\beta = 2$, 3, 5, 7, 10, and 20 °C/min. (b) The plots of logarithms of β/T_p^2 versus the conversions of reciprocal peak temperature of desorption for **R5 ⊃ 2H₂O·2MeOH**.

$$[d(\ln\beta/T_p^2)]/d(1/T_p) = -E/R \qquad (3)$$

where E is the apparent activation energy and R is the gas constant. The DTA curves for **R5 ⊃ 2H₂O·2MeOH** recorded at various heating rates β, ranging from 2 to 20 °C/min are shown in Figure8a. Two endotherms, A and B, are observed similarly to the DSC curve. The peak A is corresponding to the endotherm of desorption, the peak temperatures at different heating rates are following (Figure 8a); T_p = 76.9 (349.9), 82.6 (355.6), 86.0 (359.0), 94.2 (367.2), 97.9 (370.9) and

108.8 °C (381.8 K) at β = 2, 3, 5, 7, 10 and 20 °C/min, respectively.   Straight lines are obtained in the plot of $\log(\beta/T_p^2)$ vs. T_p^{-1}, and the method of the least squares affords the activation energies determined; E_{de2} = 73 kJ/mol.   Whereas, the peak temperatures of B are similar and do not depend on the heating rate.   That result also supports the fact that **R5** is accompanied with the phase change before its thermal decomposition.

E_{de} **Estimated by Kinetics of desorption.**   **R5** ⊃ **2H₂O·2MeOH** is reacted to desolvate to be amorphous **R5** in a single step.   Based on the standard equation for the analysis of nucleation and growth processes, the kinetics of isothermal solid-state reactions can be presented by the following equation;[23]

$$\ln[-\ln(1-\alpha)] = \ln k + m \ln t \qquad (4)$$

where α is the fraction reacted in time t, k is a constant which depends in part on the nucleation frequency and linear rate of grain growth and m is a constant that can vary according to the geometry of the system or mechanism of the reaction.   Figure9a shows α vs. t in the process of "**R5** ⊃ **2H₂O·2MeOH** → **R5**" at various temperatures.   It is apparent that the desoprtion is relative smoothly proceeded at higher temperature.   When $\ln[-\ln(1-\alpha)]$ is plotted against $\ln t$, if the range of α is limited to 0.15 – 0.50, the kinetic data give a linear plot with slope m ($\approx$ 1.24).   Thus, the desorption of **R5** ⊃ **2H₂O·2MeOH** is close to the zero order reaction ($\alpha = kt$).   The reaction rates k are calculated by the method of the least squares in α range of 0.15 – 0.50; 2.2, 4.4, 7.4 and 16.0 (10^{-3} min^{-1}) at 308, 313, 318 and 323 K respectively.   From the slope of Arrenius plot ($\ln k$ vs. T^{-1}) based on these data (Figure 9b), E can be estimated; E_{de3} = 108 kJ/mol.
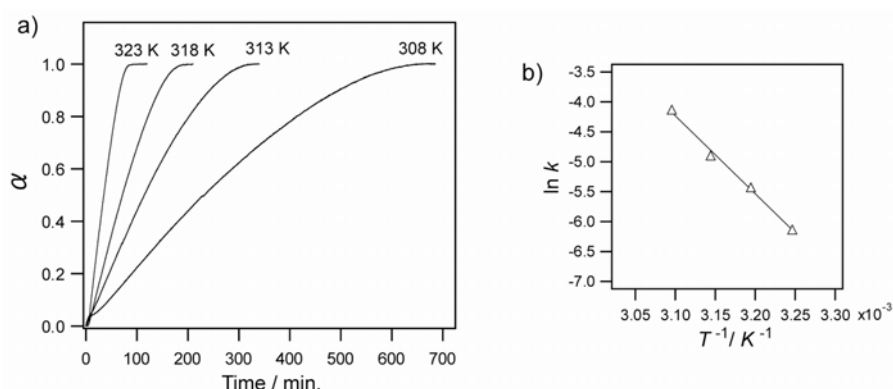
Figure 9.   (a) Desorption kinetic curves of **R5** ⊃ **2H₂O·2MeOH** at 308, 313, 318 and 323 K.   (b) Arrhenium plot of $\ln k$ vs. T^{-1}.

Mechanism and Discussion.

Several organic hosts have been investigated about desorption processes in the solid state. The difference from the case of discrete molecules is that **R5 ⊃ 2H₂O·2MeOH** forms infinite network, whose repeated rhomboid chains are bound by hydrogen bond. Therefore the extensive cooperativity would be expected between the molecules throughout the crystal, such that rearrangement can occur in a well-concerted fashion, in order to maintain its macroscopic integrity. As mentioned previously, the energy difference among states (**R5 ⊃ 2H₂O·2MeOH** and **R5**) is ΔH_{de} (-198 kJ/mol). That large energy difference would be occupied by the vaporization enthalpies of both H_2O (43.99 kJ/mol) and methanol (37.43 kJ/mol).[25] The remained energy could be considered as hydrogen bond, because the number of hydrogen bond is reduce from 8 (**R5 ⊃ 2H₂O·2MeOH**) to 2 (**R5**). Therefore, it could be considered that second endotherm of 40 kJ/mol before the decomposition of **R5** (Figure 4, the peak B) is corresponding to the energy for breaking remained hydrogen bond.

The activation energy for desorption process is estimated by three method; E_{de1} = 82 kJ/mol, E_{de2} = 73 kJ/mol and E_{de3} = 108 kJ/mol. Although the thermal decomposition of **R5 ⊃ 2H₂O·2MeOH** → **R5** is an endothermic reaction, all estimated activation energy is lower than the thermodynamic value for the reaction (ΔH_{de} = -198 kJ/mol). In general, it is difficult to discuss the mechanism of solid state reaction, because the reaction is comprised of many kinds of elementary reaction. It is because that the activation energy is obtained based on rate-determining step of some elementary reaction.
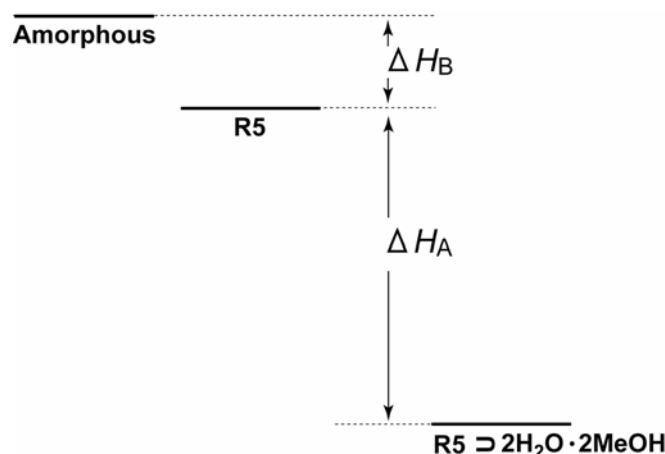
Figure 10. Schematic energy diagram for the solid-gas complexation of **R5 ⊃ 2H₂O·2MeOH** with methanol and water. Definitions are as follows: E_{de} are activation energy of acetone desorption in the processes of **R5 ⊃ 2H₂O·2MeOH** → **R5**. ΔH_A and ΔH_B are heat in the processes of **R5 ⊃ 2H₂O·2MeOH** → **R5** and **R5** → **Amorphous**, respectively.

Conclusion

This work shows the synthesis and analysis of porous frameworks using repeated rhomboid networks, and characterization of desorption process. From Co(II) and bipyridyl derivatives containing an amide group, we succeeded in producing novel repeated rhomboid networks, **R3 ~ 5**. Particularly, **R5 ⊃ 2H₂O·2MeOH** affords micropores fulfilled with guest molecules, and shows that crystal-to-crystal structural transformation is caused by adsorption/desorption of guest molecules. Such flexible porous coordination polymers offer an application to unique class of materials, which cannot be obtained in rigid porous material. Based on well-defined **R5 ⊃ 2H₂O·2MeOH**, the energy relationship among states was achieved. Both **R5 ⊃ 2H₂O·2MeOH** and **R5** form multiple hydrogen bonds to afford stable networks. This research is particularly relevant in the context of solid-state chemistry since rational design of solids has important ramifications for the development of new materials with unusual properties. We anticipate this approach to be viable for the construction of cavity-containing frameworks possessing bridging ligands not described here, and we also anticipate this approach to be applicable for the design of flexible porous materials.

Experimental Section

Materials. For 4-pcna, nicotinoyl chloride hydrochloride, nicotinic chloride hydrochloride and 4-aminomethylpyridine were obtained from Tokyo Kasei Industrial Co. $CoCl_2 \cdot 6H_2O$ and $Co(NO_3)_2 \cdot 6H_2O$ were obtained from Wako Co. $Co(SCN)_2$ were obtained from Aldrich Chemical Co.

Synthesis of *N*-(4-pycolyl)nicotinamide (4-pcna).

This ligand was readily prepared by the reaction of nicotinic chloride hydrochloride (13 g, 73 mmol) with 4-pycolylamine (7.4 mL, 73 mmol) in dry tetrahydrofuran (250 mL) in the presence of triethylamine (21 mL, 150 mmol) under N_2. The product was recrystallized from acetone/hexane in 83 % yield (8.3 g): ^{1}H NMR (DMSO) δ 4.51 (d, J = 6.0 Hz, 2H), δ 7.32 (d, J = 5.5 Hz, 2H), δ 7.52 (dd, J = 8.0 Hz; 5.0Hz, 1H), δ 8.23 (d, J = 8.0 Hz, 1H), δ 8.51 (d, J = 5.5 Hz, 2H), δ 8.72 (d, J = 5.0 Hz, 1H), δ 9.06 (s, 1H), δ 9.31 (t, J = 6.0 Hz, 1H). Elemental analysis calcd for $C_{12}H_{11}N_3O$: C, 67.59; H, 5.20; N, 19.71; found: C, 67.33; H, 5.44; N, 19.53.

$[CoCl_2(4\text{-pcna})_2]_n$ (R3).

An ethanol solution (1.5 mL) of 4-pcna (32 mg, 0.15 mmol) was carefully layered on a methanol/chloroform mixed (v/v 9:1) solvent (1.5 mL) of $CoCl_2 \cdot 6H_2O$ (17.8 mg, 0.075 mmol), where a mixed solvent of ethanol/chloroform (v/v 19:1) was placed between two layers. Violet crystals of **R3** suitable for X-ray diffraction were obtained (yield: 86%). Absorption band in visible region: 506, 536, 633 (sh), 611 (sh) nm. Elemental analysis calcd for $C_{24}H_{22}Cl_2CoN_6O_2$: C, 51.82; H, 3.99; N, 15.11, found: C, 51.63; H, 4.00; N, 15.20.

$\{[Co(NCS)_2(4\text{-pcna})_2] \cdot 2Me_2CO\}_n$ (R4 ⊃ 2Me$_2$CO).

An ethanol solution (1.5 mL) of 4-pcna (16 mg, 0.075 mmol) was carefully layered on a acetone/chloroform mixed (v/v 9:1) solvent (1.5 mL) of $Co(SCN)_2$ (6.6 mg, 0.038 mmol), where a mixed solvent of ethanol/chloroform (v/v 19:1) was placed between two layers. Red crystals of **R4 ⊃ 2Me$_2$CO** suitable for X-ray diffraction were obtained (yield: 88%). Absorption band in visible region: 493 nm. For elemental analysis these crystals were collected, and dried *in vacuo* at 373 K for 20 hours. Elemental analysis calcd for $C_{26}H_{22}CoN_8O_2S_2$: C, 51.91; H, 3.69; N, 18.63; found: C, 51.18; H, 3.58; N 18.17.

64

{[Co(4-pcna)$_2$(H$_2$O)$_2$]·2NO$_3$·2CH$_3$OH}$_n$ (R5 ⊃ 2H$_2$O·2MeOH).

An ethanol solution (1.5 mL) of 4-pcna (32 mg, 0.15 mmol) was carefully layered on a methanol/chloroform mixed (v/v 9:1) solvent (1.5 mL) of Co(NO$_3$)$_2$·6H$_2$O (21.8 mg, 0.075 mmol), where a mixed solvent of ethanol/chloroform (v/v 19:1) was placed between two layers. Orange crystals of **R5 ⊃ 2H$_2$O·2MeOH** suitable for X-ray diffraction were obtained (yield: 21%). Absorption band in visible region: 485 nm. For elemental analysis these crystals were collected, and dried *in vacuo* at room temperature for 20 hours. Elemental analysis calcd for C$_{24}$H$_{24}$CoN$_8$O$_9$: C, 45.94; H, 3.86; N, 17.86, found: C, 46.55; H, 4.02; N 18.25. The microcrystalline sample of **R5 ⊃ 2H$_2$O·2MeOH** was prepared in the same solvent, and the crystallinity was checked by X-ray powder diffraction.

Physical measurements. UV-vis reflection spectra were recorded on a Hitachi U-3500 spectrophotometer over the range from 400 to 800 nm at room temperature. IR spectra were recorded on a Perkin-Elmer 2000 FT-IR spectrophotometer with samples prepared as Nujol. All operations were carried out under ambient conditions. Thermal gravimetric analyses (TG) and differential thermal analyses (DTA) were carried out with a Rigaku Instrument TG8120 in a nitrogen atmosphere. DSC thermogram was carried out with Rigaku Instrument TG8120 in a nitrogen atmosphere at β = 5 ºC/min, and the heats of desorption was calibrated by using indium, lead, and antimony as a reference. X-ray powder diffraction (XRPD) data were collected on a Rigaku RINT-2200 (Ultima) diffractometer by using Cu-Kα radiation.

Single crystal X-ray analysis. A single crystal for **R3**, **R4 ⊃ 2Me$_2$CO** and **R5 ⊃ 2H$_2$O·2MeOH** were mounted on a glass fiber and coated with epoxy resin. For each compound X-ray data collections were carried out by a Rigaku Mercury diffractometer with graphite monochromated Mo-Kα radiation (λ = 0.71069 Å) and CCD two-dimensional detector. The sizes of the unit cells were calculated from the reflections collected on the setting angles of six frames by changing ω by 0.5º for each frame. Two different χ settings were used and ω were changed by 0.5º per frame. Intensity data were collected with a ω scan width of 0.5º. Empirical absorption correction using REQABA[26] was performed for all data. Crystal data and details of the structure determinations are summarized in Table 1, and selected bond distances and angles are listed in Table 2. For **R3**, the structure was solved by a direct method using the SIR97 program[27] and expanded using Fourier techniques.[28] For **R4 ⊃ 2Me$_2$CO**, the structure was solved by a Patterson method using the SAPI91 program[29] and expanded using Fourier techniques.[28] For **R5 ⊃ 2H$_2$O·2MeOH**, the structure was solved by a direct method using the SIR92 program[30] and expanded using Fourier

techniques.[28]   The final cycles of the full-matrix least-squares refinements were based on the all observed reflections.   All calculations were performed using the teXsan crystallographic software package of Molecular Structure Corporation.[31]   For all compounds the non-hydrogen atoms were refined anisotropically and all the hydrogen atoms were placed in the ideal positions.   In compound **R4 ⊃ 2Me₂CO** the disorder of the acetone molecule containing O(2) and C(14)-C(16) was found at final stage, and thus its atom positions were isotropically refined under a rigid condition.

References

(1)   Moulton, B.; Zaworotko, M. J. *Chem. Rev.* **2001**, *101*, 1629-1658.

(2)   Li, H.; Eddaoudi, M.; O'Keeffe, M.; Yaghi, O. M. *Nature* **1999**, *402*, 276-279.

(3)   Eddaoudi, M.; Kim, J.; Rosi, N.; Vodak, D.; Wachter, J.; O'Keeffe, M.; Yaghi, O. M. *Science* **2002**, *295*, 469-472.

(4)   Yaghi, O. M.; O'Keeffe, M.; Ockwig, N. W.; Chae, H. K.; Eddaoudi, M.; Kim, J. *Nature* **2003**, *423*, 705-714.

(5)   Uemura, K.; Kitagawa, S.; Fukui, K.; Saito, K. *J. Am. Chem. Soc.* **2003**, submitted.

(6)   Uemura, K.; Kitagawa, S.; Kondo, M.; Fukui, K.; Kitaura, R.; Chang, H.-C.; Mizutani, T. *Chem. Eur. J.* **2002**, *8*, 3586-3600.

(7)   Tong, M.-L.; Chen, X.-M.; Ye, B.-H.; Ng, S. W. *Inorg. Chem.* **1998**, *37*, 5278-5281.

(8)   Jung, O.-S.; Park, S. H.; Kim, D. C.; Kim, K. M. *Inorg. Chem.* **1998**, *37*, 610-611.

(9)   Rivas, J. C. M.; Brammer, L. *New J. Chem.* **1998**, 1315-1318.

(10)   A. L. Speck PLATON, A. M. C. T., Utrecht University (The Netherlands), **2002**.

(11)   Fujita, M.; Kwon, Y. J.; Miyazawa, M.; Ogura, K. *J. Chem. Soc., Chem. Commun.* **1994**, 1977-1978.

(12)   Kasai, K.; Aoyagi, M.; Fujita, M. *J. Am. Chem. Soc.* **2000**, *122*, 2140-2141.

(13)   Sharma, C. V. K.; Diaz, R. J.; Hessheimer, A. J.; Clearfield, A. *Cryst. Eng.* **2000**, *3*, 201-208.

(14)   Kondo, M.; Shimamura, M.; Noro, S.-i.; Kimura, Y.; Uemura, K.; Kitagawa, S. *J. Solid State Chem.* **2000**, *152*, 113-119.

(15)   Caira, M. R.; Nassimbeni, L. R.; Schubert, W.-D.; Toda, F. *Thermochim. Acta* **1992**, *206*, 265-271.

(16)   Nakamoto, K. *Infrared and Raman Spectra of Inorganic and Coordination Compounds*, 5th Edition, Wiley, New York, **1997**.

(17)   Bellamy, L. J. *Advances in Infrared Group Frequencies*, Methuen; London, **1968**.

(18)   Ghadiri, M. R.; Granja, J. R.; Milligan, R. A.; McRee, D. E.; Khazanovich, N. *Nature* **1993**, *366*, 324-327.

(19)   Haris, P. I.; Chapman, D. *Biopolymers* **1995**, *37*, 251-263.

(20)   Hartgerink, J. D.; Granja, J. R.; Milligan, R. A.; Ghadiri, M. R. *J. Am. Chem. Soc.* **1996**, *118*, 43-50.

(21)   Flynn, J. H.; Wall, L. A. *J. Polym. Sci. B* **1966**, *4*, 323-328.

(22)   Ozawa, T. *Bull. Chem. Soc. Jpn.* **1965**, *38*, 1881-1886.

(23)   Hatakeyama, T.; Zhenhai, L. *Handbook of Thermal Analysis*, Wiley, New York, **1998**.

(24)   Zivkovic, Z. D. *Thermochim. Acta* **1992**, *203*, 251-257.

(25)   Weast, R. C.; Astle, M. J.; Beyer, W. H. *CRC Handbook of Chemistry and Physics 80th ed.* CRC Press; Ohio, **1999**.

(26)   Jacobson, R. A. REQABA Empirical Absorption Correction Version 1.1-0301998, Molecular Structure Corp.: The Woodlands, TX, **1996**-**1998**.

(27)   Altomare, A.; Burla, M. C.; Camalli, M.; Cascarano, G. L.; Giacovazzo, C.; Guagliardi, A.; Moliterni, A. G. G.; Polidori, G.; Spagna, R. *J. Appl. Cryst.* **1999**, *32*, 115-119.

(28)   Beurskens, P. T.; Admiraal, G.; Beurskens, G.; Bosman, W. P.; deGelder, R.; Israel, R.; Smits, J. M. M. The DIRDIF-94 program system, Technical Report of the Crystallography Laboratory, University of Nijmegen, The Netherlands, **1994**.

(29)   Hai-Fu, F., Structure Analysis Programs with Intelligent Control, Rigaku Corporation, Tokyo, Japan, **1991**.

(30)   Altomare, A.; Burla, M. C.; Camalli, M.; Cascarano, M.; Giacovazzo, C.; Guagliardi, A.; Polidori, G. *J. Appl. Cryst.* **1994**, *27*, 435.

(31)   teXsan Crystal Structure Analysis Package, Molecular structure Corporation **1985, 1999**.

Chapter 4

Novel Flexible Frameworks of Porous Cobalt(II) Coordination Polymers Which Show Selective Guest Adsorption Based on Switching of Hydrogen Bond Pairs of Amide Groups

Abstract

Four porous crystalline coordination polymers with 2-dimensional frameworks of a double edged axe-shaped motif, $\{[Co(NCS)_2(3\text{-pia})_2]\cdot 2EtOH\cdot 11H_2O\}_n$ (**MOPA-1 ⊃ 2EtOH·11H₂O**), $\{[Co(NCS)_2(3\text{-pia})_2]\cdot 4Me_2CO\}_n$ (**MOPA-1 ⊃ 4Me₂CO**), $\{[Co(NCS)_2(3\text{-pia})_2]\cdot 4THF\}_n$ (**MOPA-1 ⊃ 4THF**) and $[Co(NCS)_2(3\text{-pna})_2]_n$ (**MOPA-2**), have been synthesized from reactions of cobalt(II) thiocyanate with *N*-(3-pyridyl)isonicotinamide (3-pia) or *N*-(3-pyridyl)nicotinamide (3-pna). X-ray crystallographic characterization reveals that the adjacent layers are stacked such that channels are created except for **MOPA-2**. The channels form a hydrogen bonding interior for guest molecules, in practice, **MOPA-1 ⊃ 2EtOH·11H₂O** contains ethanol and water molecules as guests in the channels with hydrogen bonds, whereas **MOPA-1 ⊃ 4THF** (**MOPA-1 ⊃ 4Me₂CO**) includes tetrahydrofuran (acetone) molecules. In **MOPA-1 ⊃ 2EtOH·11H₂O**, the "double edged axe-shaped" motifs in the adjacent sheets are not located over each other while the motifs in **MOPA-1 ⊃ 4THF** stack so perfectly as to overlap each other in a edge to edge fashion. This subtle change in the 3D framework is greatly associated with the template effect of the guests. Compound **MOPA-2** has no guest molecules and therefore, the amide groups in a sheet are used for hydrogen bonding links with the adjacent sheets. Removal of the guest molecules from **MOPA-1 ⊃ 2EtOH·11H₂O** and **MOPA-1 ⊃ 4THF** (**MOPA-1 ⊃ 4Me₂CO**) causes a structural conversion with color change. Pink **MOPA-1 ⊃ 2EtOH·11H₂O** cannot retain its original framework to be blue amorphous one. On the other hand, the framework of pink **MOPA-1 ⊃ 4THF** (**MOPA-1 ⊃ 4Me₂CO**) is transformed to a new crystalline framework of violet **MOPA-1**. Interestingly, **MOPA-1** reverts to original pink crystal of **MOPA-1 ⊃ 4THF** (**MOPA-1 ⊃ 4Me₂CO**) when it is exposed to vapor of THF (or acetone). Spectroscopic measurements (Visible, EPR, and IR) indicate a clue to the crystal-to-crystal transformation; on removal of the guests the amide groups are used to form the *β*-sheet type hydrogen bonding between the sheets, and thus the framework withstands significant stress on removal of guest molecules. This mechanism is attributed to the

arrangement of the adjacent sheets so suited in regularity that the β-sheet type structure forms efficiently.   The apohost **MOPA-1** does not adsorb cyclopentane, showing a guest-selectivity that in addition to the size, the hydrogen bonding capability is required for the guest molecules.   The obtained compound is categorized in a new generation one towards functional porous coordination polymers.

Introduction

The crystal engineering of coordination polymers aims to gain control of the topology and geometry of the networks formed through judicious choice of ligand and metal precursor geometry,[1-4] expanding itself by producing useful functions characteristic of a metal complex assembly. In the last decade crystalline coordination polymers have added a new dimension to solid-state coordination chemistry, occupying an important position as an alternative candidate for porous materials as well as zeolites and activated carbons.[5] The porous functions are, for instance, heterogeneous catalysis,[6] ion exchange,[7-9] molecule adsorption[10-12] and enantio-selective catalysis.[13] This development owes to the advent of thermally stable and robust open frameworks in the absence of guest molecules.[14-23] In practice, robust porous frameworks can be realized by three-dimensional linkages of coordination bond[21] or interdigitation of two-dimensional networks of coordination bond.[10,24] They are further evolving from a stage of zeolites-mimicry to creation of new function characteristic of molecularly inorganic-organic hybrid compounds.

Based on the achievement, there are two approaches to create new porous functions in coordination polymers. One is to prepare functional pores with a chemical affinity, which is related to a new class of open framework solids with the goal of being able to carry out shape- and size-selective chemical reactions within the pores of a microporous solid. The other pores are dynamic ones, which respond to the chemical and/or physical stimulus. This properties could come from the capability of the structural regeneration and recovering once collapsed by the removal of guest molecules.[25-35] This sort of compounds has a potential for specific selective guest binding by cooperative effect of physical size, shape and chemical functionalities.

Dynamic structural transformation based on flexible porous frameworks is one of the most interesting phenomena in coordination polymers, so-called new generation compounds, coupled to novel porous functions. The three types are listed in Scheme 1:

(1) Type I framework of "recoverable collapsing" has a property that by removal of guest molecules a network collapses due to the close packing force, however it regenerates under the initial condition.[25-29] (2) Type II framework of "guest-induced transformation" has a property that structural shifts in the network are induced by the simultaneously exchanging of guest molecules.[30,31,34,35] (3) Type III framework of "guest-induced reformation" has a property that removal of guest molecules makes a structure change in network to another one, however it reverts to the original one under the initial condition.[32,33] Interestingly, type II and III compounds show "crystal-to-crystal transformation", in a sense, this property results from advantage of molecularly inorganic-organic hybrid system.[35] Several instances for discrete molecular assemblies have been found.[36-40] However, reports on coordination polymers are still sparse. This is because flexibility

71

in coordination polymers is incompatible with robustness such that porous frameworks are maintained without guest molecules.
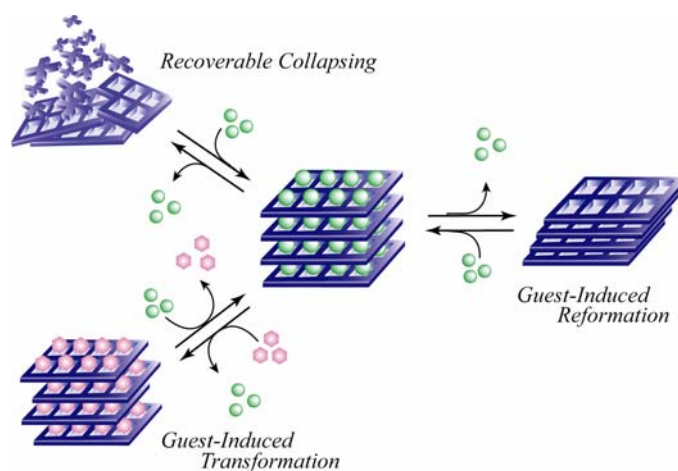
Scheme 1.

In order to create flexible porous frameworks, we first utilized a ligand flexibility by introducing spacer substituents X in between pyridyl groups, py-X-py, dissimilar to a rigid rod 4,4'-bipyridine. Secondly, we focus our attention on hydrogen-bonding networks of the organic moieties,[5] which flexibly respond and shift its structure against the guest molecules.[41,42] Although hydrogen-bonding has been widely used to construct extended organic solids possessing both condensed and open structures,[43-47] strategies for their utility in assembling porous metal-organic frameworks remain, with the exception of few reports, largely unexplored. Here, we designed amide containing ligands, *N*-(3-pyridyl)isonicotinamide (3-pia) and *N*-(3-pyridyl) nicotinamide (3-pna) as bridging ligands, which are characteristic of unsymmetrical bridge and possessing hydrogen-bonding sites.[10,48]
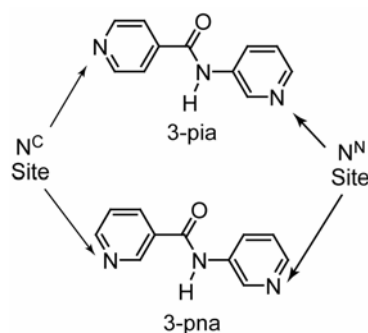
Scheme 2.

We succeeded in synthesizing four kinds of 2-dimensional porous framework-based coordination polymers of cobalt(II) thiocyanate, $\{[Co(NCS)_2(3\text{-pia})_2]\cdot2EtOH\cdot11H_2O\}_n$ (**MOPA-1 ⊃ 2EtOH·11H₂O**), $\{[Co(NCS)_2(3\text{-pia})_2]\cdot4Me_2CO\}_n$ (**MOPA-1 ⊃ 4Me₂CO**), $\{[Co(NCS)_2(3\text{-pia})_2]\cdot4THF\}_n$ (**MOPA-1 ⊃ 4THF**) and $[Co(NCS)_2(3\text{-pna})_2]_n$ (**MOPA-2**). The four types of networks in drying in vacuo show different behaviors, falling within the category of "recoverable collapsing" and "guest-induced reformation". The inclusion of incoming molecular guests is dependent not only on their size and shape but also on their chemical affinity for the amide moiety.

Results and Discussion

Crystal Structures.

Crystal data and details of the structure determinations are summarized in Table 1.

$\{[Co(NCS)_2(3\text{-pia})_2]\cdot2EtOH\cdot11H_2O\}_n$ (**MOPA-1 ⊃ 2EtOH·11H₂O**). Figure 1(a) shows a coordination environment of the cobalt ion in **MOPA-1 ⊃ 2EtOH·11H₂O**. The cobalt(II) center is octahedrally coordinated to the four nitrogen atoms of 3-pia ligands in equatorial plane, in which two types of the nitrogen donors, carbonyl pyridyl (N^C) and amino pyridyl (N^N), are coordinated to the cobalt ion in a trans fashion. All the Co-N bond distances are close to each other; Co-N(1) = 2.214(6) Å, Co-N(2) = 2.199(5) Å. The *trans* N-Co-N bond angles for NCS and pyridine ligands are 180°. The *cis* N-Co-N bond angles range from 87° to 93°, indicative of a distorted octahedral environment. In addition, the NCS groups are coordinated axially in a linear fashion with the angles of 175.8(6)° (Co-N(4)-C(12)) and 179.3(8)° (N-C-S).

The cobalt ions are linked by 3-pia ligands to form a 2-dimensinal sheet composed of a "double edged axe-shaped" motif (Figure 1(b)) with the dimension of 9 Å × 2.5 Å,[49] where two ethanol and eleven water molecules are incorporated; the ethanol molecules are trapped by hydrogen bonding with the amide moiety of O(EtOH)-N(amide) = 2.9 Å while the water molecules are hydrogen bonded to each other. The sheets do not interpenetrate, affording a layered structure. Interestingly, the bond vector of the amide carbonyl group sticks out from the sheet plane with the angle of about 61°.[50] The adjacent sheets are stacked offset with respect to each other, recognized as …ABAB…(Figure 1(c)). Therefore, oxygen atoms of the carbonyl groups on the adjacent sheets are facing each other (Figure 1(d)). The nearest Co-Co distance in a sheet is about 11.8 Å, and 9.5 Å in the adjacent sheet.

Table 1. Crystal Data and Structure Refinement for {[Co(NCS)$_2$(3-pia)$_2$]·2EtOH·11H$_2$O}$_n$ (**MOPA-1 ⊃ 2EtOH·11H$_2$O**), [Co(NCS)$_2$(3-pia)$_2$(H$_2$O)$_2$]$_n$ (**2**), {[Co(NCS)$_2$(3-pia)$_2$]·4Me$_2$CO}$_n$ (**MOPA-1 ⊃ 4Me$_2$CO**), {[Co(NCS)$_2$(3-pia)$_2$]·4THF}$_n$ (**MOPA-1 ⊃ 4THF**), [Co(NCS)$_2$(3-pna)$_2$]$_n$ (**MOPA-2**).

Compoound	MOPA-1 ⊃ 2EtOH·11H$_2$O	2	MOPA-1 ⊃ 4Me$_2$CO	MOPA-1 ⊃ 4THF	MOPA-2
chemical formula	C$_{28}$H$_{18}$CoN$_8$O$_{15}$S$_2$	C$_{24}$H$_{18}$CoN$_8$O$_4$S$_2$	C$_{36}$H$_{30}$CoN$_8$O$_6$S$_2$	C$_{40}$H$_{50}$CoN$_8$O$_6$S$_2$	C$_{24}$H$_{18}$CoN$_8$O$_2$S$_2$
formula weight	829.55	605.51	793.74	861.94	573.51
crystal system	monoclinic	monoclinic	monoclinic	monoclinic	monoclinic
space group	C2/c	P2$_1$/c	P2$_1$/n	P2$_1$/n	P2$_1$/c
a [Å]	19.730(3)	8.7267(9)	10.4196(8)	10.460(3)	8.805(3)
b [Å]	18.3287(8)	12.271(2)	14.6675(9)	15.127(8)	15.585(7)
c [Å]	14.9877(3)	13.301(2)	14.253(1)	14.3170(9)	9.5214(7)
α [°]	90	90	90	90	90
β [°]	115.2061(6)	110.1333(7)	97.5061(9)	97.006(2)	98.727(2)
γ [°]	90	90	90	90	90
V [Å^3]	4904.0(6)	1337.4(3)	2159.6(3)	2248(1)	1291.4(7)
Z	4	2	2	2	2
ρ_{calcd} [g cm^{-3}]	1.123	1.504	1.221	1.273	1.475
F(000)	1684.00	618.00	818.00	906.00	586.00
μ [mm^{-1}]	0.494	0.845	0.543	0.526	0.865
radiation [Å]	0.71069	0.71069	0.71069	0.71069	0.71069
temperature [K]	293	293	213	293	293
2θ range	5.5° < 2θ < 54.8°	5.5° < 2θ < 53.4°	5.5° < 2θ < 53.4°	5.5° < 2θ < 55.0°	5.5° < 2θ < 54.8°
GOF	2.51	2.00	1.23	2.57	2.455
no. of data collected	18180	8637	14092	15824	8620
no. of unique data	5431	2764	4521	4849	2858
no. of obsd data	2117 (I > 4.00σ(I))	2445 (I > 3.00σ(I))	2141 (I > 5.00σ(I))	2418 (I > 5.00σ(I))	1997 (I > 4.00σ(I))
no. of variables	203	173	209	221	169
R[a]	0.081	0.038	0.064	0.072	0.058
R$_w$[b]	0.107	0.069	0.093	0.1040	0.096
$\Delta\rho_{max and min}$ [e Å^{-3}]	0.59 and -0.36	0.71 and -0.54	0.86 and -0.59	0.65 and -0.46	1.04 and -0.63

[a] $R = \Sigma||Fo| - |Fc||/\Sigma|Fo|$. [b] $R_w = [(\Sigma w (|Fo| - |Fc|)^2/\Sigma wFo^2)]^{1/2}$.
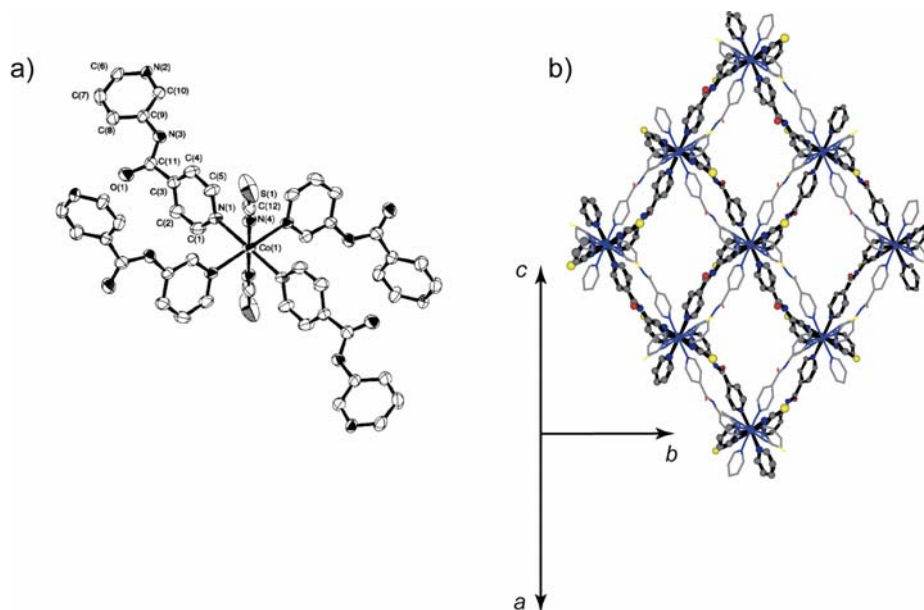
Figure 1. Crystal structure of $\{[Co(NCS)_2(3\text{-pia})_2]\cdot 2EtOH\cdot 11H_2O\}_n$ (**MOPA-1 ⊃ 2EtOH·11H$_2$O**). (a) ORTEP drawing of the cobalt center of **MOPA-1 ⊃ 2EtOH·11H$_2$O** at the 30% probability level. Hydrogen atoms and ethanol and water molecules are omitted for clarity. (b) Superposed two sheets. The thin and thick lines show the upper and lower sheet, respectively.
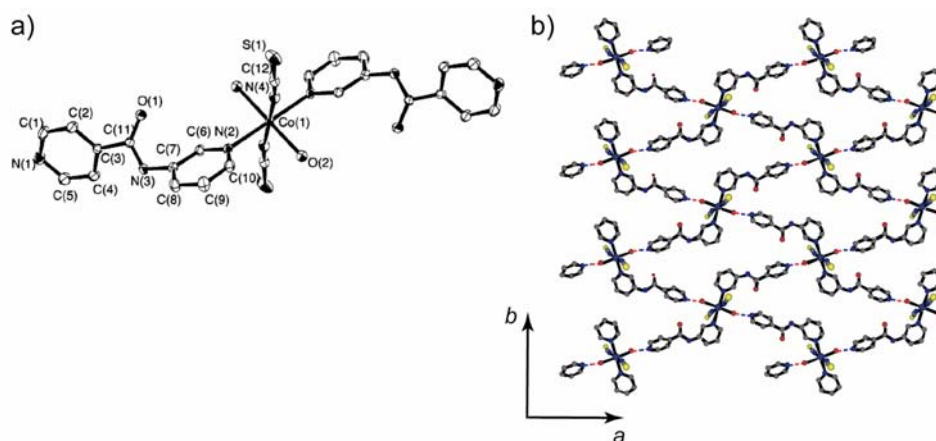
Figure 2. Crystal structure of $[Co(NCS)_2(3\text{-pia})_2(H_2O)_2]_n$ (**2**). (a) ORTEP drawing of the cobalt center of **2** at the 30% probability level. Hydrogen atoms are omitted for clarity. (b) The projection view along the *c* axis.

$[Co(NCS)_2(3\text{-pia})_2(H_2O)_2]_n$ (2). Figure 2(a) shows a coordination environment of the cobalt ion of **2**. The Cobalt(II) ion is octahedrally coordinated to the two N^N-type atoms of 3-pia ligand, two NCS groups and two water molecules. The apparent difference from

MOPA-1 ⊃ 2EtOH·11H$_2$O is recognized in a coordination mode of 3-pia ligand, which does not bridge cobalt(II) ions. The torsional twist of the pyridyl groups about the amide linkage is defined as 59° and 85° for **MOPA-1 ⊃ 2EtOH·11H$_2$O** and **2**, respectively. The NCS anion shows a bent

75
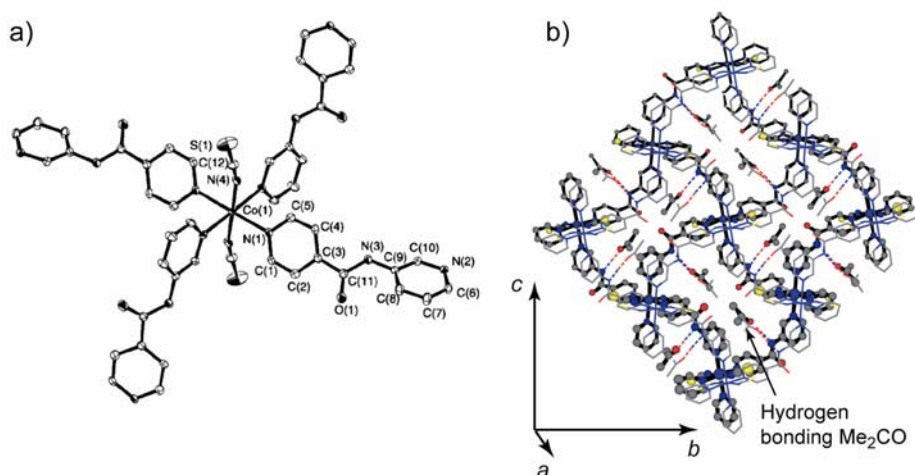
Figure 3. Crystal structure of $\{[Co(NCS)_2(3\text{-pia})_2]\cdot 4MeCO_2\}_n$ (**MOPA-1 ⊃ 4Me$_2$CO**). (a) ORTEP drawing of the cobalt center of **MOPA-1 ⊃ 4Me$_2$CO** at the 30% probability level. Hydrogen atoms and acetone molecules are omitted for clarity. (b) Superposed two sheets. The thin and thick lines show the upper and lower sheet, respectively.

coordination mode with the Co-N(4)-C(12) angle of 170.8(2)°. The coordinated water molecules are hydrogen bonded to the non-coordinated N^C atoms of the nearest-neighbor 3-pia ligands (O(2)-N(1) = 2.721(2) Å), affording a 2-dimensinal sheet (Figure 2(b)). The sheet extends along the *ab*-plane and the relationship between the sheets is …ABAB… The nearest Co-Co distance is about 14.0 Å in a sheet, and 8.7 Å in the adjacent sheet. Interestingly, the amide moieties do not interact with other groups like sulfur atoms of SCN ions. Moreover, **2** clathrates no guest molecules. Similar two-dimensional structures happen to be constructed from hydrogen bond links between coordinated water molecules and non-coordinated 4,4'-bpy.[51-53] In the case of **2**, the hydrogen bond sheet forms by use of the metal-free site of terminally coordinated 3-pia ligand.

$\{[Co(NCS)_2(3\text{-pia})_2]\cdot 4Me_2CO\}_n$ (**MOPA-1 ⊃ 4Me$_2$CO**). Compound **MOPA-1 ⊃ 4Me$_2$CO** has a coordination environment arounf the cobalt ion, similar to that of **MOPA-1 ⊃ 2EtOH·11H$_2$O**; the cobalt(II) center is octahedrally coordinated to four 3-pia ligands and the two NCS anions in a trans fashion (Figure 3(a)). Figure 3(b) shows a extended structure of **MOPA-1 ⊃ 4Me$_2$CO**. The Co-N bond distances of 3-pia ligands are slightly different (Co-N(1) = 2.171(5) Å and Co-N(2) = 2.221(4) Å). The NCS ion shows N-site coordination with a bending mode; Co-N(4)-C(12) = 164.9(5)° and N(4)-C(12)-S(1) = 177.8(6)°.

The cobalt ions are linked by 3-pia ligands to form a 2-dimensinal sheet constructed from a "double edged axe-shaped" motif with a cavity of 3.5 Å × 10.5 Å dimension. Two types of acetone molecules are included in the cavity (Figure 3(b)). One is hydrogen bonded to N

76
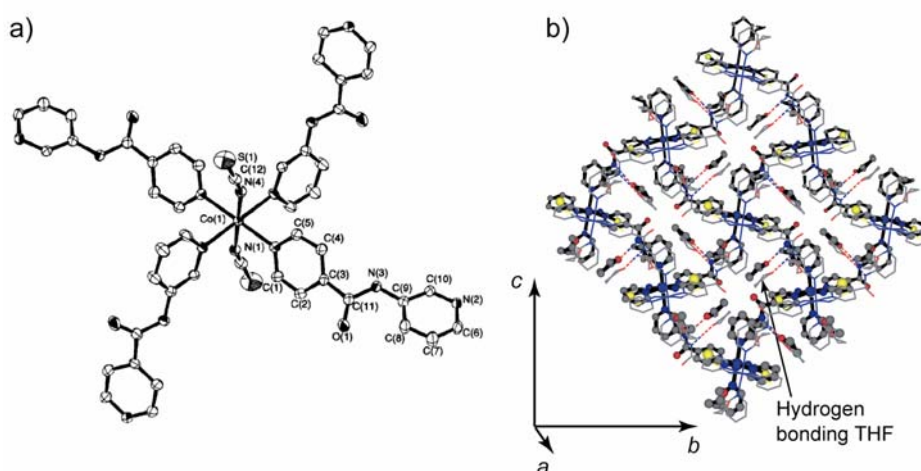
Figure 4. Crystal structure of {[Co(NCS)$_2$(3-pia)$_2$]·4THF}$_n$ (**MOPA-1 ⊃ 4THF**). (a) ORTEP drawing of the cobalt center of **MOPA-1 ⊃ 4THF** at the 30% probability level. Hydrogen atoms and THF molecules are omitted for clarity. (b) 2D-sheet which is the projection view along the a axis.
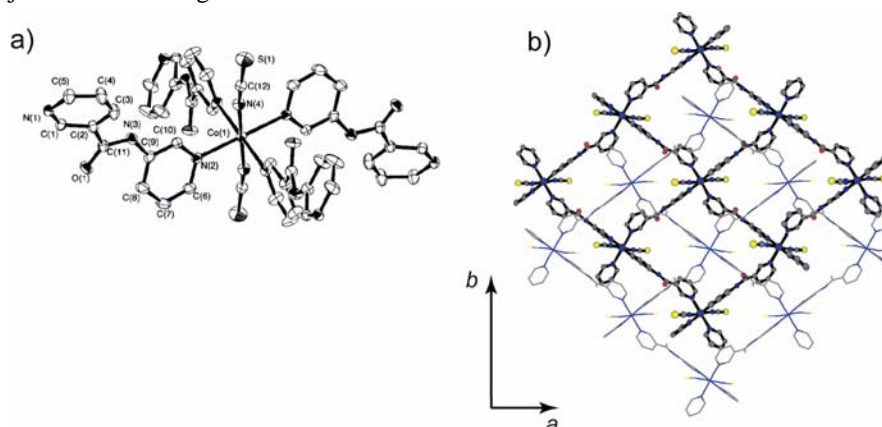
Figure 5. Crystal structure of [Co(NCS)$_2$(3-pna)$_2$]$_n$ (**MOPA-2**). (a) ORTEP drawing of the cobalt center of **MOPA-2** at the 30% probability level. Hydrogen atoms are omitted for clarity. (b) Two sheets stack along the c axis with hydrogen bond of amide moieties between the sheets. The thin and thick lines show the upper and lower sheet, respectively.

(O(Me$_2$CO)-N(amide) = 2.961(7) Å), entrapped in the cavity with the inclination to the sheet plane, while the other exists over the cavity frame without significant interactions to any atoms. As a result of the hydrogen bonding, the bond vector of the amide carbonyl group is coplanar to the sheet plane, therefore unavailable for the sheet-sheet interaction. The adjacent layers are stacked along the a axis with respect to each other such that channels are created with a double edged axe-shaped cross section (Figure 3(c) and (d)); the distance between the layers is about 10.4 Å and the thickness of each sheet is about 10.4 Å. The nearest Co-Co distance is about 11.9 Å in a sheet and 10.4 Å in the adjacent sheets.

{[Co(NCS)$_2$(3-pia)$_2$]·4THF}$_n$ (MOPA-1 ⊃ 4THF). Figure 4(a) shows an octahedral geometry of the cobalt(II) ion with the four nitrogen atoms of the two 3-pia ligands and the two NCS anions in

a trans fashion.   The distances between the cobalt ions and two types of nitrogen atoms of 3-pia are slightly different (Co-N(1) = 2.182(5) Å and Co-N(2) = 2.256(4) Å).   The NCS ion is coordinated to the cobalt ion at the nitrogen site with a bending mode; Co-N(4)-C(12) = 161.8(5)° and N(4)-C(12)-S(1) = 176.3(6)°.   The 3-pia ligand bridges two cobalt atoms to afford a 2-dimensional sheet, analogous to **MOPA-1 ⊃ 4Me₂CO** in the crystal data.   The sheet is also constructed from a double edged axe-shaped motif with dimensions of 3.2 Å × 10.4 Å, in which two types of THF molecules are included (Figure 4(b)); one is trapped inside the cavities because of hydrogen bonding with the nitrogen atom of the amide moiety (O(THF)-N(amide) = 2.928(8) Å), sitting perpendicular to the sheet plane.   The other exists over the cavity frame without significant interactions to any groups.

The sheets stack along the *a* axis to superimpose on each other in a slight offset, and the distance between the adjacent sheets is about 10.4 Å.   The nearest Co-Co distance is about 12.0 Å in a sheet and 10.4 Å in the adjacent sheets.   This feature is very similar to that of **MOPA-1 ⊃ 4Me₂CO**.

[Co(NCS)₂(3-pna)₂]ₙ (MOPA-2).   Figure 5(a) shows the local coordination sphere of the cobalt ion, indicating an octahedral geometry with the four 3-pna and the two NCS groups.   The unsymmetrical 3-pna ligand has two kinds of nitrogen atoms, N^N and N^C like 3-pia.   The Co-N distances are similar to each other; Co-N(1) = 2.240(3) Å, Co-N(2) = 2.214(3) Å.   The slightly bent mode of N-C-S ion with the angle of 178.2(4)° is observed together with Co-N(4)-C(12) angle of 172.7(4)°.   The 3-pna bridges two cobalt atoms to afford a 2-dimensinal sheet composed of a nearly square grid with the dimensions of 7.3 Å × 12.9 Å, analogous to **MOPA-1 ⊃ 2EtOH·11H₂O, MOPA-1 ⊃ 4Me₂CO** and **MOPA-1 ⊃ 4THF**.   Interestingly, the adjacent sheets stack along the *c* axis with a shift offset by 0.5(a + b) along the *ab*-plane so that the NCS group protrudes through the midpoint of the cavity of the adjacent sheet (Figure 5(b)).   The interlayer separation is about 3 Å. It is worth noting that a hydrogen bonding link of a NH---O=C (N---O = 2.874(4) Å) type between the adjacent sheets affords a 3-dimensinal network.   The framework contains no solvent molecules, attributing to closely packed layer structures with hydrogen bonds between the sheets.   The nearest Co-Co distance is about 12.2 Å in a sheet and 8.8 Å in the adjacent sheets.

Coordination polymers with Co(NCS)₂ unit, [Co(NCS)₂(bpee)₂]ₙ and [Co(NCS)₂(bpea)₂]ₙ (bpee = *trans*-1,2-bis(4-pyridyl)ethylene, bpea = 1,2-bis(4-pyridyl)ethane),[54] tend to give square-grid sheets. Among these compounds, mutual interpenetration of the sheets often occurs and therefore provides no porous frameworks.   Compounds **MOPA-1 ⊃ 2EtOH·11H₂O, MOPA-1 ⊃ 4Me₂CO** and **MOPA-1 ⊃ 4THF** also show essentially the square grid frameworks of cobalt atoms, however, interpenetration is eschewed by hydrogen bonding links between the adjacent sheets or the effective guest-inclusion.

X-ray powder diffraction.

A guest-free solid, **1**, was obtained by treating **MOPA-1 ⊃ 2EtOH·11H₂O** under reduced pressure. Removal of the guest molecules causes a significant change on the framework of **MOPA-1 ⊃ 2EtOH·11H₂O**, which was readily detected by X-ray powder diffraction (XRPD). The XRPD pattern in Figure 6 shows that the framework of **MOPA-1 ⊃ 2EtOH·11H₂O** cannot withstand a high level of stress on an extensive loss of guests, resulting in an amorphous structure. When **1** is exposed to moisture or soaked in water, a new crystalline phase **2** occurs,[55] in which two water molecules are directly coordinated to the cobalt atom, resulting in a $Co(H_2O)_2(py)_2(SCN)_2$ type chromophore. As is illustrated in Figure 6, the transformation associated with water is characterized by a process of "crystal to crystal via amorphous phase", which is, however, not reversible.
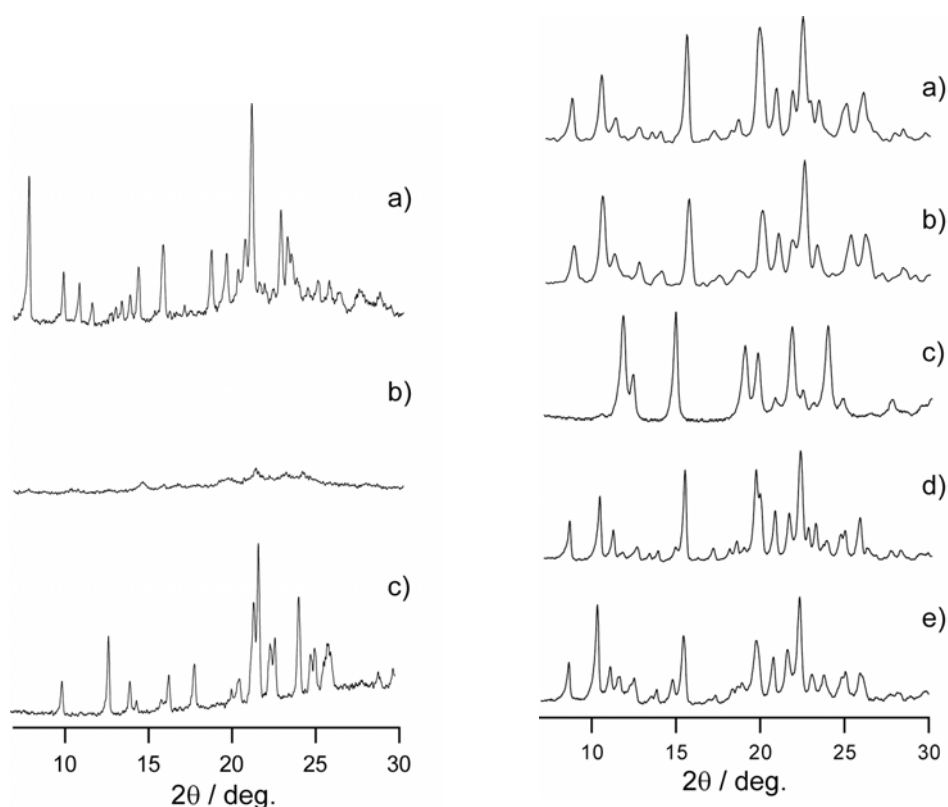
Figure 6. XRPD patterns at room temperature of (a) as-synthesized **MOPA-1 ⊃ 2EtOH·11H₂O**, (b) **1** obtained by drying **MOPA-1 ⊃ 2EtOH·11H₂O** in vacuo for 2 hours, and (c) **2** obtained after immersing **1** in an ethanol and water mixed solvent (ethanol/water, *v/v* 2:11) for 1 hour.

Figure 7. XRPD patterns at room temperature of (a) **MOPA-1 ⊃ 4THF** obtained after exposing **1** to a THF vapor for 4 days, (b) **MOPA-1 ⊃ 4Me₂CO** obtained after exposing **1** to an acetone vapor for 4 days, (c) **MOPA-1** obtained by drying **MOPA-1 ⊃ 4THF** in vacuo for 2hours, (d) **MOPA-1 ⊃ 4THF** obtained after exposing **MOPA-1** to an THF vapor for 4days, and (e) **MOPA-1 ⊃ 4Me₂CO** obtained after exposing **MOPA-1** to an acetone vapor for 4days.

79

On the other hand, when **1** is exposed to THF vapor or immersed in the solvent, a new crystalline framework of **MOPA-1 ⊃ 4THF** takes place, indicating that **1** adsorbs THF in its cavities to restore a 2-dimensinal network.   The similar phenomenon occurs in acetone, therefore affording a new crystalline framework of **MOPA-1 ⊃ 4Me$_2$CO**.   The two XRPD patterns in Figure 7(a) and (b) are in fair agreement with those calculated from single crystal data of **MOPA-1 ⊃ 4THF** and **MOPA-1 ⊃ 4Me$_2$CO**, respectively.   In this sense **1** is regarded as an apohost for THF and acetone.   Another apohost, **MOPA-1**, can be obtained by treating **MOPA-1 ⊃ 4THF** (or **MOPA-1 ⊃ 4Me$_2$CO**) under reduced pressure as shown in Scheme 3.   The sharp XRPD pattern of **4** exhibits a crystal phase, different from those of **MOPA-1 ⊃ 2EtOH·11H$_2$O, MOPA-1 ⊃ 4Me$_2$CO**, and **MOPA-1 ⊃ 4THF**. On the basis, **MOPA-1 ⊃ 4THF** changes its framework into a new one after the removal of THF. Interestingly, the original crystal structure comes back completely upon exposing to THF vapor because the peak positions and relative intensities coincide with original ones (Figure 7(d)).   The similar reversible structural change is also found in the process of the adsorption/desorption of acetone molecules.   Consequently, the apohost **MOPA-1** has capability to adsorb and to desorb THF or acetone reversibly, therefore the direct transformation from crystal to crystal is realized.
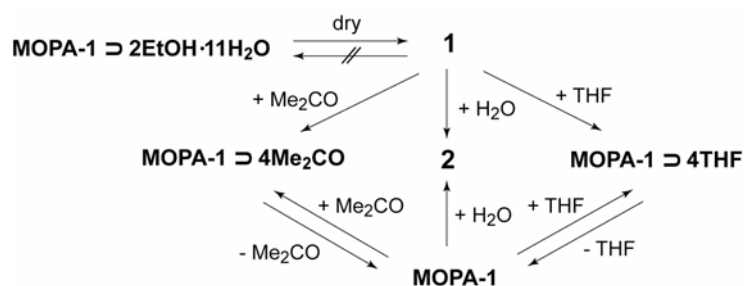
Scheme 3.

Optical and Infrared Spectra.

Figure 8 shows the reflection spectra of the compounds **MOPA-1 ⊃ 2EtOH·11H$_2$O**, **1** and **2** together with XRPD patterns.   **MOPA-1 ⊃ 2EtOH·11H$_2$O** has a main band at *ca*. 488 nm, typical of an octahedral geometry.   Removal of the guests causes the intensity to decrease, and instead, new bands appear at *ca*. 614, 570 and 513 nm in Figure 8(b).   It should be kept in mind that **1** is not uniform but amorphous.   The apparent spectral feature accompanying the color change from **MOPA-1 ⊃ 2EtOH·11H$_2$O** to **1** implies a conversion from an octahedral to a tetrahedral Co^{II} coordination geometry.[32]   Practically, blue compounds of [Co(NC$_5$H$_4$C$_2$H$_3$)$_2$Cl$_2$] and

[Co(4-vpy)$_2$Cl$_2$] (4-vpy = 4-vinylpyridine) have been demonstrated to be tetrahedral geometries.[56,57] In general, tetrahedral Co^{II} (e^{4}t$_2{}^3$) species exhibit two characteristic electronic absorptions in the near-infrared and visible regions due to the transitions ν_1 (^{4}T$_1$(F) $\leftarrow$ ^{4}A$_2$) and ν_2 (^{4}T$_1$(P) $\leftarrow$ ^{4}A$_2$), respectively.   The intensities of these absorption bands usually range from 10 to 100 L / (mol·cm) for ν_1 and from 100 to 2000 L / (mol·cm) for ν_2, and they are broadened due to spin-orbit coupling and deviations from ideal tetrahedral symmetry.[58]   The absorption bands at a longer wavelength region in Figure 8(b) could be attributed to those of a tetrahedral Co^{II}.   By comparisons with the electronic absorption spectra of the tetrahedral complexes in K$_2$[Co(NCO)$_4$] (ν_1 = 1200, ν_2 = 630, ν_3 = 590 (sh) and ν_4 = 520 (sh) nm) and Hg[Co(NCS)$_4$] (ν_1 = 1205, ν_2 = 599 nm), the new bands between 500 and 650 nm arising from the guest removal of **MOPA-1 ⊃ 2EtOH·11H$_2$O** are possibly assigned to the ν_2 transition of tetrahedral Co^{II} ions.[59,60]   In the case of **1**, however, we cannot exclude the possibility of the considerable mixing of octahedral forms with tetrahedral ones because the band intensities of octahedral forms are much lower than that of tetrahedral ones.   In **2** the peak of the reflection spectrum is 496 nm (Figure 8(c)), assigned to the octahedral form, as is illustrated by crystal structures of **MOPA-1 ⊃ 2EtOH·11H$_2$O** and **2** typical of octahedral geometries with N$_6$ and N$_4$O$_2$, respectively.
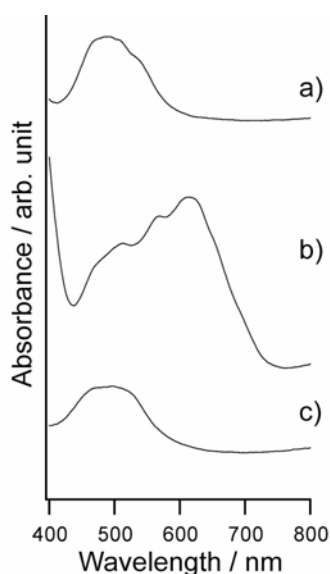
Figure 8.   Reflection spectra of in visible region, (a) as-synthesized **MOPA-1 ⊃ 2EtOH·11H$_2$O**, (b) **1** obtained by drying **MOPA-1 ⊃ 2EtOH·11H$_2$O** in vacuo for 2 hours, and (c) after immersing **1** in an ethanol and water mixed solvent (ethanol/water, v/v 2:11) for 1 hour.
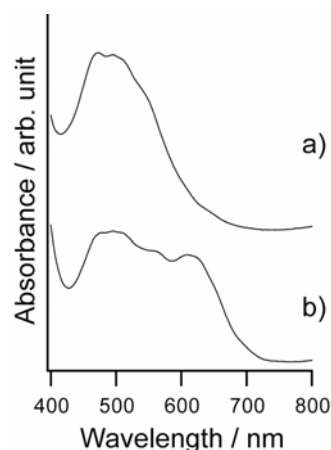
Figure 9.   Reflection spectra of in visible region, (a) as-synthesized **MOPA-1 ⊃ 4THF** and (b) **MOPA-1** obtained by drying **MOPA-1 ⊃ 4THF** in vacuo for 2 hours.

On the other hand, the apohost **MOPA-1** affords a different feature from that of **1**. Figure 9 shows the reflection spectra of the compounds **MOPA-1 ⊃ 4THF** and **MOPA-1**. Removal of THF from **MOPA-1 ⊃ 4THF** gives rise to color change from pink to violet while the crystallinity is maintained regardless of its transformation. The band at *ca*. 472 nm (Figure 9, (a)) is observed for **MOPA-1 ⊃ 4THF** while the new bands at *ca*. 608 and 560 (sh) (Figure 9, (b)) appear in **MOPA-1**. The reversibility in color between **MOPA-1 ⊃ 4THF** and **MOPA-1** is also confirmed by these reflection spectra. It has been demonstrated that a pink compound, $\{[Co(NCS)_2(4,4'\text{-bpy})_2]\cdot2(CH_3CH_2)_2O\}_n$,[53] thermally decomposes to form a violet one, $[Co(\mu\text{-NCS})(\mu\text{-SCN})(\mu\text{-}4,4'\text{-bpy})]_n$, having octahedral cobalt(II) ions with N_4S_2 chromophore. It is worth noting that the NCS anions bridges the two cobalt(II) ions. On the other hand, the cobalt(II) complex, $[Co(py)_4(NCS)_2]$ (py = pyridine),[61] with N_6 chromophore also affords the bands ($\nu_1 = 800$, $\nu_2 = 625$, $\nu_3 = 526$ and $\nu_4 = 485$ nm) in a region similar to that of **MOPA-1.** Taking account of these results, the cobalt(II) ion of **MOPA-1** could have an octahedral coordination geometry, and the donor atoms could be N_6 or N_4S_2.

With respect to asymmetric stretching vibration of thiocyanate, the criterion, which is adopted to establish the bond type, is that the thiocyanato (M-SCN) complexes exhibit very sharp, well-formed N-C stretching bands above 2100 cm^{-1}, whereas the isothiocyanato (M-NCS) complexes exhibit relatively broad and intense bands around or below 2100 cm^{-1}.[62] Strong and broad bands at 2071 cm^{-1} (**1**), 2056 cm^{-1} (**MOPA-1**) and 2056 cm^{-1} (**MOPA-2**) of the present complexes are indicative of isothiocyanato bonding mode. In case that the NCS group bridges the two metal atoms, the CN stretching frequency of the bridging group is generally higher than that of a terminal group.[61,62] Taking account of the lower frequency (2056 cm^{-1}) in **MOPA-1**, the NCS groups do not bridge any cobalt(II) atoms, indicative of the formation of a $N^{py}_4N^{NCS}_2$ chromophore. Therefore, the IR spectra also support a distorted octahedral geometry of the cobalt ion in **MOPA-1**.[58]

The IR spectra for the two guest-free apohosts (**1** and **MOPA-1**) well distinguish their structures. The N-H stretching band and the amide-I and -II bands appear in the regions of 3500 - 3100 cm^{-1} and 1700 - 1500 cm^{-1}, respectively.[62] Crystal structure of **2** shows no hydrogen bonding between the amide groups whereas **MOPA-2** has the hydrogen bonding between them. As shown in Figure 10 the β-sheet type links affords a characteristic band profile. Therefore, the two compounds are regarded as authentic samples, by which hydrogen bonding link could be identified by IR spectroscopy. The hydrogen bond-free amide groups in **2** provide a featureless band profile as in Figure 10 (b) while the hydrogen-bonded one, so-called β-sheet form of **MOPA-2** affords a structured bands in Figure 10 (d); the amide-I bands at 1608 cm^{-1} and 1660 cm^{-1}, the amide-II band at 1551 cm^{-1}, and the sharp and middle intensity peak of N-H stretching vibrations at 3303 cm^{-1} are

observed. This feature characteristic of the amide interaction is very close to those of *s-trans* type found in a cyclic peptide,[45,47,63] in good agreement with the single X-ray crystal structure. The apohost **MOPA-1** also displays a band profile as shown in Figure 10 (c), characteristic of hydrogen-bond formation within amide moieties, resulting in β-sheet type structure: amide-I bands at 1608 cm^{-1} and 1674 cm^{-1}, and the amide-II band at 1547 cm^{-1} are consistent with those of the β-sheet type structure. The observed N-H stretching frequencies at 3263 cm^{-1} also strongly support the formation of a tight network by backbone-backbone hydrogen bonding (Scheme 4). On the other hand, in **1** and **2** the amide-I and amide-II bands are relatively broad and split as well as N-H stretching broad vibration band. Because the N-H stretching band appears as a very broad band with many sub-maxima in hydrogen bond-free amides,[64] the amide moieties in **1** and **2** do not form hydrogen bonding links between adjacent sheets, consistent with the X-ray crystallographic structure of **2**.
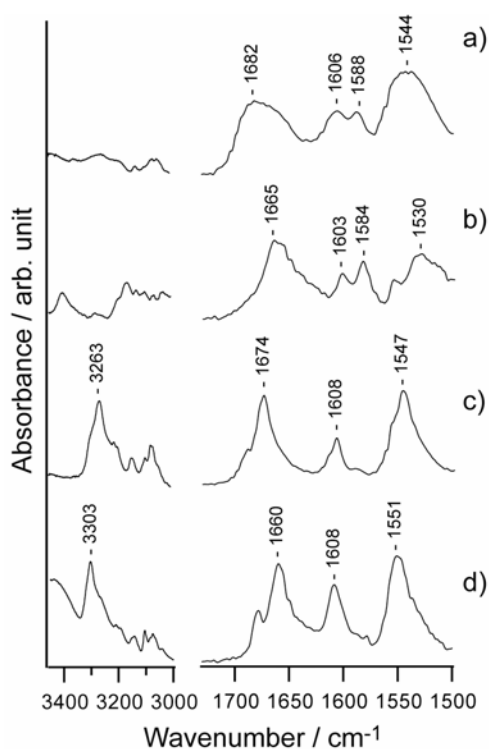
Figure 10. Infrared spectra of in amide-I and –II region (right) and N-H stretch region (left) with samples prepared as KBr pellets (a) **1**, (b) **2**, (c) **MOPA-1** and (d) **MOPA-2**.

Scheme 4.

83
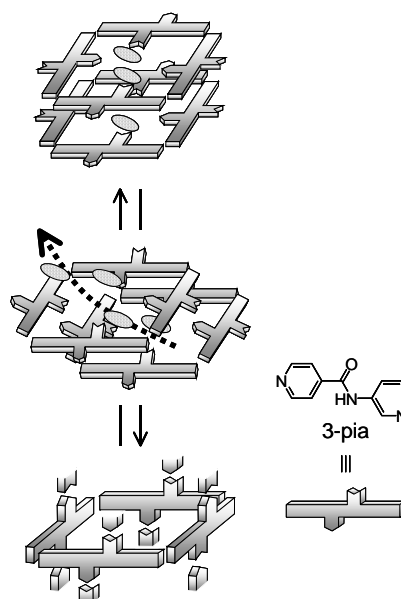
EPR.

EPR measurements for **1** and **MOPA-1** were performed in order to gain information concerning the coordination structures around the Co^{II} ion. Figure 11 shows the EPR spectra of **1**, water-added **1** (= **2**), and **MOPA-1** measured at ~15 K. The EPR spectrum of **MOPA-1** indicates well-resolved features and their EPR parameters have been determined by computer simulation as g'_1, g'_2, g'_3 = 6.4, 3.65, 2.88; A_1 = 6.8 mT [65]; the peak-to-peak line widths W_1, W_2, W_3 = 14.0, 28.0, 45.0 mT. On the other hand, **1** exhibits a broader EPR spectrum in accordance with the amorphous nature of compound **1**. The g values are estimated as $g'_1 \approx 6.8$ and $g'_2 \approx g'_3 \approx 3.3$. (Rigorous computer simulation of the spectrum of **1** was found to be difficult because of its broad nature of the spectrum). When the sample of **1** got wet by a few drops of water, the EPR spectrum changed drastically to that in Figure 11 (b), which is similar to that of **2**: computer simulation has yielded $g'_1 = g'_2 = 5.0$, $g'_3 = 2.4$; the peak-to-peak line widths $W_1 = W_2 = 27$ mT and $W_3 = 90$ mT.[66]

Several types of high-spin Co^{II} complexes have so far been studied by EPR spectroscopy,[67] and the differences in the EPR pattern between tetrahedral and octahedral Co^{II} have been well documented.[68-71] In tetrahedral Co^{II}, the ground orbital state is $^4A_2$, and thus the orbital angular momentum is well quenched, which makes the spin Hamiltonian approach appropriate. As a result, observed g values (effective g values) satisfy the relatively simple equations relating the effective g values with the zero-field splitting (ZFS) parameters D and E and the true g values, $g_\perp$ and $g_\parallel$ (or g_1, g_2, g_3 ; note that they are referred to in equations without prime).[71,72] The true g values are the g values in the original $S = 3/2$ spin Hamiltonian, and they should not be very different from 2. In axial cases ($E/D = 0$), one obtains $g'_1 = g'_2 = 2g_\perp$ and $g'_3 = g_\parallel$ for $S_z = \pm 1/2$ doublet and $g'_1 = g'_2 = 0$ and $g'_3 = 3g_\parallel$ for $S_z = \pm 3/2$ doublet. It is clear that the observed g' values for **2** and **MOPA-1** do not accord with these relations. This result also appears to hold even for **1**. In the case of an octahedral Co^{II}, on the other hand, the ground orbital state is $^4T_1$, and thus orbital degeneracy still remains.[73] Although the lower symmetry ligand field lifts the orbital degeneracy, the orbital angular momentum is generally not sufficiently quenched, which makes the simple spin Hamiltonian approach invalid. Because a large portion of orbital angular momentum remains, the relationships between the effective g values and other parameters are quite complicated. Theoretical treatment of the EPR parameters of octahedral Co^{II} was made by Abragam and Pryce,[74] who gave theoretical expressions for the effective g value and HFC parameters considering up to the second-order perturbation effects. They estimated that the effects of the second-order terms on the effective g values are ≤ 0.20. Hence, for the present purpose, the second-order term may be omitted. The zeroth-order and first-order perturbation results for the effective g values are plotted against $\Delta/|\lambda|$ in Figure 12, where Δ is the ligand-field splitting between $|^4T_1;xy\rangle$ and $|^4T_1;z\rangle$ with the value being

positive when $|^4T_1;z\rangle$ is upper, and λ is the spin-orbit coupling constant. The position $\Delta/|\lambda| = 0$ corresponds to the exact O_h symmetry, and thus the expected g' are isotropic. On the contrary, as $\Delta/|\lambda|$ goes to $\pm\infty$, the g' values approaches to the cases expected from the simple spin Hamiltonian,[75] where the distinction between tetrahedral and octahedral complexes is difficult. Figure 12 shows that the present EPR results are in good agreement with the theory and, furthermore, estimated $\Delta/|\lambda|$ values are reasonably small. Therefore, the Co^{II} ion in **2** and **MOPA-1** are in octahedral coordination environment. Even for **1**, octahedral species are also detected by EPR whereas optical spectrum exhibits tetrahedral species. We estimate $\Delta/|\lambda| = 3.4, -4.1, 3.1$ for **1**, **2** and **MOPA-1**, respectively. It is interesting to note that the sign of Δ is reversed between **1** and **2**. Finally, we mention the case in five-coordinate Co^{II} complexes. In literature, square-pyramidal and trigonal bipyramidal Co^{II} complexes have been investigated by EPR spectroscopy,[70,76,77] and shown to exhibit EPR spectra clearly different from those of **1**, **2**, and **MOPA-1**. This is reasonable because the degeneracy of the $^4T_1$ states no more occurs under the five-coordinate geometry, which makes the simple spin Hamiltonian approach fairly appropriate.
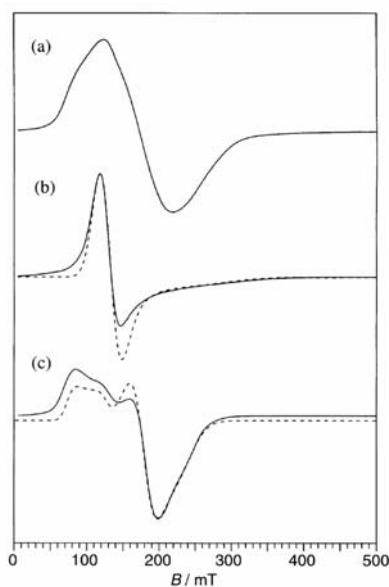
Figure 11. CW EPR spectra of powdered samples of **1** (a), water-added **1** (= **2**) (b), and **MOPA-1** (c). Experimental settings: microwave frequency, 9.000 (a), 8.992 (b), 8.998 (c) GHz; microwave power, 1mW; field modulation (100 kHz), 1 mT; temperature, 14.9 (a), 17.7 (b), 14.8 (c) K.
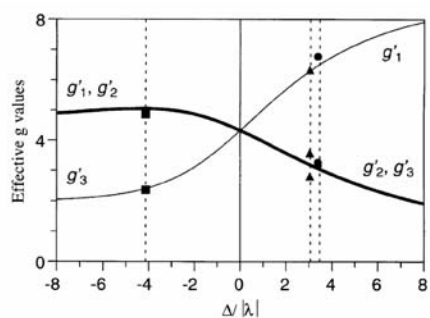
Figure 12. Effective g values calculated from the first-order perturbation equations are plotted versus $\Delta/|\lambda|$. For details, see text. The solid squares, triangles, and circles represent the experimentally obtained effective g values for **1**, water-added **1** (= **2**), and **MOPA-1**, respectively.

Selective Guest Inclusions.

Both compounds **1** and **MOPA-1** adsorb THF or acetone molecules, accompanying their framework deformation so that the guest molecules are trapped by amide moieties with hydrogen bonding. The guest selectivity was examined for organic compounds, which are classified into four groups according to the shape/size and the presence/absence of O atom available for hydrogen bonding;
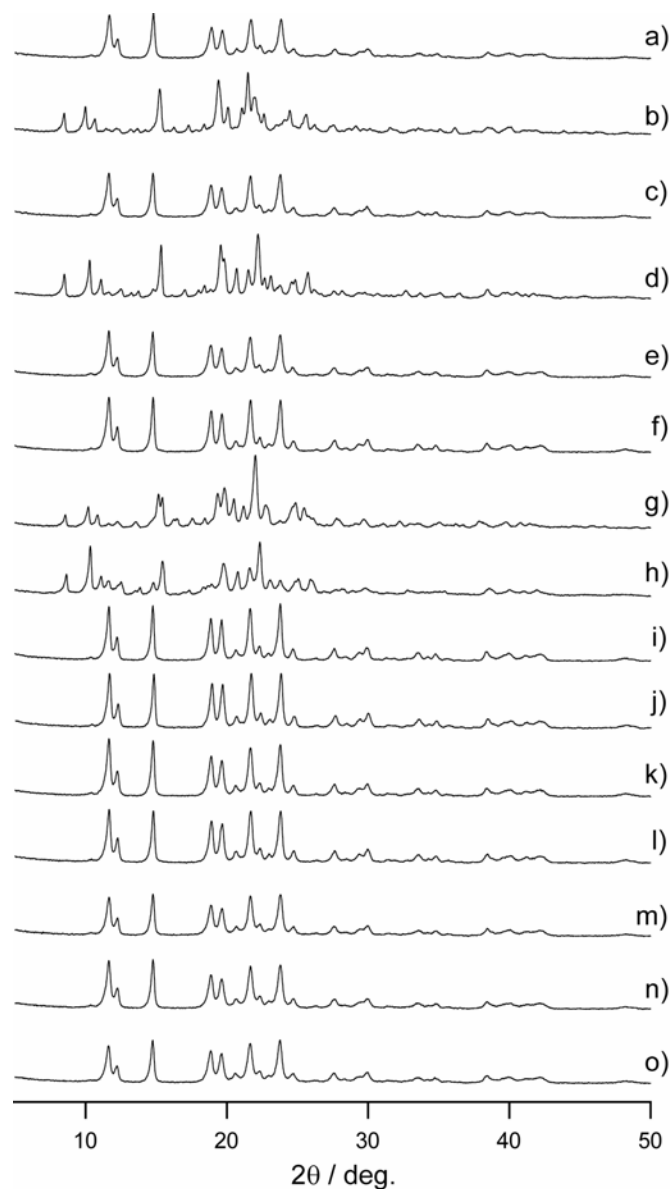
Figure 13. XRPD patterns at room temperature of (a) **MOPA-1** obtained by drying **MOPA-1 ⊃ 4THF** in vacuo for 2 hours, **MOPA-1** exposed for 4 days to (b) THF (= **MOPA-1 ⊃ 4THF**), (c) cyclopentane, (d) tetrahydropyran, (e) cyclohexane, (f) benzene, (g) 1,4-dioxane, (h) acetone (= **MOPA-1 ⊃ 4Me$_2$CO**), (i) pentane, (j) hexane, (k) heptane, (l) diethylether, (m) propylether, (n) isopropylether and (o) *t*-butyl methyl ether.

86

(group I) five and six-membered ring ethers (THF, tetrahydropyran and 1,4-dioxane), (group II) linear type ethers (diethylether, propylether, isopropylether and *t*-butyl methyl ether), (group III) ring hydrocarbons (cyclopentane, cyclohexane and benzene) and (group IV) linear alkanes (pentane, hexane and heptane).   Apohost **MOPA-1** was exposed to vapor of each compound and the XRPD pattern was measured, several of which are shown in Figure 13.   Compounds of group II - IV show no change in the peak positions and relative intensities, identical with those of the apohost **MOPA-1**, and indicating that apohost **MOPA-1** does not undergo a structural change with guest adsorption. On the other hand all the compounds of group I exhibit guest inclusion.   By considering the fact that cyclopentane and THF (cyclohexane and tetrahydropyran/1,4-dioxane) are similar in size and shape, a guest molecule for apohost **MOPA-1** should possess at least one hydrogen-bonding site. Apohost **MOPA-1** also has shape selectivity of the guest inclusion, because **MOPA-1** does not include linear-shaped ether, diethylether, propylether, isopropylether and *t*-butyl methyl ether. Guest molecule adsorption in coordination polymers has so far been found for hydrophobic apohost whose driving force may be a sort of π-π stacking.[6,78]   On the contrary to the robust framework having hydrophobic cavities, we designed the cavities with structural flexibility accompanying with hydrogen bonding site.   This is indeed successful.   Consequently, the apohost **MOPA-1** pave the way to the selective inclusion system reflecting to the size/shape and hydrogen bonding capability.

Scheme 5.

Highly Selective
Guest Inclusion
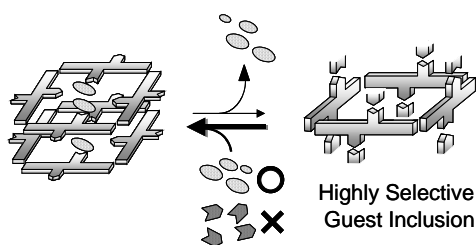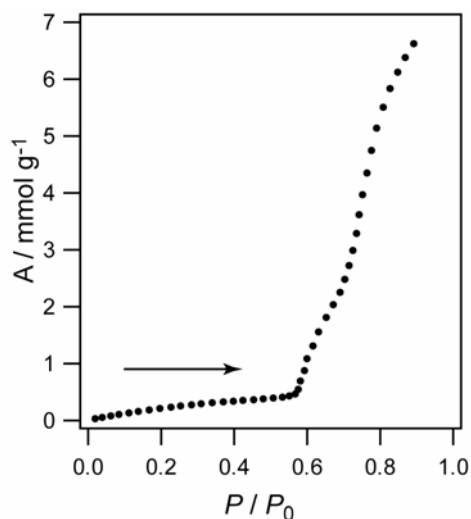
Figure 14.   Isotherm for acetone vapor adsorption at 293 K of apohost **MOPA-1** from 0.005 to 0.229 atom. P_0 is a saturated vapor pressure, 0.244 atom, of acetone at 293 K.

In the process of adsorption/desorption, there is a remarkable difference between guest-free **1** and apohost **MOPA-1**, it is an important point whether or not the structural regularity is maintained for a whole process; "amorphous to crystal" and "crystal to crystal" for **1** and **MOPA-1**, respectively. Now, a question arises as to why "**MOPA-1 ⊃ 2EtOH·11H₂O** to **1**" is "crystal to amorphous" and "**MOPA-1 ⊃ 4THF** (**MOPA-1 ⊃ 4Me₂CO**) to **MOPA-1**" is "crystal to crystal" on the removal guest molecules. When we recall the crystal structures, the following point would answer the question; whether or not 2-dimensional sheets regularly stack with hydrogen-bond formation, namely, β-sheet typed structure forms (Scheme 4). In **MOPA-1 ⊃ 2EtOH·11H₂O**, the "double edged axe-shaped" motifs in the adjacent sheets are not located over each other (Figure 1 (c)), whereas in **MOPA-1 ⊃ 4THF** (**MOPA-1 ⊃ 4Me₂CO**), the motifs stack so perfectly as to overlap in a edge to edge fashion (Figure 3 (c)). Due to this regularity, the sheets in **MOPA-1** can stack efficiently with locking mechanism by forming β-sheet type structure, and thus, withstands significant stress on removal of guest molecules.

As mentioned previous section, both **1** and **MOPA-1** adsorb THF *vapor* (or acetone) showing "amorphous to crystal" and "crystal to crystal" transformation, respectively. Figure 14 shows the isotherms of acetone adsorption of **MOPA-1** at 293 K. The isotherm shows an abrupt rise at $P/P_0 \cong$ 0.58 and reach to the saturation point of *ca.* 6.9 mmol g^{-1}, which corresponds to that estimated based on the crystal structure. This characteristic adsorption profile would support the conversion of a phase A (apohost, β-sheet) without guests in the pore to a phase B (adsorbed form, trap) with the guests.[79] The adsorption isotherm of CH₄ for **MOPA-1** at 298 K reveals no uptake into the micropores at all, indicating that the channel of **MOPA-1** is not large enough to incorporate CH₄ molecules (3.8 × 3.8 Å).[80]

Conclusion

From cobalt(II) thiocyanate and bipyridyl derivatives having the amide group, we succeeded in providing novel coordination polymers with flexible 2-dimensinal sheets. Such sheets transform their structure to other ones accompanying with adsorption/desorption of guest molecules. {[Co(NCS)₂(3-pia)₂]·2EtOH·11H₂O}$_n$ (**MOPA-1 ⊃ 2EtOH·11H₂O**) changes to amorphous **1**, {[Co(NCS)₂(3-pia)₂]·4Me₂CO}$_n$ (**MOPA-1 ⊃ 4Me₂CO**) and {[Co(NCS)₂(3-pia)₂]·4THF}$_n$ (**MOPA-1 ⊃ 4THF**) are transformed to β-sheet typed crystalline **MOPA-1**, whose porous structures are maintained. The clue to maintain crystallinity in **MOPA-1** is a gadget that the amide moiety plays not only a role in trapping guest molecules but also in linking sheets. Therefore, the

reversible adsorption is restricted to the apohost **MOPA-1,** which also shows selectivity for guest molecules in shape and chemical affinity.

The compound obtained in this work is one of representations of new generation coordination polymers. The structural change of amorphous **1** to crystalline **MOPA-1 ⊃ 4THF** (**MOPA-1 ⊃ 4Me₂CO**) is categorized in "Recoverable Collapsing", while the reversible change of crystalline **MOPA-1** to crystalline **MOPA-1 ⊃ 4THF** (**MOPA-1 ⊃ 4Me₂CO**) is categorized in "Guest-Induced Reformation". In our case "crystal to crystal" transformation with color change is more effective than "amorphous to crystal" in the adsorption property. However, "amorphous to crystal" transformation means a kind of restoration by organic guest molecules, which is, therefore, a restoring agent. This system would imply a healing material based on coordination polymers. Such dynamic behaviors of coordination polymers at present provide a new concept that porous properties of coordination polymer do not require robustness, and the advantage of inorganic/organic hybrid compound would open up a new functional chemistry towards dynamic porous materials.

Experimental Section

Materials. For 3-pia and 3-pna ligand, isonicotinic chloride hydrochloride, nicotinic chloride hydrochloride and 3-aminopyridine were obtained from Tokyo Kasei Industrial Co. $Co(SCN)_2$ and $CoSO_4 \cdot xH_2O$ were obtained from Aldrich Chemical Co. NH_4SCN was obtained from Wako Co.

{[Co(NCS)$_2$(3-pia)$_2$]·2EtOH·11H$_2$O}$_n$ (MOPA-1 ⊃ 2EtOH·11H$_2$O)

An ethanol solution (1.5 mL) of 3-pia (14.9 mg, 0.075 mmol) was gently layered on acetone/chloroform (*v/v* 9:1) solution (1.5 mL) of $Co(SCN)_2$ (6.6 mg, 0.038 mmol), where a mixed solvent of ethanol/chloroform (*v/v* 19:1, 1.5 mL) was placed between the two layers. After seven weeks, red single crystals formed at room temperature. For elemental analysis these crystals were collected, and dried in vacuo for 2 hours. Yield: 88%; elemental analysis calcd (%) for $C_{24}H_{18}CoN_8O_2S_2$ (573.52): C 50.26, H 3.16, N 19.54; found C 50.26, H 3.92, N 18.23.

[Co(NCS)$_2$(3-pia)$_2$] (1)

An ethanol solution (40 mL) of 3-pia (0.198 g, 1 mmol) was added to acetone solution of (20 mL) of $Co(SCN)_2$ (88 mg, 0.50 mmol), and stirred at room temperature for 10 minutes. Then pink powder was collected by filtration and dried in vacuo for 2 hours. During the drying process, the color of the product changed to blue, which is ([Co(NCS)$_2$(3-pia)$_2$]·2.5H$_2$O) in good agreement with that from elemental analysis. Elemental analysis calcd (%) for $C_{24}H_{23}CoN_8O_{4.5}S_2$ (618.56): C 46.60, H 3.75, N 18.12; found C 47.58, H 3.58, N 17.36.

[Co(NCS)$_2$(3-pia)$_2$(H$_2$O)$_2$]$_n$ (2)

Blue powder of **1** was immersed in ethanol/water (*v/v* 2/11) for one month at room temperature, and small (0.05 × 0.05 × 0.02 mm) orange crystals were obtained. Another synthetic method is that an acetonitrile solution (1.5 mL) of 3-pia (29.9 mg, 0.15 mmol) was gently layered on water solution (1.5 mL) of $CoSO_4 \cdot xH_2O$ (11.6 mg, 0.075 mmol) and ammonium thiocyanate (11.4 mg, 0.15 mmol), where a mixed solvent of acetonitrile/water (*v/v* 1:1, 1.5 mL) was placed between the two layers. After three weeks, orange single crystals formed at room temperature. These crystals were collected and dried in vacuo for 2 hours. Yield: 80%; elemental analysis calcd (%) for $C_{24}H_{22}CoN_8O_4S_2$ (609.55): C 47.29, H 3.64, N 18.38; found C 46.93, H 3.64, N 18.80.

{[Co(NCS)$_2$(3-pia)$_2$]·4Me$_2$CO}$_n$ (MOPA-1 ⊃ 4Me$_2$CO)

Blue powder of **1** was immersed in acetone for three weeks at room temperature, resulting in red crystals. For elemental analysis, these crystals were collected and dried in vacuo for 2 hours. Elemental analysis calcd (%) for C$_{24}$H$_{18}$CoN$_8$O$_2$S$_2$ (573.52): C 50.26, H 3.16, N 19.54; found C 49.50, H 3.13, N 19.44.

{[Co(NCS)$_2$(3-pia)$_2$]·4THF}$_n$ (MOPA-1 ⊃ 4THF)

A THF solution (1.5 mL) of 3-pia (29.9 mg, 0.15 mmol) was gently layered on a mixed THF/chloroform (*v/v* 9:1) solution (1.5 mL) of Co(SCN)$_2$ (13.1 mg, 0.079 mmol), where a mixed solvent of THF/chloroform (*v/v* 19:1, 1.5 mL) was placed between the two layers. The layered solution was stood for seven weeks at room temperature, giving red crystals. For elemental analysis, these crystals were collected and dried in vacuo for 2 hours. Yield: 81%; elemental analysis calcd (%) for C$_{24}$H$_{18}$CoN$_8$O$_2$S$_2$ (573.52): C 50.26, H 3.16, N 19.54; found C 49.40, H 3.23, N 19.77.

[Co(NCS)$_2$(3-pna)$_2$]$_n$ (MOPA-2)

An ethanol solution (1.5 mL) of 3-pna (14.9 mg, 0.075 mmol) was gently layered on acetone/chloroform solution (*v/v* 9:1, 1.5 mL) of Co(SCN)$_2$ (6.6 mg, 0.038 mmol), where ethanol/chloroform solution (*v/v* 19:1; 1.5 mL) was layered between the two layers. The solution was stood for seven weeks at room temperature, giving red crystals. These crystals were collected and dried in vacuo for 2 hours. Yield: 78%; elemental analysis calcd (%) for C$_{24}$H$_{18}$CoN$_8$O$_2$S$_2$ (573.52): C 50.26, H 3.16, N 19.54; found C 49.70, H 3.31, N 19.83.

X-ray crystal analysis. A single crystal for **2** was mounted on a glass fiber and coated with epoxy resin, and those for other compounds were sealed in a glass capillary. For each compound X-ray data collections were carried out by a Rigaku Mercury diffractometer with graphite monochromated Mo-Kα radiation (λ = 0.71069 Å) and CCD two-dimensional detector. The sizes of the unit cells were calculated from the reflections collected on the setting angles of seven frames by changing ω by 0.5° for each frame. Two different χ settings were used and ω were changed by 0.5° per frame. Intensity data were collected in 480 frames with a ω scan width of 0.5°. Empirical absorption correction using REQABA[81] was performed for all data. For **MOPA-1 ⊃ 2EtOH·11H$_2$O**, the structure was solved by a direct method using the SIR88 program[82] and expanded using Fourier techniques.[83] For **2**, the structure was solved by a Patterson method using the SAPI91 program[84] and expanded using Fourier techniques.[83] For **MOPA-1 ⊃ 4Me$_2$CO**, the structure was solved by a

direct method using the SIR97 program[85] and expanded using Fourier techniques.[83]   For **MOPA-1 ⊃ 4THF** and **MOPA-2**, the structure was solved by a direct method using the SIR92 program[86] and expanded using Fourier techniques.[83]   The final cycles of the full-matrix least-squares refinements were based on the observed reflections ($I > 5\sigma(I)$ for **MOPA-1 ⊃ 4Me2CO** and **MOPA-1 ⊃ 4THF**, $I > 4\sigma(I)$ for **MOPA-1 ⊃ 2EtOH·11H$_2$O** and **MOPA-2**, $I > 3\sigma(I)$ for **2**).   All calculations were performed using the teXsan crystallographic software package of Molecular Structure Corporation.[87,88]   For all compounds the non-hydrogen atoms were refined anisotropically and all the hydrogen atoms were placed in the ideal positions.   In compound **MOPA-1 ⊃ 2EtOH·11H$_2$O** ethanol molecule containing O(2), C(13) and C(14), and water molecules containing O(3)-O(8) were refined isotropically.   In compound **2** water molecule of O(2) was refined isotropically.   In compound **MOPA-1 ⊃ 4Me$_2$CO** the disorder of the acetone molecule containing O(3) and C(16)-C(18) was found at final stage, and thus its atom positions were isotropically refined under a rigid condition.   In compound **MOPA-1 ⊃ 4THF** the disorder of the THF molecule containing O(3) and C(17)-C(20) was found at final stage, and thus its atom positions were isotropically refined under a rigid condition.

Physical Measurements.   Continuous-wave (CW) EPR spectra were recorded on a JEOL RE-3X spectrometer equipped with an Air-Product Heli-Tran cryostat.   The microwave frequency was measured using an Advantest R5372 frequency counter, and the magnetic field was repeatedly calibrated with diphenylpicrylhydrazyl (DPPH) and Mn^{2+} in MgO.   UV-VIS reflection spectra were recorded on a Hitachi U-3500 spectrophotometer over the range from 400 to 800 nm at room temperature.   Elemental analyses were taken on Yanaco C, H, N Corder MT-5.   IR spectra were recorded on a Perkin-Elmer 2000 FT-IR spectrophotometer with samples prepared as KBr pellets.   X-ray powder diffraction (XRPD) data were collected on a Rigaku RINT-2200HF (Ultima) diffractometer or a SHIMADZU XD-610 X-ray diffractometer by using Cu-Kα radiation.   The adsorption isotherms of gaseous acetone were measured using FMS-BG gravimetric adsorption equipment from BEL JAPAN.

References and Notes

(1) Batten, S. R.; Robson, R. *Angew. Chem. Int. Ed.* **1998**, *37*, 1460-1494.

(2) Yaghi, O. M.; Li, H.; Davis, C.; Richardson, D.; Groy, T. L. *Acc. Chem. Res.* **1998**, *31*, 474-484.

(3) Hagrman, P. J.; Hagrman, D.; Zubieta, J. *Angew. Chem. Int. Ed.* **1999**, *38*, 2638-2684.

(4) Zaworotko, M. J. *Chem. Comm.* **2001**, 1-9.

(5) Desiraju, G. R. *Nature* **2001**, *412*, 397-400.

(6) Fujita, M.; Kwon, J. Y.; Washizu, S.; Ogura, K. *J. Am. Chem. Soc.* **1994**, *116*, 1151-1152.

(7) Robinson, F.; Zawarotko, M. J. *J. Chem. Soc., Chem. Commun.* **1995**, 2413-2414.

(8) Yaghi, O. M.; Li, H. *J. Am. Chem. Soc.* **1996**, *118*, 295-296.

(9) Hoskins, B. F.; Robson, R. *J. Am. Chem. Soc.* **1990**, *112*, 1546-1554.

(10) Kondo, M.; Yoshitomi, T.; Seki, K.; Matsuzaka, H.; Kitagawa, S. *Angew. Chem. Int. Ed.* **1997**, *36*, 1725-1727.

(11) Li, H.; Eddaoudi, M.; Groy, T. L.; Yaghi, O. M. *J. Am. Chem. Soc.* **1998**, *120*, 8571-8572.

(12) Kondo, M.; Okubo, T.; Asami, A.; Noro, S.-I.; Yoshitomi, T.; Kitagawa, S.; Ishii, T.; Matsuzaka, H.; Seki, K. *Angew. Chem. Int. Ed.* **1999**, *38*, 140-143.

(13) Seo, J. S.; Whang, D.; Lee, H.; Jun, S. I.; Oh, J.; Jeon, Y. J.; Kim, K. *Nature* **2000**, *404*, 982-986.

(14) Kiang, Y.-H.; Gardner, G. B.; Lee, S.; Xu, Z.; Lobkovsky, E. B. *J. Am. Chem. Soc.* **1999**, *121*, 8204-8215.

(15) Sawaki, T.; Aoyama, Y. *J. Am. Chem. Soc.* **1999**, *121*, 4793-4798.

(16) Li, H.; Eddaoudi, M.; O'Keeffe, M.; Yaghi, O. M. *Nature* **1999**, *402*, 276-279.

(17) Chui, S. S.-Y.; Lo, S. M.-F.; Charmant, J. P. H.; Orpen, A. G.; Williams, I. D. *Science* **1999**, *283*, 1148-1150.

(18) Eddaoudi, M.; Li, H.; Yaghi, O. M. *J. Am. Chem. Soc.* **2000**, *122*, 1391-1397.

(19) Chen, B.; Eddaoudi, M.; Reineke, T. M.; Kampf, J. W.; O'Keeffe, M.; Yaghi, O. M. *J. Am. Chem.Soc.* **2000**, *122*, 11559-11560.

(20) Biradha, K.; Hongo, Y.; Fujita, M. *Angew. Chem. Int. Ed.* **2000**, *39*, 3843-3845.

(21) Noro, S.-I.; Kitagawa, S.; Kondo, M.; Seki, K. *Angew. Chem. Int. Ed.* **2000**, *39*, 2082-2084.

(22) Chen, B.; Eddaoudi, M.; Hyde, S. T.; O'Keeffe, M.; Yaghi, O. M. *Science* **2001**, *291*, 1021-1023.

(23) Eddaoudi, M.; Moler, D. B.; LI, H.; Chen, B.; Reineke, T. M.; O'keeffe, M.; Yaghi, O. M. *Acc. Chem. Res.* **2001**, *34*, 319-330.

(24) Kitagawa, S.; Kondo, M. *Bull. Chem. Soc. Jpn.* **1998**, *71*, 1739-1753.

(25) Min, K. S.; Suh, M. P. *Chem. Eur. J.* **2001**, *7*, 303-313.

(26) Tabares, L. C.; Navarro, J. A. R.; Salas, J. M. *J. Am. Chem. Soc.* **2001**, *123*, 383-387.

(27) Choi, H. J.; Lee, T. S.; Suh, M. P. *Angew. Chem. Int. Ed.* **1999**, *38*, 1405-1408.

(28) Pan, L.; Woodlock, E. B.; Wang, X.; Zheng, C. *Inorg. Chem.* **2000**, *39*, 4174-4178.

(29) Li, H.; Davis, C. E.; Groy, T. L.; Kelley, D. G.; Yaghi, O. M. *J. Am. Chem. Soc.* **1998**, *120*, 2186-2187.

(30) Min, K. S.; Suh, M. P. *J. Am. Chem. Soc.* **2000**, *122*, 6834-6840.

(31) Jung, O.-S.; Kim, Y. J.; Lee, Y.-A.; Park, J. K.; Chae, H. K. *J. Am. Chem. Soc.* **2000**, *122*, 9921-9925.

(32) Beauvais, L. G.; Shores, M. P.; Long, J. R. *J. Am. Chem. Soc.* **2000**, *122*, 2763-2772.

(33) Kiritsis, V.; Michaelides, A.; Skoulika, S.; Golhen, S.; Ouahab, L. *Inorg. Chem.* **1998**, *37*, 3407-3410.

(34) Jung, O.-S.; Kim, Y. J.; Lee, Y.-A.; Chae, H. K.; Jang, H. G.; Hong, J. *Inorg. Chem.* **2001**, *40*, 2105-2110.

(35) Noro, S.-i.; Kitaura, R.; Kondo, M.; Kitagawa, S.; Ishii, T.; Matsuzaka, H.; Yamashita, M. *J. Am. Chem. Soc.* **2002**, *124*, 2568-2583.

(36) Larionova, J.; Chavan, S. A.; Yakhmi, J. V.; Froystein, A. G.; Sletten, J.; Sourisseau, C.; Kahn, O. *Inorg. Chem.* **1997**, *36*, 6374-6381.

(37) Buss, C. E.; Anderson, C. E.; Pomije, M. K.; Lutz, C. M.; Britton, D.; Mann, K. R. *J. Am. Chem. Soc.* **1998**, *120*, 7783-7790.

(38) Soldatov, D. V.; Ripmeester, J. A.; Shergina, S. I.; Sokolov, I. E.; Zanina, A. S.; Gromilov, S. A.; Dyadin, Y. A. *J. Am. Chem. Soc.* **1999**, *121*, 4179-4188.

(39) Nossov, A. V.; Soldatov, D. V.; Ripmeester, J. A. *J. Am. Chem. Soc.* **2001**, *123*, 3563-3568.

(40) Soldatov, D. V.; Henegouwen, A. T.; Enright, G. D.; Ratcliffe, C. I.; Ripmeester, J. A. *Inorg. Chem.* **2001**, *40*, 1626-1636.

(41) Endo, K.; Sawaki, T.; Koyanagi, M.; Kobayashi, K.; Masuda, H.; Aoyama, Y. *J. Am. Chem. Soc.* **1995**, *117*, 8341-8352.

(42) Thaimattam, R.; Xue, F.; Sarma, J. A. R. P.; Mak, T. C. W.; Desiraju, G. R. *J. Am. Chem. Soc.* **2001**, *123*, 4432-4445.

(43) MacNicol, D. D.; McKendrick, J. J.; Wilson, D. R. *Chem. Soc. Rev.* **1978**, *7*, 65-87.

(44) Ung, A. T.; Bishop, R.; Craig, D. C.; Dance, I. G.; Scudder, M. L. *J. Chem. Soc., Chem. Commun.* **1991**, 1012-1014.

(45) Ghadiri, M. R.; Granja, J. R.; Milligan, R. A.; McRee, D. E.; Khazanovich, N. *Nature* **1993**, *366*, 324-327.

(46) Ung, A. T.; Gizachew, D.; Bishop, R.; Scudder, M. L.; Dance, I. G.; Craig, D. C. *J. Am. Chem. Soc.* **1995**, *117*, 8745-8756.

(47) Hartgerink, J. D.; Granja, J. R.; Milligan, R. A.; Ghadiri, M. R. *J. Am. Chem. Soc.* **1996**, *118*, 43-50.

(48) Kondo, M.; Asami, A.; Chang, H.-c.; Kitagawa, S. *Cryst. Eng.* **1999**, *2*, 115-122.

(49) The size is measured by considering van der Waals radii for constituting atoms. Hereafter, all the size-estimation of pore is made in this way.

(50) The least squared plane is calculated with cobalt atoms at the vertices of a double edged axe-shaped motif.

(51) Blake, A. J.; Hill, S. J.; Hubberstey, P.; Li, W.-S. *J. Chem. Soc., Dalton Trans.* **1997**, 913-914.

(52) Zaworotko, M. J. *Chem. Soc. Rev.* **1994**, 283-288.

(53) Lu, J.; Paliwala, T.; Lim, S. C.; Yu, C.; Niu, T.; Jacobson, A. J. *Inorg. Chem.* **1997**, *36*, 923-929.

(54) Park, S. H.; Kim, K. M.; Lee, S.; Jung, O.-S. *Bull. Korean Chem. Soc.* **1998**, *19*, 79-82.

(55) The XRPD patterns of the microcrystalline sample is in good agreement with the simulated one.

(56) Bryan, R. F.; Manning, A. R. *Chem. Commun.* **1968**, 1220-1222.

(57) Laing, M.; Horsfield, E. *Chem. Commun.* **1969**, 902-903.

(58) Lever, A. B. P. *Inorganic Electronic Spectroscopy*, 2nd edition, Elsevier, Amsterdam **1984**.

(59) Cotton, F. A.; Goodgame, D. M. L.; Sacco, M. G. A. *J. Am. Chem. Soc.* **1961**, *83*, 4157-4161.

(60) Cotton, F. A.; Goodgame, M. *J. Am. Chem. Soc.* **1961**, *83*, 1777-1780.

(61) Liptay, G.; Burger, K.; Papp-Molnar, E.; Szebeni, S.; Ruff, F. *J. Inorg. Nucl. Chem.* **1969**, *31*, 2359-2366.

(62) Nakamoto, K. *Infrared and Raman Spectra of Inorganic and Coordination Compounds*, 5th Edition, Wiley, New York, **1997**.

(63) Kim, H. S.; Hartgerink, J. D.; Ghadiri, M. R. *J. Am. Chem. Soc.* **1998**, *120*, 4417-4424.

(64) Bellamy, L. J. *Advances in Infrared Group Frequencies*, Methuen, London, **1968**.

(65) Hyperfine coupling (HFC) is not included for the peaks g'_2, g'_3.

(66) HFC is not included for this compound.

(67) Weckhuysen, B. M.; Verberckmoes, A. A.; Uytterhoeven, M. G.; Mabbs, F. E.; Collison, D.; Boer, E. d.; Schoonheydt, R. A. *J. Phys. Chem. B* **2000**, *104*, 37-42.

(68) Bencini, A.; Benelli, C.; Gattenschi, D.; Zanchini, C. *Inorg. Chem.* **1980**, *19*, 1301-1304.

(69) Banci, L.; Benelli, C.; Gatteschi, D.; Mani, F. *Inorg. Chem.* **1982**, *21*, 1133-1136.

(70) Makinen, M. W.; Kuo, L. C.; Yim, M. B.; Wells, G. B.; Fukuyama, J. M.; Kim, J. E. *J. Am. Chem. Soc.* **1985**, *107*, 5245-5255.

(71) Drulis, H.; Dyrek, K.; Hoffmann, K. P.; Hoffmann, S. K.; Weselucha-Birczynska, A. *Inorg. Chem.* **1985**, *24*, 4009-40125.

(72) Pilbrow, J. R. *J. Mag. Reson.* **1978**, *31*, 479-490.

(73) Griffith, J. S. *In The Theory of Transition Metal Ions*, Cambridge University Press, London, **1961**.

(74) Abragham, A.; Pryce, M. H. *Proc. Roy. Soc. A* **1951**, *205*, 173-191.

(75) In the calculation, the effective Lande factors α, α' were set as 1.5, which is the value for the $^4T_1(F)$ state.

(76) Bencini, A.; Benelli, C.; Gatteschi, D.; Zanchini, C. *Inorg. Chem.* **1979**, *18*, 2526-2528.

(77) Bencini, A.; Benelli, C.; Gatteschi, D.; Zanchini, C. *Inorg. Chem.* **1980**, *19*, 3839-3842.

(78) Yaghi, O. M.; Li, G.; Li, H. *Nature* **1995**, *378*, 703-706.

(79) Li, D.; Kaneko, K. *Chem. Phys. Lett.* **2001**, *335*, 50-56.

(80) Kitaura, R.; Fujimoto, K.; Noro, S.-i.; Kondo, M.; Kitagawa, S. *Angew. Chem. Int. Ed.* **2002**, *41*, 133-135.

(81) Jacobson, R. A. REQABA Empirical Absorption Correction Version 1.1-0301998, Molecular Structure Corp. The Woodlands, TX, (USA) **1996-1998**.

(82) Burla, M. C.; Camalli, M.; Cascarano, G.; Giacovazzo, C.; Polidori, G.; Spagna, R.; Viterbo, D. *J. Appl. Cryst.* **1989**, *22*, 389-303.

(83) Beurskens, P. T.; Admiraal, G.; Beurskens, G.; Bosman, W. P.; deGelder, R.; Israel, R.; Smits, J. M. M., The DIRDIF-94 program system, Technical Report of the Crystallography Laboratory, University of Nijmegen, (The Netherlands), **1994**.

(84) Hai-Fu, F., Structure Analysis Programs with Intelligent Control, Rigaku Corporation, Tokyo, Japan, **1991**.

(85) Altomare, A.; Burla, M. C.; Camalli, M.; Cascarano, G. L.; Giacovazzo, C.; Guagliardi, A.; Moliterni, A. G. G.; Polidori, G.; Spagna, R. *J. Appl. Cryst.* **1999**, *32*, 115-119.

(86) Altomare, A.; Burla, M. C.; Camalli, M.; Cascarano, M.; Giacovazzo, C.; Guagliardi, A.; Polidori, G. *J. Appl. Cryst.* **1994**, *27*, 435.

(87) teXsan Crystal Structure Analysis Package, Molecular structure Corporation **1985, 1992**.

(88) teXsan Crystal Structure Analysis Package, Molecular structure Corporation **1985, 1999**.

Chapter 5

A Contrivance for a Dynamic Porous Framework.   Cooperative Guest Adsorption Based on Square Grids Connected by Amide-Amide Hydrogen Bonds

Abstract

Flexible porous coordination polymers containing amide groups as a function origin have been synthesized and categorized as "Metal-Organic Polymer with Amide Groups" (**MOPA**). Bispyridyl ligands with a spacer of amide group afford 2-dimensional (2-D) motifs with a deformed square grid, resulting in 3-dimensional (3-D) frameworks of $[Co(NO_3)_2(3\text{-pna})_2]_n$ (**MOPA-3**), $[Co(Br)_2(3\text{-pna})_2]_n$ (**MOPA-4**) and $\{[Co(NCS)_2(4\text{-peia})_2]\cdot 4Me_2CO\}_n$ (**MOPA-5 ⊃ 4Me₂CO**) (3-pna = *N*-3-pyridylnicotinamide, 4-peia = *N*-(2-Pyridin-4-yl-ethyl)-isonicotinamide), where the 2-D motifs are bound by complementary hydrogen bond between the amide groups.   In the case of the **MOPA-5 ⊃ 4Me₂CO**, the amide groups form a contrivance for a dynamic porous framework because of their relevant position and orientation in the mutual nearest neighboring motifs. Consequently, **MOPA-5 ⊃ 4Me₂CO** shows *amorphous* (non-porous)-to-*crystal* (porous) structural rearrangement in Me_2CO adsorption/desorption process, where 2-D motifs are maintained.   This cooperative phenomena associated with guest inclusion is examined by thermodynamic analysis. The rearrangement in Me_2CO adsorption is induced by weak dispersive force ($\Delta H_{ad} = -25$ kJ/mol), which is comparable to acetone vaporization enthalpy ($\Delta H_{vap} = 30.99$ kJ/mol).   Our results imply that porous coordination polymer is often much more dynamic than generally believed.

Introduction

In a decade, coordination polymers have been extensively studied and added a new dimension to materials-directed coordination chemistry. The synthetic method is rapidly developing from accidental to rational stage,[1-10] affording porous frameworks, which could be relevant for storage and exchange of specific guests, catalysis and guest alignment.[11-15] One of the recent targets for the porous coordination polymers is a robust framework such as inorganic zeolites,[10,16] and large pores with high specific surface area.[17] In addition to such targets, an approach to create other properties, characteristic of porous coordination polymers, has been explored and the most interesting is a dynamic micropore, which responds to a chemical stimulus.[18,19] This properties could come from a sort of "soft" framework with bistability, whose two states go back from and forth to one of counter parts; a system could exist in one or two states for the same values of external field parameters. Recently, several articles[19-37] have been reported about dynamic porous coordination polymers which show framework transformation accompanying with adsorption/desorption of guest molecules as shown in equation 1,
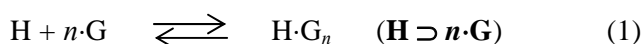
$$H + n \cdot G \quad \rightleftharpoons \quad H \cdot G_n \quad (\mathbf{H} \supset \mathbf{n} \cdot \mathbf{G}) \qquad (1)$$

where H is apohost, G is guest molecule, and n is stoichiometry of accommodated guest vs. apohost.[38] These new types of porous coordination polymers are expected to provide characteristic functionality such as highly selective guest inclusions[19,30] and reversible magnetic modulation.[22,37,39,40]

There are two kinds of forms for apohost; one is "crystal" and the other is "amorphous" (Scheme 1). When an apohost is amorphous, such structural transformation is regarded as "recoverable collapse". Therefore, the approach to create such a transformation could be applicable to brittle materials systems.[41] A unique adsorption property is expected to this amorphous-to-crystal phase transformation. Several coordination polymers recover their crystallinity with the aid of *liquid* solvents, like as a recrystallization process.[33-35] On the other hand, the transformation to a crystal form merely upon exposure to guest *vapor* has been observed for several compounds.[36,37] A clue for this flexible but ordered structure is to set a contrivance for a framework, by which amorphous-to-crystal transformation could be realized. For the purpose, it is useful to take advantages of organic ligands, which possess weak interaction such as hydrogen bond, and therefore the utilization could have great contribution to a wide range of framework formation.
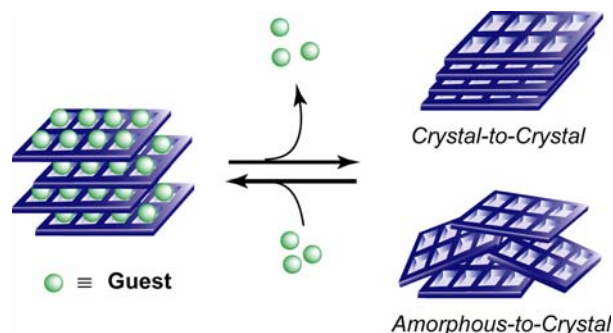
Scheme 1.

Although there are various combinations of hydrogen bond-type gadgets in structural motifs, a layer-type motif would operate well for creating dynamic but reversible porous framework, which exhibits structural transformation caused by external stimuli, the event occurring either within the layer or in between the layers.[19,24]   When py-Xi (Yi)-py (py = pyridine, spacer Xi and Yi = functional group) type ligands are employed, 2-D networks are readily formed; straight type rod ligands have so far afforded a square grid,[12,24,42-56] rectangular grid,[57-61] herringbone, brick wall, bilayer and so on.[7,8]   Among all possible these networks from py-Xi (Yi)-py, the square grid (Xi = Yi) or rectangular grid (Xi ≠ Yi) polymers are of particular importance because they could control over the spatial dimensions of grids and chemistry of the interior of channels by modifying the spacer group (Xi and Yi) in the ligand.   Once the size of channels in such a square-grid system is fixed, another important factor is the stacking modes of the grids in the nearest neighbor layers.   It has been reported that for coordination polymers of planar square grid, three types of stacking modes are typically observed as follows (Scheme 2);

i) Edge-to-edge type: grids in the nearest neighbor layers eclipse in edge-to-edge fashion (or short-slipped manner), designated as …AAA….[19,24,46,51]

ii) Interpenetration type: square grids are intimately inter-locked with other(s) in the same sort of topological relationship.[42,49,54,56,62,63]

iii) Staggered type: grids deposit on each other in an offset fashion, designated as …ABAB… (or …ABCABC…).[12,43-48,50-53,55]

Scheme 2.

The types ii) and iii) hinder effective pores, since the cavities in a layer are usually obstructed by adjacent layers. However, even if the interpenetration or staggered manner occurs, we expect the presence of voids for an inclusion of small-molecule when we use longer ligands.[43,49] Square grids of $\{[Ni(L)_2(NO_3)_2]\cdot 4(o\text{-xylene})\}_n$ (L = py-PhPh-py, py = pyridine) in staggered manner afford large pores,[43] resulting in a 3-D held porous network.

On this background, we focus on stacking modes of square grids controlled by hydrogen bond, which are associated with dynamic pores. "Metal-Organic Polymer with Amide Groups" (**MOPA**) is one of candidates in relevant to those having square grids with hydrogen bond in staggered fashion, where **MOPA** including L-Amide-L type ligand (L = ligand containing coordination donor atom) form complementary hydrogen bonding (so-called β-sheet) between 2D motifs. Such form of hydrogen bond is similar to that of amide binding of cyclic peptide,[64,65] and useful for achieving pores in coordination polymers. In this manuscript, **MOPA**s (**MOPA-3 ~ 5**) based on this β-sheet were synthesized (Scheme 3), characterized by X-ray crystallography and sorption measurements, and particularly discussed about the adsorption/structural transformation of **MOPA-5 $\supset$ 4Me$_2$CO** based on thermodynamic analysis.

3-pia, 3-pna

4-peia

Scheme 3.

Table 1. Crystal Data and Structure Refinement for $[Co(NO_3)_2(3\text{-pna})_2]_n$ (**MOPA-3**), $[CoBr_2(3\text{-pna})_2]_n$ (**MOPA-4**) and $\{[Co(NCS)_2(4\text{-peia})_2]\cdot 4Me_2CO\}_n$ (**MOPA-5 ⊃ 4Me₂CO**).

Compoound	MOPA-3	MOPA-4	MOPA-5 ⊃ 4Me₂CO
Chemical formula	$C_{22}H_{18}CoN_8O_8$	$C_{22}H_{16}Br_2CoN_6O_2$	$C_{40}H_{26}CoN_8O_6S_2$
formula weight	581.37	615.15	837.75
crystal dimensions [mm]	$0.40 \times 0.30 \times 0.20$	$0.24 \times 0.20 \times 0.10$	$0.50 \times 0.40 \times 0.30$
crystal system	orthorhombic	orthorhombic	monoclicic
space group	$Pbcn$	$Ccca$	$P2_1/c$
a [Å]	18.3004(6)	10.481(7)	11.115(3)
b [Å]	10.759(3)	19.03(1)	22.046(7)
c [Å]	11.458(2)	10.894(8)	9.717(3)
α [°]	90	90	90
β [°]	90	90	100.834(7)
γ [°]	90	90	90
V [Å³]	2255.9(8)	2172(2)	2338(1)
Z	4	4	2
ρ_{calcd} [g cm⁻³]	1.712	1.881	1.190
$F(000)$	1188	1212	858
μ [mm⁻¹]	0.832	4.515	0.505
radiation [Å]	0.71069	0.71069	0.71069
temperature [K]	223	293	293
2θ range	$5.5° < 2\theta < 54.1°$	$5.5° < 2\theta < 54.9°$	$5.5° < 2\theta < 55.0°$
GOF	1.45	1.44	2.58
no. of data collected	11611	11978	24767
no. of unique data	1673	1211	5324
no. of obsd data	1673	1211	2526 ($I > 5.00\sigma(I)$)
no. of variables	167	86	195
$R^{[a]}$	0.066	0.053	0.083
R_w	0.125 [b]	0.137 [b]	0.132 [c]

[a] $R = \Sigma||Fo| - |Fc||/\Sigma|Fo|$, [b] $R_w = \{\Sigma w[(Fo^2 - Fc^2)^2]/[(\Sigma wFo^2)^2]\}^{1/2}$, [c] $R_w = [\Sigma w(|Fo| - |Fc|)^2/(\Sigma wFo^2)]^{1/2}$.

Results and Discussion

Crystal structures.   Crystallographic data for **MOPA**s are summarized in Table 1.

   [Co(NO₃)₂(3-pna)₂]ₙ (MOPA-3).   In **MOPA-3**, the cobalt(II) center is octahedrally coordinated to each nitrogen atom of four 3-pna in equatorial plane, where two types of the nitrogen donors, carbonyl pyridyl (N^C) and amino pyridyl (N^A), are located in a *cis* fashion (Figure 1a).   The two Co-N bond distances are close to each other; Co-N(1) = 2.174(5) Å, Co-N(2) = 2.167(5) Å.   In addition, the two oxygen atoms of NO_3^- groups are coordinated axially with the distance of 2.089(5) Å.   The *cis* N-Co-N or N-Co-O bond angles range from 83° to 104°, indicative of a distorted octahedral environment.   The cobalt ions are linked by 3-pna to yield a honeycomb-shaped grid with the dimension of 10.8 Å × 10.8 Å.   The square grids do not interpenetrate, affording a layered structure.   It is worth noting that hydrogen-bonding links of the NH---O=C (N---O = 3.170(7) Å) groups between the adjacent layers create complementary-amide binding network (Figure 1b).   Adjacent layers are slipped in one direction by approximately 5.7 Å so that the axial NO_3^- groups on one layer project into the channels along the *b* axis.   The framework contains no solvent molecules, attributed to a closely packed layer structure with hydrogen bonds between the layers.   The nearest Co-Co distance is about 10.8 Å in a layer, and 7.5 Å in the adjacent layer.

   [Co(Br)₂(3-pna)₂]ₙ (MOPA-4).   In **MOPA-4**, the cobalt(II) center is also coordinated to the four nitrogen atoms of 3-pna in equatorial plane (Figure 1c).   In addition, two bromide atoms are coordinated axially with the distance of 2.594(2) Å.   The *trans* Br-Co-Br bond angle is 180°.   The *cis* N-Co-N bond angles range from 87° to 93° indicative of a distorted octahedron.   The cobalt ions are linked by 3-pna to afford a honeycomb-shaped grid with the dimension of 10.9 Å × 10.9 Å (Figure 1d), as well as **MOPA-3**.   These layers also do not interpenetrate, affording a layered structure.   As shown in Figure 1c, the amide moiety is disordered about the twofold axis running through the 3-pna ligands.   Noticeably, the 2-D layers stack in a slipped fashion along the *a* axis with hydrogen bonding links of NH---O=C (N---O = 3.263(8) Å) between the layers.   Coordinated bromide anions on one layer project into the channels along the *c* axis with close distance of Br---Br = 5.294(4) Å.   The nearest Co-Co distance is about 10.5 Å in a layer, and 7.6 Å in the adjacent layer.

   {[Co(NCS)₂(4-peia)₂]·4Me₂CO}ₙ (MOPA-5 ⊃ 4Me₂CO).   In **MOPA-5 ⊃ 4Me₂CO**, the cobalt(II) center is octahedrally coordinated to each nitrogen atom of four 4-peia in equatorial plane, where two types of the nitrogen donors, carbonyl pyridyl (N^C) and ethyl pyridyl (N^E), are located in a trans fashion (Figure 2a).   All the Co-N bond distances are close to each other; Co-N^C = 2.220(5) Å, Co-N^E = 2.191(6) Å.   The trans N-Co-N bond angles for NCS and pyridine ligands are 180°.   The cis N-Co-N bond angles range from 88.2(2)° to 91.8(2)°.   The NCS groups are coordinated
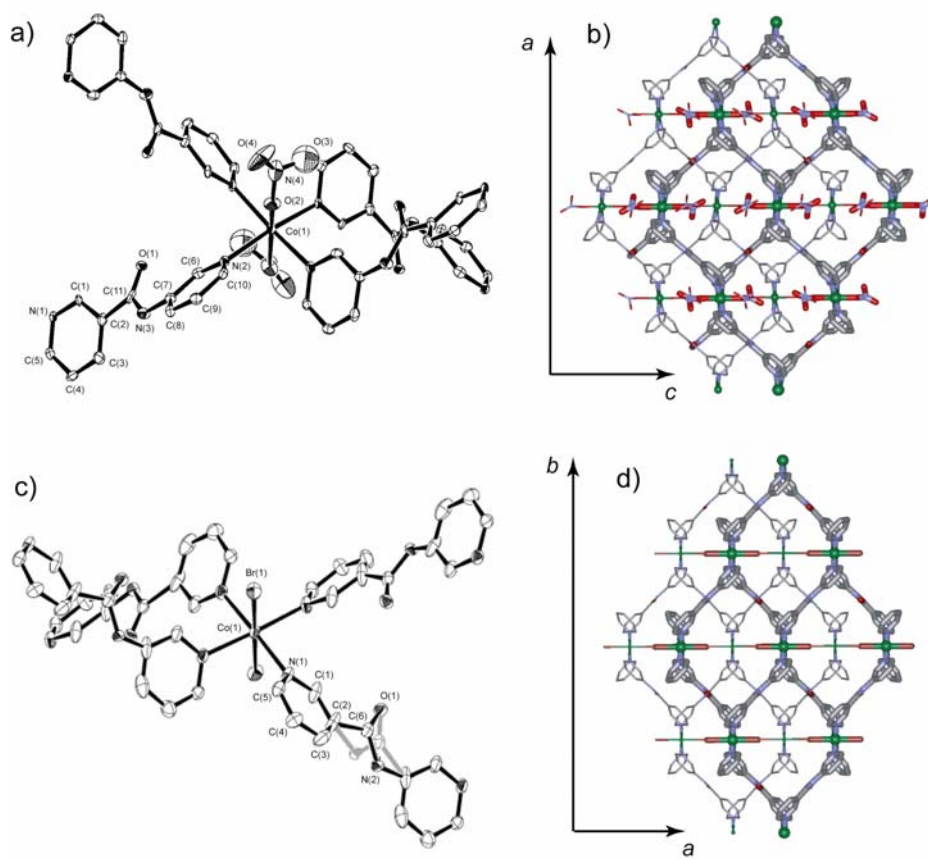
Figure 1. Crystal structure of [Co(NO$_3$)$_2$(3-pna)$_2$]$_n$ (**MOPA-3**) and [Co(Br)$_2$(3-pna)$_2$]$_n$ (**MOPA-4**). (a) ORTEP drawing of the cobalt center of **MOPA-3** at the 30% probability level. Hydrogen atoms are omitted for clarity. (b) Crystal view of **MOPA-3** along the *b* axis. Two layers stack with hydrogen bond of amide moieties between the layers. The thin and thick lines show the upper and lower layer, respectively. (c) ORTEP drawing of the cobalt center of **MOPA-4** at the 30% probability level. Hydrogen atoms are omitted for clarity. The amide moiety is disordered about the twofold axis running through the 3-pna ligand. (d) Crystal view of **MOPA-4** along the *c* axis. Two layers stack with hydrogen bond of amide moieties between the layers. The thin and thick lines show the upper and lower layer, respectively.

axially in a slightly bending mode with the angles of 172.5(6)° (Co-N(4)-C(14)) and 177.3(8)° (N-C-S). The cobalt ions are linked by 4-peia to form a 2-D layer composed of a square grid motif with the dimension of 15.8 Å × 15.8 Å. Interestingly, the adjacent layers stack along the *c* axis with a offset by 0.5(*a* + *b*) along the *ab*-plane, and the NCS group protrudes through the midpoint of the cavity of the adjacent layer eschewing interpenetration (Figure 2b). It is worth noting that hydrogen-bonding links of the NH---O=C (N---O = 2.780(7) Å) groups between the adjacent layers create complementary-amide binding network. A channel with the dimension of 4.4 Å × 4.4 Å is observed,[66] running along the *c* axis, in spite of the mutual slip of the neighboring layers (Figure 2b and 2c). These channels create 46 % void, where acetone molecules are accommodated with no

103
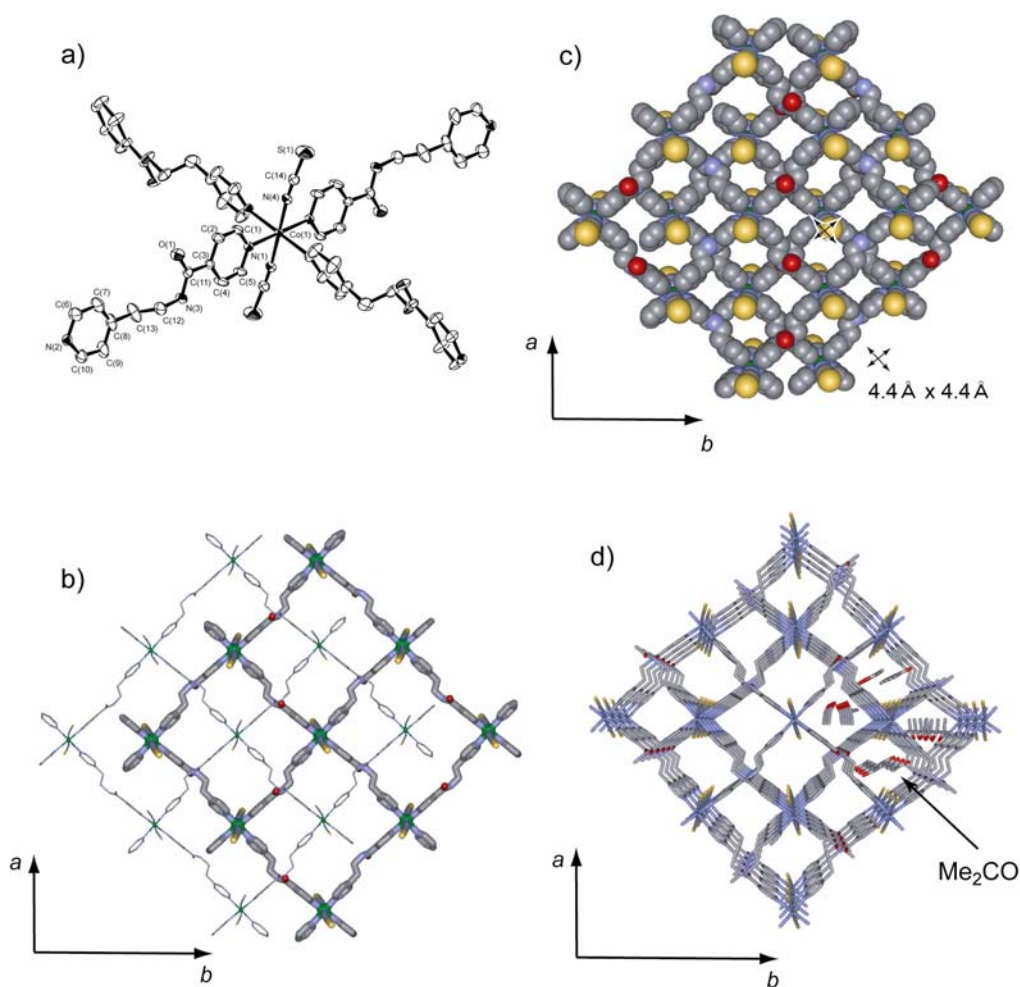
Figure 2. Crystal structure of {[Co(NCS)$_2$(4-peia)$_2$]·4Me$_2$CO}$_n$ (**MOPA-5 ⊃ 4Me$_2$CO**) and {[Co(NCS)$_2$(4-peia)$_2$]·4THF}$_n$ (**MOPA-5 ⊃ 4THF**). (a) ORTEP drawing of the cobalt center of **MOPA-5 ⊃ 4Me$_2$CO** at the 30% probability level. Hydrogen atoms and acetone molecules are omitted for clarity. (b) Two layers stack of **MOPA-5 ⊃ 4Me$_2$CO** along the *c* axis with hydrogen bond of amide moieties between the layers. Acetone molecules are omitted for clarity. The thin and thick lines show the upper and lower layer, respectively. (c) Space-filling representation for two layers stacking in the crystal structure of **MOPA-5 ⊃ 4Me$_2$CO** along the *c* axis. (d) Crystal structure of **MOPA-5 ⊃ 4Me$_2$CO** with acetone molecules along the *c* axis.

significant interaction (Figure 2d). All pyridine planes in this crystal are parallel to the *c* axis, forming interior panels, and, therefore, resulting in hydrophobic space. Acetone molecules show a guest-column in the channel but highly disordered. The ethylene moiety in 4-peia assumes a staggered ethane-conformation about the C-C bond. The hydrogen bonds between the amide groups afford a dipole vector array, however these dipole vectors are cancelled out with neighboring one. Compound **MOPA-5 ⊃ 4THF**, which includes THF molecules, has the similar cell parameters and isostructural with **MOPA-5 ⊃ 4Me$_2$CO**. **MOPA-5 ⊃ 4THF** also form 2-D layer

which are connected by hydrogen-bonding link (NH---O=C (N---O = 2.79(1) Å) between the adjacent layers as shown in Supporting Information.

Comparison of MOPA-3 ~ 5 with Other Square Grdis.

Selected 2-D square grids comprised of octahedral metal cations and bpy (4,4'-bipyridine) analogues (= 1 : 2) are summarized in Table 2. From $Co(NCS)_2$ and bpy analogues (= 1 : 2), 2-D layers are rationally obtained because two thiocyanate ions tend to terminally coordinate to a cobalt(II) ion at axial position.[19,48,49,56] What is important at this stage is mutual relationship between the layer motifs. Among compounds synthesized to date, a ligand longer than bpy prefers the formation of interpenetrating (type-(ii)) to noninterpenetrating grid structures (See Scheme 2),[1] precluding their frames from porous materials. On the other hand, short bridging ligands favor the formation of the staggered fashion of grids in the adjacent layers (type-(iii)), resulting in no pores. Therefore, in order to create useful cavities, a certain gadget is required. Inspection of Table 2 reveals that the gadgets are (1) template of guests,[43,46] or (2) interlayer hydrogen bond with a staggered fashion.[19,43,46]

To attain a pore frame, each grid must preclude interpenetration. Herein, **MOPA**s fulfil such requirement because complementary hydrogen bond between amide moieties in neighboring layers take an important role in superposing each layers in staggered fashion. In **MOPA-3** and **MOPA-4**, in spite of the difference in counter anions, all square grids show staggered relationship ascribed to complementary-amide binding. Although interpenetration is eschewed, "ABAB" stacking does not afford channels due to cavities occupied with metals and anions in neighbouring layers. In **MOPA-5 ⊃ 4Me₂CO** containing relative longer 4-peia ligand, 1-dimensional (1-D) channels successfully form, because the SCN groups protrude perpendicular to layers. Moreover, 2-D layers of $\{[Co(NCS)_2(3\text{-pia})_2]\cdot2EtOH\cdot11H_2O\}_n$ (**MOPA-1 ⊃ 2EtOH·11H₂O**) and $\{[Co(NCS)_2(3\text{-pia})_2]\cdot4Me_2CO\}_n$ (**MOPA-1 ⊃ 4Me₂CO**) (3-pia = *N*-3-pyridylisonicotinamide) form edge-to-edge manner (type-(i)) and afford channels, which accommodate guest molecules by hydrogen bond with the amide group.[19] Therefore, **MOPA**s are suitable for construction of channels.

105

Table 2. Summary of the Bridging Ligands, Ligand Lengths, Open Areas and Stacking Manners found in selected Square Grids.

Ligand	Ligand length [Å]	Open area [Å^2] [c]	Stacking manner [d]	Metal + Anion	Reference
pyrazine	2.8	none	(iii)	Co(II) + SCN$^-$	48
pyrazine	2.8	none	(iii)	Zn(II) + Br$^-$	47
4,4'-bipyridine	7.1	none	(ii)	Zn(II) + SiF$_6^-$	42
4,4'-bipyridine	7.1	6.8	(iii)	Cd(II) + NO$_3^-$	12
4,4'-bipyridine	7.1	16.4	(iii)	Co(II) + SCN$^-$	48
py-CH$_2$CH$_2$-py	9.4	none	(ii)	Co(II) + SCN$^-$	56
py-CHCH-py	9.5	none	(ii)	Co(II) + SCN$^-$	56
mppe [a]	9.5	none	(ii)	Co(II) + SCN$^-$	63
py-Azo-py	9.0	9.0	(ii)	Co(II) + SCN$^-$	49
py-Antharacene-py	11.4	17.6	(i)	Ni(II) + NO$_3^-$	46
py-Ph-py	11.4	4.2	(iii), HB [e]	Ni(II) + NO$_3^-$	46
py-PhPh-py	15.7	47.3	(iii), HB [e]	Ni(II) + NO$_3^-$	43
py-X-py [b]	19.8	11.5	(iii)	Cu(II) + NO$_3^-$	44
3-pia (**MOPA-1 ⊃ 2EtOH·11H$_2$O**)	8.5	9.0 × 2.5	(i)	Co(II) + SCN$^-$	19
3-pia (**MOPA-1 ⊃ 4Me$_2$CO**)	8.5	3.5 × 10.5	(i)	Co(II) + SCN$^-$	19
3-pna (**MOPA-2**)	8.4	none	(iii), HB [e]	Co(II) + SCN$^-$	19
4-peia (**MOPA-5 ⊃ 4Me$_2$CO**)	11.4	19.4	(iii), HB [e]	Co(II) + SCN$^-$	this study

[a] 1-methyl-1'-(4-pyridyl)-2-(4-pyrimidyl)ethylene.   [b] 9,9-bis[(S)-2-methylbutyl]-2,7-bis(4-pyridylethynyl)fluorine.   [c] The size is measured by considering the van der Waals radii for constituent atoms.   [d] three types of packing manner are typically observed; (i) edge-to-edge manner, (ii) interpenetration and (iii) staggered manner (See Scheme 2).   [e] Each sheet is connected with adjacent sheet by interlayer hydrogen bond.

106

Thermal Analysis of MOPA-5 ⊃ 4Me₂CO.

   As seen in crystal structure analysis, **MOPA-5 ⊃ 4Me₂CO** includes acetone molecules as a guest. The acetone desorption was monitored by thermal gravimetry (TG). Figure 3 shows the TG thermograms for **MOPA-5 ⊃ 4Me₂CO** over the temperature range from 30 to 500 °C at a heating rate of $\beta = 5$ °C/min. The observed weight loss of acetone molecules is in agreement with that calculated for the corresponding crystal structure. The TG data for compound **MOPA-5 ⊃ 4Me₂CO** indicates two stages for weight loss of the guest molecules; three acetone molecules (observed 19.0 %, calculated 20.2 %) in the temperature range 30 ~ 80 °C, immediately followed by another weight loss of one acetone molecule (observed 4.3 %, calculated 6.7 %). The resultant species, $[Co(NCS)_2(4\text{-peia})_2]_n$ (**MOPA-5**), is stable up to 215 °C, and then gradually decomposes with loss of two 4-peia ligands (observed 53.7 %, calculated 52.7 %).
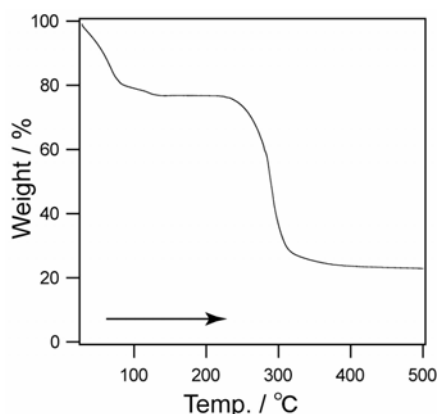
Figure 3. TG analysis of **MOPA-5 ⊃ 4Me₂CO** over the temperature range from 30 to 500 °C at a heating rate of $\beta = 5$ °C/min under the N₂ atmosphere.

Recoverable Collapsing of MOPA-5 ⊃ 4Me₂CO.

   Removal of the guest molecules causes a significant change on the framework of **MOPA-5 ⊃ 4Me₂CO**. The two stages on desorption by heating **MOPA-5 ⊃ 4Me₂CO** reveal the formation of $[Co(NCS)_2(4\text{-peia})_2]_n$ (**MOPA-5**), *via* $\{[Co(NCS)_2(4\text{-peia})_2] \cdot Me_2CO\}_n$ (**MOPA-5 ⊃ Me₂CO**). **MOPA-5 ⊃ Me₂CO** was also obtained by treating **MOPA-5 ⊃ 4Me₂CO** under reduced pressure at room temperature, which was readily detected by X-ray powder diffraction (XRPD) and IR. The XRPD pattern of **MOPA-5 ⊃ Me₂CO** shows an amorphous form with sub-maximum peaks (Figure 4b). Since positions of those sub-maximum peaks are different from those in **MOPA-5 ⊃ 4Me₂CO**, **MOPA-5 ⊃ Me₂CO** is new form. Guest-free solid, **MOPA-5**, was obtained by treating **MOPA-5 ⊃ 4Me₂CO** under reduced pressure at 373 K. The framework of **MOPA-5 ⊃ 4Me₂CO** cannot

107

withstand a high level of stress on an extensive loss of the guest, resulting in amorphous form as shown in Figure 4c.   On the other hand, the XRPD pattern in Figure 4d is in good agreement with those of as-synthesized and calculated from single crystal data of **MOPA-5 ⊃ 4Me₂CO**, therefore, it is concluded that the original crystal structure comes back completely upon exposing to acetone vapor.

IR spectra shows the information of amide environment of **MOPA-5 ⊃ Me₂CO** and **MOPA-5**. The N-H stretching and amide-I/-II bands appear in the regions of 3500 - 3100 cm^{-1} and 1700 - 1500 cm^{-1}, respectively.[65,67-69]   The amide moieties in **MOPA-5 ⊃ 4Me₂CO** provide structured bands which are characteristic of *s-trans* complementary-amide hydrogen bond as shown in Figure 4a; N-H stretching vibration, the amide-I/-II bands are observed at 3303 cm^{-1}, 1644 cm^{-1}, and 1553 cm^{-1}, respectively.   In **MOPA-5 ⊃ Me₂CO**, the broadening of band width is observed at 3299 cm^{-1}, 1649 cm^{-1} and 1548 cm^{-1}, respectively.   In **MOPA-5**, N-H stretching and amide-I/-II bands are observed at 3276 cm^{-1}, 1650 cm^{-1} and 1533 cm^{-1} (1553 cm^{-1}, shoulder) respectively, and encounter further broadening.   Since the amide-II is bending band, the lower shifts indicates weakening of the hydrogen bonds.[67,70]   Therefore, the strength of complementary amide-amide hydrogen bonds in **MOPA-5** becomes weaker in **MOPA-5 ⊃ 4Me₂CO**.

IR data also shows the reconstruction of the porous structure by complementary-amide hydrogen bond; broader bands of **MOPA-5** in the N-H stretching and amide-I/-II bands change to the original ones (3301, 1644 and 1553 cm^{-1}).   "Amorphous **MOPA-5** → crystalline **MOPA-5 ⊃ 4THF**" regeneration is also induced by THF vapor, which is shown in Supporting Information.   We concluded that there are three different states, characterized by guest accomodation, namely $\{[Co(NCS)_2(4\text{-peia})_2]\cdot 4Me_2CO\}_n$ (**MOPA-5 ⊃ 4Me₂CO**), $\{[Co(NCS)_2(4\text{-peia})_2]\cdot Me_2CO\}_n$ (**MOPA-5 ⊃ Me₂CO**) and $[Co(NCS)_2(4\text{-peia})_2]_n$ (**MOPA-5**), which are summarized as reaction equation of eq. 2 and eq. 3.

$$\textbf{MOPA-5} + Me_2CO \quad \rightleftarrows \quad \textbf{MOPA-5} ⊃ \textbf{Me}_2\textbf{CO} \qquad (2)$$

$$\textbf{MOPA-5} ⊃ \textbf{Me}_2\textbf{CO} + 3Me_2CO \quad \rightleftarrows \quad \textbf{MOPA-5} ⊃ \textbf{4Me}_2\textbf{CO} \qquad (3)$$
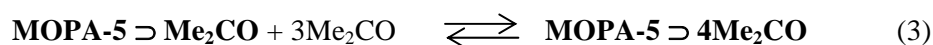
In addition to the information of hydrogen bonding modes among layers, it is necessary to investigate the integrity of layers in amorphous **MOPA-5**.   In order to gain information concerning the coordination structures around the Co^{II} ion in **MOPA-5**, EPR measurements were performed. Figure 5 shows the EPR spectra of **MOPA-5 ⊃ 4Me₂CO**, **MOPA-5 ⊃ Me₂CO**, and **MOPA-5** measured at ~15 K.   The EPR spectrum of **MOPA-5 ⊃ 4Me₂CO** indicates well-resolved features and their EPR parameters have been determined by computer simulation as $g'_1, g'_2, g'_3 = 5.7, 4.0,$
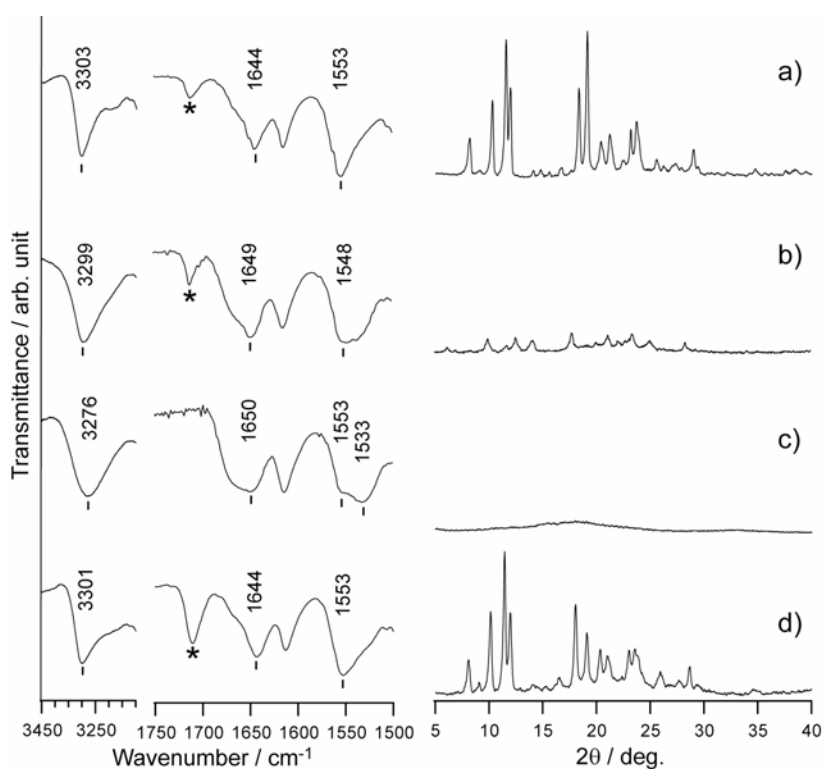
Figure 4. XRPD patterns (right) and IR spectra (left) in the region of N-H stretching, amide-I and amide-II bands at room temperature of (a) as-synthesized **MOPA-5 ⊃ 4Me₂CO**, (b) **MOPA-5 ⊃ Me₂CO** obtained by drying **MOPA-5 ⊃ 4Me₂CO** *in vacuo* for 20 hours at room temperature, (c) **MOPA-5** obtained by drying **MOPA-5 ⊃ 4Me₂CO** *in vacuo* for 20 hours at 373 K, (d) **MOPA-5 ⊃ 4Me₂CO** obtained by exposing **MOPA-5** to an acetone vapor for 4 days. Asterisk exhibits the C=O stretching band of acetone molecule.

2.8; $A_1 = 8.0$ mT[71]; the peak-to-peak line widths W_1, W_2, $W_3 = 20$, 40, 25 mT. On the other hand, **MOPA-5 ⊃ Me₂CO** and **MOPA-5** exhibit broad EPR spectra in accordance with the amorphous nature of these compounds. The g values are estimated as $g'_{center} \approx 4.0$ (**MOPA-5 ⊃ Me₂CO**) and $g'_{center} \approx 3.9$ (**MOPA-5**). (Computer simulation of the spectra of **MOPA - 5 ⊃ Me₂CO** and **MOPA - 5** was found to be difficult because of their broad nature).

Several types of high-spin Co^{II} complexes have so far been studied by EPR spectroscopy,[72] and the differences in the EPR pattern between tetrahedral and octahedral Co^{II} have been well documented.[73-76] In tetrahedral Co^{II}, the ground orbital state is $^4A_2$, and thus the orbital angular momentum is well quenched, which makes the spin Hamiltonian approach appropriate.[76,77] However, the observed g values for three compounds do not accord, similarly to the case reported previously.[19] In the case of an octahedral Co^{II}, on the other hand, the ground orbital state is $^4T_1$, and thus orbital degeneracy still remains.[78] Theoretical treatment of the EPR parameters of octahedral Co^{II} was made by Abragam and Pryce,[79] who gave theoretical expressions for the

109
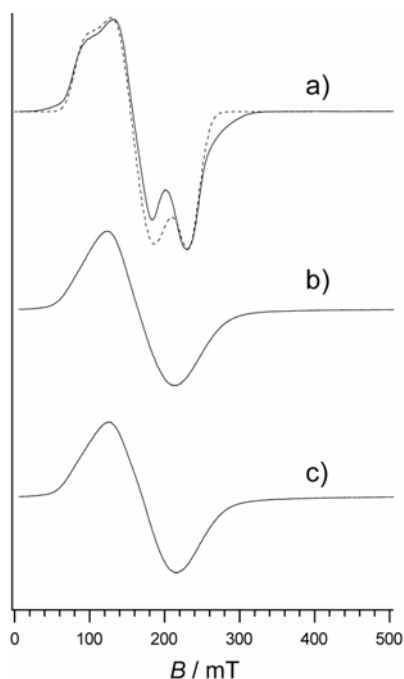
Figure 5. CW EPR spectra of powdered samples of a) **MOPA-5 ⊃ 4Me₂CO**, b) **MOPA-5 ⊃ Me₂CO**, and c) **MOPA-5**. Experimental setting: microwave frequency, a) 8.998, b) 8.993, and c) 8.996 GHz; microwave power, 1mW; field modulation, 1mT; temperature 15 K

effective g value and HFC parameters considering up to the second-order perturbation effects. The perturbation result for the effective g values are plotted against $\Delta/|\lambda|$, where Δ is the ligand-field splitting between $|^4T_1;xy\rangle$ and $|^4T_1;z\rangle$ with the value being positive when $|^4T_1;z\rangle$ is upper, and λ is the spin-orbit coupling constant. We estimate $\Delta/|\lambda| = 2.1$, ~0, ~0 for **MOPA-5 ⊃ 4Me₂CO**, **MOPA-5 ⊃ Me₂CO** and **MOPA-5**, respectively.[80] The present EPR results are in good agreement with the theory and, therefore, the Co^{II} ion in **MOPA-5 ⊃ Me₂CO** and **MOPA-5** are in octahedral coordination environment as well as **MOPA-5 ⊃ 4Me₂CO**.

Throughout the characterization of series of **MOPA-5** by XRPD, IR and EPR, we conclude that the 2-D motif of **MOPA-5** does not collapse. Although the layer framework in **MOPA-5** is maintained, the XRPD pattern shows that **MOPA-5** is not crsytalline (Figure 4c). The pattern is attributed to the random layer slip against the neighboring layers, accompanying with the deformation of grid framework.

Desorption and Energetics.

As mentioned previously, **MOPA-5 ⊃ 4Me₂CO** is desolvated, *via* **MOPA-5 ⊃ Me₂CO**, to be amorphous **MOPA-5**. In both desorption processes, "**MOPA-5 ⊃ Me₂CO → MOPA-5**" and "**MOPA-5 ⊃ 4Me₂CO → MOPA-5 ⊃ Me₂CO**", the activation energies of desorption (E_{de1} and E_{de2}, respectively) are estimated by recording TG curves at various heating rates (β) and by plotting $\log\beta$ vs $1/T$ at a given extent of desorption, according to the eq. 4.[81,82]

$$\ln\beta = -1.0516 E_{de}/RT + \text{const.} \qquad (4)$$

The results of the thermogravimetry at various heating rates are plotted against the reciprocal absolute temperature in Figure 6. It is apparent that these curves can be superposed by lateral shifts. For the process of "**MOPA-5 ⊃ 4Me₂CO → MOPA-5 ⊃ Me₂CO**" at 50% desorption, $T = 49.6$ (322.6), 53.0 (326.0), 57.9 (330.9), 65.1 (338.1), 66.2 (339.2) and 78.3 °C (351.3 K) at β = 2, 3, 5, 7, 10 and 20 °C/min. For the process of "**MOPA-5 ⊃ Me₂CO → MOPA-5**" at 50% desorption, $T =$ 97.4 (370.4), 103.2 (376.2), 108.1 (381.1), 111.1 (384.1), 114.6 (387.6) and 122.8 °C (395.8 K) at β = 2, 3, 5, 7, 10 and 20 °C/min. In the insert of Figure 6, the logarithms of the heating rates are plotted against the reciprocal absolute temperature, until which point the weight of the sample decreases to a 50% desorption. Straight lines are obtained and the method of the least squares affords the activation energies determined; $E_{de1} = 108$ kJ/mol and $E_{de2} = 71$ kJ/mol.
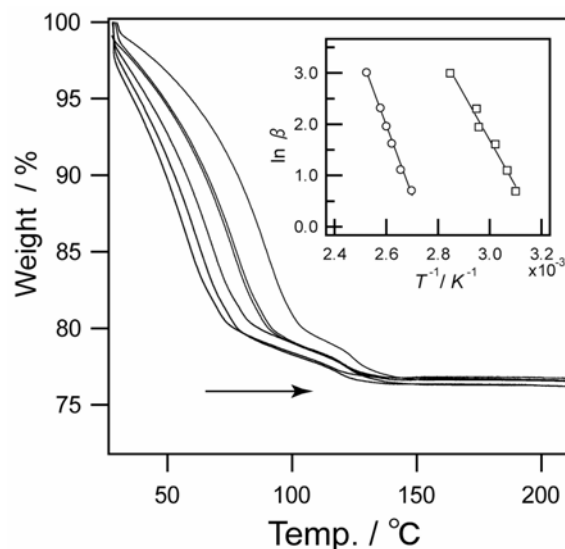
Figure 6. The thermogravimetric curves of **MOPA-5 ⊃ 4Me₂CO** plotted against the reciprocal absolute temperature. Heating rate; a, 2 °C/min; b, 3 °C/min; c, 5 °C/min; d, 7 °C/min; e, 10 °C/min; f, 20 °C/min. Insert: The plots of logarithms of heating rate (β) versus the conversions of reciprocal absolute temperature of 50 % desorption for **MOPA-5 ⊃ 4Me₂CO** (open square) and **MOPA-5 ⊃ Me₂CO** (open circle).

111

Isothermal Adsorption/Desorption Experiment.

Recently, several literature on adsorption behavior of porous coordination polymers have reported.[2,14,19,20,27,83-87]   When one look more carefully at the behavior of the adsorption, the actual porous coordination polymers, responsible for uptaking the adsorbates, tend to undergo guest-directed framework transformation,[19,20,27,86,88] dissimilar to zeolites and activated carbons. The mechanism of this transformation should be investigated in details, and the present **MOPA-5** system is suitable for in-depth study on adsorption/desorption properties.

MOPA-5 shows no N_2 adsorption at 77 K adsorb as shown in Figure 7a. Moreover, the adsorption isotherm of CH_4 for **MOPA-5** at 298 K reveals no uptake into the micropores but only surface adsorption.[89]   These result indicates **MOPA-5** does not maintain channels available for N_2 (3.64 Å) and CH_4 molecules (3.8 Å).[20,87]

Since **MOPA-5** shows structural regeneration when exposed to acetone vapor, acetone adsorption/desorption experiment was carried out on **MOPA-5**.   Figure 7b shows the adsorption/desorption isotherms for acetone over the relative pressure range from 0 to 0.9 at 298 K. The adsorption isotherm shows a slight increase and an abrupt rise at $P/P_0 = 0.76$.   This characteristic adsorption profile clearly indicates a conversion of amorphous **MOPA-5** to a crystalline **MOPA-5 ⊃ 4Me$_2$CO**.[86]   On the other hand, the desorption isotherm shows a monotonus decrease as if the pores were maintained until a sudden drop at $P/P_0 = 0.05$.   A large range of hysteresis loop based on the structural conversion is realized in this compound, which could not be obtained in rigid porous materials.

Threshold Points for Adsorption.

Figure 7c shows the Hill plot (eq. 5), of acetone adsorption on **MOPA-5** at 298 K.

$$\log [Y / (1-Y)] = n \log P + \log K \qquad (5)$$

where Y $(0 < Y < 1)$ is the extent of complexation (adsorption), which is often used to describe cooperative or allosteric binding processes in homogeneous solutions.   It may be more important, however, that this treatment of the binding data according to a homogeneous host-guest complexation fails to give a linear correlation for the whole pressure range.   The acetone adsorption curve is characterized by a sharp threshold point (P_{th}), consisting of three stages, which are characterized by different slopes: a prebinding region at $P < P_{th}$, the vertical region at $P \cong P_{th}$, and a milder follow-up region at $P > P_{th}$.   The vertical one at $P \cong P_{th}$ ($P_{th}/P_0 = 0.76$) indicates a remarkably cooperative nature of adsorption around P_{th}.
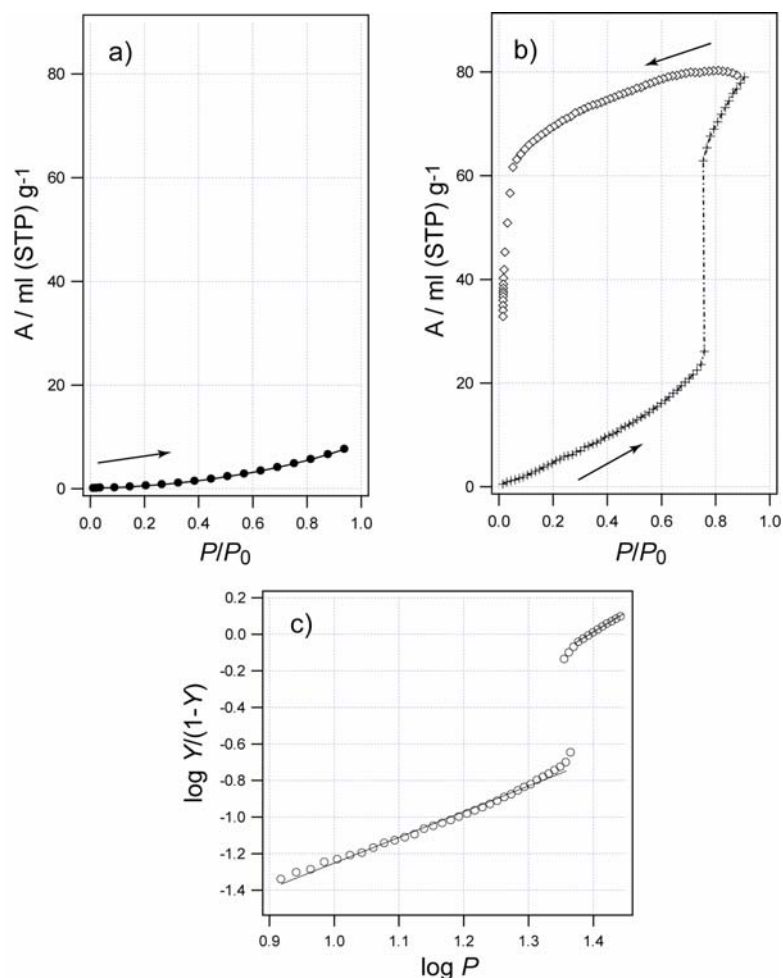
Figure 7. (a) Isotherm for N_2 adsorption (filled circle) at 77 K of **MOPA-5** over the pressure range from 0.003 to 0.939 atom. P_0 is a saturated vapor pressure, 1.022 atom, of N_2 at 77 K. (b) Isotherm for acetone vapor adsorption (cross) and desorption (open square) at 298 K of **MOPA-5** over the pressure range from 0.507 to 27.756 kPa. P_0 is a saturated vapor pressure, 30.593 kPa, of acetone at 298 K. (c) Hill plot for the adsorption curve of (b), where Y ($0 < Y < 1$) and P are the extent of complexation and pressure (kPa), respectively.

Isothermal acetone adsorption curves were obtained at various temperature, 288, 293, 298, 303, 308 and 313 K. The three stages of the Hill plots are also observed for all the temperatures. Figure 8a clearly shows the dependence of P_{th} on the temperature: the P_{th} values decrease with decrease in temperature; 17.3 (288), 21.2 (293), 23.2 (298), 28.8 (303 K), 34.8 (308 K) and 40.9 kPa (313 K). Since P_{th} values could be regarded as the equilibrium pressure for the reaction of acetone inclusion, their temperature dependence allows us to evaluate the associated enthalpy change on acetone adsorption process based on the following eq. 6,

$$d \ln P_{th}/d(1/T)) = \Delta H_{ad}/R \qquad (6)$$

where R and ΔH_{ad} denote the gas constant and the adsorption enthalpy of gas, respectively. The plot of ln P_{th} vs $1/T$, according to eq. 6, yields a straight line (Figure 8b), whose slope leads to ΔH_{ad} = -25 kJ/mol for the inclusion of acetone.
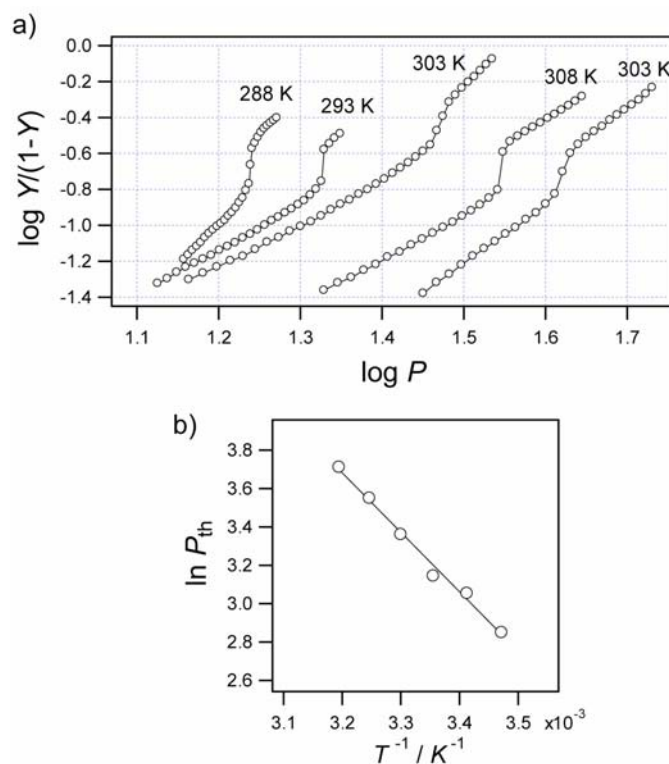
Figure 8. (a) Hill plot for the acetone adsorption curve of **MOPA-5** at 288, 293, 303, 308 and 313 K. (b) Plot of ln P_{th} against T^{-1}.

Mechanism and Thermodynamics in Relation to Structural Regeneration.

MOPA-5 does not contain channels, but nevertheless undergoes the inclusion of acetone molecules. Several organic hosts and metal-organic architectures exhibit the ability to switch between dense and open forms responding to guest molecules.[88,90-99] The new aspect of **MOPA-5** ⊃ **4Me₂CO** is solid form conversion based on infinite 2-D layers bound by complementary hydrogen bond. As mentioned previously, it is apparent that the 2-D structural integrity is maintained during the reaction. The structural regeneration by the inclusion of acetone is associated with change of the hydrogen bonding mode: the accommodation of acetone molecules in each grid of the 2-D motif could control the orientation of the amide hydrogen bonds, thus the overall relationship between the motifs comes back to the former **MOPA-5** ⊃ **4Me₂CO**, where extensive cooperativity must exist.

Previously, the energy diagram for the adsorption/desorption of some organic networks was fortunately constructed and reported.[88] In general, it is difficult to discuss the mechanism of solid state reaction, because the reaction is comprised of many kinds of elementary reaction. Figure 9

shows a schematic energy diagram for the acetone adsorption/desorption of **MOPA-5**, based on the results of TG and adsorption measurements. DSC measurement shows two separated endotherms of desorption for **MOPA-5 ⊃ 4Me₂CO**, however it is difficult to estimate the desorption enthalpy, because **MOPA-5 ⊃ 4Me₂CO** is unstable at room temperature and decomposes with loss of acetone molecules, usually with concominant rearrangement of the host compound to the non-porous compound. Therefore, the energy difference among states could be calculated from ΔH_{ad} (-25 kJ/mol), that is, $\Delta H_{ad1} = \Delta H_{ad} = -25$ kJ/mol and $\Delta H_{ad2} = 3\Delta H_{ad} = -75$ kJ/mol, and activation energy ($E_{de1} = 108$ kJ/mol and $E_{de2} = 71$ kJ/mol) were obtained as mentioned previously. Although the thermal decomposition of **MOPA-5 ⊃ 4Me₂CO → MOPA-5 ⊃ Me₂CO** is an endothermic reaction, the activation energy ($E_{de2} = 71$ kJ/mol) is lower than the thermodynamic value for the reaction ($\Delta H_{ad2} = -75$ kJ/mol). It is because that the activation energy is obtained based on rate-determining step of some elementary reaction.

As seen in energy diagram of the acetone adsorption process, **MOPA-5** transfer to **MOPA-5 ⊃ Me₂CO** with the energy barrier, and follows to smoothly second transformation to be **MOPA-5 ⊃ 4Me₂CO**. It is surprising that acetone inclusion enthalpy (ΔH_{ad} (-25 kJ/mol)) is close to acetone vaporization enthalpy ($\Delta H_{vap} = 30.99$ kJ/mol).[100] Thus, even weak dispersive forces can exert a profound influence over solid-sate transformation.
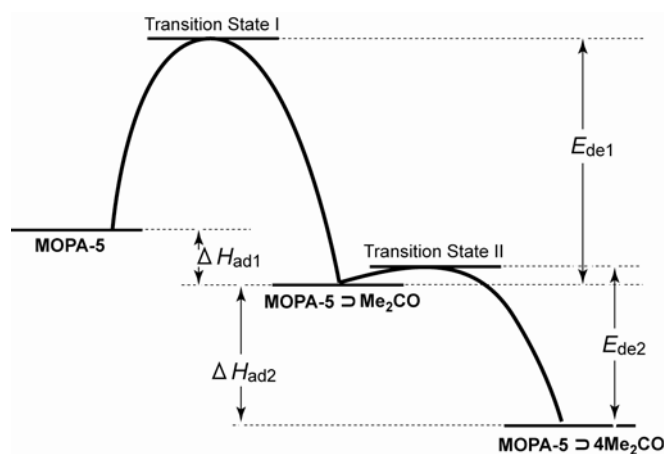
Figure 9. Schematic energy diagram for the solid-gas complexation of **MOPA-5** with gaseous acetone. Definitions are as follows: E_{de1} and E_{de2} are activation energy of acetone desorption in the processes of **MOPA-5 ⊃ Me₂CO → MOPA-5** and **MOPA-5 ⊃ 4Me₂CO → MOPA-5 ⊃ Me₂CO**, respectively. ΔH_{ad1} and ΔH_{ad2} are heat of guest binding in the processes of **MOPA-5 → MOPA-5 ⊃ Me₂CO** and **MOPA-5 ⊃ Me₂CO → MOPA-5 ⊃ 4Me₂CO**, respectively.

115

Adsorption Kinetics and Cooperative Adsorption.

A following kinetic model for diffusion of molecules into carbon molecular sieves have been used,[85,101,102]

$$M_t/M_e = 1 - \exp(-kt) \qquad (7)$$

where M_t is the mass uptake at time t, M_e is the mass uptake at equilibrium, and k is the kinetic rate constant. Figure 10 shows M_t/M_e (fractional uptake for the pressure increment) versus time for adsorption increments and for acetone adsorption. The adsorption kinetics can be compared in terms of the rate constant, which can be determined from either the gradient of the $\ln(1 - M_t/M_e)$ against time plot. Figure 10 shows M_t/M_e and $\ln(1 - M_t/M_e)$ against time plot of isotherm point 1, 2 and 52 on the acetone adsorption measurement at 298 K (See Figure 7b). As mentioned previously, the acetone isotherm consists of three regions: $P < P_{th}$, $P \cong P_{th}$, and $P > P_{th}$ ($P_{th} = 23.2$ kPa at 298 K). The isotherm point 1 (0 - 0.442 kPa) and 2 (0.442 - 0.888 kPa) belong to $P < P_{th}$ region, and isotherm point 52 (22.686 - 23.708 kPa) belong to $P \cong P_{th}$ region.

As shown in the graphs of M_t/M_e versus time of isotherm point 1 and 2 (Figure 10a and 10b), these profiles are characterized by a rapid uptake of 0.4-0.6 of the total uptake for the pressure increment followed by a slow uptake. The kinetic measurements for the first adsorption pressure increment are subject to larger uncertainty than the other kinetic measurements, because there is a change pressure, which introduces conduction through the gas, resulting in larger temperature fluctuation at the start of the pressure increment.[85] The slow uptake region has a linear graph of $\ln(1 - M_t/M_e)$ versus time. The M_t/M_e versus time profile of isotherm point 52 shows the linearly increase until the total uptake (Figure 10c). The curve of $\ln(1 - M_t/M_e)$ versus time indicates that the kinetic
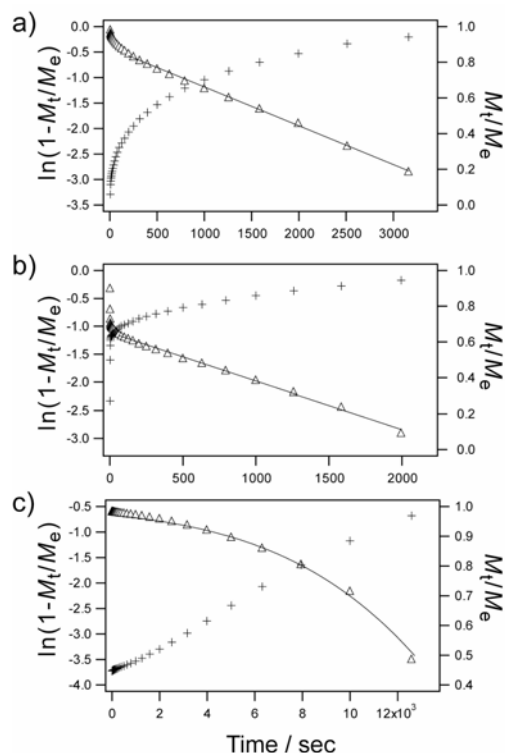
Figure 10. Analysis of acetone vapor adsorption kinetics on **MOPA-5** at 298 K for the pressure increment: (a) isotherm point 1 (0 - 0.442 kPa), (b) isotherm point 2 point (0.442 - 0.888 kPa), and (c) isothermpoint point 52 (22.686 - 23.708 kPa). The calculated profile for the M_t/M_e versus time graphs (cross) and $\ln(1 - M_t/M_e)$ versus time graphs (open triangle).

116

rate constant k is increasing for each time passes. Such amplified adsorption is attributed to the cooperative phenomena that **MOPA-5** include acetone molecules accompanying with structural regeneration.

Conclusion

This work demonstrates (1) the rational construction of flexible porous frameworks using square grids, and (2) characterization of cooperative adsorption with thermal analysis. In addition, we showed a new contrivance for dynamic porous coordination polymers based on flexible amide-amide hydrogen bond.

(1): From $Co(SCN)_2$ and bipyridyl derivatives containing an amide group, we succeeded in producing new square grid frameworks, **MOPA-3 ~ 5**, which have complementary-amide binding manner eschewing interpenetrating. Particularly, **MOPA-5 ⊃ 4Me₂CO** affords micropores fulfilled with guest molecules, and shows that structural transformation *via* amorphous is caused by adsorption/desorption of guest molecules. Such flexible porous coordination polymers offers an application to unique class of materials, which cannot be obtained in rigid porous material, in this case, large hysteresis loop on adsorption/desorption measurements, and leading to amplification of adsorption for specific guest.

(2): Based on well-defined **MOPA-5 ⊃ 4Me₂CO**, the energy diagram was achieved. Our results imply that coordination polymer is often much more dynamic than generally believed and that weak dispersive forces induces structural rearrangement in a well-concerted fashion. Although many porous coordination polymers have been synthesized and reported, in our present stage of knowledge, the report of thermal analysis is sparse. Thermodyanmic parameters calculated in the present course of study are also useful to analyze the thermal behavior of porous coordination polymers.

This research is particularly relevant in the context of solid-state chemistry since rational design of solids has important ramifications for the development of new materials with unusual properties. We anticipate this approach to be viable for the construction of cavity-containing frameworks possessing bridging ligands not described here, and we also anticipate this approach to be applicable for the design of flexible porous materials.

Experimental Section

Materials. Isonicotinic chloride hydrochloride, nicotinic chloride hydrochloride, 3-aminopyridine and 4-(2-aminoethyl)pyridine were obtained from Tokyo Kasei Industrial. $Co(SCN)_2$ was obtained from Aldrich Co.

Synthesis of *N*-(3-pyridyl)nicotinamide (3-pna)

The ligand was prepared by the reaction of nicotinic chloride hydrochloride (15.2 g, 85 mmol) with 3-aminopyridine (8.0 g, 85 mmol) in dry tetrahydrofuran (220 mL) in the presence of triethylamine (25 mL, 179 mmol) under N_2.   The product was recrystallized from acetone/hexane in 47 % yield (8.0 g): ^{1}H NMR (DMSO) δ 7.58 (dd, J = 8.5 Hz; 5.0 Hz, 1H), δ 7.58 (dd, J = 8.0 Hz; 5.0 Hz, 1H), δ 8.18 (d, J = 8.5 Hz, 1H), δ 8.29 (d, J = 8.0 Hz, 1H), δ 8.33 (d, J = 5.0 Hz, 1H), δ 8.78 (d, J = 5.0 Hz, 1H), δ 8.92 (s, 1H), δ 9.12 (s, 1H), δ 10.64 (s, 1H).   Elemental analysis calcd for $C_{11}H_9N_3O$ (199.2): C, 66.32; H, 4.55; N, 21.09; found: C, 65.80; H, 4.47; N, 20.89.

Synthesis of *N*-(2-pyridin-4-yl-ethyl)-isonicotinamide (4-peia)

The ligand was prepared by the reaction of isonicotinic chloride hydrochloride (15.0 g, 84.4 mmol) with 4-(2-aminoethyl)pyridine (10.0 mL, 84.4 mmol) in dry tetrahydrofuran (280 mL) in the presence of triethylamine (24 mL, 170 mmol) under N_2.   The product was recrystallized from acetone/hexane in 55 % yield (10.6 g): ^{1}H NMR (DMSO) δ 2.87 (t, J = 7.0 Hz, 2H), δ 3.54 (q, J = 7.0 Hz, 2H), δ 7.26 (d, J = 4.5 Hz, 2H), δ 7.67 (d, J = 4.5 Hz, 2H), δ 8.45 (d, J = 4.5 Hz, 2H), δ 8.70 (d, J = 4.5 Hz, 2H), δ 8.86 (t, J = 7.0 Hz, 1H).   Elemental analysis calcd for $C_{13}H_{13}N_3O$ (227.3): C, 68.70; H, 5.77; N, 18.49; found: C, 68.56; H, 5.74; N, 18.54.

[Co(NO$_3$)$_2$(3-pna)$_2$]$_n$ (MOPA-3)

An ethanol solution (1.5 mL) of 3-pna (29.9 mg, 1.5 mmol) was carefully layered on a acetone/chloroform mixed (v/v 9:1) solvent (1.5 mL) of $Co(NO3)_2$ (21.8 mg, 0.75 mmol), where a mixed solvent of ethanol/chloroform (v/v 19:1) was placed between two layers (yield: 37 %). Elemental analysis calcd for $C_{22}H_{18}CoN_8O_8$ (581.4): C, 45.45; H, 3.12; N, 19.27; found: C, 44.80; H, 3.23; N, 19.06.

[CoBr$_2$(3-pna)$_2$]$_n$ (MOPA-4)

An ethanol solution (1.5 mL) of 3-pna (14.9 mg, 0.075 mmol) was carefully layered on a methanol/chloroform mixed (v/v 9:1) solvent (1.5 mL) of $CoBr_2$ (8.2 mg, 0.038 mmol), where a

mixed solvent of ethanol/chloroform (v/v 19:1) was placed between two layers (yield: 22 %). Elemental analysis calcd for $C_{22}H_{18}Br_2CoN_6O_2$ (617.2): C, 42.81; H, 2.94; N, 13.62; found: C, 42.31; H, 3.31; N, 12.92.

{[Co(NCS)$_2$(4-peia)$_2$]·4Me$_2$CO}$_n$ (MOPA-5 ⊃ 4Me$_2$CO)

A solution of 4-peia (6.81 mg, 0.03 mmol) in acetone (1.5 mL) was gently layered on to a solution of Co(SCN)$_2$ (2.63 mg, 0.015 mmol) in acetone/chloroform (v/v 9:1, 1.5 mL), with a mixed solvent of acetone/chloroform (v/v 19:1, 1.5 mL) placed between the two layers (yield: 50 %).   For elemental analysis these crystals were collected, and dried *in vacuo* at room temperature for 24 hours. Elemental analysis calcd for $C_{31}H_{32}CoN_8O_3S_2$ (687.7): C, 54.14; H, 4.69; N, 16.29; found: C, 53.47; H, 4.55; N, 16.10.   The microcrystalline sample for physico-chemical measurements was prepared in the same solvent, and the crystallinity was checked by X-ray powder diffraction.

X-ray crystal structure determination.   For each compound, a single crystal was mounted on a glass fiber and coated with epoxy resin.   X-ray data collection for each crystal was carried out on a Rigaku Mercury diffractometer with graphite monochromated MoKα radiation (λ = 0.71069 Å) and a CCD two-dimensional detector.   The size of the unit cells were calculated from the reflections collected on the setting angles of six frames by changing by 0.5° for each frame.   Three different settings were used and were changed by 0.5° per frame.   Intensity data were collected with a scan width of 0.5°.   Empirical absorption correction by using REQABA[103] was performed for all data. For **MOPA-3**, the structure was solved by direct methods by using the SIR88 program[104] and expanded by using Fourier techniques.[105]   For **MOPA-4**, the structure was solved by Patterson methods by using the DIRDIF94 program[106] and expanded by using Fourier techniques.[105]   For **MOPA-5 ⊃ 4Me$_2$CO**, the structure was solved by direct methods by using the SIR97 program[107] and expanded by using Fourier techniques.[105]   All calculations were performed with the teXsan crystallographic software package of Molecular Structure Corporation.[108]   For all compounds, the non-hydrogen atoms were refined anisotropically and all hydrogen atoms were placed in the ideal positions.   In compound **MOPA-3** nitrate anions containing O(3), and 3-pna containing C(7) were refined isotropically.   In compound **MOPA-5 ⊃ 4Me$_2$CO**, acetone molecules containing O(2), O(3) and C(15)-C(20) were found at the final stage, and thus its atom positions were isotropically refined under a rigid condition.

Physical measurements.   Thermal gravimetry (TG) was carried out with a Rigaku Instrument TG8120 in a nitrogen atmosphere.   IR spectra were recorded on a Perkin-Elmer 2000 FTIR

spectrophotometer with samples prepared with Nujol.   X-ray powder diffraction (XRPD) data were collected on a Rigaku RINT-2200HF (Ultima) diffractometer with CuKα radiation. Continuous-wave (CW) EPR spectra were recorded on a JEOL RE-3X spectrometer equipped with an Air-Product Heli-Tran cryostat.   The microwave frequency was measured using an Advantest R5372 frequency counter, and the magnetic field was repeatedly calibrated with diphenylpicrylhydrazyl (DPPH) and Mn^{2+} in MgO.

Measurement of Adsorption.   The adsorption isotherm of CH_4 was measured by using FMS-BG gravimetric adsorption equipment from BEL JAPAN.   The adsorption isotherms and kinetics measurements of gaseous acetone and N_2 were measured by using BELSORP18-Plus volumetric adsorption equipment from BEL JAPAN.   In the sample chamber (~ 17.5 mL) maintained at $T \pm$ 0.03 K was placed the adsorbent sample (~ 50 mg), which had been prepared at 373 K and 10^{-1} Pa prior to measurement of the isotherms.   The larger gas chamber (179.85 mL) with a pressure gauge was kept at $(T + 20) \pm 0.1$ K.   The acetone used to generate the vapor was degassed fully by repeated evacuation and vapor equilibration cycles of the liquid supply side of the vapor reservoir. Helium gas at a certain pressure was introduced in the gas chamber and was allowed to diffuse into the sample chamber by opening a valve.   The change in pressure allowed an accurate determination of the volume of the total gas phase.   The complexation was monitored in a similar manner by using a guest vapor in place of helium.   The amount of guest adsorbed was calculated readily from pressure difference $(P_{cal} - P_e)$, where P_{cal} is the calculated pressure with no guest adsorption, and P_e is the observed equilibrium pressure.   All operations were computer-controlled and automatic.

References and Notes

(1)   Batten, S. R.; Robson, R. *Angew. Chem. Int. Ed.* **1998**, *37*, 1460-1494.

(2)   Li, H.; Eddaoudi, M.; O'Keeffe, M.; Yaghi, O. M. *Nature* **1999**, *402*, 276-279.

(3)   Hagrman, P. J.; Hagrman, D.; Zubieta, J. *Angew. Chem. Int. Ed.* **1999**, *38*, 2638-2684.

(4)   Noro, S.-I.; Kitagawa, S.; Kondo, M.; Seki, K. *Angew. Chem. Int. Ed.* **2000**, *39*, 2082-2084.

(5)   Seki, K. *Chem. Comm.* **2001**, 1496-1497.

(6)   Desiraju, G. R. *Nature* **2001**, *412*, 397-400.

(7)   Moulton, B.; Zaworotko, M. J. *Chem. Rev.* **2001**, *101*, 1629-1658.

(8)   Zaworotko, M. J. *Chem. Comm.* **2001**, 1-9.

(9)   Eddaoudi, M.; Kim, J.; Rosi, N.; Vodak, D.; Wachter, J.; O'Keeffe, M.; Yaghi, O. M. *Science* **2002**, *295*, 469-472.

(10)   Yaghi, O. M.; O'Keeffe, M.; Ockwig, N. W.; Chae, H. K.; Eddaoudi, M.; Kim, J. *Nature* **2003**, *423*, 705-714.

(11)   Hoskins, B. F.; Robson, R. *J. Am. Chem. Soc.* **1990**, *112*, 1546-1554.

(12)   Fujita, M.; Kwon, J. Y.; Washizu, S.; Ogura, K. *J. Am. Chem. Soc.* **1994**, *116*, 1151-1152.

(13)   Yaghi, O. M.; Li, H. *J. Am. Chem. Soc.* **1996**, *118*, 295-296.

(14)   Kondo, M.; Yoshitomi, T.; Seki, K.; Matsuzaka, H.; Kitagawa, S. *Angew. Chem. Int. Ed.* **1997**, *36*, 1725-1727.

(15)   Langley, P. J.; Hulliger, J. *Chem. Soc. Rev.* **1999**, *28*, 279-291.

(16)   Eddaoudi, M.; Moler, D. B.; LI, H.; Chen, B.; Reineke, T. M.; O'keeffe, M.; Yaghi, O. M. *Acc. Chem. Res.* **2001**, *34*, 319-330.

(17)   Noro, S.-i.; Kitagawa, S.; Yamashita, M.; Wada, T. *Chem. Comm.* **2002**, 222-223.

(18)   Kitagawa, S.; Kondo, M. *Bull. Chem. Soc. Jpn.* **1998**, *71*, 1739-1753.

(19)   Uemura, K.; Kitagawa, S.; Kondo, M.; Fukui, K.; Kitaura, R.; Chang, H.-C.; Mizutani, T. *Chem. Eur. J.* **2002**, *8*, 3586-3600.

(20)   Kitaura, R.; Fujimoto, K.; Noro, S.-i.; Kondo, M.; Kitagawa, S. *Angew. Chem. Int. Ed.* **2002**, *41*, 133-135.

(21)   Kitaura, R.; Seki, K.; Akiyama, G.; Kitagawa, S. *Angew. Chem. Int. Ed.* **2003**, *42*, 428-431.

(22)   Halder, G. J.; Kepert, C. J.; Moubaraki, B.; Murray, K. S.; Cashion, J. D. *Science* **2002**, *298*, 1762-1765.

(23)   Cussen, E. J.; Claridge, J. B.; Rosseinsky, M. J.; Kepert, C. J. *J. Am. Chem. Soc.* **2002**, *124*, 9574-9581.

(24)   Biradha, K.; Hongo, Y.; Fujita, M. *Angew. Chem. Int. Ed.* **2002**, *41*, 3395-3398.

(25)   Biradha, K.; Fujita, M. *Angew. Chem. Int. Ed.* **2002**, *41*, 3392-3395.

(26)   Suh, M. P.; Ko, J. W.; Choi, H. J. *J. Am. Chem. Soc.* **2002**, *124*, 10976-10977.

(27)   Seki, K. *Phys. Chem. Chem. Phys.* **2002**, *4*, 1968-1971.

(28)   Takamizawa, S.; Nakata, E.-i.; Yokoyama, H.; Mochizuki, K.; Mori, W. *Angew. Chem. Int. Ed.* **2003**, *42*, 4331-4334.

(29)   Serre, C.; Millange, F.; Thouvenot, C.; Nogues, M.; Marsolier, G.; Louer, D.; Ferey, G. *J. Am. Chem. Soc.* **2002**, *124*, 13519-13526.

(30)   Makinen, S. K.; Melcer, N. J.; Parvez, M.; Shimizu, G. K. H. *Chem. Eur. J.* **2001**, *7*, 5176-5182.

(31)   Edgar, M.; Mitchell, R.; A. M. Z. Slawin; Lightfoot, P.; Wright, P. A. *Chem. Eur. J.* **2001**, *7*, 5168-5175.

(32)   Alberti, G.; Brunet, E.; C. Dionigi; Juanes, O.; Mata, M. J. d. l.; RodrIguez-Ubis, J. C.; Vivani, R. *Angew. Chem. Int. Ed.* **1999**, *38*, 3351-3353.

(33)   Choi, H. J.; Lee, T. S.; Suh, M. P. *Angew. Chem. Int. Ed.* **1999**, *38*, 1405-1408.

(34)   Min, K. S.; Suh, M. P. *Chem. Eur. J.* **2001**, *7*, 303-313.

(35)   Cao, R.; Sun, D.; Liang, Y.; Hong, M.; Tatsumi, K.; Shi, Q. *Inorg. Chem.* **2002**, *41*, 2087-2094.

(36)   Tabares, L. C.; Navarro, J. A. R.; Salas, J. M. *J. Am. Chem. Soc.* **2001**, *123*, 383-387.

(37)   Maspoch, D.; Ruiz-molina, D.; Wurst, K.; Domingo, N.; Cavallini, M.; Biscarini, F.; Tejada, J.; Rovira, C.; Veciana, A. J. *Nature Mater.* **2003**, *2*, 190-195.

(38)   Hereafter, the number *n* is defined for the ratio of [the amount of adsorbed guest molecules]/[asymmetric unit of the crystal].

(39)   Larionova, J.; Chavan, S. A.; Yakhmi, J. V.; Froystein, A. G.; Sletten, J.; Sourisseau, C.; Kahn, O. *Inorg. Chem.* **1997**, *36*, 6374-6381.

(40)   Usuki, N.; Ohba, M.; Okawa, H. *Bull. Chem. Soc. Jpn.* **2002**, *75*, 1693-1698.

(41)   White, S. R.; Sottos, N. R.; Geubelle, P. H.; Moore, J. S.; Kessler, M. R.; Sriram, S. R.; Brown, E. N.; Viswanathan, S. *Nature* **2001**, *409*, 794-797.

(42)   Gable, R. W.; Hoskins, B. F.; Robson, R. *J. Chem. Soc., Chem. Commun.* **1990**, 1677-1678.

(43)   Biradha, K.; Hongo, Y.; Fujita, M. *Angew. Chem. Int. Ed.* **2000**, *39*, 3843-3845.

(44)   Pschirer, N. G.; Ciurtin, D. M.; Smith, M. D.; Bunz, U. H. F.; Loye, H.-C. z. *Angew. Chem. Int. Ed.* **2002**, *41*, 583-585.

(45)   Aoyagi, M.; Biradha, K.; Fujita, M. *Bull. Chem. Soc. Jpn.* **2002**, *73*, 1369-1373.

(46)   Biradha, K.; Fujita, M. *J. Chem. Soc. Dalton Trans* **2000**, 3805-3810.

(47)   Bourne, S. A.; Kilkenny, M.; Nassimbeni, L. R. *J. Chem. Soc. Dalton Trans* **2001**,

1176-1179.

(48)   Lu, J.; Paliwala, T.; Lim, S. C.; Yu, C.; Niu, T.; Jacobson, A. J. *Inorg. Chem.* **1997**, *36*, 923-929.

(49)   Kondo, M.; Shimamura, M.; Noro, S.-i.; Minakoshi, S.; Asami, A.; Seki, K.; Kitagawa, S. *Chem. Mater.* **2000**, *12*, 1288-1299.

(50)   Haynes, J. S.; Rettig, S. J.; Sams, J. R.; Thompson, R. C.; Trotter, J. *Can. J. Chem.* **1987**, *65*, 420-426.

(51)   Tong, M.-L.; Ye, B.-H.; Cai, J.-W.; Chen, X.-M.; Ng, S. W. *Inorg. Chem.* **1998**, *37*, 2645-2650.

(52)   Biradha, K.; Domasevitch, K. V.; Moulton, B.; Seward, C.; Zaworotko, M. J. *Chem. Comm.* **1999**, 1327-1328.

(53)   Biradha, K.; Domasevitch, K. V.; Hogg, C.; Moulton, B.; Power, K. N.; Zaworotko, M. J. *Cryst. Eng.* **1999**, *2*, 37-45.

(54)   Real, J. A.; Andres, E.; Munoz, M. C.; Julve, M.; Granier, T.; Bousseksou, A.; Varret, F. *Science* **1995**, *268*, 265-267.

(55)   Real, J. A.; Munno, G. D.; Munoz, M. C.; Julvel, M. *Inorg. Chem.* **1991**, *30*, 2701-2704.

(56)   Park, S. H.; Kim, K. M.; Lee, S.; Jung, O.-S. *Bull. Korean Chem. Soc.* **1998**, *19*, 79-82.

(57)   MacGillivray, L. R.; Groeneman, R. H.; Atwood, J. L. *J. Am. Chem. Soc.* **1998**, *120*, 2676-2677.

(58)   Groeneman, R. H.; MacGillivray, L. R.; Atwood, J. L. *Chem. Comm.* **1998**, 2735-2736.

(59)   Tong, M.-L.; Chen, X.-M.; Yu, X.-L.; Mak, T. C. W. *J. Chem. Soc. Dalton Trans* **1998**, 5-6.

(60)   Kawata, S.; Kitagawa, S.; Kondo, M.; Furuchi, I.; Munakata, M. *Angew. Chem. Int. Ed.* **1994**, 1759-1761.

(61)   Zheng, L.-M.; Fang, X.; Lii, K.-H.; Song, H.-H.; Xin, X.-Q.; Fun, H.-K.; Chinnakali, K.; Razak, I. A. *J. Chem. Soc. Dalton Trans* **1999**, 2311-2316.

(62)   Shin, D. M.; Lee, I. S.; Chung, Y. K.; Lah, M. S. *Inorg. Chem.* **2003**, *42*, 5459-5461.

(63)   Shin, D. M.; Lee, I. S.; Chung, Y. K.; Lah, M. S. *Chem. Comm.* **2003**, 1036-1037.

(64)   Bong, D. T.; Clark, T. D.; Granja, J. R.; Ghadiri, M. R. *Angew. Chem. Int. Ed.* **2001**, *40*, 988-1011.

(65)   Ghadiri, M. R.; Granja, J. R.; Milligan, R. A.; McRee, D. E.; Khazanovich, N. *Nature* **1993**, *366*, 324-327.

(66)   The size is measured by considering van der Waals radii for constituting atoms.   Hereafter, all the size-estimation of pore is made in this way.

(67)   Bellamy, L. J. *Advances in Infrared Group Frequencies*, Methuen; London, **1968**.

(68)   Haris, P. I.; Chapman, D. *Biopolymers* **1995**, *37*, 251-263.

(69)   Hartgerink, J. D.; Granja, J. R.; Milligan, R. A.; Ghadiri, M. R. *J. Am. Chem. Soc.* **1996**, *118*, 43-50.

(70)   As the NH bond becomes longer (hydrogen bond becomes stronger) and easier to stretch the orbitals of the nitrogen atom take on more *p* character, which makes the bond more directional and harder to bend.   Therefore, hydrogen shifts the amide-II band to higher frequencies.

(71)   Hyperfine coupling (HFC) is not included for the peaks g'_2, g'_3.

(72)   Weckhuysen, B. M.; Verberckmoes, A. A.; Uytterhoeven, M. G.; Mabbs, F. E.; Collison, D.; Boer, E. d.; Schoonheydt, R. A. *J. Phys. Chem. B* **2000**, *104*, 37-42.

(73)   Bencini, A.; Benelli, C.; Gattenschi, D.; Zanchini, C. *Inorg. Chem.* **1980**, *19*, 1301-1304.

(74)   Banci, L.; Benelli, C.; Gatteschi, D.; Mani, F. *Inorg. Chem.* **1982**, *21*, 1133-1136.

(75)   Makinen, M. W.; Kuo, L. C.; Yim, M. B.; Wells, G. B.; Fukuyama, J. M.; Kim, J. E. *J. Am. Chem. Soc.* **1985**, *107*, 5245-5255.

(76)   Drulis, H.; Dyrek, K.; Hoffmann, K. P.; Hoffmann, S. K.; Weselucha-Birczynska, A. *Inorg. Chem.* **1985**, *24*, 4009-40125.

(77)   Pilbrow, J. R. *J. Mag. Reson.* **1978**, *31*, 479-490.

(78)   Griffith, J. S. *In The Theory of Transition Metal Ions*, Cambridge University Press; London, **1961**.

(79)   Abragham, A.; Pryce, M. H. *Proc. Roy. Soc. A* **1951**, *205*, 173-191.

(80)   Effective *g* values calculated from the first-order perturbation equations are plotted versus $\Delta/|\lambda|$ is reasonable.

(81)   Flynn, J. H.; Wall, L. A. *J. Polym. Sci. B* **1966**, *4*, 323-328.

(82)   Ozawa, T. *Bull. Chem. Soc. Jpn.* **1965**, *38*, 1881-1886.

(83)   Kondo, M.; Okubo, T.; Asami, A.; Noro, S.-I.; Yoshitomi, T.; Kitagawa, S.; Ishii, T.; Matsuzaka, H.; Seki, K. *Angew. Chem. Int. Ed.* **1999**, *38*, 140-143.

(84)   Kepert, C. J.; Rosseinsky, M. J. *Chem. Comm.* **1999**, 375-376.

(85)   Fletcher, A. J.; Cussen, E. J.; Prior, T. J.; Rosseinsky, M. J.; Kepert, C. J.; Thomas, K. M. *J. Am. Chem. Soc.* **2001**, *123*, 10001-10011.

(86)   Li, D.; Kaneko, K. *Chem. Phys. Lett.* **2001**, *335*, 50-56.

(87)   Pan, L.; Adams, K. M.; Hernandez, H. E.; Wang, X.; Zheng, C.; Hattori, Y.; Kaneko, K. *J. Am. Chem. Soc.* **2003**, *125*, 3062-3067.

(88)   Dewa, T.; Endo, K.; Aoyama, Y. *J. Am. Chem. Soc.* **1998**, *120*, 8933-8940.

(89)   Isotherm for methane adsorption at 298 K of **MOPA-5** from 0.5 to 70 atom is measured.

(90) Miyata, M.; Shibakami, M.; Chirachanchai, S.; Takemoto, K.; Kasai, N.; Miki, K. *Nature* **1990**, *343*, 446-447.

(91) Bourne, S. A.; Nassimbeni, L. R.; Toda, F. *J. Chem. Soc. Perkin Trans. II* **1991**, *1335-1341*.

(92) Barbour, L. J.; Caira, M. R.; Coetzee, A.; Nassimbeni, L. R. *J. Chem. Soc. Perkin Trans. II* **1995**, 1345-1349.

(93) Ung, A. T.; Gizachew, D.; Bishop, R.; Scudder, M. L.; Dance, I. G.; Craig, D. C. *J. Am. Chem. Soc.* **1995**, *117*, 8745-8756.

(94) Endo, K.; Sawaki, T.; Koyanagi, M.; Kobayashi, K.; Masuda, H.; Aoyama, Y. *J. Am. Chem. Soc.* **1995**, *117*, 8341-8352.

(95) Endo, K.; Koike, T.; Sawaki, T.; Hayashida, O.; Masuda, H.; Aoyama, Y. *J. Am. Chem. Soc.* **1997**, *119*, 4117-4122.

(96) Thaimattam, R.; Xue, F.; Sarma, J. A. R. P.; Mak, T. C. W.; Desiraju, G. R. *J. Am. Chem. Soc.* **2001**, *123*, 4432-4445.

(97) Atwood, J. L.; Barbour, L. J.; Jerga, A.; Schottel, B. L. *Science* **2002**, *298*, 1000-1002.

(98) Soldatov, D. V.; Ripmeester, J. A.; Shergina, S. I.; Sokolov, I. E.; Zanina, A. S.; Gromilov, S. A.; Dyadin, Y. A. *J. Am. Chem. Soc.* **1999**, *121*, 4179-4188.

(99) Soldatov, D. V.; Ripmeester, J. A. *Chem. Eur. J.* **2001**, *7*, 2979-2994.

(100) Weast, R. C.; Astle, M. J.; Beyer, W. H. *CRC Handbook of Chemistry and Physics 80th ed.* CRC Press; Ohio, **1999**.

(101) Foley, N. J.; Thomas, K. M.; Forshaw, P. L.; Stanton, D.; Norman, P. R. *Langmuir* **1997**, *13*, 2083-2089.

(102) Harding, A. W.; Foley, N. J.; Norman, P. R.; Francis, D. C.; Thomas, K. M. *Langmuir* **1998**, *14*, 3858-3864.

(103) Jacobson, R. A. REQABA Empirical Absorption Correction Version 1.1-0301998, Molecular Structure Corp.: The Woodlands, TX, **1996-1998**.

(104) Burla, M. C.; Camalli, M.; Cascarano, G.; Giacovazzo, C.; Polidori, G.; Spagna, R.; Viterbo, D. *J. Appl. Cryst.* **1989**, *22*, 389-303.

(105) Beurskens, P. T.; Admiraal, G.; Beurskens, G.; Bosman, W. P.; deGelder, R.; Israel, R.; Smits, J. M. M. The DIRDIF-94 program system, Technical Report of the Crystallography Laboratory, University of Nijmegen, The Netherlands, **1994**.

(106) Beurskens, P. T.; Admiraal, G.; Beurskens, G.; Bosman, W. P.; Garcia-Granda, S.; Gould, R. O.; Smits, J. M. M.; Smykalla, C., The DIRDIF program system, Technical Report of the Crystallography Laboratory, University of Nijmegen, The Netherlands, **1992**.

(107) Altomare, A.; Burla, M. C.; Camalli, M.; Cascarano, G. L.; Giacovazzo, C.; Guagliardi, A.;

Moliterni, A. G. G.; Polidori, G.; Spagna, R. *J. Appl. Cryst.* **1999**, *32*, 115-119.

(108)   teXsan Crystal Structure Analysis Package, Molecular structure Corporation **1985, 1999**.

Chapter 6

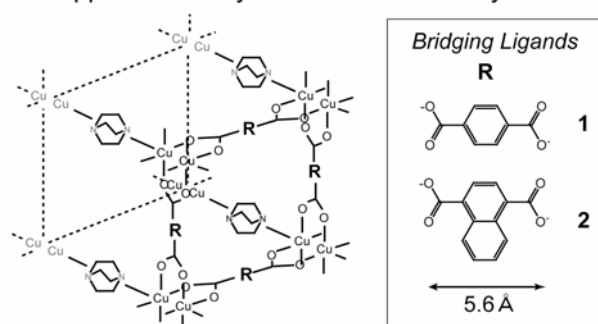*n*-Pentane and Isoprene Adsorption on Three-Dimensional Porous Coordination Polymers

Abstract

Equilibrium adsorption isotherms of *n*-pentane and isoprene were measured for two 3-dimensional (3-D) porous coordination polymers, $[Cu_2(p\text{-}OOC\text{-}Ph\text{-}COO)_2TED]_n$ (**1**) and $[Cu_2(1,4\text{-}OOC\text{-}Nap\text{-}COO)_2TED]_n$ (**2**) (p-OOC-Ph-COO = terephthalic acid, 1,4-OOC-Nap-COO = 1,4-naphthalenedicarboxylic acid, TED = triethylenediamine).   All the adsorption isotherms exhibit a Type-I curve, characteristic of physisorption in micropores.   For each isotherm, adsorption parameters, such as the adsorption amount (m_{max} and W_0), were obtained according to Langmuir, Freundlich and Dubinin-Radushkevich (DR) equations.   The observed adsorption amounts (m_{max} and W_0) of both *n*-pentane and isoprene for **1** increase with decreasing temperature (278-308 K).   The Freundlich theory indicates such adsorption propensies are attributed to the surface of the adsorbent to have a range of adsorption sites each having different adsorbate-adsorbent heats of adsorption.

Introduction

Separation of mixtures, i.e. alkanes and alkenes, is an important activity in the petroleum and petrochemical industries. Adsorption is especially effective for the separation of gas mixtures and different low molecular weight hydrocarbon isomers, which are usually difficult to separate using distillation. A major application of zeolites is in the separation of mixtures based on the differences in the adsorption capacity.[1] A large number of industrial applications in separation processes have been developed with zeolites as adsorbents. For example, selective sorption on zeolites is often used for separation of alkane mixtures, and the linear alkanes are the desired components and need to be separated from the alkane mixture.[1,2]

Recent advent of coordination polymers have paved the way to porous materials because their frameworks are essentially designable based on a variety of coordination geometries of metal centers and multifunctionality of bridging organic parts,[3-6] therefore affording desirable high porosity and/or flexibility. Although many kinds of 3-D porous coordination polymers have been reported, attempt of hydrocarbon adsorption focusing on separation is still sparse. It is due to that coordination polymers tend to provide hydrophilic pores. Recently, 3-D networks $[Cu_2(p\text{-OOC-Ph-COO})_2TED]_n$ (**1**), which consist of 2-D layers of copper(II) terephthalate and pillar ligands of triethylenediamine (TED) were reported.[7-10] This copper(II) dicarboxylate system has hydrophobic cavity by nature, thus, available for selective adsorption of nonpolar hydrocarbon molecules not only for storage but also separation applications (Scheme 1).


Scheme 1.

In this manuscript, we synthesized the 3-D porous compounds including a new $[Cu_2(1,4\text{-OOC-Nap-COO})_2TED]_n$ (**2**) of 1,4-naphthalenedicarboxylic and carried out adsorption measurements for *n*-pentane and isoprene, which form a mixture unseparable by usual distillation. From the results, we demonstrate the relations between the structures and adsorption properties.

128

Results and Discussion

Structures and Physical Properties of 1 and 2.

Two kinds of 3-D coordination polymer, $[Cu_2(OOC\text{-}R\text{-}COO)_2TED]_n$ (R = Ph (**1**), naphthalene (**2**)), were synthesized by heterogeneous reaction between porous dicarboxylates and TED as a pillared ligand. The structures of **1** and **2** were studied by X-ray powder diffraction (XRPD), as shown in Figure 1. Since the observed peak positions of **1** and **2** are well coincided, both compounds form similar lattice dimensions. Considering the structure of **1** mentioned in previous report,[9] **2** also forms 3-D non-interpenetrated framework.

The physical properties such as particle size distribution of **1** and **2** are given in Table 1. The estimated specific surface areas (pore volumes) of **1** and **2** are 1891 (0.70) and 441 m^2/g (0.08 cm^3/g), respectively. The pore size distributions obtained from the N_2 adsorption based on HK approach show the mean pore sizes of about 7.4 Å (**1**) and 4.0 Å (**2**). In spite of similar dimensions in both compounds, the pore size of **2** is smaller, which is attributed to occupying pores with the bulky naphthalene rings.
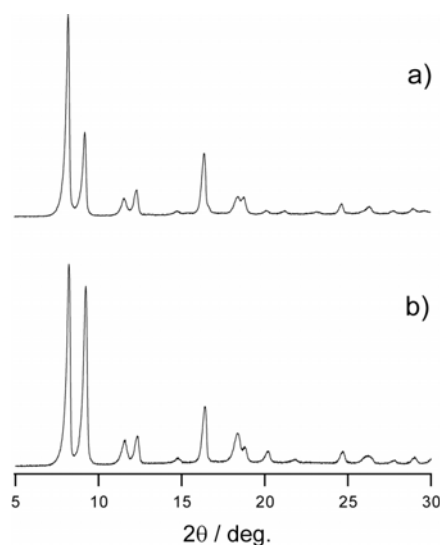
Figure 1. XRPD patterns of (a) $[Cu_2(p\text{-}OOC\text{-}Ph\text{-}COO)_2TED]_n$ (**1**) and (b) $[Cu_2(1,4\text{-}OOC\text{-}Nap\text{-}COO)_2TED]_n$ (**2**).

Table 1. Physical Properties of **1** and **2**.

Property	**1** [a]	**2**
bulk density [g/cm^3]	0.83	0.98
BET surface area [m^2/g]	1891	441
pore volume [cm^3/g]	0.70	0.08 [b]
pore diamerter [Å]	7.4	4.0 [c]
porosity [%]	58	8

[a] The properties obtained from ref. [9]   [b] Estimated from the obtained values based on DR plot of N$_2$ adsorption at 77 K.   [c] Estimated from HK method.

Equilibrium Adsorption Isotherms.

Adsorption isotherms of *n*-pentane and isoprene were measured at various temperatures in the range between 278 and 308 K and are plotted in Figure 2.   The equilibrium data exhibited a Type-I isotherm and showed no apparent hysteresis on desorption.   For each of these isotherms Langmuir, Freundlich and DR adsorption parameters were calculated, and these parameters are shown in Table 2.   The Langmuir model can also be expressed as a linear equation relating amount of adsorption m, (ml g^{-1}), to the adsorption parameters a and m_{max} as

$$P/m = 1/am_{\mathrm{max}} + P/m_{\mathrm{max}} \qquad (1)$$

where a is the distribution coefficient and is reflecting kinetically as the adsorption rate constant, k_{ads} (ml g^{-1} s^{-1}) is devided by the desorption rate constant k_{des} (s^{-1}), P is the adsorptive pressure, and m_{max} is defined as the maximum adsorbent capacity.   Freundlich model is similar in nature to the Langmuir model.   In this theory Θ, the fraction of occupied adsorption sites on the surface of the adsorbent, can be expressed as

$$\Theta = k'P^{1/n} \qquad (2)$$

where k' and $1/n$ are empirical constant.   Expressing Θ in terms of mass of adsorbate, m, a linear response should be obtained from eq. 2 by plotting log m as a function of log P as follows

$$\log m = 1/n \log P + k \qquad (3)$$

where k represents log $(k'm_{\mathrm{max}})$.   Dubinin-Radushkevich (DR) equation which has the form

$$\ln W = \ln W_0 + (A/\beta E_0)^2 \qquad (4)$$

where P_0 is saturated vapor pressure, W and W_0 are the amount of adsorption at P/P_0 and the saturated amount of adsorption, E_0 is a characteristic adsorption energy, and the parameter of A is Polanyi's adsorption potencial defined as $A = RT \ln(P_0/P)$. The parameter of β is affinity coefficient related to the adsorbate-adsorbent interaction. Langmuir and DR analysis were used to determine the saturated amount of adsorption and the adsorption energy in a series of coordination polymers. Langmuir plots have linearity in the all P/P_0 region. All DR plots were almost linear in the higher P/P_0 region, giving the saturated amount of adsorption W_0 and adsorption energy βE_0.

As seen in Table 2, the experimentally measured adsorption amount (m_{max} and W_0) of both *n*-pentane and isoprene on **1** increase with decreasing temperature, except for 318 K. It can be seen that isoprene adsorption is higher than *n*-pentane adsorption in all temperatures. Figure 3 shows adsorption isotherms of *n*-pentane and isoprene on **1** at 278 K. *n*-Pentane reveals a rapid rise more than isoprene in **1** in lower pressure range, which tendency is observed in all temperatures. The diameter and the length of *n*-pentane are about 5.1 and 6.0 Å, respectively. The diameter of the molecule is less than the pore diameter of **1**. Therefore, the molecules are able to penetrate in **1** and move relatively easily in pores.
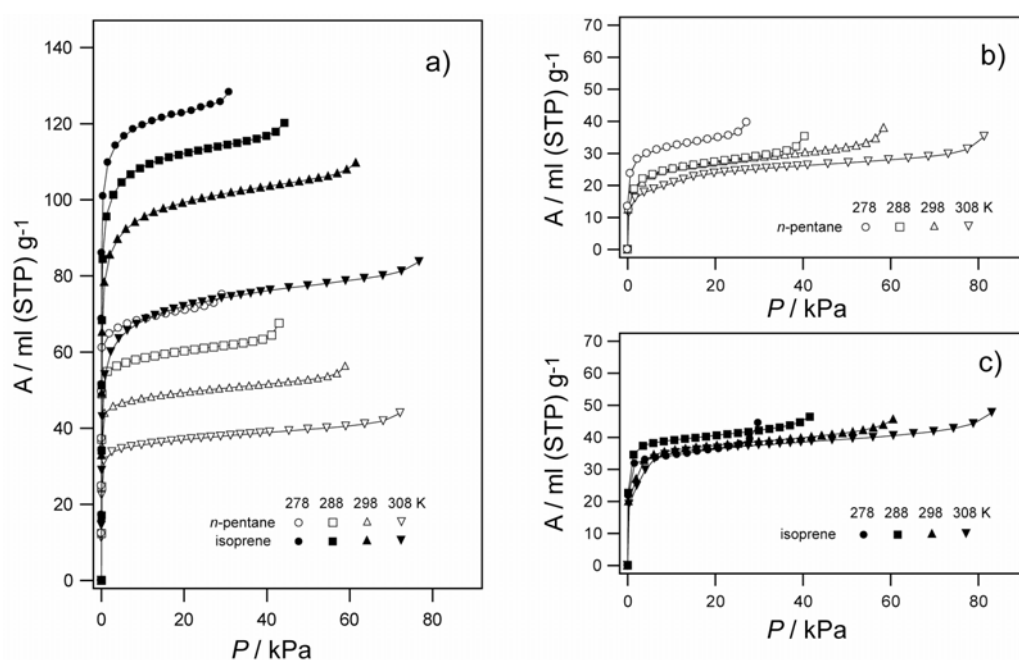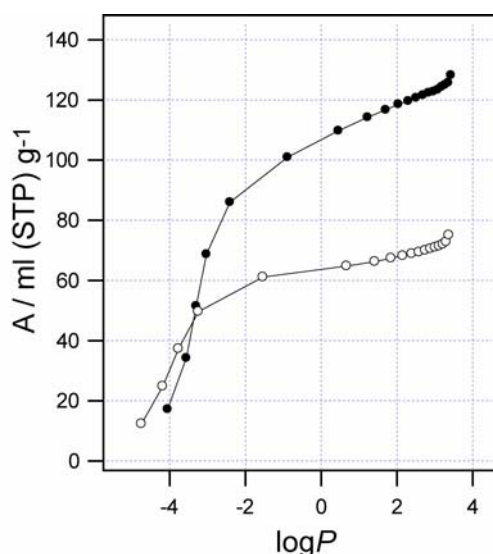

Figure 2. Isotherm for *n*-pentane (open symbol) and isoprene (filled symbol) adsorption at various temperatures on **1** (a) and **2** (b)(c).

Table 2. Characteristic Parameters of *n*-Pentane and Isoprene Adsorption on **1** and **2**.

	Compd.	T [K]	Langmuir parameters			Freundlich parameters			DR parameters		
			m_{max} [ml(STP)g^{-1}]	a	R^2	n	k	R^2	W_0 [ml(STP)g^{-1}]	βE_0 [kJ/mol]	R^2
1	*n*-pentane	278	73.0	3.34	0.999	30.4	1.8	0.983	67.5	35.9	0.967
		288	63.3	1.96	0.999	24.2	1.7	0.993	58.8	32.6	0.993
		298	53.4	1.01	0.998	23.2	1.6	0.987	49.0	32.1	0.953
		308	41.1	0.65	0.998	20.2	1.5	0.993	37.3	30.0	0.974
		318	74.8	0.99	1.000	29.7	1.8	0.993	73.3	26.6	0.960
1	isoprene	278	126.1	3.77	0.999	20.4	2.0	0.992	121.9	23.0	0.993
		288	117.8	1.89	0.999	16.6	2.0	0.984	112.5	22.9	0.987
		298	107.6	0.96	0.999	15.0	1.9	0.994	101.6	21.8	0.991
		308	80.4	0.63	0.998	11.7	1.8	0.996	75.5	20.6	0.978
		318	121.5	0.55	0.999	13.9	1.9	0.986	114.9	22.7	0.994
2	*n*-pentane	278	36.3	1.25	0.997	7.6	1.4	0.983	32.6	16.0	0.997
		288	31.1	0.56	0.995	6.7	1.3	0.995	27.4	13.6	0.993
		298	32.5	0.37	0.995	6.9	1.3	0.997	28.7	13.3	0.996
		308	29.9	0.23	0.994	6.1	1.2	0.997	26.9	11.7	0.995
		318	33.8	0.25	0.994	9.6	1.3	0.996	29.2	19.5	0.983
2	isoprene	278	37.7	1.53	0.998	20.0	1.5	0.971	34.9	22.1	0.951
		288	43.6	1.10	0.998	18.2	1.5	0.982	40.5	22.1	0.992
		298	42.7	0.48	0.997	13.3	1.5	0.990	38.7	18.0	0.993
		308	42.3	0.37	0.997	14.0	1.5	0.990	38.8	18.8	0.982
		318	43.9	0.19	0.996	6.3	1.3	0.990	33.0	20.0	0.998

Figure 3. Isotherm for *n*-pentane (open circle) and isoprene (filled circle) adsorption on **1** at 278 K.

In the case of **2**, the experimentally measured adsorption amount (m_{max} and W_0) of both *n*-pentane and isoprene are similar in all temperatures. As well as **1**, it can be seen that isoprene adsorption is higher than *n*-pentane adsorption in all temperatures. Since the diameter of the molecule (*n*-pentane and isoprene) is slightly larger than the pore diameter (4.0 Å) of **2** estimated from N_2 adsorption, some specific adsorption mechanism related to framework mobility would be expected.

Effect of Temperature on the Calculated Langmuir, Freundlich and DR Parameters.

The Langmuir parameter *a*, the distribution coefficient, is kinetically reflecting k_{ads}/k_{des}, where k_{ads} is the adsorption rate constant and k_{des} is the desorption rate constant of the adsorptive molecule. It can be seen in Table 2 that a decrease in temperature results in an increase in the value of *a* calculated for the adsorption of most of the compounds which is in agreement with the basic kinetic theory of adsorption of gases. However, it can be seen from Table 2 that a decrease in the temperature at which adsorption takes place results in an increase of the m_{max} values. This increase in the value of m_{max} with decreasing temperature is not consistent with the definition of m_{max} in the Langmuir theory. The Langmuir theory assumes that all adsorption sites on the surface of the adsorbent are energically homogeneous.

The Freundlich parameter *n* is also temperature dependent. An interpretation of this can be based on the hypothesis that the reciprocal of this parameter, $1/n$, is linearly dependent on temperature. As temperature increases there are less available adsorption sites within the range of lower energies resulting in fewer molecules being adsorbed. Looking at Table 2, this is seen to be

133

the case for the adsorption of all compounds at 278-308 K.   By contrast, however, the calculated n for at 318 K does not follow this propensity.

The Freundlich theory assumes the surface of the adsorbent to have a range of adsorption sites each having different adsorbate-adsorbent heats of adsorption associated with them.   The values of m_{max} in Table 2 suggest that the distribution of available adsorption sites on the surface of adsorbent, and not the actual total number of adsorption sites as suggested by the Langmuir m_{max}, changes with temperature.   As temperature decreases the number of available sites increases, and this is consistent with an increase in the Langmuir a parameter.   The m_{max} value calculated from Langmuir isotherm is defined as a measure of the number of available adsorption sites that are actually present on the surface of the adsorbent.   Since $\Theta = m/m_{max}$ the value of k in Table 2 equates to the value of $\log(k'm_{max})$ where k' is an empirical constant.   Thus if the m_{max} parameter used in the Freundlich isotherm represents the total number of adsorption sites, then the value of k should remain constant over the range of temperatures at which the adsorption occurred.   As seen in Table 2, the value of k remains relatively constant over the range of temperatures studied.

The parameter W_0 of the DR analysis is related to the adsorbent pore structure.   The values of W_0 which are shown in Table 2 are of the same magnitude as those of m_{max}.   The βE_0 is the parameter, which expresses the adsorption affinity of the adsorption system, decreases in increasing temperature.
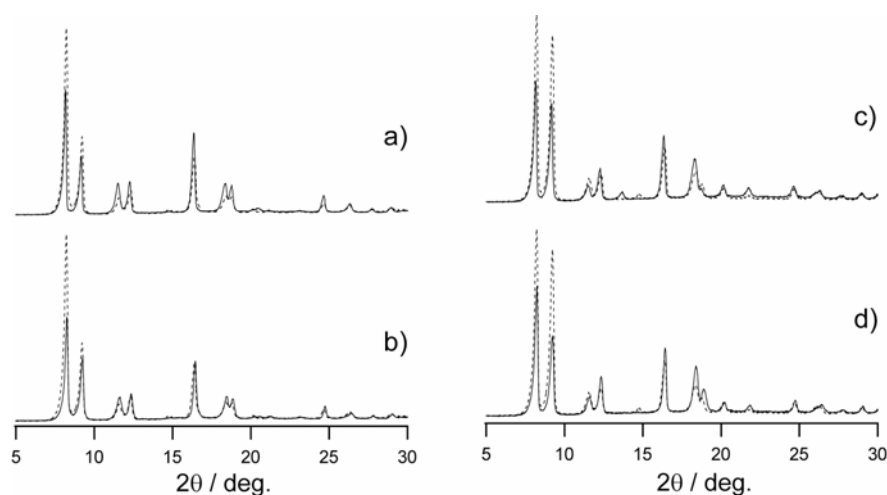
Figure 4.   XRPD patterns of (a) **1** exposed to *n*-pentane vapor for 1 day, (b) **1** exposed to isoprene vapor for 1 day, (c) **2** exposed to *n*-pentane vapor for 1 day, and (d) **2** exposed to isoprene vapor for 1 day.   Broken lines in (a)-(b) and (c)-(d) are XRPD patterns of fresh **1** and **2**, respectively.

Sorption Reversibility.

Figure 4 shows the XRPD patterns of exposed **1** and **2** to *n*-pentane or isoprene vapor. In all patterns the relative intensities are different from original ones, however, the peak positions are similar. Thus, both **1** and **2** show no significant change in crystallinity during *n*-pentane/isoprene adsorption process. To verify the adsorption reproducibility, **1** and **2** after adsorption measurements repeated for 5 cycles was checked by XRPD. The sharp peaks coincided with those of as-prepared samples are observed, thus, **1** and **2** maintain their frameworks.

Heat of Adsorption.

The βE_0 leads to the isosteric heat of adsorption $q_{\text{st, }1/e}$ at the fraction filling of $1/e$ by the equation

$$q_{\text{st, }1/e} = \beta E_0 + \Delta H_{\text{vap}} \qquad (5)$$

where ΔH_{vap} is the heat of vaporization of bulk liquid. From the eq 5, the isosteric heats of adsorption are estimated. Considering the heat of vaporization of *n*-pentane is 25.79 kJ/mol, the $q_{\text{st, }1/e}$ values are 57.9 and 39.1 kJ/mol at *n*-pentane adsorption on **1** and **2**, respectively. Compared with the reported isosteric heats of *n*-pentane adsorption on various porous compounds (Table 3), these values are reasonable. Taking into account for that the compounds having larger pore diameters show relatively larger isosteric heat, the difference among **1** and **2** is attributed to the adsorbate-adsorbate interaction in the pore system.

Table 3. Isosteric Heats of *n*-Pentane Adsorption on Various Reported Compounds, **1** and **2**.

Compd.	Surface Area [m^2/g]	Pore diameters [Å]	q_{iso} [kJ/mol]	ref
0.3 wt.-% Pt/Al$_2$O$_3$	81	-	28.6	11
PA 400 Silica Gel	670	22	37.2	12
ZSM-5/silicate	-	5.1×5.4	41.8	13
Zeolite 5A	-	5.0	52.3	14
1	1891	7.4	55.8	This work
2	441	4.0	37.5	This work

Adsorption Properties at 318 K.

There is several reports of temperature-programmed adsorption (TPA) on porous materials,[15,16] which show the adsorption amounts have dependency on environmental temperatures. That is an example of the influence of adsorbed-phase concentration on the solid diffusion flux. In that case

the decrease in adsorbed concentration dominates any increase in solid diffusivity leading to a slower overall uptake rate. 3-D porous coordination polymers also show the discontinuous tendency in rising temperature as shown in Table 2. At 318 K, which is above of boiling point of both *n*-pentane and isoprene, the propensity of adsorbed amounts shows discontinuity.

Particularly, isoprene adsorption on **2** at 318 K shows characteristic isotherm profile (Figure 5). The saturated amount at 318 K is similar to those at 278-308 K, however, isotherm exhibits two steps adsorption/desorption process. In adsorption process, the amount rapidly rises until 20 kPa, then slightly increases. Such specific adsorption could be attributed to the flexibility of framework, and controlled release of guest molecules can be expected by thermal programmed with coordination polymers.
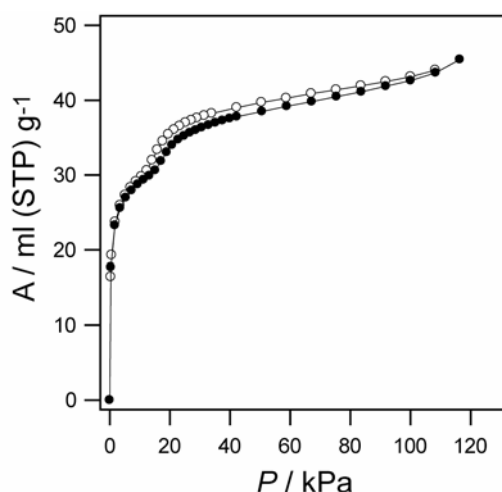
Figure 5. Isotherm for isoprene adsorption/desorption on **1** at 318 K; adsorption (filled circle) and desorption (open circle). Saturated vapor pressure at 318 K: isoprene; 105.89 kPa.

Conclusion

The detailed study of adsorption of *n*-pentane and isoprene on 3-D porous coordination polymers, **1** and **2**, was performed. The isotherm data correlated well with the Langmuir, Fruendlich and DR model for all of the system studied. In **1**, higher saturation capacities of *n*-pentane and isoprene are observed in lower temperature, except for 318 K. From DR analysis, the difference of βE_0 values is observed among *n*-pentane and isoprene on same adsorbents. Such energy differences are expected for the separation, and modulated pore properties based on coordination polymers would afford more specific inclusion process.

Experimental Section

Materials. Terephthalic acid and 1,4-naphthalenedicarboxylic acid were obtained from Tokyo Kasei Industrial. Copper(II) sulfate pentahydrate was obtained from Wako Co. *n*-Pentane (b.p.: 307-308 K, 99 %) was obtained from Kanto Chemical Co. and distilled for adsorption. Isoprene (b.p.: 309 K, anhydrous, 99 %) was obtained from Aldrich Co.

[Cu$_2$(*p*-OOC-Ph-COO)$_2$TED]$_n$ (1)

A methanol solution (10 cm^3) of copper(II) sulfate pentahydrate (0.31 g) was added to a methanol solution (200 cm^3) of *p*-OOC-Ph-COO (terephthalic acid, 0.21 g) and formic acid (2.0 cm^3). After the mixture was allowed to stand for 3 days at 313 K, a toluene solution (12.5 cm3) of TED (triethylenediamine, 0.07 g) was added to the mixture, which was then allowed to react at 433 K in an autoclave for 6 hours. A light blue precipitate was collected, and dried at 373 K under a vacuum.

[Cu$_2$(1,4-OOC-Nap-COO)$_2$TED]$_n$ (2)

A methanol solution (10 cm^3) of copper(II) sulfate pentahydrate (0.155 g) was added to a methanol solution (100 cm^3) of 1,4-OOC-Nap-COO (1,4-naphthalenedicarboxylic acid, 0.105 g) and formic acid (1.0 cm^3). After the mixture was allowed to stand for 3 days at 313 K, a toluene solution (12.5 cm^3) of TED (triethylenediamine, 0.07 g) was added to the mixture, which was then allowed to react at 433 K in an autoclave for 6 hours. A green precipitate was collected, and dried at 373 K under a vacuum. Elemental analysis calcd (%) for C$_{30}$H$_{24}$Cu$_2$N$_2$O$_8$ (667.61): C 53.97, H 3.62, N 4.20; found C 52.53, H 3.64, N 4.07.

Measurement of Adsorption. The adsorption isotherms and kinetics measurements of gaseous *n*-pentane and isoprene were measured by using BELSORP18-Plus volumetric adsorption equipment from BEL JAPAN. In the sample chamber (~ 17.5 mL) maintained at $T \pm 0.03$ K was placed the adsorbent sample (~ 300 mg), which had been prepared at 373 K and 10^{-1} Pa prior to measurement of the isotherms. The larger gas chamber (179.85 mL) with a pressure gauge was kept at $(T + 20) \pm$ 0.1 K. The *n*-pentane and isoprene used to generate the vapor was degassed fully by repeated evacuation and vapor equilibration cycles of the liquid supply side of the vapor reservoir. Helium gas at a certain pressure was introduced in the gas chamber and was allowed to diffuse into the sample chamber by opening a valve. The change in pressure allowed an accurate determination of the volume of the total gas phase. The complexation was monitored in a similar manner by using a

guest vapor in place of helium.　　The amount of guest adsorbed was calculated readily from pressure difference ($P_{cal} - P_e$), where P_{cal} is the calculated pressure with no guest adsorption, and P_e is the observed equilibrium pressure.　　All operations were computer-controlled and automatic.

　　The saturated vapor pressures were calculated using the following equation

$$\log_{10}p = A - B / (T + C) \qquad (6)$$

where p is the saturated vapor pressure (Torr), T is the temperature in degrees Celsius, and A, B, and C are constants defined by the adsorbate.　　n-Pentane: $A = 6.85221$, $B = 1064.63$, $C = 232$; isoprene: $A = 7.01187$, $B = 1126.159$, $C = 238.884$.

References

(1) Denayer, J. F. M.; Meyer, K. D.; Martens, J. A.; Baron, G. V. *Angew. Chem. Int. Ed.* **2003**, *42*, 2774-2777.

(2) Choudary, N. V.; Kumar, P.; Bhat, T. S. G.; Cho, S. H.; Han, S. S.; Kim, J. N. *Ind. Eng. Chem. Res.* **2002**, *41*, 2728-2734.

(3) Kitagawa, S.; Kondo, M. *Bull. Chem. Soc. Jpn.* **1998**, *71*, 1739-1753.

(4) Li, H.; Eddaoudi, M.; O'Keeffe, M.; Yaghi, O. M. *Nature* **1999**, *402*, 276-279.

(5) Eddaoudi, M.; Moler, D. B.; LI, H.; Chen, B.; Reineke, T. M.; O'keeffe, M.; Yaghi, O. M. *Acc. Chem. Res.* **2001**, *34*, 319-330.

(6) Eddaoudi, M.; Kim, J.; Rosi, N.; Vodak, D.; Wachter, J.; O'Keeffe, M.; Yaghi, O. M. *Science* **2002**, *295*, 469-472.

(7) Seki, K. *Chem. Comm.* **2001**, 1496-1497.

(8) Seki, K. *Phys. Chem. Chem. Phys.* **2002**, *4*, 1968-1971.

(9) Seki, K.; Mori, W. *J. Phys. Chem. B* **2002**, *106*, 1380-1385.

(10) Seki, K. *Langmuir* **2002**, *18*, 2441-2443.

(11) Gonenc, Z. S.; Yildirim, R.; Beler-Baykal, A. B.; Onsan, Z. I. *Applied Catalysis A: General* **1993**, *103*, 35-42.

(12) Al-Sahhaf, T. A.; Sloan, E. D.; Hlnes, A. L. *Ind. Eng. Chem. Process Des. Dev.* **1981**, *20*, 658-662.

(13) Sun, M. S.; Talu, O.; Shah, D. B. *J. Phys. Chem.* **1996**, *100*, 17276-17280.

(14) Silva, J. A. C.; Rodrigues, A. E. *Ind. Eng. Chem. Res.* **1997**, *36*, 493-500.

(15) Li-feng, C.; Rees, L. V. C. *Zeolites* **1988**, *8*, 310-316.

(16) Kim, D. J.; Kim, J. W.; Yie, J. E.; Moon, H. *Ind. Eng. Chem. Res.* **2002**, *41*, 6589-6592.

General Conclusion

The author investigated the rational synthesis and characterization of the coordination polymers toward the new functional materials, which involve the dynamic phenomenon of the frameworks. In order to obtain dynamic porous coordination polymers, the author tried to construct with elastic hydrogen bonds. Total 29 coordination polymers (1-D motif: **A1 ~ 5** and **R1 ~ 5**, 2-D motif: **MOPA-1 ~ 5**, 3-D motif: **1** and **2**), which accommodate guest molecules, have been synthesized and characterized, and studied on the correlation between the crystal dimensionality and properties.

In Chapter 1, the author synthesized novel 1-D chains, **A1 ~ 5**, by self-assembly method with coordination bond and hydrogen bond. Although structural controls in new topological system with the py-CO-NH-CH$_2$-py organic ligands are rather difficult because of the free rotation of NH-CH$_2$ bond, **A1 ~ 3** form 1-D chains aligned in parallel in the crystal. All chains form cationic 1-D chain to accommodate anions as guest molecules with elastic hydrogen bonds.

In Chapter 2 and 3, from octahedral coordinated metals and bipyridyl derivatives containing an amide group, we succeeded in producing novel 1-D repeated rhomboid networks, **R1 ~ 5**. Particularly, in **R5 ⊃ 2H$_2$O·2MeOH** each repeated rhomboid chain stack with edge-to-edge manner to afford micropores fulfilled with guest molecules, and shows crystal-to-crystal structural transformation caused by adsorption/desorption of guest molecules, which is attributed to multiple hydrogen bonds in the structure.

In Chapter 4, from Co(SCN)$_2$ and bipyridyl derivatives having the amide group, the author succeeded in providing novel coordination polymers with flexible 2-D sheets. Such sheets transform their structure to other ones accompanying with adsorption/desorption of guest molecules. **MOPA-1 ⊃ 4Me$_2$CO (MOPA-1 ⊃ 4THF)** are transformed to *β*-sheet typed crystalline **MOPA-1**, whose porous structures are maintained. The clue to maintain crystallinity in **MOPA-1** is a gadget that the amide moiety plays not only a role in trapping guest molecules but also in linking sheets. Therefore, the reversible adsorption is restricted to the apohost **MOPA-1,** which also shows selectivity for guest molecules in shape and chemical affinity.

In Chapter 5, From Co(SCN)$_2$ and bipyridyl derivatives containing an amide group, we succeeded in producing new square grid frameworks, **MOPA-3 ~ 5**, which have complementary-amide binding manner eschewing interpenetrating. Particularly, **MOPA-5 ⊃ 4Me$_2$CO** affords micropores fulfilled with guest molecules, and shows that structural transformation *via* amorphous is caused by adsorption/desorption of guest molecules. Thermodyanmic results imply that coordination polymer

141

is often much more dynamic than generally believed and that weak dispersive forces induces structural rearrangement in a well-concerted fashion.

In Chapter 6, the detailed study of adsorption of *n*-pentane and isoprene on robust 3-D porous coordination polymers, **1** and **2**, was performed.   The unique propensity was observed.

The author principally showed the three topics, that is, (1) rational synthesis of coordination polymers including hydrogen bonds, (2) construction of dynamic porous framework, and (3) thermodynamic analysis on adsorption/desorption of guest molecules.

(1): Although it was difficult to predict self-assembled structures from the bridging ligands including both coordination sites and hydrogen bonding sites, py-NHCO-py type ligands are useful for new class of "crystal engineering".   It is because that the amide moiety of their ligands could create hydrogen bonding interaction sites in the network and cross-linking to coordination-based motifs.   A new structural dimension is added to coordination networks with *β*-sheet motif having a linking capability to a network structure; 1-D → 2-D (Chapter 1) and 2-D → 3-D (Chapter 5).

(2): The author anticipates the contrivance for dynamic porous coordination polymer is the introducing of hydrogen bonds into the frameworks.   Base on amide-including ligands, four types of flexible coordination polymers were obtained; "1-D chain *crystal-to-crystal*" (Chapter 1), "1-D repeated rhomboid *crystal-to-crystal*" (Chapter 3), "2-D sheet *crystal-to-crystal*" (Chapter 4), and "2-D sheet *amorphous-to-crystal*" (Chapter 5).   Such dynamic behaviors of coordination polymers at present provide a new concept that porous properties of coordination polymer do not require robustness, and the advantage of inorganic/organic hybrid compound would open up a new functional chemistry towards dynamic porous materials.

(3): Although many porous coordination polymers have been synthesized and reported, in our present stage of knowledge, the report of thermal analysis is sparse.   Thermodyanmic parameters calculated in this thesis (Chapter 3 and 5) are also useful to analyze the thermal behavior of porous coordination polymers, especially for dynamic behaviors of the framework.

List of Publications

General Introduction

Dynamic Porous Properties of Coordination Polymers Inspired by Hydrogen Bonds

Kitagawa, S.; Uemura, K. *Chem. Soc. Rev.* submitted.

Chapter 1. Cationic Ag(I)-Amide One-dimensional Coordination Polymers with β-Sheet and Helical Structures. New Second Structure Motif Constructed by Metallo-Amino Acids

Uemura, K.; Kondo, M.; Kitagawa, S. *Chem. Eur. J.* to be submitted.

Chapter 2. Sythesis and Structures of Coordination Polymers with 4,4'-Dipyridylsulfide

Kondo, M.; Shimamura, M.; Noro, S.-i.; Kimura, Y.; Uemura, K.; Kitagawa, S. *J. Solid State Chem.* **2000**, *152*, 113-119.

Chapter 3. Construction of Repeated Rhomboid-Typed Coordinatin Polymers Having Guest-Incorporated Cavities. Analysis of Flexible Structural Transformation with Thermodynamic Analysis

Uemura, K.; Kitagawa, S. *Inorg. Chem.* submitted.

Chapter 4. Novel Flexible Frameworks of Porous Cobalt(II) Coordination Polymers Which Show Selective Guest Adsorption Based on Switching of Hydrogen Bond Pairs of Amide Groups

Uemura, K.; Kitagawa, S.; Kondo, M.; Fukui, K.; Kitaura, R.; Chang, H.-C.; Mizutani, T. *Chem. Eur. J.* **2002**, *8*, 3586-3600.

Chapter 5. A Contrivance for a Dynamic Porous Framework. Cooperative Guest Adsorption Based on Square Grids Connected by Amide-Amide Hydrogen Bonds

Uemura, K.; Kitagawa, S.; Fukui, K.; Saito, K. *J. Am. Chem. Soc.* in press.

Chapter 6. *n*-Pentane and Isoprene Adsorption on Three-Dimensional Porous Coordination Polymers

Uemura, K.; Kitagawa, S. *Langmuir* to be submitted.

List of Presentations

(1) Thermal Analysis of Cooperative Adsorption on Porous Co(II) Coordination Polymers
   Uemura, K.; Kitagawa, S.
   First Symposium if Institute for Fundamental Chemistry, Kyoto, November 2003
   (Poster Presentation)

(2) Thermal Analysis of Cooperative Adsorption on Porous Co(II) Coordination Polymers
   Uemura, K.; Kitagawa, S.
   53th Symposium on Coordination Chemistry of Japan, Yamagata, September 2003
   (Poster Presentation)

(3) Cooperative Adsorption of Porous Coordination Polymers Constructed by Complementary
   Hydrogen Bonds
   Uemura, K.
   Summer Seminar of Young Coordination Chemist's Association Japan, Augast 2003

(4) Porous Coordination Polymers Having Amide Triger for Structural Transformation
   Uemura, K.; Uemura, T.; Kitagawa, S.
   Nano-Science of Advanced Metal Complexes, Institute for Molecular Science Okazaki,
   March 2003 (Poster Presentation)

(5) Two-dimensional Coordination Polymer Including Amide-Amide Hydrogen Bond Which
   Shows the Healing Property
   Uemura, K.; Horike, S.; Uemura, T.; Kitagawa, S.
   81th Annual Meeting of Chemical Society of Japan, Tokyo, March 2003

(6) Synthesis and Structures of New Coordination Polymers with Ag(I) and Amide Containing
   Ligands
   Uemura, K.; Kumamoto, Y.; Horike, S.; Kitagawa, S.
   52th Symposium on Coordination Chemistry of Japan, Tokyo, September 2002

(7)   Novel Flexible Frameworks of Porous Cobalt(II) Coordination Polymers Which Show Selective Guest Adsorption Based on Switching of Hydrogen Bond Pairs of Amide Groups

Uemura, K.

Gordon Research Conference on ORGANIC STRUCTURE & PROPERTIES, SPring-8 Hyogo, July 2002 (Poster Presentation)

(8)   Synthesis and Structures of New Coordination Networks Demonstrating Structural Change with Simultaneous Exchange of Counter Anions

Uemura, K.; Kumamoto, Y.; Kitagawa, S.

81th Annual Meeting of Chemical Society of Japan, Tokyo, March 2002

(9)   Synthesis and Structures of New Coordination Polymers with Ag(I) and Amide Including Ligand

Kumamoto, Y.; Uemura, K.; Horike, S.; Kitagawa, S.

81th Annual Meeting of Chemical Society of Japan, Tokyo, March 2002

(Poster Presentation)

(10)   Novel Cobalt(II) Coordination Polymers Which Afford Reversible Crystal-to-crystal Transformation Responding to Guest Molecules

Uemura, K.; Kitagawa, S.; Kondo, M.; Fukui, K.

International Symposium on Cooperative Phenomena of Assembled Metal Complexes, Osaka, November 2001 (Poster Presentation)

(11)   Synthesis of New Porous Coordination Networks with Guest Chromism

Uemura, K.; Kitaura, R.; Horike, S.; Kondo, M.; Kitagawa, S.

51th Symposium on Coordination Chemistry of Japan, Matsue, September 2001

(12)   Synthesis of New Coordination Networks Demonstrating Structural Change Responding to the Included Guest Molecule

Uemura, K.; Kitaura, R.; Kondo, M.; Kitagawa, S.

79th Annual Meeting of Chemical Society of Japan, Hyogo, March 2001

(13)   Synthesis and Structures of the New Ag(I) Coordination Polymers Having
         Pycolylisonicotinamide
         Uemura, K.; Kondo, M.; Kitagawa, S.
         2000 International Chemical Congress of Pacific Basin Societies, Hawaii, December 2000
         (Poster Presentation)

(14)   Synthesis of New Coordination Networks Demonstrating the Structural Change Responding
         to the Included Guest Molecule
         Kondo, M.; Uemura, K.; Kitagawa, S.
         47th Symposium on Organometallic Chemistry of Japan, Nagoya, October 2000

(15)   Synthesis of New Coordination Networks Demonstrating the Structural Change Responding
         to the Included Guest Molecule
         Kondo, M.; Uemura, K.; Kitagawa, S.
         49th SPSJ Symposium on Macromolecules, Sendai, September 2000

(16)   Synthesis and Structure of Coordination Polymers with Amide-Containing Ligand
         Uemura, K.; Kondo, M.; Kitagawa, S.
         International Symposium on New Horizons of Coordination Chemistry towards the 21st
         Century, Kusatsu, September 2000 (Poster Presentation)

(17)   Synthesis of New Porous Coordination Networks with Guest Chromism
         Uemura, K.; Kondo, M.; Kitagawa, S.
         50th Symposium on Coordination Chemistry of Japan, Kusatsu, September 2000

(18)   Synthesis, Crystal Structure and Property of Co(II)-Pyridylnicotinamide Coordination
         Polymer
         Uemura, K.; Kondo, M.; Kitagawa, S.; Seki, K.
         78th Annual Meeting of Chemical Society of Japan, Chiba, March 2000

(19)   Synthesis and Structures of Coordination Polymers with Pyridylnicotinamide
         Uemura, K.; Kondo, M.; Asami, A.; Kitagawa, S.
         49th Symposium on Coordination Chemistry of Japan, Sapporo, September 1999
         (Poster Presentation)